(20) 3-1

AFML-TR-67-205

DEVELOPMENT OF MANUFACTURING METHODS AND PROCESSES FOR FLUXLESS BRAZING TO ALUMINUM THIN WALL TUBING AND FOIL

G. Martin
AVCO Corporation

TECHNICAL REPORT AFML-TR-67-205
July 1967
PROJECT 8-317

Air Force Materials Laboratory
Directorate of Laboratories
Air Force Systems Command
Wright-Patterson Air Force Base, Ohio

NOTICE

When Government drawings, specifications, or other data are used for any purpose other than in connection with a definitely related Government procurement operation, the United States Government thereby incurs no responsibility nor any obligation, whatsoever; and the fact that the Government may have formulated, furnished, or in any way supplied the said drawings, specifications, or other data, is not to be regarded by implication or otherwise as in any manner licensing the holder or any other person or corporation, or conveying any rights or permission to manufacture, use, or sell any patented invention that may in any way be related thereto.

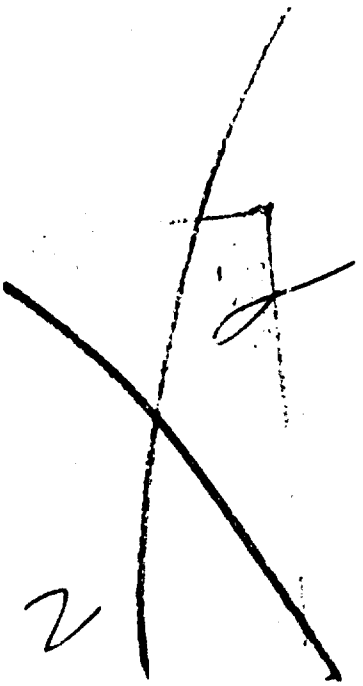

Copies of this report should not be returned unless return is required by security considerations, contractual obligations, or notice on a specific document.

(U)
Security Classification

DOCUMENT CONTROL DATA · R&D

(Security classification of title, body of abstract and indexing annotation must be entered when the overall report is classified)

1 ORIGINATING ACTIVITY (Corporate author)
Aerostructures Division
AVCO Corporation
Nashville 1, Tennessee

400 166

2a REPORT SECURITY CLASSIFICATION
(U)

2b GROUP

3 REPORT TITLE
(6)
DEVELOPMENT OF MANUFACTURING METHODS AND PROCESSES FOR FLUXLESS BRAZING TO ALUMINUM THIN WALL TUBING AND FOIL.

4 DESCRIPTIVE NOTES (Type of report and inclusive dates)
(9)
Final Technical Report. [redacted] 15 June 1965 to 15 April 1967.

5 AUTHOR(S) (Last name, first name, initial)
(10)
Martin, Geoffrey Martin.

6. REPORT DATE	7a. TOTAL NO. OF PAGES	7b. NO. OF REFS
(11) 5 June 1967 Jul 67	(12) 243 p.	--

8a. CONTRACT OR GRANT NO. (15) AF33(615)-2783 ≠

b. PROJECT NO. (16) 7351-8-317

c.

d.

9a. ORIGINATOR'S REPORT NUMBER(S)
(18) (19) AFML-TR-67-205

9b. OTHER REPORT NO(S) (Any other numbers that may be assigned this report)

10. AVAILABILITY/LIMITATION NOTICES This document is subject to special export controls and each transmittal to foreign governments or foreign nationals may be made only with prior approval of the Advanced Fabrication Techniques Branch, Manufacturing Technology Division, Air Force Materials Laboratory, Wright-Patterson AFB, Ohio 45433.

11. SUPPLEMENTARY NOTES

12. SPONSORING MILITARY ACTIVITY
Air Force Materials Laboratory
Advanced Fabrication Techniques Branch
MATF, Wright-Patterson Air Force Base, Ohio

13. ABSTRACT This program had the overall objectives of developing and/or establishing process(es) or limits for fluxless brazing and diffusion bonding composites fabricated from aluminum alloy foils, thin sheet, and thin walled tubing, and to demonstrate the optimum process on small, complex hardware samples applicable for aerospace applications. (U)

Simulated material service environments included--thermal environments ranging from -400 F (-240 C) to 500 F (260 C), and corrosive environmental testing per MIL-A-5090D. Corrosive and thermal environments were limited to 100 hours. (U)

Composite evaluations were limited to small thin walled tube shell heat exchangers, multi-layer plate fin heat exchangers, honeycomb sandwich structural panels, and ultra light split turbulent surface extended fin thermal conditioning panels. (U)

Basic joints and composite testing for materials and methods included--vibration, reverse stress cycling, thermal cycling, extended elevated temperature environment up to 100 hours, salt fog environments for 100 hours, and proof pressure reliability testing of joints and materials for gaseous or liquid heat exchanger applications. (U)

Suitability of the fluxless brazing method and materials for complex lightweight hardware composites was demonstrated. (U)

(continued)

DD FORM 1 JAN 64 1473

(U)
Security Classification

KEY WORDS	LINK A		LINK B		LINK C	
	ROLE	WT	ROLE	WT	ROLE	WT

INSTRUCTIONS

1. ORIGINATING ACTIVITY: Enter the name and address of the contractor, subcontractor, grantee, Department of Defense activity or other organization *(corporate author)* issuing the report.

2*a*. REPORT SECURITY CLASSIFICATION: Enter the overall security classification of the report. Indicate whether "Restricted Data" is included. Marking is to be in accordance with appropriate security regulations.

2*b*. GROUP: Automatic downgrading is specified in DoD Directive 5200.10 and Armed Forces Industrial Manual. Enter the group number. Also, when applicable, show that optional markings have been used for Group 3 and Group 4 as authorized.

3. REPORT TITLE: Enter the complete report title in all capital letters. Titles in all cases should be unclassified. If a meaningful title cannot be selected without classification, show title classification in all capitals in parenthesis immediately following the title.

4. DESCRIPTIVE NOTES: If appropriate, enter the type of report, e.g., interim, progress, summary, annual, or final. Give the inclusive dates when a specific reporting period is covered.

5. AUTHOR(S): Enter the name(s) of author(s) as shown on or in the report. Enter last name, first name, middle initial. If military, show rank and branch of service. The name of the principal author is an absolute minimum requirement.

6. REPORT DATE: Enter the date of the report as day, month, year; or month, year. If more than one date appears on the report, use date of publication.

7*a*. TOTAL NUMBER OF PAGES: The total page count should follow normal pagination procedures, i.e., enter the number of pages containing information.

7*b*. NUMBER OF REFERENCES: Enter the total number of references cited in the report.

8*a*. CONTRACT OR GRANT NUMBER: If appropriate, enter the applicable number of the contract or grant under which the report was written.

8*b*, 8*c*, & 8*d*. PROJECT NUMBER: Enter the appropriate military department identification, such as project number, subproject number, system numbers, task number, etc.

9*a*. ORIGINATOR'S REPORT NUMBER(S): Enter the official report number by which the document will be identified and controlled by the originating activity. This number must be unique to this report.

9*b*. OTHER REPORT NUMBER(S): If the report has been assigned any other report numbers *(either by the originator or by the sponsor)*, also enter this number(s).

10. AVAILABILITY/LIMITATION NOTICES: Enter any limitations on further dissemination of the report other than those imposed by security classification, using standard statements such as:

(1) "Qualified requesters may obtain copies of this report from DDC."

(2) "Foreign announcement and dissemination of this report by DDC is not authorized."

(3) "U. S. Government agencies may obtain copies of this report directly from DDC. Other qualified DDC users shall request through

_____."

(4) "U. S. military agencies may obtain copies of this report directly from DDC. Other qualified users shall request through

_____."

(5) "All distribution of this report is controlled. Qualified DDC users shall request through

_____."

If the report has been furnished to the Office of Technical Services, Department of Commerce, for sale to the public, indicate this fact and enter the price, if known.

11. SUPPLEMENTARY NOTES: Use for additional explanatory notes.

12. SPONSORING MILITARY ACTIVITY: Enter the name of the departmental project office or laboratory sponsoring *(paying for)* the research and development. Include address.

13. ABSTRACT: Enter an abstract giving a brief and factual summary of the document indicative of the report, even though it may also appear elsewhere in the body of the technical report. If additional space is required, a continuation sheet shall be attached.

It is highly desirable that the abstract of classified reports be unclassified. Each paragraph of the abstract shall end with an indication of the military security classification of the information in the paragraph, represented as *(TS)*, *(S)*, *(C)*, or *(U)*.

There is no limitation on the length of the abstract. However, the suggested length is from 150 to 225 words.

14. KEY WORDS: Key words are technically meaningful terms or short phrases that characterize a report and may be used as index entries for cataloging the report. Key words must be selected so that no security classification is required. Identifiers, such as equipment model designation, trade name, military project code name, geographic location, may be used as key words but will be followed by an indication of technical context. The assignment of links, rules, and weights is optional.

DD FORM 1473

13. ABSTRACT (cont'd)

Limitations of the applicability of diffusion bonding aluminum alloy composites at temperatures below the state-of-the-art brazing temperatures were exposed. (U)

Feasibility of developing filler metal alloys exhibiting low flow temperatures was demonstrated. (U)

Details of illustrations in this document may be better studied on microfiche.

DEVELOPMENT OF MANUFACTURING METHODS AND PROCESSES FOR FLUXLESS BRAZING TO ALUMINUM THIN WALL TUBING AND FOIL

G. Martin

Form 1473

ABSTRACT

This program had the overall objectives of developing and/or establishing process(es) or limits for fluxless brazing and diffusion bonding composites fabricated from aluminum alloy foils, thin sheet, and thin walled tubing, and to demonstrate the optimum process on small, complex hardware samples applicable for aerospace applications.

Simulated material service environments included--thermal environments ranging from -300 F (-184 C) to 500 F (260 C), and corrosive environmental testing per MIL-A-5090D. Corrosive and thermal environments were limited to 100 hours.

Composite evaluations were limited to small thin walled tube shell heat exchangers, multi-layer plate fin heat exchangers, honeycomb sandwich structural panels, and ultra light split turbulent surface extended fin thermal conditioning panels.

Basic joints and composite testing for materials and methods included--vibration, reverse stress cycling, thermal cycling, extended elevated temperature environment up to 100 hours, salt fog environments for 100 hours, and proof pressure reliability testing of joints and materials for gaseous or liquid heat exchanger applications.

Suitability of the fluxless brazing method and materials for complex lightweight hardware composites was demonstrated.

Limitations of the applicability of diffusion bonding aluminum alloy composites at temperatures below the state-of-the-art brazing temperatures were exposed.

Feasibility of developing filler metal alloys exhibiting low flow temperatures was demonstrated.

The primary investigations and surveys were:

- Availability and properties of wrought aluminum alloys in foil, sheet, and thin wall tubing forms survey.
- Methods for achieving metallic node joints for fabrication of aluminum honeycomb core blankets survey.
- Investigation of chemical cleaning systems for pre-joining preparation.
- Determination of state-of-the-art materials brazed joint properties at cryogenic and elevated temperatures.
- Evaluation of the effect of brazing on the corrosion resistance of selected aluminum alloys.

- o Fabrication and testing of complex hardware brazements.
- o Evaluation of low pressure diffusion bonded joints and applicability of method for fabricating lightweight structures.
- o Feasibility of developing experimental braze filler metal systems for joining aluminum at temperatures lower than those required for the state-of-the-art systems.

Primary accomplishments were:

- o Materials availability and properties were reviewed and tabulated, which exposed that aluminum alloys suitable for brazing are not readily available as foil. That commercial braze filler metals are only available as powder, wire, or sheet. However, the study concluded that aluminum alloy foils could be produced by rerolling, and that braze alloy available as sheet could be reduced to foil for experimental purposes by chemical milling.
- o Aluminum honeycomb core with metallic nodes suitable for brazing methods were surveyed. Ultrasonic welding was found to be applicable, while diffusion bonding (Astroweld) was a possibility.
- o Candidate alkaline and acid base chemical cleaning systems were reviewed and two were proven to be satisfactory systems for prebrazing surface conditioning. (A third system previously developed and proven by the contractor as satisfactory for fluxless brazing was compared and eventually used for all brazing evaluations conducted.)
- o Relative atmospheric oxide formation rates for candidate base metal aluminum alloys were determined.
- o Capillary rise power and bridging characteristics of two commercial braze filler metals on 6061 aluminum were demonstrated.
- o Satisfactory ultrasonic welded aluminum honeycomb core blankets were produced without development.
- o Fluxless brazing with commercially available materials was demonstrated as being suitable for structural, cryogenic, and elevated temperature environments for complex aerospace composites.
- o A low pressure diffusion bonding process with commercially available materials, was successfully developed and demonstrated for joints which can be positively held in intimate contact during joining, but was limited in multi-joint lightweight composite applications, and as such is not a suitable alternate method to the fluxless brazing process.

o The feasibility of developing new brazing filler metals with lower wetting and flow temperatures than the state-of-the-art (commercially available) materials was established. Experimental aluminum base complex systems exhibited minimum effective wetting temperatures up to 50 F lower than the present available systems, with acceptable joint strengths.

Of the systems investigated the AlSi + Cu ternary offered the best combination of strength versus wetting temperature. The AlSi + Mg system offered the lowest wetting temperature. The AlSi + In system based on its microstructure, is a potential candidate for corrosive environment applications, although in this area, the AlSi + Mg ternary based on known data, should also exhibit good corrosion resistance.

This abstract is subject to special export controls and each transmittal to foreign governments or foreign nationals may be made only with prior approval of the Air Force Materials Laboratory, MATF, Wright-Patterson Air Force Base, Ohio 45433.

CONTENTS

CONTENTS

CONTENTS

TABLES

ILLUSTRATIONS

ILLUSTRATIONS

ILLUSTRATIONS

ILLUSTRATIONS

ILLUSTRATIONS

SECTION 1.0

INTRODUCTION

Corrosive flux residue had been a major drawback in the use of brazed aluminum for aerospace composite applications. As late as 1963 it had been assumed that aluminum base filler metals without flux, would not wet aluminum due to the oxide film. Since the aluminum oxide forms readily at room temperature in air, it was considered necessary to have a reducing flux present at the work interface to promote wetting during brazing. Thus, entrapped flux residue resulted in catastrophic corrosion, which limited the use of aluminum to open brazed joint applications.

Because of the properties exhibited by certain aluminum alloys, it was highly desirable to develop a method for producing non-corrosive complex aluminum brazements for the resolution of many aerospace application problems.

Studies conducted by AVCO/AD on the relative oxide formation rates for various alloys showed that each alloy oxidized at a rate different from that of other alloys and generally that alloys having lower alloying constituent content reacted quicker with oxygen in air. It was also seen that the reaction (oxide formation) in air at room temperature continued for periods longer than twenty four hours, or in other words the oxide film was not completed in the period immediately after bare aluminum was exposed to air. It was further seen that moisture present in air acted as a catalyst, while heat accelerated the oxide formation rate.

Studies of the behavior of a AlSi binary system on aluminum surfaces, which had been reduced of oxides, within a period of twenty four hours, showed that the binary system exhibited wetting and flow when heated to 1075 F (580 C). It was further learned that wetting could be accomplished in an inert gas environment, if the free oxygen and moisture content of the gaseous environment was not extensive. As a result of this work, brazing of aluminum alloys having a solidus of 1100 F (593 C) or higher, using AlSi base filler metals, was developed and established as a practical process.

The principle objective of the subject program, was to broaden the scope of the state-of-the-art of this fluxless brazing process, and demonstrate the applicability of the materials and process for fabricating ultra-light complex aluminum composites for structural and thermal applications.

Secondary, but important objectives included investigations to determine the feasibility of alternate backup approaches, since the AlSi system may not be optimum for all complex composite applications,

especially if the relatively high brazing temperature proved restrictive. Low pressure intermediate temperature diffusion bonding, utilizing the identical material systems as used for fluxless brazing, was one alternate. The second alternate covered investigations to determine the feasibility of developing new filler metal systems, with both approaches directed to achieving sound metallurgical joints at temperatures below that required for the state-of-the art brazing (1075 F).

The objective of this report is to describe the work and accomplishments during the period from June 15, 1965 to April 15, 1967 toward the selection of materials processes and fabrication techniques for fluxless brazing and diffusion bonding complex structural and heat exchanger composites for advanced structures and systems. The program was divided into the two inter-related phases delineated below:

Phase I as reported in Sections 2 through 6 inclusive covered---- Material availability survey--- Material properties review--- Aluminum honeycomb core node joining techniques survey--- Review and evaluation of chemical cleaning systems--- Basic properties of brazed joints--- Investigation of low pressure diffusion bonding--- Investigation of new braze filler metals.

Phase II as reported in Sections 7 through 9 inclusive covered---- Application of state-of-the art brazing process to complex hardware composites--- Application of diffusion bonding technique to complex hardware composites--- Demonstration of the feasibility of applying new candidate braze filler metals for joining complex hardware composites.

Note: It is important to note that the metal preparation and brazing procedures for all joining evaluations were conducted as outlined in Subsection 4.2.3--- Any deviations from this are stated in the appropriate subsections.

SECTION 2.0

MATERIAL AVAILABILITY AND HONEYCOMB CORE FABRICATION TECHNOLOGY SURVEY

A review was conducted to accumulate data on material availability, honeycomb core fabrication technology, and mechanical and physical properties of aluminum alloys in foil, thin sheet, and thin wall tubing forms. This was a minimum effort review conducted for the purpose of program planning, and was performed at the program's inception.

Eight aluminum alloys--2020, 2219, 3003, 5052, 6061, 6951, 7139, and 7005--were pre-program candidate selections as being broadly representative of the commercial and experimental alloys being offered the aerospace industry. Selections included four alloys (3003, 6061, 6951, 7005) approved by AVCO/AD for fluxless brazing of various types of aerospace hardware. The 2020, 2219, and 7139 alloys were chosen from the more recent alloys developed by the aluminum industry, as the properties of these three alloys would add much to lightweight composite material in future applications.

Four of the candidate materials, aluminum alloys 3003, 6061, 6951, and 7005 were available and appeared compatible. Alloys 2020 and 2219 were not compatible with commercially available filler metal braze temperatures. Alloy 5052 was rejected as a material candidate as recent investigations proved the alloy to be highly susceptible to filler metal intergranular penetration. Alloy 7139 was not available except in 10,000 pound mill runs.(1)

The major consideration in the honeycomb core fabrication technology review, was the need for compatibility between the node joining fabrication process and the fluxless brazing process. Of the three (3) node joining approaches reviewed, only ultrasonic welded honeycomb core had been produced. This had been limited to experimental core blanket fabrication, but appeared satisfactory for evaluation in this program.

2.1 Material Availability

The review of the candidate alloys for their availability showed that general warehouse stocks were poor. Many items required mill runs of minimum buys from 2,000 to 10,000 pounds with up to 18 weeks delivery. Some of these procurement difficulties were anticipated as it was planned to procure wrought sheet stock thicker than required, and subsequently, chemically milling to the gage required.

Table 2-1 is a tabulation which showed the availability of alloys in the sheet and/or foil form. Close tolerance, small diameter, thin walled extruded tubing was readily available in small quantities

(1) Alcoa research laboratories supplied sheet from their stock.

of random lengths with short deliveries for most aluminum alloys.

The 6061 alloy required for honeycomb core foil could be rerolled from available 0.008 inch sheet. The 6951 and 7005 alloy sheet required for the program could be chemical milled from available thicknesses of 0.070 and 0.060 inches respectively.

Table 2-1

Availability of Sheet and Foil Forms

Alloys available in sheet and/or foil from warehouse stocks:

Thickness	Alloys Available	
.002	3003	
.003	3003	
.006	3003	
.008	3003	6061
.010	3003	6061
.016	3003	6061
.020	3003	6061
.032	3003	6061

Alloys requiring minimum buy mill runs:

Thickness	Alloy Types and Minimum Buy Quantities		
.002	6061 (2000 lbs)	2020 (NA)	2219 (NA)
.003	6061 (2000 lbs)	2020 (NA)	2219 (NA)
.006	6061 (2000 lbs)	2020 (NA)	2219 (NA)
.008		2020 (NA)	2219 (2000 lbs)
.010		2020 (NA)	2219 (2000 lbs)
.016		2020 (2000 lbs)	2219 (2000 lbs)
.020		2020 (2000 lbs)	2219 (2000 lbs)
.032		2020 (2000 lbs)	2219 (2000 lbs)
.002	6951 (NA)	7005 (NA)	7139 (NA)
.003	6951 (NA)		7139 (NA)
.006	6951 (NA)		7139 (NA)
.008	6951*(10,000 lbs)	7005 (2000 lbs)	7139 (NA)
.010-.032	6951*(10,000 lbs)	7005 (2000 lbs)	7139 (10,000 lbs)

(NA) Not Available
* Available as braze sheet core in 1,000 lb. mill runs

2.2 Honeycomb Core Fabrication Technology

A review was conducted on the current status and potential for manufacturing aluminum honeycomb core with all metal node joints. The honeycomb was required to be suitable for core in fluxless brazed honeycomb sandwich composites. The review was limited to the following node joining approaches: a) Diffusion Bonding, b) Resistance Welding, and c) Ultrasonic Welding.

Diffusion bonded aluminum honeycomb was not available. The progress appeared promising but was reported to be requiring further development.

Resistance welded aluminum honeycomb was not available. No research activity for resistance welding of aluminum honeycomb nodes was reported. Anticipated problems in resistance welding are summarized below:

- o Surface conditioning of spot weld areas would be critical.
- o Current rise must be extremely fast, making repeatability of welding schedule difficult for thin foil.
- o Electrode tip surfaces would constantly require cleaning.
- o Metal burning and expulsion from weld areas would be severe, and thus critical for foil.

Ultrasonic welded aluminum honeycomb core meeting the AMS 5850 configuration requirements had been manufactured by Kentucky Metals, Inc., for developmental purposes.

The ultrasonic welding equipment incorporated a single welding head. Welding pressures are applied normal to the node interface and reacted against a cantilevered pin. The length and cross section of this pin is critical. Welding pressures which deflect the pin causes the joint to skid, and results in incomplete joining. Core blanket size is theoretically unlimited. (However, without changes to the floor-to-welding position of existing equipment the blanket size is limited to 6' x 4'.) Core blanket thickness is currently limited by the cell size as below:

Cell Size	Blanket Thickness
1/8 Inch	1/2 Inch
3/16 "	1 "
1/4 "	1/1/2 "
3/8 "	2 "
1/2 "	3 "

Characteristics of ultrasonic welding:

- o Temper of foil affects degree of reduction of foil gage across node joint. Does not affect metallurgical quality of joint.
- o Electrodes generate considerable heat and require forced cooling.
- o Welds can be made without prior surface conditioning. Mild contamination by oils, dirt, and oxides are broken down ultrasonically.
- o Core, while not necessarily desirable, can be chemically milled to reduce the ribbon gage, but appears limited to not more than 40 percent reduction of the original ribbon thickness. This limit is due to the metal reduction at each node during welding.

- o Welding frequency is approximately 20 kc.
- o Electrode tips are made from tool steel.
- o Damaged cell walls or unwelded nodes in welded core blankets cannot be repaired by ultrasonic welding, as welding force is applied normal to surface of each joint.

Ultrasonic welded aluminum honeycomb core costs and quality can be greatly reduced and improved respectively by improving equipment design without further research in the basic joining technology.

Ultrasonic welding of 6061 aluminum core nodes is illustrated in Figure 2-1. Blanket configuration was 12 inches by 12 inches by 3/8 inches thick with 3/8 inch square cell. Material was .008 in. thick and in condition "0".

FIGURE 2-1 ULTRASONIC WELDING OF ALUMINUM HONEYCOMB CORE NODES COURTESY • KENTUCKY METALS INC.

2.3 Base Metal Alloy and Filler Metal Alloy Reference Data

A review and tabulation of physical and mechanical properties of selected aluminum alloys and commercial filler metals was made to provide quick references and comparisons.

Table 2-2 shows the reference data for commercial braze sheets. A review of this data shows brazing range for the 10 percent Si clad surfaces to be 1080 F to 1120 F, while the 7.5 percent Si clad surfaces range from 1100 F to 1140 F.

Reference data for the commercial fillers is shown in Table 2-3. Alcoa's alloy Numbers 4043, 716, and 719 were available in wire form only, and as such, were not applicable for use with the structures conceived for this program. Braze alloys 713 and 718 were available in sheet form and have melting ranges from 1070 F to 1135 F which is comparable to the commercial braze sheets. The 4045 alloy could be obtained in foil form for experimental purposes by chemical melting away the core alloy of Number 23 braze sheet.

Tables 2-4 and 2-5 provide a comprehensive tabulation of non-heat treatable and heat treatable alloys respectively. The solidus temperatures of alloys below 1100 F (593 C) prohibits brazing with state-of-the-art filler metals.

Certain base metal alloys, such as 2219, may be classified as unbrazeable--if optimum heat treatment is required, since the solutioning temperature and solidus temperature spreads are too narrow, unless higher remelt brazed joints can be developed.

Table 2-6 presents short time tensile properties at cryogenic and elevated temperatures as developed by AVCO/AD.

Braze Sheet No.	No. of Sides Clad	Core Alloy	Melting Range Of Core	Cladding[5] Composition	% Cladding On Each Side For Sheet Thickness	Brazing[1] Range, °F
11[2]	1	3003	1190-1210	7.5% Si	10% For .063" and Less 5% For .064" and Over	1100-1140
12[2]	2	3003	1190-1210	7.5% Si	10% For .063" and Less 5% For .064" and Over	1100-1140
21[2]	1	6951	1140-1210	7.5% Si	10% For .090" and Less 5% For .091" and Over	1100-1120
22[2]	2	6951	1140-1210	7.5% Si	10% For .090" and Less 5% For .091" and Over	1100-1120
23[2]	1	6951	1140-1210	10% Si	10% For .090" and Less 5% For .091" and Over	1080-1120
24[2]	2	6951	1140-1210	10% Si	10% For .090" and Less 5% For .091" and Over	1080-1120
100[2][3]	1	3003	1190-1210	7.5% Si	10% For .063" and Less 5% For .064" and Over	1100-1140
M845F[2][4]		M705	1125-1195	10% Si		1080-1120

(1) Manufacturers Recommended Range.
(2) Available Only In 1,000 Pounds Minimum Mill Runs.
(3) Core is clad on one side with brazing alloy, and on other side with alclad.
(4) Core - X7005
(5) Balance Aluminum

Braze Sheets - Reference Data

Table 2-2

Alloy No.	Class	Composition							Melting[2] Range, °F	Product Form
		Si	Cu	Fe	Zn	Mg	Mn	Cr		
4043	B-AlSi-1	4.0-6.0	0.30[1]	0.80[1]	0.10[1]	0.05[1]	0.05[1]		1070-1165	Wire
713	B-AlSi-2	6.8-8.2	0.25[1]	0.80[1]	0.20[1]				1070-1135	Sheet
716	B-AlSi-3	9.3-10.7	3.3-4.7	0.80[1]	0.20[1]	0.15[1]	0.15[1]	0.15[1]	970-1085	Wire
4045[3]		9.0-11.0	0.25[1]	0.80[1]	0.20[1]				1080-1120	Cladding
718	B-AlSi-4	11.0-13.0	0.30[1]	0.80[1]	0.20[1]	0.10[1]	0.15[1]		1070-1080	Wire & Sheet
719		9.5-10.5	3.5-4.5	0.80[1]	9.5-10.5				960-1040	Wire

(1) Maximum Percentage

(2) Manufacturers Recommended Range

(3) 714 Braze Alloy

Commercial Filler Metals - Reference Data

Table 2-3

Alloy No.	Temper	Chemical Composition							
		Si	Fe	Cu	Mn	Mg	Cr	Zn	Ti
1060	0	0.25	0.35	0.05	0.03	0.03		0.05	0.03
1100	0	1.0 Si+Fe		0.20	0.05			0.10	
3003	0	0.6	0.7	0.20	1.0-1.5			0.10	
3004	0	0.30	0.70	0.25	1.0-1.5	0.8-1.3		0.25	
5050	0	0.40	0.70	0.20	0.10	1.0-1.8	0.10	0.25	
5052	0	0.45 Si+Fe		0.10	0.10	2.2-2.8	0.15-0.35	0.10	
5083	0	0.40	0.40	0.10	0.3-1.0	4.0-4.9	0.05-0.25	0.25	0.15
5086	0	0.40	0.50	0.10	0.2-0.7	3.5-4.5	.05- .25	0.25	0.15
5154	0	0.45 Si+Fe		0.10	0.10	3.1-3.9	.15- .35	0.20	0.20
5454	0	0.40 Si+Fe		0.10	.50-1.0	2.4-3.0	.05-0.2	0.25	0.20
5456	0	0.40 Si+Fe		0.10	0.5-1.0	4.7-5.5	.05-0.2	0.25	0.20

Alloy No.	Ultimate Tensile Strength, PSI						Tensile Yield Strength, PSI					
	-300°F	-112°F	+75°F	+212°F	+300°F	+500°F	-300°F	-112°F	+75°F	+212°F	+300°F	+5
1060			10,000						4,000			
1100	24,000	15,000	13,000	11,000	8,500	4,000	6,000	5,500	5,000	5,000	4,500	
3003	33,000	20,000	16,000	13,000	11,000	5,000	8,500	7,000	6,000	5,000	5,000	
3004	42,000	28,000	26,000	26,000	22,000	10,000	13,000	11,000	10,000	10,000	10,000	
5050	36,000	23,000	21,000	21,000	19,000	9,000	10,000	8,500	8,000	8,000	8,000	
5052	44,000	30,000	28,000	28,000	24,000	12,000	16,000	13,000	13,000	13,000	13,000	
5083	60,000	43,000	44,000	44,000	30,000	16,000	24,000	21,000	22,000	22,000	18,000	
5086	56,000	39,000	38,000	38,000	30,000	16,000	20,000	17,000	17,000	17,000	17,000	
5154	53,000	35,000	35,000	35,000	29,000	16,000	16,000	17,000	17,000	17,000	17,000	
5454	54,000	37,000	36,000	36,000	30,000	16,000	20,000	17,000	17,000	17,000	17,000	
5456	63,000	46,000	45,000	45,000	30,000	16,000	27,000	23,000	23,000	23,000	20,000	

(1) Elevated temperature properties shown subsequent to 10,000 hours at temperature.
(2) Endurance limits based on 500,000,000 reversed stress cycles.
(3) CAL/GM

No
Pr

um Alloys - Non Heat-Treatable - Physical and
Mechanical Properties - Reference Data

Ti	Melting Range, °F	Density Lbs/Cu. In.	Thermal Conductivity, CGS -350°F	Thermal Conductivity, CGS +77°F	Thermal Conductivity, CGS +500°F	Specific Heat (3) +212°F	Coefficient of Thermal Expansion Per °F X 10^6 -58°F To +68°F	Coefficient of Thermal Expansion Per °F X 10^6 +68°F To 212°F	Coefficient of Thermal Expansion Per °F X 10^6 68°F To 392°F	Coefficient of Thermal Expansion Per °F X 10^6 68°F To 572°F
0.03	1195-1215	0.098		0.56		0.225	12.1	13.1	13.6	14.2
	1190-1215	0.098	0.81	0.53		0.23	12.2	13.1	13.7	14.2
	1190-1210	0.099		0.42		0.23	12.0	12.9	13.5	13.9
	1165-1210	0.098		0.39		0.23	12.0	12.9	13.4	13.9
	1155-1205	0.097		0.46		0.23	12.1	13.2	13.7	14.2
	1125-1200	0.097	0.19	0.33		0.23	12.1	13.2	13.7	14.2
0.15	1075-1185	0.096		0.28		0.23	12.3	13.2	13.8	14.3
0.15	1085-1185	0.096		0.30		0.23	12.2	13.2	13.8	14.3
0.20	1100-1190	0.096	0.14	0.30		0.23	12.3	13.3	13.8	14.4
0.20	1115-1195	0.097		0.32		0.23	12.1	13.1	13.6	14.2
0.20	1055-1180	0.096		0.28		0.23	12.3	13.3	13.9	14.4

+5 F	Elongation, % +300°F	+500°F	-300°F	-112°F	+75°F	Modulus of Elasticity X 10^6 +212°F	+300°F	+500°F	-300°F	+75°F	+500°F	Fatigue (2) PSI +75°F
					43					10.0		3,000
2	4,500	2,000	55	48	45	45	55	75		10.0		5,000
0	5,000	3,500	46	42	43	40	47	65		10.0		7,000
7	10,000	7,500	38	38	25	25	35	60		10.0		14,000
0	8,000	7,500			24					10.0		13,000
0	13,000	8,000	45	36	30	35	45	80	11.2	10.2	7.0	16,000
0	18,000	11,000	36	30	25	38	45	70		10.3		22,000
0	17,000	11,000	45	36	30	40	50	70		10.3		21,000
0	17,000	11,000	45	36	25	30	40	70		10.2		17,000
0	17,000	11,000	39	30	25	30	40	70		10.2		19,000
0	20,000	11,000	30	26	25	35	45	70		10.3		22,000

Table 2-4

2

Alloy No.	Temper	Chemical Composition Limits, %								
		Si	Fe	Cu	Mn	Mg	Cr	Zr	Zn	Ti
2014	T6	0.5-1.2	1.0	3.9-5.0	0.4-1.2	0.2-0.8	0.10		0.25	0.15
2020	T6	0.40	0.40	4.0-5.0	0.3-0.8	0.03			0.25	0.10
2024	T86	0.50	0.50	3.8-4.9	0.3-0.9	1.2-1.8	0.10		0.25	
2219	T62	0.20	0.30	5.8-6.8	0.2-0.4	0.02		0.1-0.25	0.10	0.02-0.1
6061	T6	0.4-0.8	0.7	0.15-0.4	0.15	0.8-1.2	0.15-0.35		0.25	0.15
6951	T6	0.2-0.5	0.8	0.14-0.4	0.1	0.4-0.8			0.2	
7005	T63(4)	0.35	0.35	0.10	0.2-0.7	1.0-1.8	0.06-0.20	0.06-0.20	4.2-5.0	0.01-0.06
7075	T6	0.5	0.7	1.2-2.0	0.30	2.1-2.9	0.18-0.4		5.1-6.1	0.20
7139	T63	0.30	0.40	0.10	0.1-0.4	2.3-3.3	0.06-0.25		3.5-4.5	0.01-0.06
7178	T6	0.5	0.7	1.6-2.4	0.30	2.4-3.1	0.18-0.4		6.3-7.3	0.20

Alloy No.	Ultimate Tensile Strength, PSI						Yield Strength, PSI					
	-300°F	-112°F	75°F	212°F	300°F	500°F	-300°F	-112°F	75°F	212°F	300°F	500°
2014	87,000	74,000	70,000	62,000	40,000	9,000	79,000	69,000	60,000	56,000	35,000	7,50
2020	99,000	91,000	87,000	81,000	69,000	19,000	92,000	84,000	79,000	75,000	67,000	17,00
2024	91,000	80,000	75,000	70,000	55,000	12,000	84,000	76,000	70,000	66,000	51,000	9,00
2219	74,000	65,000	60,000	55,000	45,000	27,000	50,000	46,000	42,000	40,000	33,000	20,00
6061	60,000	48,000	45,000	42,000	34,000	7,500	48,000	43,000	40,000	38,000	31,000	5,00
6951			39,000						33,000			
7005			54,000						46,000			
7075	100,000	87,000	83,000	66,000	25,000	11,000	90,000	77,000	73,000	62,000	21,000	8,50
7139			63,000						55,000			
7178	106,000	96,000	88,000	86,500	32,000		96,000	86,000	78,000	77,000	29,000	

(1) Elevated temperature properties shown subsequent to 10,000 hrs. at temperature, except 1,000 Hrs. for 2020-T6.
(2) Based on 500,000,000 reversed stress cycles.
(3) CAL/GM
(4) Solution heat treated and aged by ALCOA.

luminum Alloys - Heat-Treatable - Physical
nd Mechanical Properties - Reference Data

	Ti	Melting Range, °F	Density Lbs/Cu. In.	Thermal Conductivity, CGS 77°F	Thermal Conductivity, CGS 212°F	Specific Heat (3)	Coefficient of Thermal Expansion Per °F X 10^6 -58°F To 68°F	68°F To 212°F	68°F To 392°F	68°F To 572°F
5	0.15	950-1180	0.101	0.37		0.23	12.0	12.5	13.1	13.6
5	0.10	975-1190	0.098	0.21				12.8	13.3	13.6
5		935-1180	0.100	0.35		0.23	11.9	12.6	13.2	13.7
0	0.02-0.1	1010-1190	0.102	0.30				12.4		13.4
5	0.15	1100-1205	0.098	0.40		0.23	12.1	13.0	13.5	14.1
		1140-1210	0.098	0.52				13.0		
0	0.01-0.06	1125-1195	0.101	0.36				13.2	13.5	14.0
1	0.20	890-1175	0.101	0.31		0.23	12.1	12.9	13.5	14.4
5	0.01-0.06			0.31						
3	0.20	890-1165	0.102	0.30		0.23	12.0	13.0	13.6	14.5

°F			Elongation, %						Modulus of Elasticity, X 10^6			Fatigue Properties (2) (Endurance Limit) PSI
00	300°F	500°F	-300°F	-112°F	75°F	212°F	300°F	500°F	-300°F	75°F	500°F	75°F
00	35,000	7,500	14	12	13	14	15	45	11.2	10.6	7.0	18,000
00	67,000	17,000	2	3	6	5	8	24		11.1		23,000
00	51,000	9,000	5	5	5	6	11	55	11.2	10.6	7.0	18,000
00	33,000	20,000	13	11	10	14	16	18	11.9	10.6		15,000
	31,000	5,000	22	18	17	18	20	60	11.2	10.0	7.0	14,000
					13					10.0		
00					12					10.3		19,000
	21,000	8,500	14	14	11	15	30	65	11.2	10.4	5.0	22,000
					13							
	29,000		9	11	11	18	36			10.4		22,000

TA for 2020-T6.

TABLE 2-5

2

Aluminum Alloy No.	Temper	-300°F	-100°F	R.T.	1 Hr @ +185°F	50 Hrs @ +185°F	100 Hrs @ +185°F	1 Hr @ +300°F	50 Hrs @ +300°F	100 Hrs @ +300°F
				ULTIMATE TENSILE STRENGTH, PSI						
6951	T6	47,491	42,871	39,946	37,836	37,607	37,998	34,865	35,043	35,183
7005	T6	57,646	53,160	47,240	41,994	43,509	42,610	37,038	37,846	37,306
5052		37,364	30,123	29,364	28,732	28,834	29,341	27,092	27,700	28,466
5454		43,816	35,601	34,454	33,781	33,851	33,856	32,154	31,879	32,326
6061	T6	55,508	49,227	45,811	43,309	43,489	43,395	37,928	40,031	39,505
3003		25,249	18,009	16,068	14,738	14,671	14,670	12,333	12,461	12,866
2024	T6	68,345	63,608	61,076	60,582	60,695	59,383	54,414	54,761	55,556
				YIELD STRENGTH, PSI						
6951	T6	39,529	36,671	35,243	34,015	33,974	34,284	32,308	32,425	32,614
7005	T6	49,625	45,335	40,967	38,233	39,741	39,085	34,876	36,776	35,839
5052					13,497	13,154	13,682	11,909	13,603	15,235
5454					15,779	16,258	14,000	14,205	14,198	14,806
6061	T6	47,291	41,049	39,608	38,263	37,954	37,199	36,311	36,396	35,242
3003					7,740	7,353	8,639	7,315	6,957	6,799
2024	T6	49,363	47,101	45,474	45,857	46,204	46,835	41,975	42,258	42,336
				ELONGATION IN 2 INCHES, PERCENT						
6951	T6	10.1	10.5	9.83	10.67	10.0	10.3	14.0	14.2	--
7005	T6	11.0	11.0	11.33	11.75	11.17	13.2	13.5	13.0	13.3
5052					22.5	21.7	22.0	29.7	31.2	26.3
5454					20.3	20.8	21.0	29.3	31.3	26.5
6061	T6	11.3	11.0	11.2	11.0	11.2	11.7	15.0	14.3	14.5
3003					31.5	31.0	32.5	40.2	36.3	36.1
2024	T6	10.2	10.3	9.5	9.8	10.0	10.0	14.5	13.0	13.8

- o Sub-zero results are based on a 15 minute soak
- o Results are based on the average of six (6) specimen
- o Results were obtained after simulated braze temperatures and subsequent heat treatment by AVCO/AD

Aluminum Alloys - Heat and Non-Heat Treatable
Typical Tensile Properties - Reference Data

Table 2-6

SECTION 3.0

PRE-BRAZE SURFACE CONDITIONING OF ALUMINUM ALLOYS

3.1 Aluminum Oxide - Problem and Approach

Because alumina cannot be reduced to aluminum with a reducing gas under thermal conditions below the melting point of aluminum and its alloys, and because the existing braze filler metals presently available on the market are essentially non-reducing, the method for surface preparation of base metal aluminum alloys and the degree of environment protection subsequent to cleaning and during brazing is a major factor in successful brazing of aluminum alloys.

Aluminum forms an amorphous oxide film at room temperature in air; initiation of this reaction is instantaneous. However, it appears that the oxidization resistance of the surface of an aluminum alloy does increase with time, suggesting that a continuous film is not formed instantly, but occurs over a period of hou s. It is believed that this condition is partly due to the alloying constitions and surface imperfections. It is known that the oxide film formed with heat is more inert than that formed at room temperature.

Chemical removal of oxide films from base metal aluminum alloys should be confined to systems using a final cold water rinse only, and dried mechanically or in air at room temperature or lower. Hydrated aluminum oxide molecules formed at room temperature are less inert than fused dehydrated Al_2O_3 (aluminum reduces water at room temperature, giving a trihydrate molecule, above 180 F a monohydrate molecule is produced, higher temperatures initiate the final conversion to alumina).

Base metal aluminum alloys when heated to 200 F or above in the presence of distilled water exhibit a tarnished surface effect. This condition is more noticeable with some tap waters. This surfacing is a film weakly bonded to the normal oxide film. This effect decreases with the purity level of aluminum. Commercially pure aluminum is only mildly affected. Thus far, the film has not been identified chemically. This surface effect inhibits braze filler metal wetting and can not be tolerated for optimum quality joint preparation.

Numerous alkaline and acid cleaning systems are used in industry, any of which that chemically removes the oxide film is a candidate preparation system for brazing. Initially, this investigation included the evaluation of five chemical cleaning systems for pre-braze surface conditioning. Base metal aluminum alloys selected for surfacing studies were: 2020, 2219, 3003, 5052, 6061, 6951, 7005 and 7139.

During the evaluation, a sixth cleaning system (designated as system Number 2) was added, since it had already been evaluated with some success by the contractor prior to contract award. As noted in Subsection 3.2, one of the initially selected systems (designated as system Number 6) was subsequently dropped, leaving five for continued evaluation.

A comparison of the results of the six systems investigated, to that of an existing system being used by AVCO/AD for aluminum brazing programs, showed that the system in use was equal to those evaluated. Because this system was immediately available, it was used for all investigations reported in Sections 3.0 through 9.0. This system, for the purpose of this report, was designated Number 7.

The evaluation included the following:

- o Metal removal rates.
- o Secondary surface residues.
- o Atmospheric oxide formation and inertness as formed from one hour through 24 hours at room temperature on selected aluminum alloy surfaces.
- o Confirmation of candidate cleaning systems, by determining the surface condition of the 6061 and 7005 base metal aluminum alloys prepared by the Number 1, 2, and 4 cleaning systems. The evaluation included spot braze wetting, flow, and filler metal to aluminum alloy interface diffusion mode.

3.2 Chemical Systems Evaluated for Surface Conditioning

Each candidate chemical system is discussed separately below:

System Number 1

Composition

Sodium Hydroxide	5% by Weight
Sodium Phosphate	0.2% by Weight
Water	Balance
Operating Temperature	140 - 180 F
Immersion Time	0.5 Minutes

Discussion - Aluminum and Solution Reactions and Comments:

Sodium phosphate serves as water softener. Sodium phosphate also imparts alkalinity, rinseability, and some buffer action, and is a fair emulsifier.

An excess of phosphates to take care of water additions and to allow the phosphates to exercise other beneficial effects, such as detergency is desirable.

Hot aqueous solutions of sodium hydroxide provide alkaline cleaning. Sodium hydroxide reaction with aluminum is exothermic, and produces hydrogen gas and sodium aluminate, thus solution temperature changes depends on the relationship between work surface area, rate of metal removal and tank volume which is critical. Uniform finishes thus may be more difficult to obtain with large loads or rapid dissolution etching rates and more rapidly depletion of the chemical constituents in the bath.

Reactions

$$2\ Al + 2\ NaOH + 2\ H_2O \longrightarrow 2\ NaAlO_2 + 3\ H_2$$

$$Al_2O_3\ XH_2O + 2\ NaOH \longrightarrow 2\ NaAlO_2 + XH_2O$$

Typical solution control is maintained by regular titration of samples to determine free sodium hydroxide and sodium aluminate (aluminum). In a common method of operation, the concentration of free sodium hydroxide is not permitted to fall below 3.5 or 4 oz. per gallon when a uniform, medium deep etch is required. The normal working concentration of aluminum is about 2.5% by weight.

When the aluminum content of the solution approaches 7 to 10 oz. per gallon, the finish may become brighter and more reflective; this indicates that the solution is nearly exhausted and should be partly or completely replaced.

Determination of specific gravity is also useful in solution control. A solution that has a specific gravity of 1.15 to 1.18 while maintaining a free sodium hydroxide content of 4 to 5 oz. per gallon is considered to be approaching exhaustion.

Sequestrant, such as gluconic acid, sodium gluconate, the glucamines, and sorbitol are added to alkalin solution to prevent the formation of hydrated alumina. If permitted to form, this compound coats tank walls and heating coils with difficult-to-remove scale. Sequestrants also increase the life of the bath by preventing the formation of scale and by reducing the accumulation of sludge in the tank. They are added in concentrations of 1 to 5 percent.

During the cleaning operation smut (a gray-to-black residual film) is deposited on the surface of the work. This deposit usually consists of iron, silicon, copper or other alloy constituents (in an aluminum base material) that are insoluble in sodium hydroxide.

The smut can be removed by following solutions: 50 percent HNO_3 by volume, one part HF to three parts HNO_3, sulfuric acid 22 - 25 percent by weight and sodium dichromate 3 - 4 percent by weight.

Sodium hydroxide detergent ability is very poor for the non-saponifiable oils (mineral oil) and has poor rinsing properties.

System Number 2 (Added)

Composition	
Sodium Hydroxide.	5% by Weight
Water	Balance
Operating Temperature	140 - 160°F
Immersion Time.	0.5 Minutes

See write-up on Alkaline Cleaning System Number 1 for sodium hydroxide discussion of aluminum solution reactions and comments.

System Number 3

Composition	
Trisodium Phosphate	5% by Weight
Sodium Metasilicate	2.5% by Weight
Water	Balance
Operating Temperature	140 - 160 F
Immersion Time.	5 Minutes

Discussion - Aluminum solution reactions and comments:

Trisodium phosphate serves as water softener and imparts alkalinity, rinseability, some buffer action, and is a fair emulsifier. Trisodium phosphate contributes more alkali to a cleaner than other phosphates but is less efficient as a water softener. Trisodium phosphate softens water by a reaction that produces undesirable insoluble precipitates.

Sodium metasilicate has the following properties: Excellent emulsifiers, good buffer at ph above 9, holds soil in suspension, and provides active alkalinity.

System Number 4

Composition	
Nitric Acid (42°BE)	50% by Volume
Hydrofluoric Acid (48%)	18% by Volume
Water	Balance
Operating Temperature	Room
Immersion Time	5 Minutes

Discussion - Aluminum solution reactions and comments:

Acid etching of alloys containing high silicon may be used to remove oxides smut. Acid etch containing HNO_3 and HF is an excellent smut remover. However, exotherm must be controlled. The following alloys show smut residues: 6061, 6951, 2219, X7005.

Reaction with HF

$$2\,Al + 6HF \longrightarrow 2AlF_3 + 3H_2$$

$$Al_2O_3 + 6HF \longrightarrow 2AlF_3 + 3H_2O$$

$$SiO_2 + 4HF \longrightarrow SiF_4 + 2H_2O$$

Nitric Acid

When a dilute solution of nitric is acted upon by any of the metals occurring above hydrogen in the electro-chemical series of metal, it is expected that hydrogen would be evolved. Hydrogen is evolved with a few of the alloying metals such as magnesium.

Nitric acid is a strong oxidizing agent, while hydrogen has strong reducing properties. It is reasonable to suppose that nitric acid would be reduced by any hydrogen set free, yielding reduction products. Experiments show that this happens. The reduction product formed depends upon the metal, the concentration of the acid, the temperature, and other conditions which the reaction takes place. The more common reduction products can be summarized as follows:

+5	+4	+3	+2	+1	0	-3
HNO_3	NO_2	HNO_2	NO	N_2O	N	NH_3

The most common reduction product evolved when nitric acid reacts with metal are nitrogen dioxide, and nitric oxide. The more concentrated the nitric acid, the greater is the tendency for NO_2 to be formed.

Reaction

Dilute Solution HNO_3

$$4H_2O + 2\,Al + 6HNO_3 \longrightarrow 2Al\,(NO_3)_2 \cdot 4H_2O + 3H_2$$

5 - 20% HNO_3 25 - 30°C

$$Al + 4HNO_3 \longrightarrow Al\,(NO_3)_3 + NO + 2H_2O$$

System Number 5

Composition

Sulfuric Acid (66°Be)	10% by Volume
Hydrofluoric Acid (48%)	2.3% by Volume
Water	87.7% by Volume
Chromic Acid	3.75% by Weight Total
Temperature	150 - 160°F
Immersion Time	5 Minutes

System Number 5 (cont'd)

This type of solution is sometimes used for removal of solution heat treatment stains with little etching of the metal. The etch rate varies as much as 20 times for various aluminum alloys.

System Number 6

Composition	
Phosphoric Acid	7.0% by Volume
Water	93% by Volume
Chromic Acid	2% by Weight Total
Temperature	110 to 150°F
Immersion Time	5 Minutes

This solution showed no appreciable reaction and evaluation of this system was not pursued.

System Number 7

Composition	
Sulfuric Acid (60°Be)	35% by Volume
Tap Water	Balance
Temperature	150°F
Immersion Time	4 - 5 Minutes

This system had been proven by the contractor as satisfactory for all brazeable base metal aluminum alloys and commercially available braze sheets and aluminum filler metals.

3.3 Metal Etching Characteristics of Chemical Cleaning Systems Evaluated

The metal removal rates of six chemical cleaning systems were determined for the following aluminum alloys: 2219, 3003, 5052, 6061, 6951, and 7005. A removal rate not exceeding 0.0002 inches (0.2 mils) per minute is desirable, as this will allow for reasonable immersion times for complex components, thus ensuring that all surfaces are completely bare of oxide. Fast milling rates on thin members could result in undesirable local thinning. In some cases chemical etching may preferentially attack the surface, especially at grain boundaries, which may be structurally undesirable, brazing of such surfaces may also result in abnormal diffusion. The metal removal rates for systems 1, 2, 3, 4, 5 and 7 of eight selected aluminum alloys is shown in Table 3-1.

Table 3-1

Etch Rate of Chemical Cleaning Systems Evaluated

System Numbers	Alloy 2020 Mils Per[1] Minute	Alloy 2219 Mils Per[1] Minute	Alloy 5052 Mils Per[1] Minute	Alloy 6061 Mils Per[1] Minute
1	0.20	0.15	0.7	0.20
2	0.25	0.15	1.1	0.15
3	--	0.45	0.05	0.06
4	0.12	0.08	0.09	0.09
5	--	0.10	0.32	0.08
7	--	0.04	0.08	0.07

System Number	Alloy 3003 Mils Per[1] Minute	Alloy 6951 Mils Per[1] Minute	Alloy X7005 Mils Per[1] Minute	Alloy 7139 Mils Per[1] Minute
1	0.20	0.2	0.205	0.25
2	0.15	0.15	0.11	0.25
3	0.04	0.04	0.05	--
4	0.07	0.09	0.10	0.06
5	0.06	0.07	0.05	--
7	0.06	0.08	0.05	0.05

(1) Average of eight specimens

3.4 Aluminum Oxide Inertness Test Method

The contractors standard method for comparing the aluminum surface oxide levels of various alloys, when used in conjunction with a known shelf life of a referee aluminum alloy which is classified as brazeable, provided a way of determining the surface oxide inertness and predicting the allowable shelf life of aluminum alloys. A standard test solution is used which is outlined and discussed below:

Aluminum Oxide Test Solution

Sulfuric Acid (66°Be) . . . . . .35% by Volume
Water . . . . . .Balance
Temperature . . . . . .70 ± 5°F
Immersion Time. . . . . .Until Hydrogen Evolves

Visible hydrogen released from sample surface indicates a bare metal surface. Immersion time of specimens in test solution up to the reaction can be plotted against hours of specimen in air subsequent to initial removal of oxides. The reaction is explained as follows:

When a dilute solution of sulfuric acid is reacted with aluminum, there are latent periods of inactivity during which the oxide film

is being dissolved. This is followed by violent reaction, with the release of hydrogen. The aluminate ion usually exist in the hydrate form ($AlO_2 \cdot 2H_2O$).

$$Al_2O_3 + 3H_2SO_4 \longrightarrow 3H_2O + Al_2(SO_4)_3$$

$$Al + 3H_2SO_4 \longrightarrow Al_2(SO_4)_3 + 3H_2$$

Elements such as copper, below hydrogen in the electro-chemical level, will not liberate hydrogen from sulfuric acid.

$$Cu + 2H_2SO_4 \longrightarrow CuSO_4 + SO_2 + 2H_2O$$

3.5 Measurement of Surface Oxidization Rate of Selected Aluminum Alloys

The following aluminum alloys: 2020, 2219, 3003, 5052, 6061, 6951, 7005, and 7139, were surface conditioned to an oxide-free state using five of the seven (7) chemical systems discussed in Section 3.2. These alloys were subsequently placed in air at 72 F for periods of one hour through 24 hours, RH was controlled to 50 - 65 percent. Specimen of these alloys were tested for reaction time using the Avco standard aluminum oxide inertness test described in Section 3.4. The results of these evaluations are shown in Figures 3-1 through 3-8, also in Table 3-2. The results show that surface oxide formation rate in air is lowest for the 2219 and 2020 alloys. The remaining alloys in increasing oxide formation rate are 7139, 6951, 6061, 7005, 3003, and 5052.

3.6 Brazeability of Selected Aluminum Alloys Conditioned with Candidate Cleaning Systems

The seven (7) cleaning systems described in Section 3.2 were reviewed and three (3) systems, Number 1, 2, and 4 were selected for surface brazeability evaluations. The Number 3 and 5 systems were discarded as both had wide variances of etch rates for the six (6) alloys used for surface evaluations. The Number 6 system was discarded for incomplete oxide removal. The Number 7 system was not evaluated as it was a proven system.

Two parent metal aluminum alloys (6061 and 7005) were surface conditioned with Number 1, 2, and 4 cleaning systems and spot brazed with 4045 filler metal.

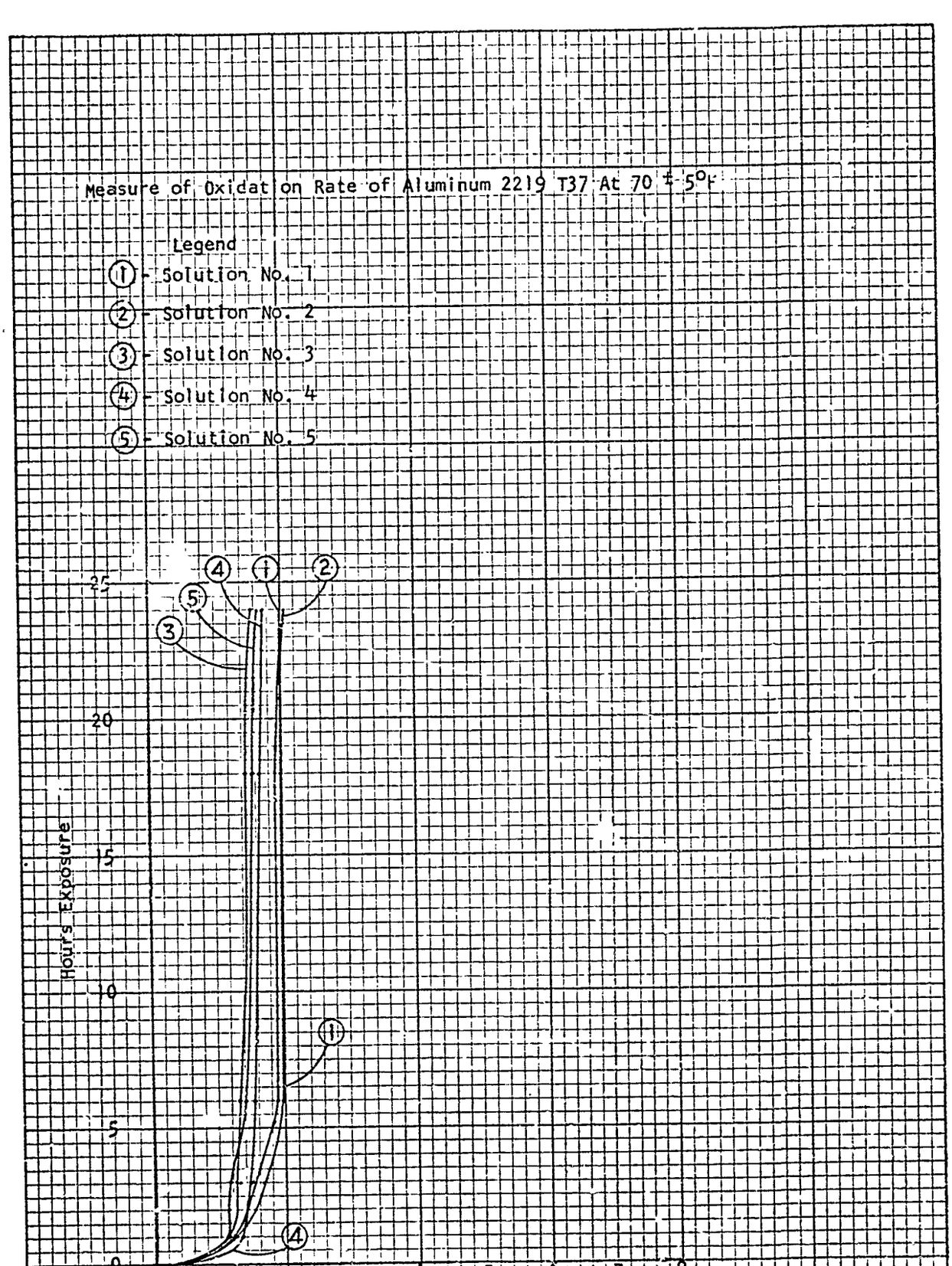
Measure of Oxidation Rate of Aluminum 2219 T37 At 70 ± 5°F
Legend
① - Solution No. 1
② - Solution No. 2
③ - Solution No. 3
④ - Solution No. 4
⑤ - Solution No. 5
Hours Exposure
25
20
15
10
5
0
0
1
2
3
4
5
6
7
8
Reaction Time, Min

Figure 3-1

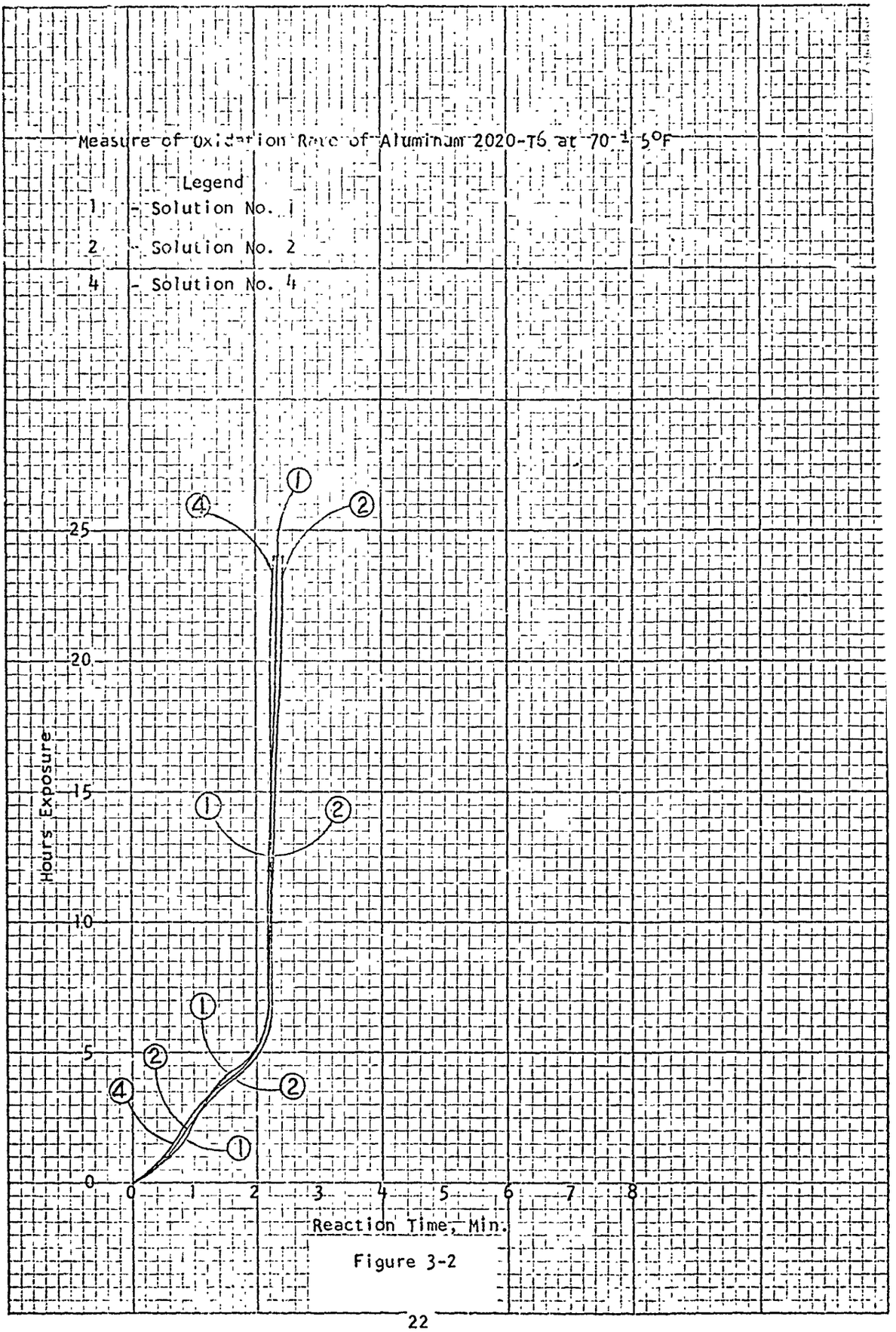
Measure of Oxidation Rate of Aluminum 2020-T6 at 70 ± 5°F
Legend
1 - Solution No. 1
2 - Solution No. 2
4 - Solution No. 4
Hours Exposure
25
20
15
10
5
0
0
1
2
3
4
5
6
7
8
Reaction Time, Min.

Figure 3-2

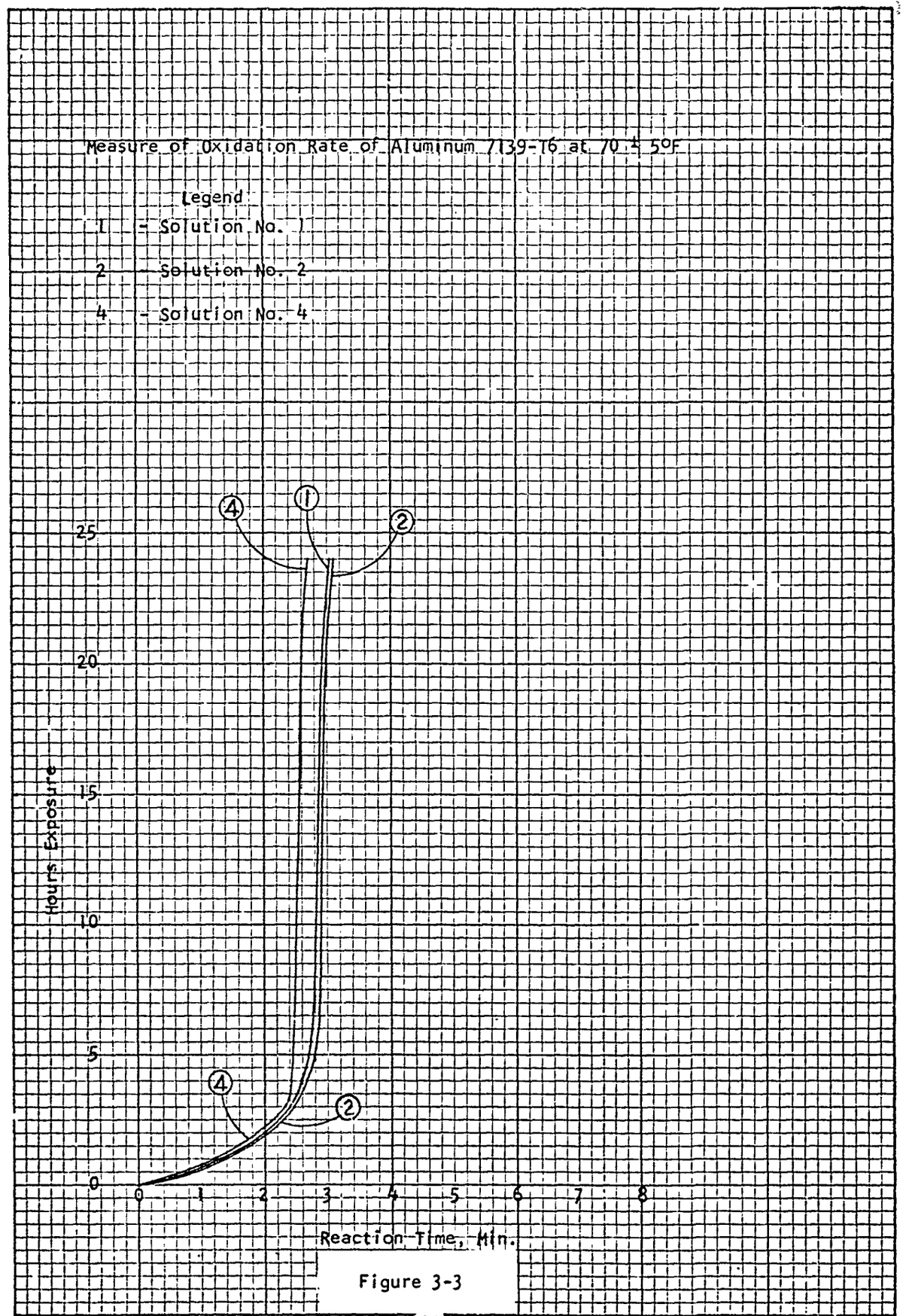
Measure of Oxidation Rate of Aluminum 7139-T6 at 70 ± 5°F
Legend
1 - Solution No. 1
2 - Solution No. 2
4 - Solution No. 4
Hours Exposure
25
20
15
10
5
0
0
1
2
3
4
5
6
7
8
Reaction Time, Min.

Figure 3-3

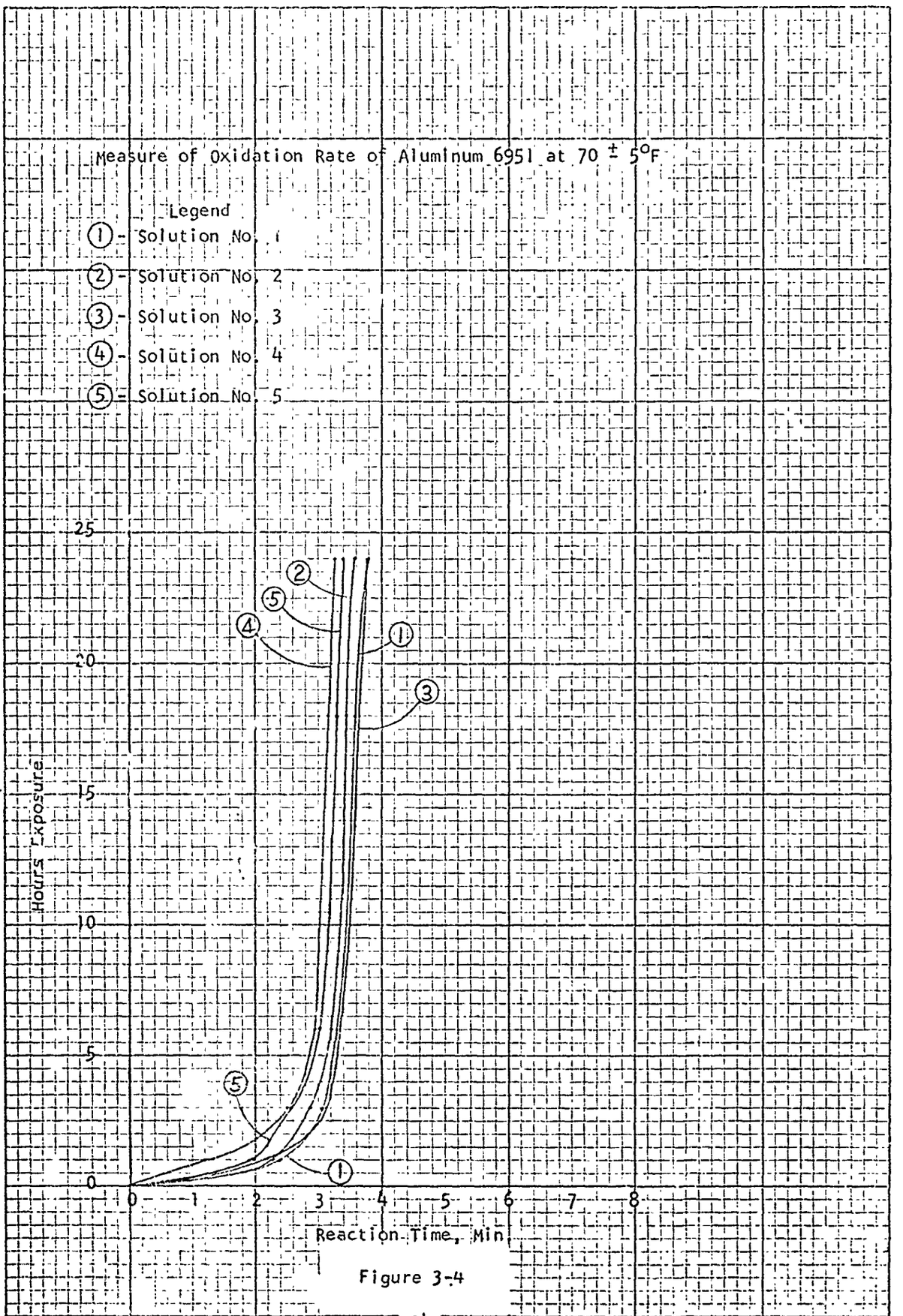
Measure of Oxidation Rate of Aluminum 6951 at 70 ± 5°F
Legend
① - Solution No. 1
② - Solution No. 2
③ - Solution No. 3
④ - Solution No. 4
⑤ - Solution No. 5
Hours Exposure
25
20
15
10
5
0
0
1
2
3
4
5
6
7
8
Reaction Time, Min

Figure 3-4

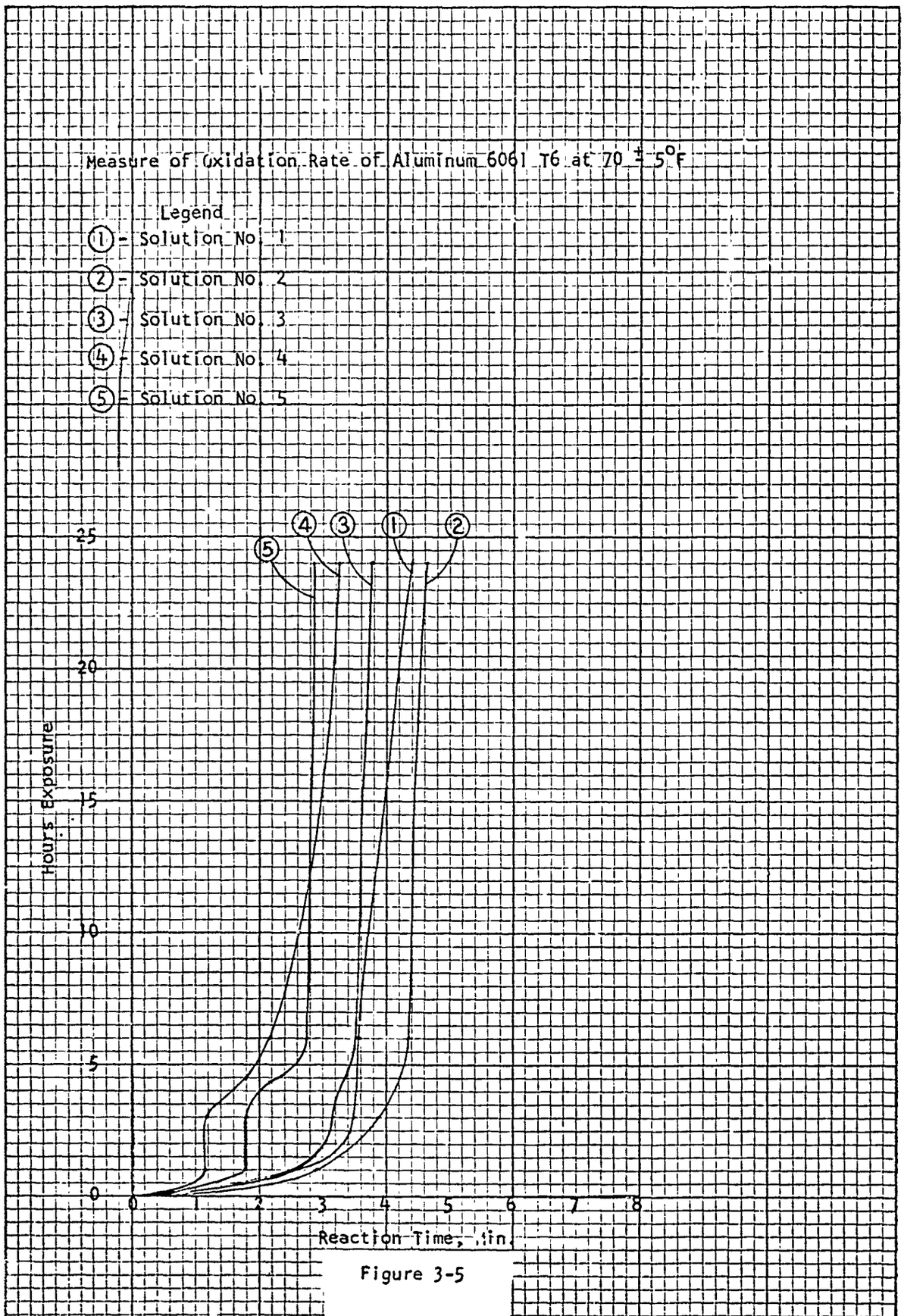
Measure of Oxidation Rate of Aluminum 6061 T6 at 70 ± 5°F
Legend
① - Solution No. 1
② - Solution No. 2
③ - Solution No. 3
④ - Solution No. 4
⑤ - Solution No. 5
Hours Exposure
0
5
10
15
20
25
0
2
3
4
5
6
7
8
Reaction Time, Hrs.

Figure 3-5

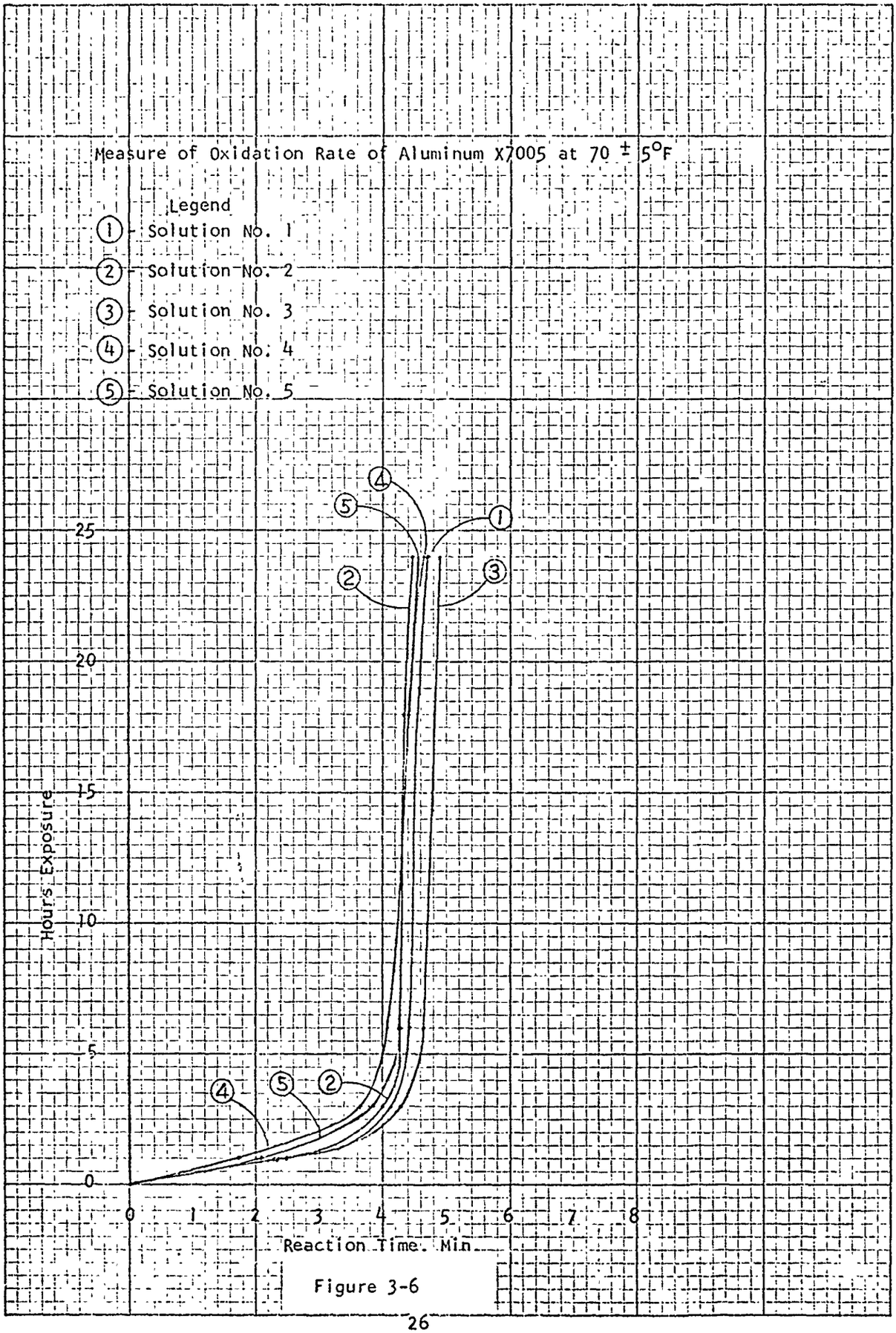
Measure of Oxidation Rate of Aluminum X7005 at 70 ± 5°F
Legend
1 - Solution No. 1
2 - Solution No. 2
3 - Solution No. 3
4 - Solution No. 4
5 - Solution No. 5
Hours Exposure
0
5
10
15
20
25
0 1 2 3 4 5 6 7 8
Reaction Time. Min

Figure 3-6

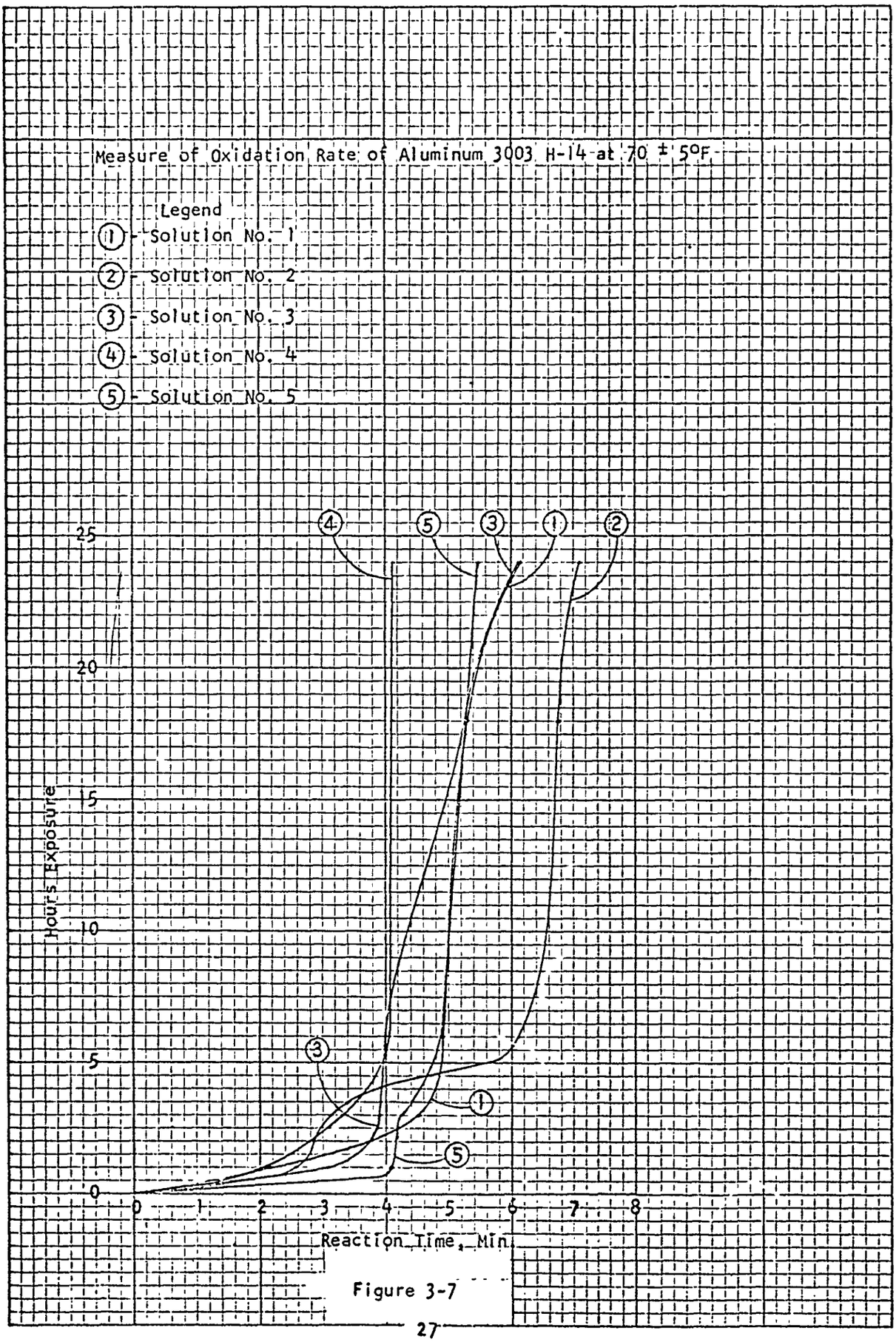
Measure of Oxidation Rate of Aluminum 3003 H-14 at 70 ± 5°F
Legend
① - Solution No. 1
② - Solution No. 2
③ - Solution No. 3
④ - Solution No. 4
⑤ - Solution No. 5
Hours Exposure
0
5
10
15
20
25
0
1
2
3
4
5
6
7
8
Reaction Time, Min.

Figure 3-7

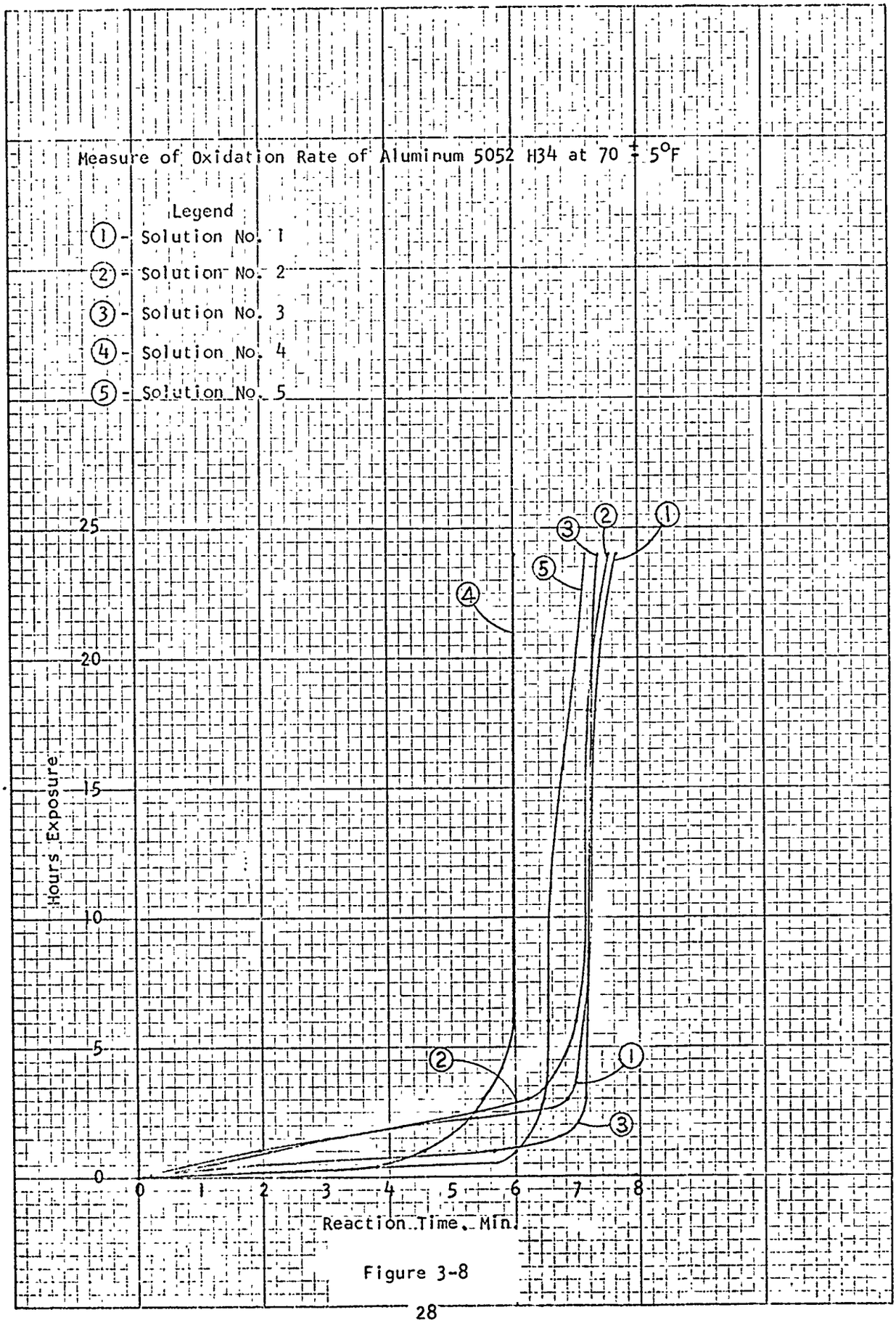
Measure of Oxidation Rate of Aluminum 5052 H34 at 70 ± 5°F
Legend
① - Solution No. 1
② - Solution No. 2
③ - Solution No. 3
④ - Solution No. 4
⑤ - Solution No. 5
Hours Exposure
0
5
10
15
20
25
0
1
2
3
4
5
6
7
8
Reaction Time, Min.

Figure 3-8

TABLE 3 -2

MEASURE OF OXIDATION RATE OF ALUMINUM ALLOYS AT 70 ± 5°F

Exposure Time (Hours)	Reaction Time Solution No.1 (Minutes)	Reaction Time Solution No.2 (Minutes)	Reaction Time Solution No.3 (Minutes)	Reaction Time Solution No.4 (Minutes)	Reaction Time Solution No.5 (Minutes)
			2020-T6		
1	0.60	0.58		0.54	
3	1.15	1.18		1.10	
6	2.15	2.22		2.15	
12	2.20	2.27		2.23	
18	2.30	2.35		2.28	
24	2.35	2.42		2.33	
			3003 H-14		
1	2.18	2.57	3.07	2.08	4.03
3	4.50	3.13	3.88	3.30	4.22
6	4.91	6.11	3.98	4.02	4.90
18	5.30	6.75	5.25	4.09	5.27
24	6.16	7.10	6.11	4.13	5.46
			2219 T-37		
1	1.23	1.20	1.16	1.35	1.11
3	1.64	1.56	1.22	1.44	1.13
6	1.95	1.89	1.31	1.52	1.42
18	1.95	1.90	1.45	1.64	1.57
24	1.98	2.02	1.54	1.72	1.65
			6061 T-6		
1	2.55	2.90	2.58	1.15	1.78
3	3.50	3.86	3.18	1.88	1.80
6	3.58	4.36	3.56	2.17	2.75
18	4.10	4.49	3.69	3.10	2.82
24	4.40	4.61	3.75	3.25	2.85
			5052 H-34		
1	2.10	1.95	5.67	4.58	6.00
3	6.82	6.20	7.13	5.50	6.47
6	7.11	6.98	7.18	5.98	6.52
18	7.31	7.20	7.25	6.00	6.89
24	7.66	7.55	7.38	6.01	7.19
			6951		
1	2.40	2.28	2.20	1.20	1.99
3	3.06	2.87	3.09	2.50	2.59
6	3.31	3.21	3.35	2.94	3.03
18	3.58	3.44	3.65	3.15	3.30
24	3.80	3.58	3.78	3.23	3.40
			X7005		
1	2.30	2.34	2.50	1.75	2.10
3	4.13	4.00	4.30	3.66	3.87
6	4.42	4.25	4.65	4.07	4.25
18	4.55	4.38	4.81	4.40	4.41
24	4.70	4.47	4.91	4.65	4.58
			7139-T6		
1	1.30	1.33		1.22	
3	2.40	2.46		2.34	
6	2.78	2.84		2.45	
12	2.82	2.88		2.52	
18	2.90	2.95		2.58	
24	3.03	3.08		2.70	

3.6.1 Preparation of Specimen for Wetting, Flow, and Diffusion

- 6061 and 7005 base metal aluminum alloy sheet stock was sheared to strips approximately 4 inches long by 1.5 inches wide and 1.125 inches respectively. All specimen were approximately 0.050 inch thick.

  Type 4045 braze filler metal foil 0.0025 inch thick was blanked out to washers having a 1/2 inch O.D. and 3/32 inch I.D.

  Each base metal aluminum alloy specimen had blind holes drilled 0.025 inch deep by 0.063 inch diameter to allow for indexing braze washer with a CRES pin, blind holes were to prevent loss of filler metal to back surface of specimen.

- Chemical Preparation of Specimen

  Each of the aluminum alloys and filler metals were cleaned to the schedule below:

Specimen Number	Aluminum Alloy	Braze Filler	Cleaning System Number	Immersion Time	Temp. °F
1	6061	4045	1	30 Sec.	140
2	7005	4045	1	30 Sec.	140
3	7005	4045	4	60 Sec.	72
4	6061	4045	4	60 Sec.	72
5	7005	4045	2	30 Sec.	140
6	6061	4045	2	30 Sec.	140

- Specimen were batch brazed as illustrated in Figure 3-9.

- Braze Cycle

  Specimen were held at 1072 F to 1076 F for four (4) minutes, in dry argon environment (argon purity approximately 20 PPM total of moisture and free oxygen).

3.6.2 Evaluation of Results

- From visual examination, the Number 2 system produced a grained finish, whereas the Number 1 and 4 systems showed a uniform surface removal overall.

- Visual flow on the three (3) 6061 alloy specimen showed a slightly higher flow for the specimen prepared with the Number 1 and 4 systems.

- Visual flow on the three (3) 7005 alloy specimen was slightly greater for the Number 2 and 4 cleaning systems than for that of the Number 1 system.

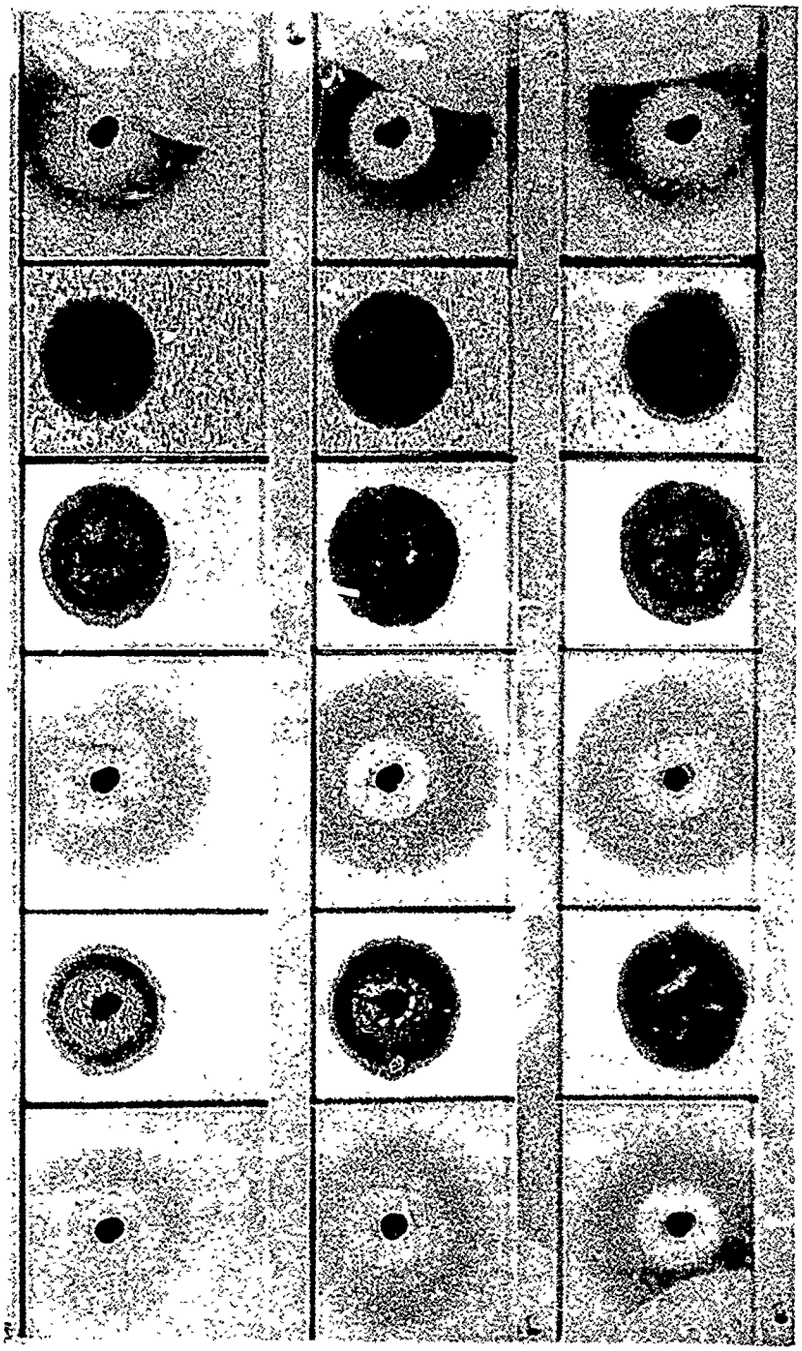

ALUMINUM ALLOY 6061
SOLUTION NO. 1

ALUMINUM ALLOY X7005
SOLUTION NO. 1

ALUMINUM ALLOY X7005
SOLUTION NO. 4

ALUMINUM ALLOY 6061
SOLUTION NO. 4

ALUMINUM ALLOY X7005
SOLUTION NO. 2

ALUMINUM ALLOY 6061
SOLUTION NO. 2

FIGURE 3-9 BATCH SPOT BRAZING SPECIMENS

- The cross sections of the brazed filler metal to the parent metal interfaces were examined in the as-polished condition to determine the wetting edge. A Knoop hardness indentation was used as a marker at this point, and for each additional 0.1 inch in from this point up to the blind hole (filler metal button index). The depth of diffusion was examined at each point. This was accomplished by measuring the distance from the back side of the parent metal up to the first noticeable signs of diffusion. In the unetched condition there was a very slight, visible diffusion of filler metal into the base metal. Etching of the samples showed up a very obvious diffusion of filler metal into parent metal. These results are shown in Table 3-3. Figure 3-10 graphically shows the measured depth of the filler metal above the parent metal's thickness as well as the depth of diffusion into the parent metal, for each of the two parent metals and three cleaning solutions at the various markers (Knoop indentations) mentioned above.

  Figure 3-11 is a series of four microphotographs of the parent and filler metal interface cross section showing the Knoop indentations, and illustrates typical information from which the data for Table 3-3 and Figure 3-10 was prepared.

  Inspection of these micrographs showed a dark area located below the original interface. The lower edge of the darker area would be considered the maximum depth of the effects of the filler metal during the brazing cycle. It might be postulated that the molten filler metal dissolved the lower melting point alloys of the base metal leaving the higher melting point particles in a solid state as precipitates, and that this occurred to the depth of the lower edge of the darker area. Furthermore, after the brazing cycle of four minutes was completed these samples were furnace cooled which left the precipitates suspended in the matrix; therefore, the precipitates are very detectable from the lower melting point matrix material. If the samples had been solution heat treated and artificially aged, the precipitates would most likely have been partly dissolved into the matrix material.

- Upon closely examining the three cleaning system's effects on the two base metals, and keeping in mind that this particular investigation was concerned only with the cleaning system's effect on the diffusion mode of the filler metal into the parent metal, it was concluded that the Number 2 and Number 4 systems provide a somewhat more compatible surface for wetting than the Number 1 system.

Base Metal	Distance[1] (Inches)	Cleaning System No. 2		Cleaning System No. 4		Cleaning System No. 1	
		A (2)	B (3)	A (2)	B (3)	A (2)	B (3)
6061	0.0	0.0000	0.0000	0.0006	0.0000	0.0034	0.0000
	0.1	0.0005	0.0001	0.0057	0.0000	0.0066	0.0000
	0.2	0.0031	0.0001	0.0081	0.0015	0.0093	0.0011
	0.3	0.0101	0.0014	0.0089	0.0015	0.0093	0.0014
7005	0.0	0.0004	0.0003	0.0000	0.0000	0.0021	0.0000
	0.1	0.0039	0.0005	0.0056	0.0002	0.0042	0.0001
	0.2	0.0057	0.0014	0.0056	0.0011	0.0042	0.0001
	0.3	0.0047	0.0002	0.0045	0.0003	0.0058	0.0012

(1) Distance - The zero mark was taken at a point that looked like the first signs of wetting, on a microscopic basis, on the sample in the unetched condition.

(2) A - Depth of diffusion below the original thickness.

(3) B - Filler metal thickness above original thickness.

Measurement of Filler Metal Diffusion

TABLE 3-3

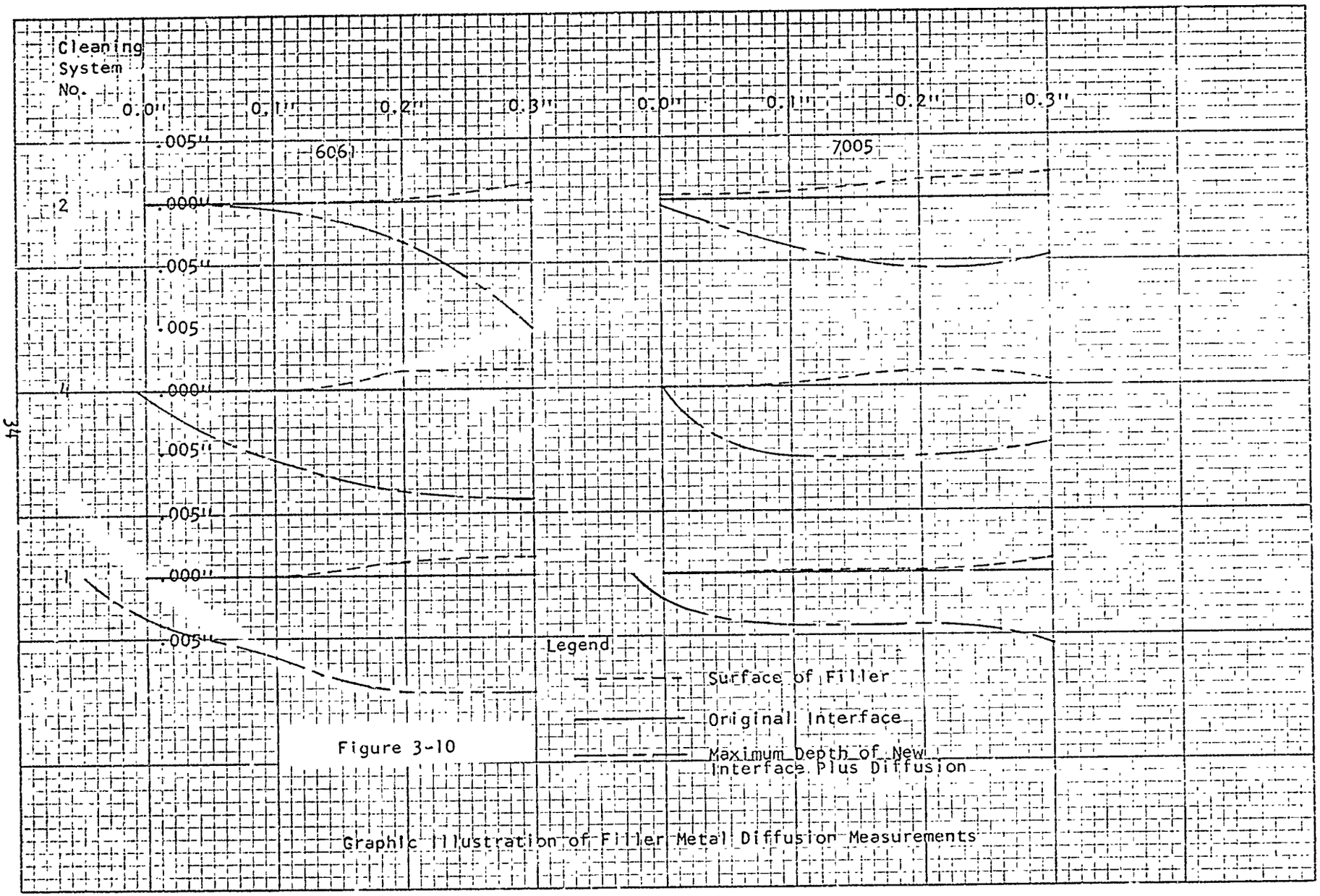

Figure 3-10

Graphic Illustration of Filler Metal Diffusion Measurements

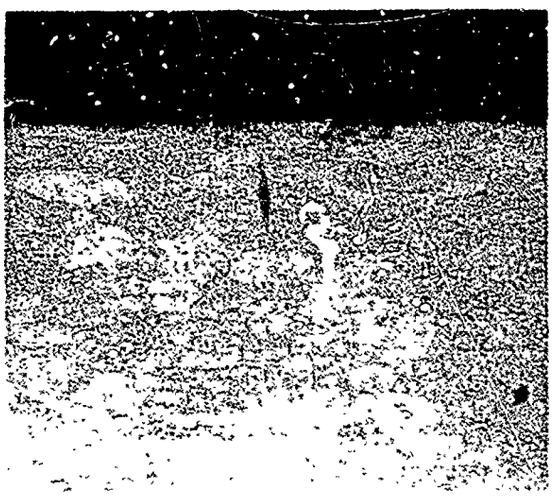

Mount #345

a) Marker locating extreme edge of wetted area condition. (100X)

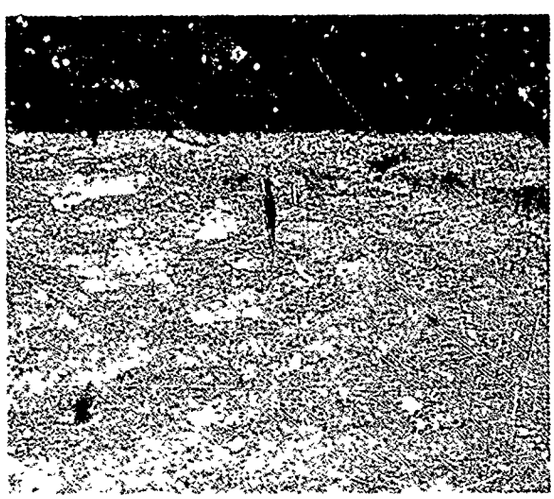

Mount #345

b) Marker locating point 0.1 inch in toward blind hole from edge. (100X)

7005 Parent Metal - 4045 Filler Metal - Cleaned by No. 1 System

Figure 3- 11

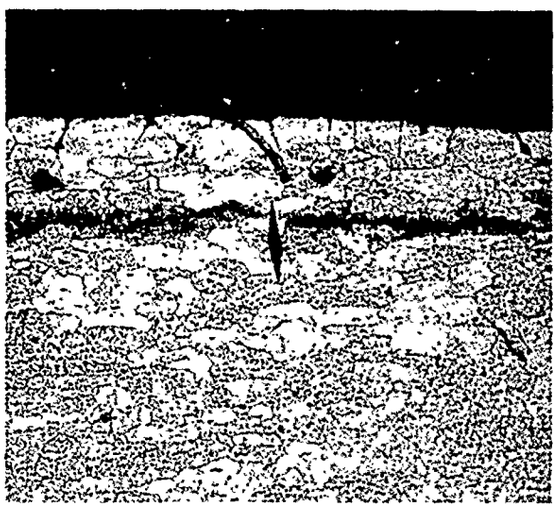

Mount #345

c) Marker locating point 0.2 inches in toward blind hole from wetted edge. 100X.

Mount #345

d) Marker locating point 0.3 inches in toward blind hole from wetted edge. The blind hole is located just beyond the right edge of micrograph. 100X.

7005 Parent Metal - 4045 Filler Metal - Cleaned by No. 1 System

Figure 3-11

SECTION 4.0

FLUXLESS BRAZING - DEVELOPMENT OF BASIC JOINT PROPERTIES AND DATA

4.1 Scope. This investigation concerned the evaluation of selected material systems which were commercially available, for the purpose of establishing brazing data, and basic joint properties, such that the results could be screened, and appropiately used for subsequent feasibility and manufacturing limit investigations of thin gage-complex multi-joint composites for cryogenic and elevated temperature applications. The investigation was conducted as four separate tasks as delineated below:

- o Thermal environment effect on properties of brazed joints.
- o Fatigue resistance of brazed laminated plate versus homogeneous plate.
- o Evaluation of the effect of corrosive plus elevated temperature environment on brazed aluminum surfaces.
- o Evaluation of capillary rise and bridging of two commercially available aluminum base braze filler metals.

4.2 Thermal Environment Effect on Properties of Brazed Joints State-Of-The-Art Materials

This investigation established the shear strength of lapped metal to metal, and flatwise tensile strength of honeycomb core to flat plate brazed joints. The data derived from this evaluation formed a technical base for processing and evaluating more complex light-weight hardware, as well as providing basic properties for brazed aluminum not previously reported within the industry. Testing was performed at -300 F, room temperature, and elevated temperatures, up to 500 F. Each of the temperatures above room temperature included soaking periods of 25 hours, 50 hours, and 100 hours for the lap shear specimen. The honeycomb sandwich flatwise tensile specimen were subjected to short times only. Materials selected were representative of the commercially available heat treatable aluminum alloys which were classified as brazeable with the 4045 (714) braze filler metal.

Over-lapped metal to metal brazed joints exhibited satisfactory shear strengths throughout the thermal environment limits. As the test temperatures approached 500 F the brazed joint strengths exceeded that of the base aluminum alloys.

Only minor lap shear failing load spreads between individual specimen were recored at each test temperature. This was attributed to specimen preparation techniques which provided a repeatable joint area between each of the specimen, and to performing the shear tests with a standardized strain rate of 0.5 in/min.

Initial lap shear values obtained were slightly higher than actual, due to the formation of minor fillets along the edges of the overlapping area. This problem was eliminated by using an improved joint configuration. The results obtained from this type of joint are reported in Table 4-3 of this report, and are considered reliable. Table 4-1 which shows the joint strengths with fillets, therefore, should be used as a reference only.

A close observation of the lap shear specimen during shear testing to failure, showed no noticeable distortion or bending. The base metal alloy members remained essentially parallel to the direction of loading, thus it was reasonable certain that no compound loading of the joints occurred (tensile shear).

The flatwise tensile evaluation of the first two (2) honeycomb sandwich test panels showed an excess of filler diffusion of the core ribbons at the face sheet to core ribbon fillet transition. This caused brittle failure type fractures at -300 F. An improvement (reduction) in the diffusion level at the joint transitions was accomplished, by reducing the thickness of braze filler metal from 0.003 inches to 0.0017 inches, and by shortening the brazing time above 1075 F from $7\frac{1}{2}$ minutes to $4\frac{1}{2}$ minutes. This improvement was effected on test panels Number 3 and 4.

4.2.1 Evaluation of Lap Shear Properties

Three base metal aluminum alloys and one braze filler metal alloy were selected for the following:

Base Metal Alloy	Reasons for Selection
6061	Good brazeability with or without flux.
6951	Good brazeability with or without flux. Commonly used as core for braze sheets.
7005	Good brazeability with or without flux. Less sensitive to solutioning quenching rates than most alloys, an important factor in the heat treatment of complex brazed composites.
Filler Metal Alloy	
4045	Exhibits good brazing characteristics without flux. Is available in braze sheet form.

4.2.1.1 Preparation of Metal to Metal Joint Specimen (Lap Shear)

Double lapped sheet metal (Type I) specimen details are illustrated in Figure 4-1a.

Double Lapped Joint Details (Type I)

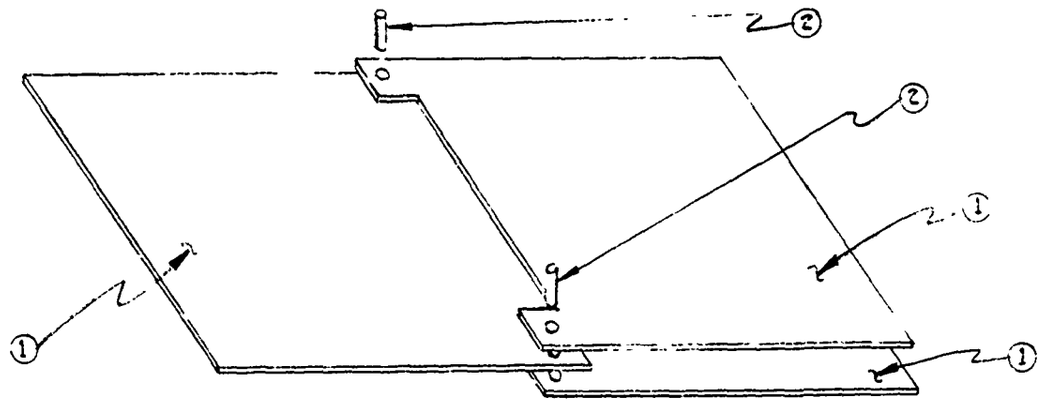

① 6061 Al Alloy-0.054" Thick ② Indexing Pins 1/8" Dia.

Figure 4-1a

Indexing holes were drilled to locate items such that an over-lap of 0.040 inches could be maintained.

The braze filler metal foil was preplaced as shown in Figure 4-1b. Spacer plates were incorporated to provide a constant package thickness, to ensure that the contact pressure during brazing was applied normal to the joint surface.

Filler Metal Placement - Double Lapped Joints

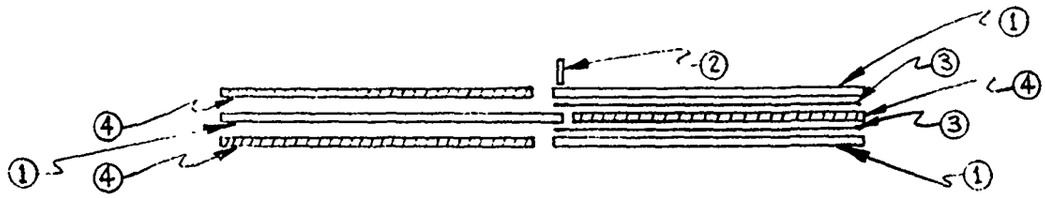

① 6061 Al Alloy-0.054" Thick ② Indexing Pins 1/8" Dia.
③ 4045 Braze Foil-0.003" Thick ④ Al Spacer Plates

Figure 4-1b

Since braze sheets can be incorporated into most lightweight composite brazements, it was considered logical to select one of the braze filler metals commonly used for braze sheets. However, the alloy is not available in foil form. Foil was obtained by chemical milling the core alloy from Number 23 braze sheet, by this method braze alloy foil sheets up to 24" x 24" x 0.003" ± 0.0002" thick was made available for the program.

4.2.1.2 Brazing of Metal to Metal Joint Specimen

Specimen details were surface conditioned by chemical cleaning per system Number 7 (reference Section 3.0), and laid up for brazing. Stack up and envelope braze package and associate tooling is illustrated in Figure 4-2.

Typical Unitized Tooling and Brazement Package

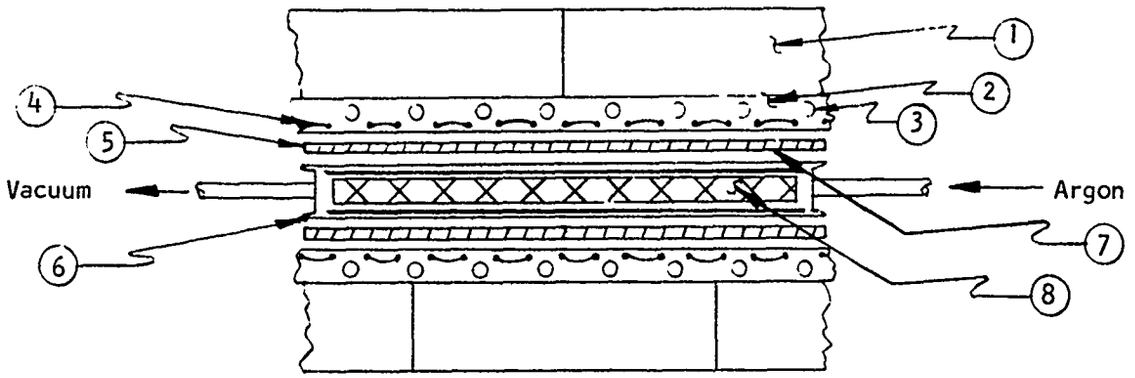

1) Glasrock brick backup
2) Silica ceramica platens
3) Cooling ports
4) Zoned electric heating elements
5) Thermocouple sheet
6) Stainless steel brazing envelope
7) Glide sheet
8) Brazement

Figure 4-2

The complete enveloped brazing package was evacuated, and then back filled with argon. This replacement purge cycle was repeated eight (8) times. A partial vacuum of 22"Hg was pulled on the envelope system, and work was heated to 1075 F at approximately 1000 F/hr. Work was held between 1075 F and 1080 F for five (5) minutes and then cooled. Partical vacuum at brazing temperature was 8"Hg. Note: Moisture content of argon gas at envelope exit after one (1) purge cycle was approximately 1500 PPM. After eight (8) purge cycles the moisture content had dropped to 20 PPM. Time between envelope sealing and brazing was eighteen (18) hours.

4.2.1.3 Thermal Environment

Specimen heat treated to the T6 condition were subjected to thermal environment conditions. Lap shear strength was determined at each of the temperatures selected. Thermal environment temperatures and soaking times were as below:

Temperature	Time at Temperature		
-300°F	10 Minutes		
Room Temperature	N.A.		
300°F	25 Hrs.	50 Hrs.	100 Hrs.
350°F	25 Hrs.	50 Hrs.	100 Hrs.
500°F	25 Hrs.	50 Hrs.	100 Hrs.

4.2.1.4 Effect of Thermal Environment on Shear Strength

The joint strengths for the 6951, 6061 and 7005 alloy Type I specimen are shown in Table 4-1. However, due to the effect of filleting along the edges of the shear interfaces, it is questionable as to whether an accurate analysis could be made. However, the one outstanding characteristic of the 6951 and 7005 alloy joints was that soaking between 350 F and 500 F generally lowered the strength of the base metal alloy components more so than the brazed joint interfaces and joint matrix, which resulted in the base metal components failing. This was not true for the 6061 alloy specimen soaked for 25 hours at 350 F and 500 F for 100 hours. This difference between the 6951 and 7005 alloys to that of the 6061 specimen was attributed to the fact that the 6061 alloy specimen had smaller fillets.

An investigation of the shear strength of filletless lapped joints was conducted and is discussed in detail in Section 4.2.1.5.

4.2.1.5 Evaluation of Effect of Fillets on Total Strength of Lapped Joint Specimen

Because it was necessary to confine the over-lap of each specimen to not more than 0.040 inches to ensure that the specimen failure would occur in the joint, any filler metal filleting along the joint edges would add noticeably to the total strength of the joint. The additional strength from filleting was not known, and it was considered necessary to determine this by testing and comparing strength of joints with fillets to those joints without fillets.

An improved single lap brazed joint design (Type II) which eliminated the joint edge fillets was used to determine more accurately the shear strength of the lapped joints. Single lap shear specimen for each of the base metal alloys (6061, 6951, 7005) were tested at -300 F, RT and 300 F. The specimen without fillets failed at lower

Shear Strength of Brazed Joints vs Time and Temperature[2]
(Reference Only - See Table 4-3)

Alloy No.	Temper	SHEAR STRENGTH, PSI										
		-300°F	RT	300°F			350°F			500°F		
		10 Min.		25 Hrs	50 Hrs	100 Hrs	25 Hrs	50 Hrs	100 Hrs	25 Hrs	50 Hrs	100 Hrs
6951	T6	19,312	19,213	17,362	16,034	15,911	25,312(1)	(1)	14,883	7,660	(1)	(1)
.054" Tk		20,006	18,883	16,497	18,309	18,824	27,129(1)	15,413	(1)	(1)	(1)	(1)
		18,945	18,033	15,706	14,725	15,730	24,800(1)	16,682	(1)	(1)	(1)	(1)
	Avg.	19,421	18,693	16,521	16,356	16,821	25,747	16.602				
6061	T6	28,019	20,676	19,734	18,555	18,100	27,290(1)	18,167	15,671	8,194	7,351	(1)
.054" Tk		29,372	24,134	18,810	19,370	18,662	26,730(1)	17,774	15,942	8,087	7,464	(1)
		29,113	25,529	19,573	17,663	16,608	27,100(1)	18,492	15,720	8,243	7,464	(1)
	Avg.	28,835	23,446	19,372	18,529	17,590	27,040	18,144	15,777	8,160	7,426	
X7005	T6	26,668	21,364	17,323	13,799	15,466	26,416(1)	(1)	(1)	(1)	(1)	(1)
		28,495	22,442	14,284	14,080	15,092	25,924(1)	12,470	(1)	(1)	(1)	(1)
		28,397	18,737	15,616	17,294	16,083	26,120(1)	(1)	(1)	(1)	(1)	(1)
		27,853(3)	20,848	15,616	15,576	15,547	26,153					

(1) Specimen broke outside of brazed joint.
(2) Type I Joint - Double lap - 0.04" Over Lap
(3) This value questionable - incorrect strain rate used.

Note: All specimen tested at environmental temperature.

Table 4-1

values than the original double lapped specimen. A comparison is made in Table 4-2 below:

Table 4-2

Shear Strength[4] of Brazed Joints
Type I vs Type II

Base Metal Alloy	Specimen Type	Shear (PSI) -300°F	Shear (PSI) RT	Shear (PSI) 300°F[3]	Crosshead Rate In/Min
6951	I[1]	19,421	18,693	16,566	0.05
6951	II[2]	17,907	17,510	15,402	0.05
6061	I	28,835	23,446	18,497	0.05
6061	II	25,108	22,160	17,180	0.05
7005	I	27,833	20,848	15,579	0.05
7005	II	20,558	19,810	15,006	0.05

(1) Double lapped - with fillets
(2) Single lap - no fillets
(3) Soak at 300°F for 50 hours
(4) All testing conducted at referenced environment temperature

The width of the Type II joint was machined subsequent to brazing and heat treatment (condition T6), which eliminated fillets. A single lap configuration was used, as it was not practical to machine the joint edge where the two members over-lap the single member.

The two joint configuration (Type I and Type II) are photographically illustrated in Figures 4-3 and 4-4.

Users of this data are advised to use the shear values tabulated in Table 4-3, which provides the interface shear only, with fillets eliminated.

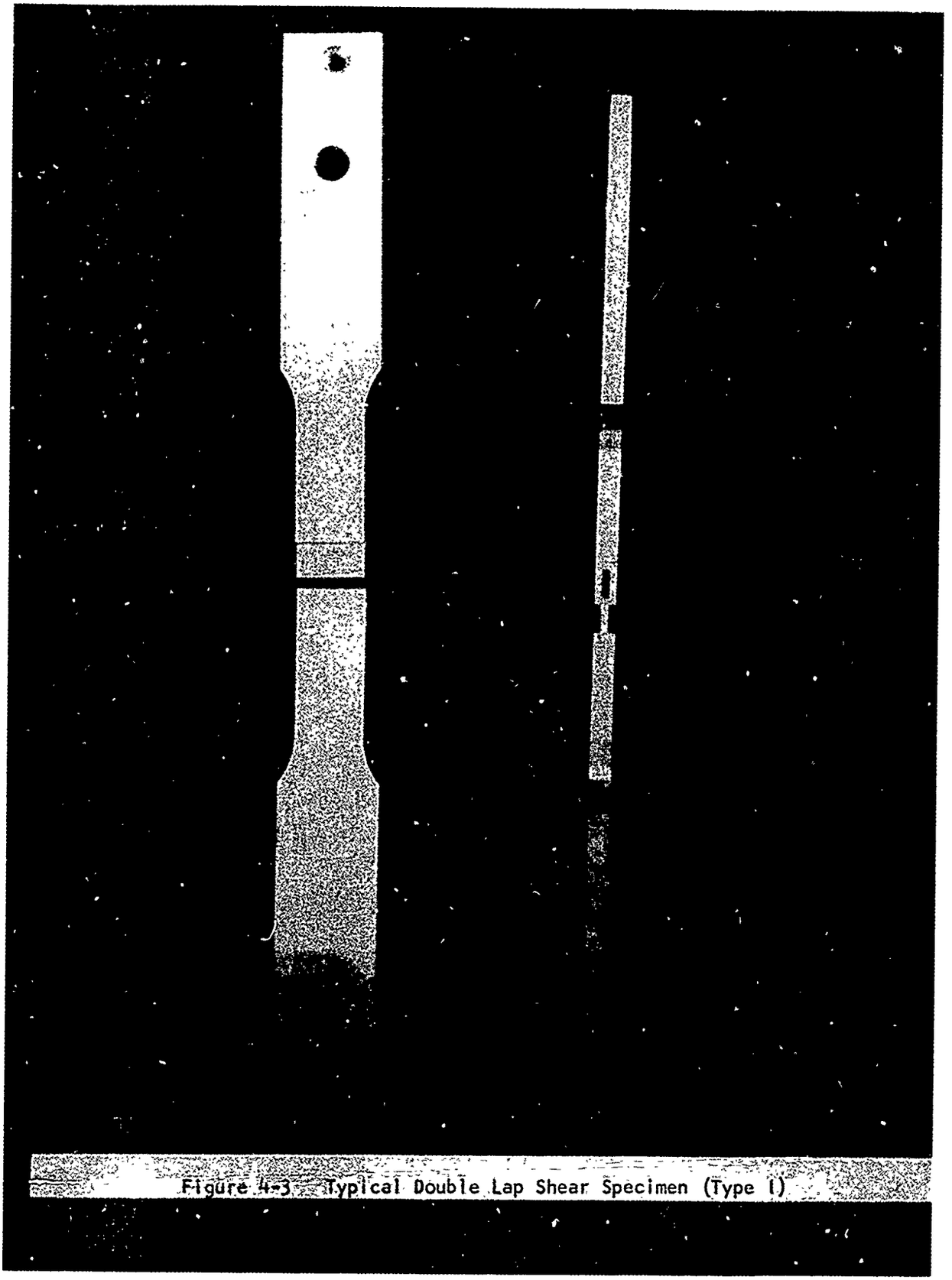

Figure 4-3 Typical Double Lap Shear Specimen (Type I)

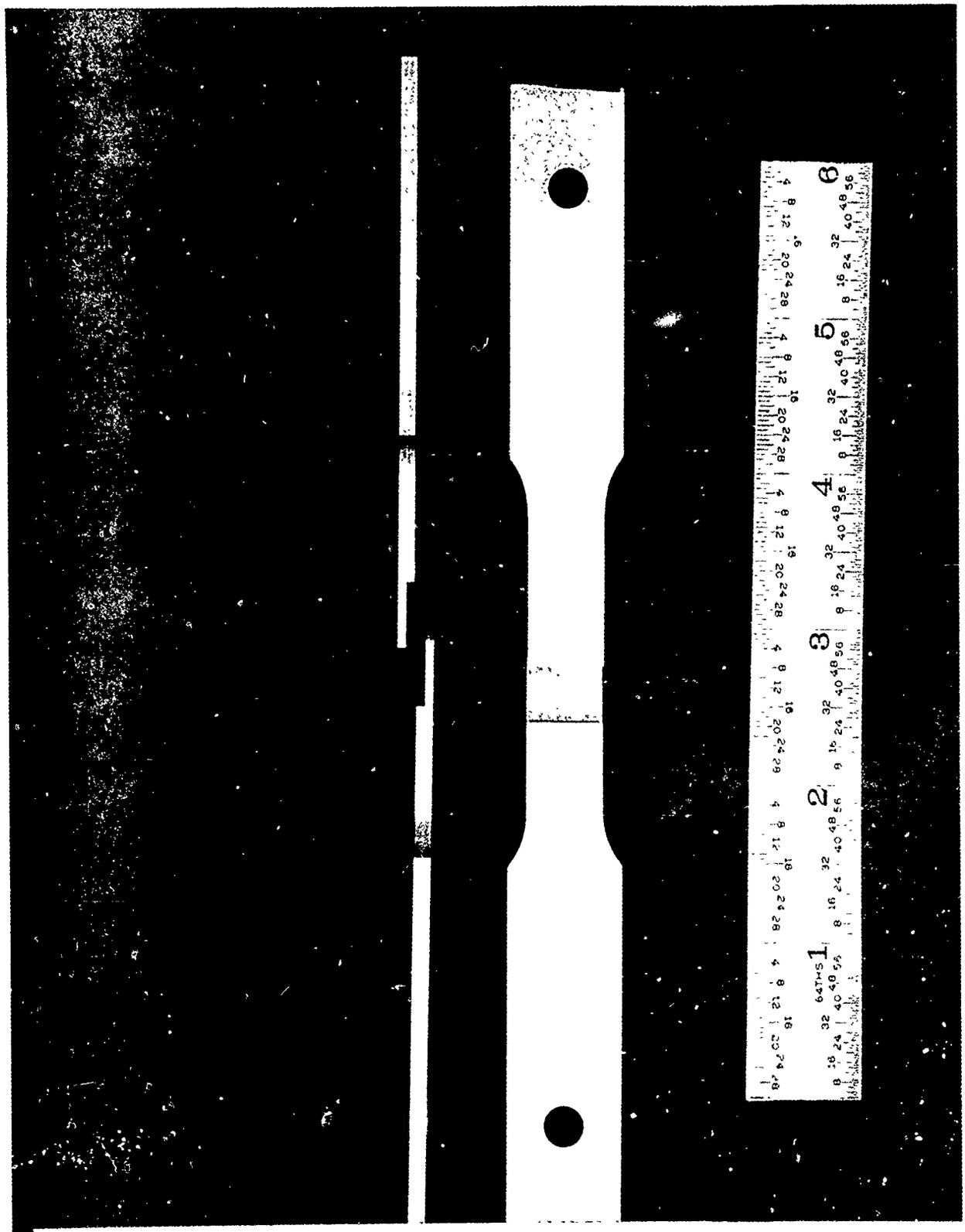

Figure 4-4 Typical Single Lap Shear (Type II)

Average Shear Strength[3] of Brazed Lapped Joints

-300°F to 500°F

Base Metal Alloy	Specimen Type	Shear (PSI) -300°F	Shear (PSI) RT	Shear (PSI) 300°F (up to 100 hrs)				Crosshead Rate In/Min
6951	11	17,907	17,519	15,402				0.05
6061	11	25,108	22,160	17,180				0.05
7005	11	20,558	19,810	15,006				0.05
		Shear (PSI) 350°F 25 Hrs.	Shear (PSI) 350°F 50 Hrs.	Shear (PSI) 350°F 100 Hrs.	Shear (PSI) 500°F 25 Hrs.	Shear (PSI) 500°F 50 Hrs.	Shear (PSI) 500°F 100 Hrs.	
6951	1[2]	(1)	14,942	(1)	(1)	(1)	(1)	0.05
6061	1[2]	(1)	16,329	14,199	7,344	6,683	(1)	0.05
7005	1[2]	(1)	(1)	(1)	(1)	(1)	(1)	0.05

(1) Exceeded strength of base metal alloy
(2) PSI calculated at 90 percent of recorded value
(3) All testing conducted at referenced environment temperature

Table 4-3

4.2.1.6 Microstructure Analysis of Brazed and Thermal Conditioned Lapped Joints

A microscopic evaluation confirmed the presence of fillets along the joint interface edges across each specimen. The amount of silicon present as idiomorphic dendrites was more pronounced in the fillet areas of the 6951 and 7005 base metal alloy joint, than in the fillet of the 6061 base metal alloy joints. Between the base metal interfaces, the silicon approached the allotriomorphic type, which is partly due to the slight mechanical force applied during brazing which assists in reducing any surface buffer effect, and creates a condition which promotes silicon diffusion across the joint interfaces. Thus the no pressure areas (fillets) should exhibit a higher retention of filler metal alloying constituents.

No microscopic studies were conducted on joints subjected to elevated temperature soaking, as similar systems were evaluated as part of an alternate joining process (diffusion bonding) evaluation.

Figures 4-5, 4-6 and 4-7 are typical photomicrographs of the three base metal aluminum alloy brazed joints.

Photomicrograph of 6951 - 4045 Brazed Joint System

Mount #336
Base Metal Alloy - 6951
Filler Alloy - 4045
Condition - Brazed T6
Etchant - Boric Acid + HF
Magnification - 100X

Figure 4-5

Photomicrograph of 6061 - 4045 Brazed Joint System

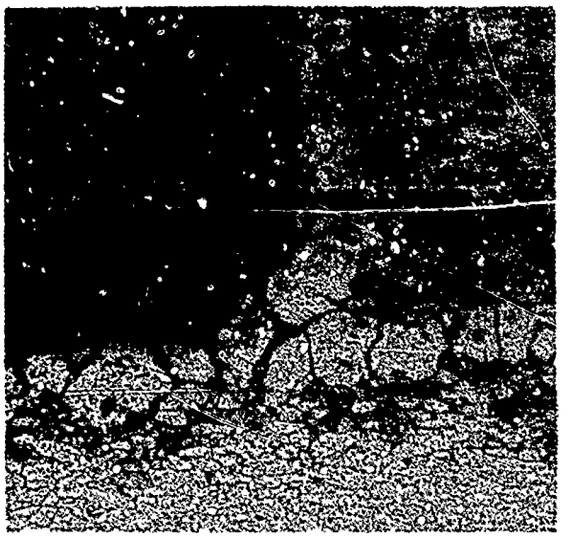

Mount #336
Base Metal Alloy - 6061
Filler Alloy - 4045
Condition - Brazed T6
Etchant - Boric Acid + HF
Magnification- 100X

Figure 4-6

Photomicrograph of 7005 - 4045 Brazed Joint System

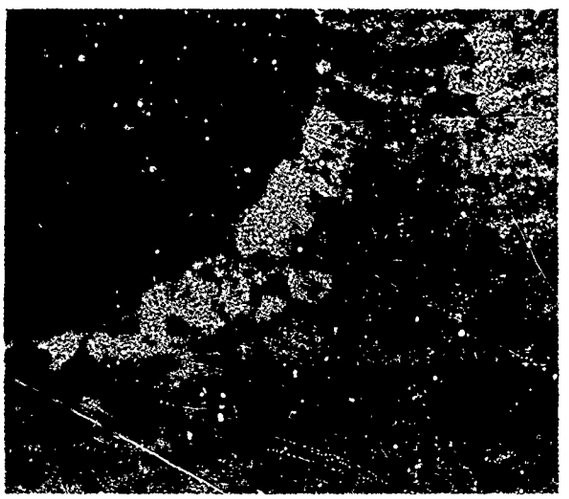

Mount #336
Base Metal Alloy - 7005
Braze Alloy - 4045
Condition - Brazed T6
Etchant - Boric Acid + HF
Magnification - 100X

Figure 4-7

4.2.2 Thermal Effect on Flatwise Tensile Properties of Brazed Honeycomb Sandwich

A series of four (4) 12 inch by 12 inch honeycomb sandwich test panels were brazed, heat treated to condition T6 and flatwise tensile tested at -300 F, room temperature, 300 F, 350 F, and 500 F. Each of the four panels were sectioned into 1 inch by 1 inch square specimen and bonded to aluminum pull blocks for testing purposes. Each of the specimen were held at the test temperature for 10 minutes and then loaded to failure.

Three (3) base metal aluminum alloys and one (1) braze filler metal were selected as the panel components for reasons stated below:

Face Sheet Alloy	Core Alloy	Filler Alloy	
7005			Good brazeability. Low sensitivity to solutioning quenching rates.
6951			Good brazeability. Available as braze sheet core.
	6061		Good brazeability. Available in thin sheet.
		4045	Exhibits good brazing characteristics. Available as braze sheet with 6951 or 3003, can be produced with 7005.

The material combinations for each of the four (4) test panels were:

Panel No.	Face Sht. Alloy	Face Sht. Thickness	Core Alloy	Ribbon Thickness	Ribbon Height	Cell Size	Filler Thickness	Filler Form
1	7005	0.050"	6061	0.008"	0.357"	3/8"	0.003"	Foil (Solid)
2	6951	0.059"	6061	0.008"	0.357"	3/8"	0.003"	Foil (Solid)
3	7005	0.050"	6061	0.008"	0.357"	3/8"	0.003"	Foil (Pierced)
4	6951	0.059"	6061	0.008"	0.357"	3/8"	0.003"	Foil (Pierced)

Figure 4-8 shows one of the four (4) test panels as brazed and heat treated.

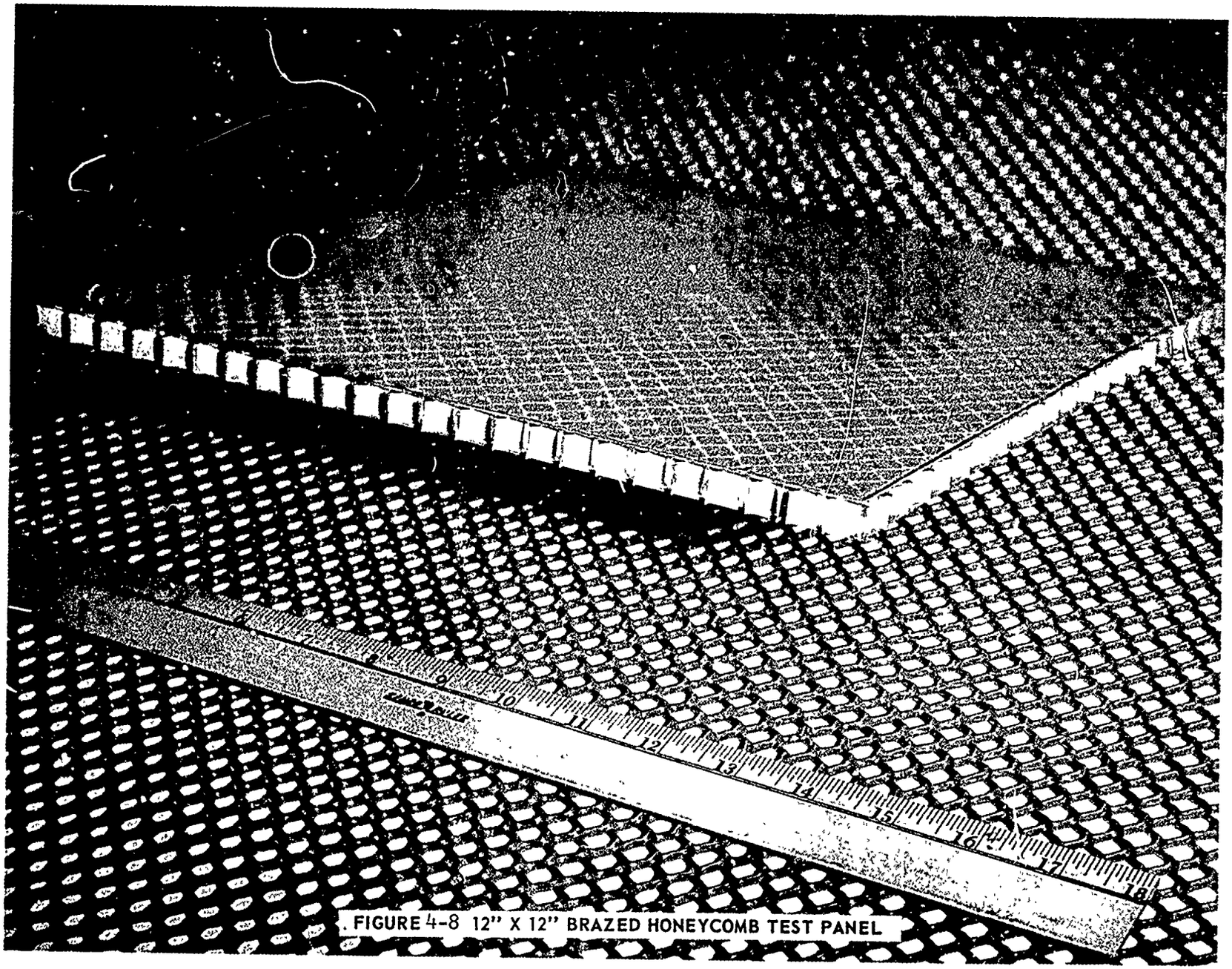

FIGURE 4-8 12" X 12" BRAZED HONEYCOMB TEST PANEL

A summary analysis of the findings of the tests and evaluations performed on the four (4) initial test panels produced to the above material combinations is made in the following:

General Comment

The data obtained from this initial investigation indicated that the structural properties obtained thus far are attractive for room temperature and elevated temperature applications up to 500 F for short periods of time. However, there is a need to minimize the filler metal embrittling effect on the core ribbon to face sheet joint transition areas for cryogenic applications, which may include a high frequency cyclic stress service.

Specific Comments

- The 0.003 inch thick braze filler metal foil used in the first two panels was excessive for the amount of joint surface area to be brazed. This plus a somewhat long brazing cycle ($7\frac{1}{2}$ minutes above 1075 F) caused an over diffusion condition of the thin core ribbon members by the aluminum silicon filler metal. Base metal alloy grain growth and diffusion was predominant in the ribbon joint transition areas.

- A reduction in the amount of filler metal used for joining the Number 3 and 4 test panels was accomplished by pie cing the braze filler metal foil. This reduced the available filler metal for joining to an equivalent foil thickness of 0.0017 inches. Also the time at brazing (above 1075 F) was reduced to $4\frac{1}{2}$ minutes. This showed a reduction in the base metal microsturcture change over that of the Number 1 and 2 panels, but not to the degree which was considered optimum. It was concluded that a further reduction in the amount of filler metal available for joining was desirable. However, an increase in the ribbon surface area in contact with the filler metal, by reducing the core cell size, would be an equivalent corrective approach. It is doubtful that a reduction in the filler metal attack would give a substantial increase in flatwise tensile properties of the composites, but the embrittled areas of the joints would be less susceptible to premature brittle failure such as under repeated load cycling conditions, or loading in a cryogenic environment.

- The honeycomb core ribbon was perforated to permit inert gas purging for brazing. There was evidence of crack propagation from these holes. This type of failure was more noticeable for the tests conducted at room temperature and above. Whereas, at the -300 F test temperature the less ductile joint condition at the ribbon to fillet transition was more susceptible to any notched effects caused by microscopic filler metal erosion of the base metal grain boundary to surface junctions.

- o The air quenching rate for the Number 3 and 4 panels was less than that for the Number 1 and 2 panels. This no doubt was the prime reason for the lower tensile values of the 6061 ribbon members. Quenching (AQ) rates were low, to avoid warping. The Number 3 and 4 panels exhibited less joint transition type failures than did the Number 1 and 2 panels under the -300 F condition.

4.2.2.1 Process and Brazing Method

The precleaning and brazing methods for four (4) test panels was identical to that reported in Subsection 4.2.1.2 of this report. Excepting that the time at brazing above 1075 F was $7\frac{1}{2}$ minutes for panels Number 1 and 2, and $4\frac{1}{2}$ minutes for panels Number 3 and 4.

4.2.2.2 Flatwise Tensile Properties of Brazed Honeycomb Sandwich Test Panels at -300 F through 500 F.

Flatwise tensile properties for each of the four flat test panels are presented in Table 4-4.

Honeycomb Brazed Panel - Flatwise Tensile Properties
-300°F to 500°F

Test Temperature Degrees F 10 (Min.)	Total Area (In^2)	Average Ribbon Area ($In.^2$)	Average Ribbon[4] Tensile Stress at Failure (PSI)	Predominant Failure Mode
		Test Panel Number 1		
-300	1	0.045	32,222	(1)
72	1	0.045	36,805	(3)
300	1	0.045	33,629	(3)
350	1	0.045	31,480	(3)
500	1	0.045	27,420	(3)
		Test Panel Number 2		
-300	1	0.045	37,476	(1)
72	1	0.045	36,476	(2)
300	1	0.045	33,333	(2)
350	1	0.045	29,716	(3)
500	1	0.045	26,320	(3)
		Test Panel Number 3		
-300	1	0.045	34,851	(3)
72	1	0.045	31,119	(2)
300	1	0.045	29,222	(2)
350	1	0.045	29,010	(2)
500	1	0.045	27,535	(2)
		Test Panel Number 4		
-300	1	0.045	31,444	(3)
72	1	0.045	32,851	(2)
300	1	0.045	30,111	(2)
350	1	0.045	28,906	(2)
500	1	0.045	23,284	(2)

(1) Failed at joint transition - fillet to core ribbon
(2) Failed in core ribbons
(3) Type (1) and (2)
(4) Average of three (3) or more specimen

Table 4-4

4.2.2.3 Flatwise Honeycomb Sandwich Tensile Failure Modes

Failure Mode Number 1

Figure 4-9 photographically illustrates a typical tensile failure at the fillet to core ribbon transition.

Heavy braze filler metal build up at right of ribbon was due to a burr at the ribbon edge, caused by machining the core blanket prior to brazing.

Section shown was removed from portion of panel Number 4, tested at -300 F.

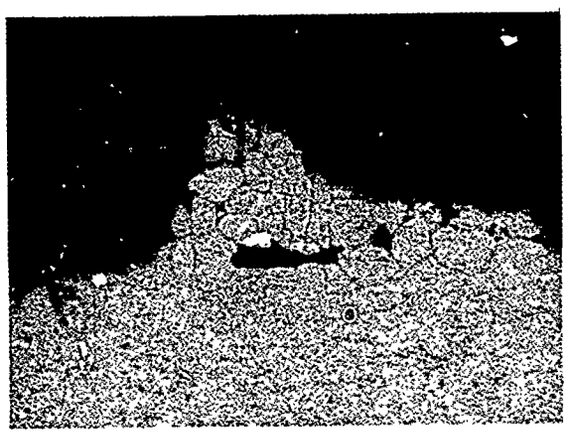

Mount #378
Etchant - Boric Acid + HF
Test Temperature -300 F
Failing Stress - 34.1 KSI
Panel No. 4
Magnification - 100X

Figure 4-9

Failure Mode Number 2

Figure 4-10 photographically illustrates a typical core ribbon failed in tension. Considerable neck down of the 6061 alloy ribbon member occurred before fracturing.

Section was removed from portion of panel Number 3, tested at -300 F.

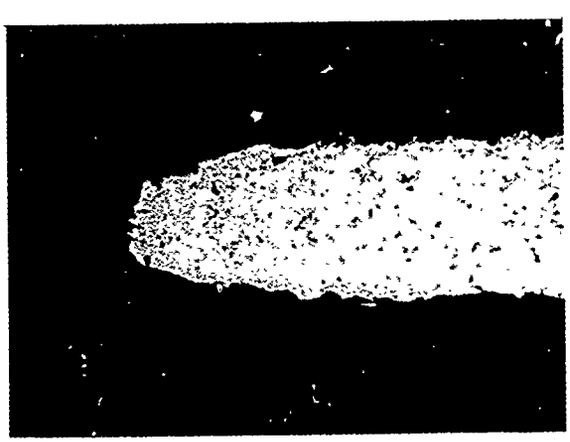

Mount #342
Etchant - Boric Acid + HF
Test Temperature -300 F
Failing Stress - 34 KSI
Panel No. 3
Magnification-100X

Figure 4-10

4.3 Fatigue Resistance of Brazed Laminated Plate vs Homogeneous Plate

In order that brazed aluminum composites could be considered for future structural applications, it was necessary to determine if any serious degrading of the fatigue resistance of the base metal alloys was affected by the brazing temperature and/or braze metal. A limited investigation was conducted for this purpose.

Fixed cantilever constant amplitude fatigue testing was investigated on brazed two ply 6061, 6951, and 7005 aluminum alloy plates. Braze filler metal alloy Number 4045 was used to braze each interface. Specimen configuration conformed to the RR Moore type as shown in Figure 4-11. All specimen were 0.06 inches thick.

In order that the results of the ply specimen could be compared to a reliable reference standard, a series of homogeneous specimen of each base metal aluminum alloy, having the same configuration, thickness and heat treated condition (T6), were fatigue tested at the same amplitudes as the ply plates.

The S-N curves (Figures 4-12, 4-13, and 4-14) were developed from five (5) identical stress levels; each level was an average of three specimen. The S-N curves demonstrated that, if any down grading of the base metal alloys occurred as a result of brazing, it was more than offset by the laminating effect (for the 0.06 inch thickness evaluated) as the endurance limits of all three types of brazed laminates exceeded those of homogeneous plates of the same thickness.

The fatigue resistance endurance limit break even thickness point between laminated brazed plate and homogeneous plate was not determined, but would be less than the 0.06 inch thickness investigated.

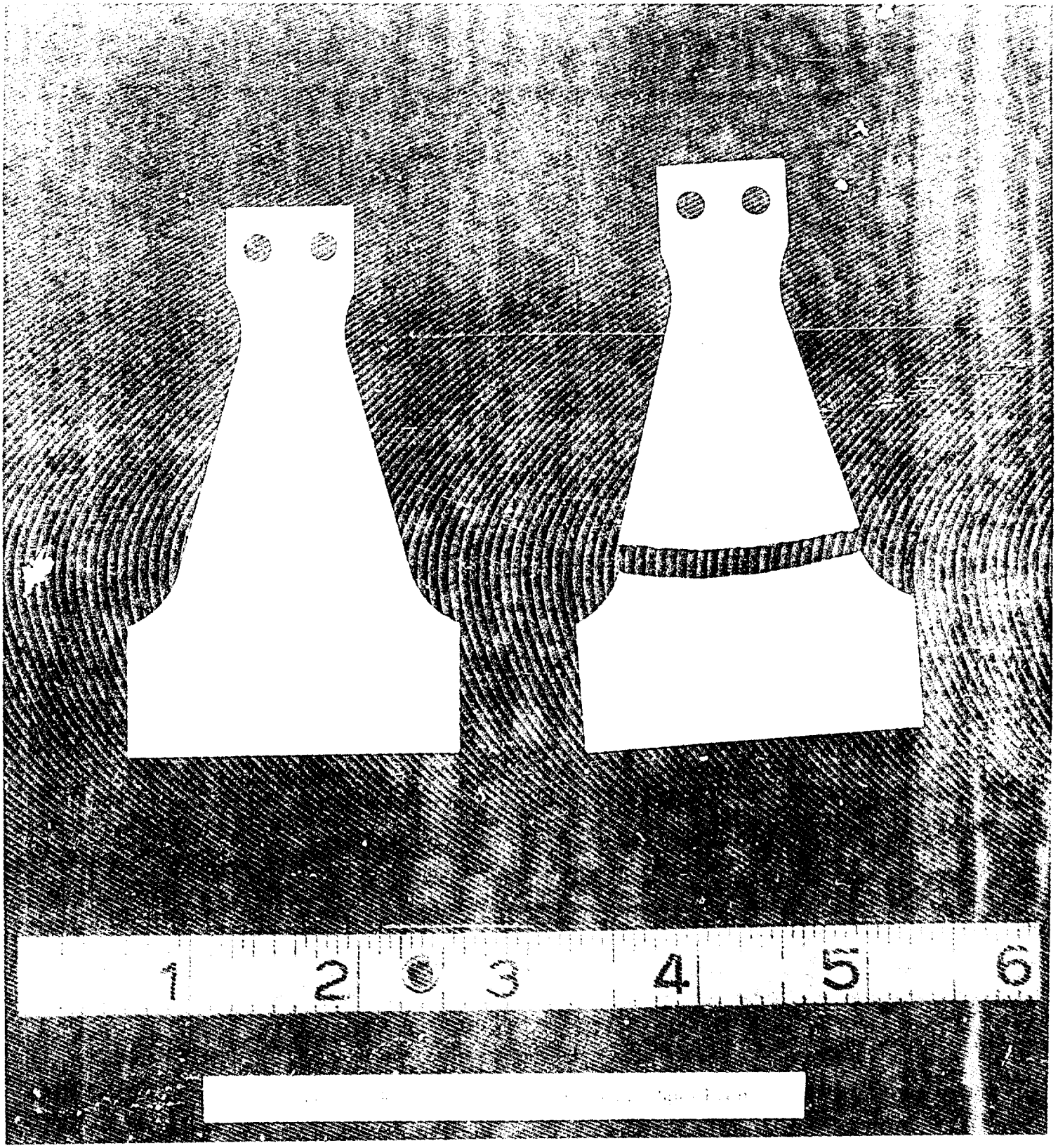
1
2
3
4
5
6

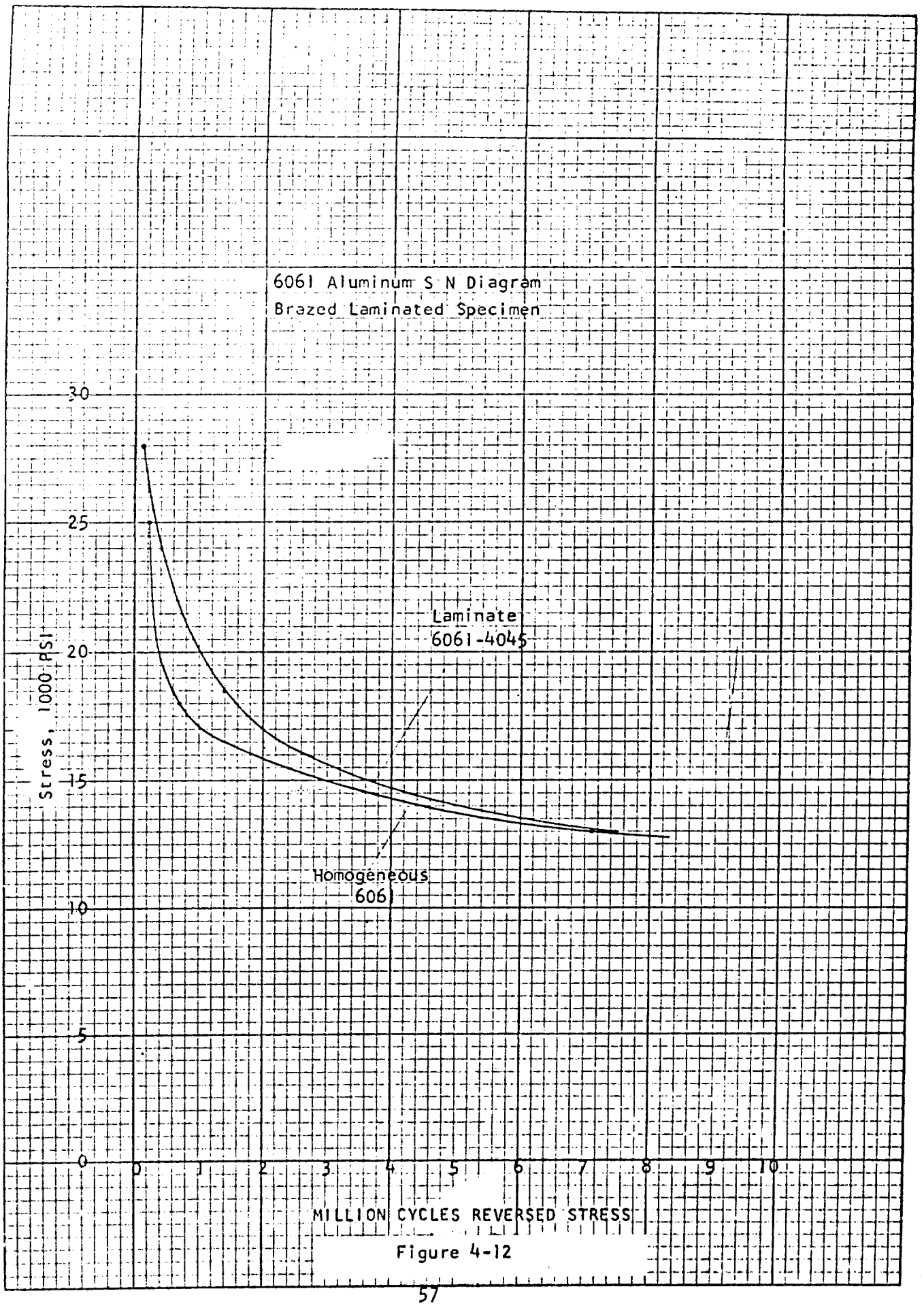
6061 Aluminum S N Diagram
Brazed Laminated Specimen
Laminate
6061-4045
Homogeneous
6061
Stress, 1000 PSI
30
25
20
15
10
5
0
0
1
2
3
4
5
6
7
8
9
10
MILLION CYCLES REVERSED STRESS

Figure 4-12

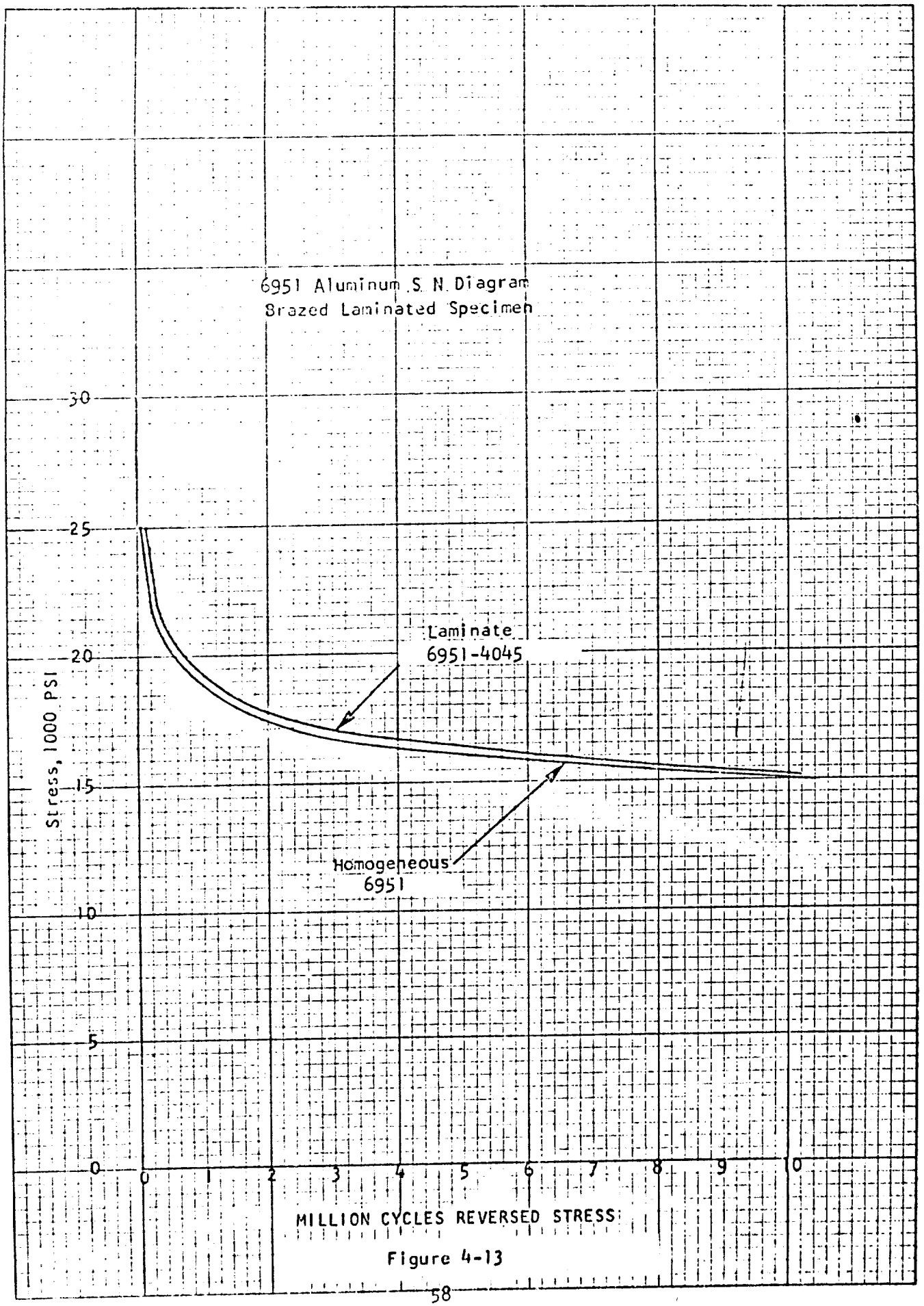
6951 Aluminum S. N. Diagram
Brazed Laminated Specimen
Stress, 1000 PSI
30
25
20
15
10
5
0
Laminate
6951-4045
Homogeneous
6951
0
1
2
3
4
5
6
7
8
9
10
MILLION CYCLES REVERSED STRESS

Figure 4-13

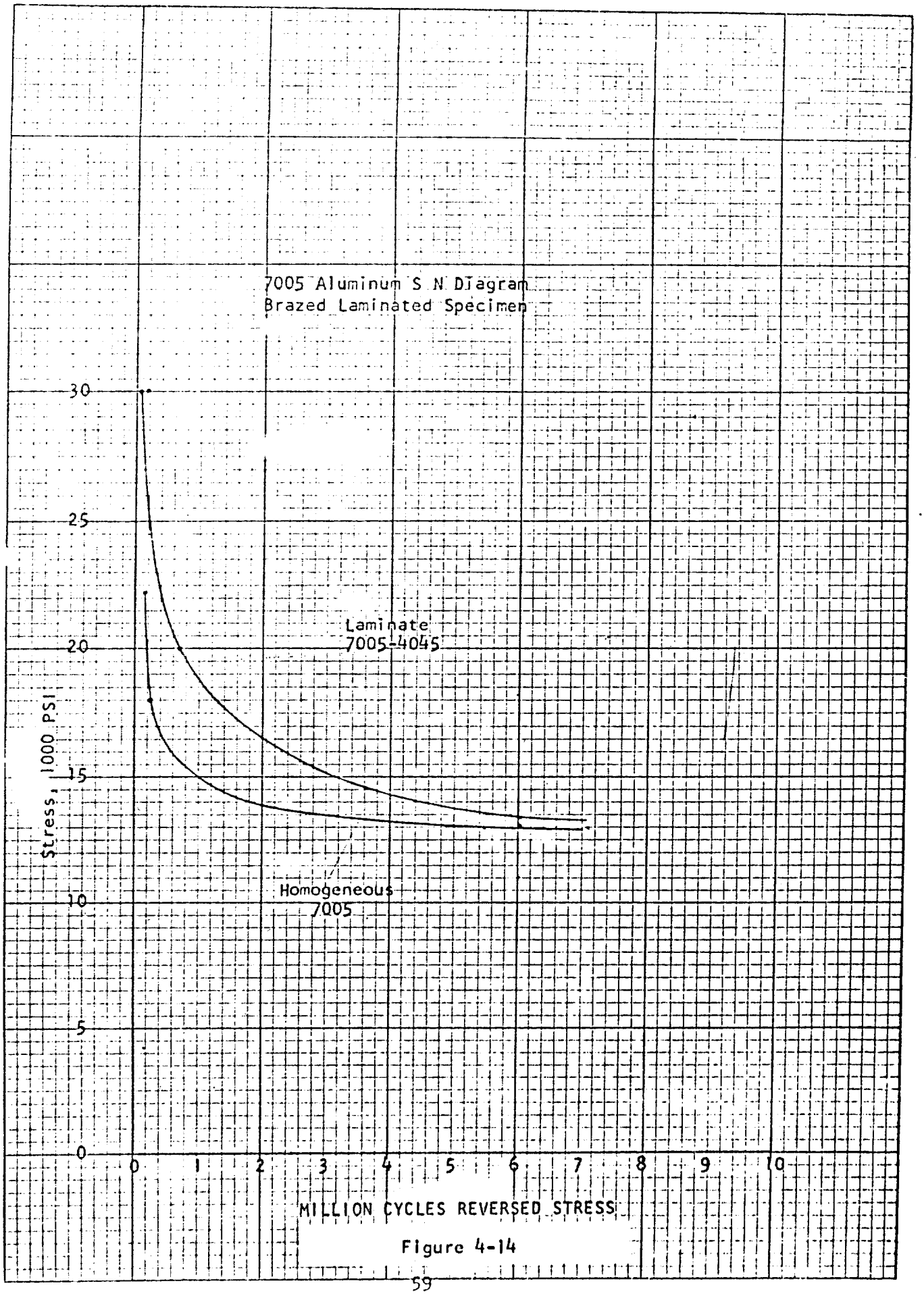
7005 Aluminum S N Diagram
Brazed Laminated Specimen
Laminate
7005-4045
Homogeneous
7005
Stress, 1000 PSI
30
25
20
15
10
5
0
0
1
2
3
4
5
6
7
8
9
10
MILLION CYCLES REVERSED STRESS

Figure 4-14

4.4 Effect of Corrosive and Elevated Temperature Environments on Brazed Aluminum Surfaces

An investigation was conducted to establish the relative corrosion resistance of brazed surfaces, interfaces and areas adjacent to wetted areas of selected aluminum alloys. For this purpose, three heat treatable base metal alloys (6061, 6951 and 7005) and one braze filler metal (4045) were evaluated. The investigation included an elevated temperature environment added subsequent to the corrosive environment.

Flat sheet specimen were surface spot brazed using 3 mill thick filler metal buttons. The specimen preparation and brazing cycles were as reported in Subsection 4.2.1.2.

The accelerated corrosion and thermal environment test was conducted as below:

- o A series of button spot brazed specimen were subjected to salt fog environment per Federal Test Method 151A for a 5 percent sodium chloride aquaous solution.
- o Groups (series) of the specimen that had been subjected to the salt fog test as above, were subjected to elevated temperatures of 300 F, 350 F and 500 F for periods of 25 hours, 50 hours, and 100 hours at each of these temperatures.
- o Each specimen was sectioned through the center of the brazed area and examined microscopically. The viewing field included base metal unbrazed (bare), bare base metal to filler metal wetted junctions, braze metal to base metal interfaces, and braze metal surfaces.

The 6061 alloy, both at the bare surfaces and brazed surfaces exhibited a higher resistance to corrosion than did the 7005 and 6951 alloys. The 7005 alloy gave a slightly lower resistance, while the 6951 alloy showed considerably less corrosion resistance.

In all cases, the corrosion occurred at the high energy areas (grain boundaries). Little, if any, surface pitting was found, except at the grain boundary to surface junctions.

No evidence of electrochemical corrosion could be attributed to bi-alloy electrode potential differences at the interfaces or adjacent areas. However, heavy concentrations of the braze metal filler's silicon constituent suffered preferential attack, due to the constituent being anodic to the filler matrix. This suggests

that metal to metal brazed joints would have good corrosion resistance, but that filleted joints (fillet matrix normally retain greater percentage of γ silicon than that of sandwiched metal to metal joints) exposed to a corrosive media would be more susceptible to corrosion if the fillets retained concentrations of alloying constituents anodic to the surrounding matrix.

The effect of subjecting the brazed specimen to elevated temperatures subsequent to the salt fog environment was less detrimental than was first concluded. There was evidence that the grain boundary attack had increased after the thermal environment, however, by re-evaluating the specimen that were subjected to salt fog only, it was found that the corrosion had continued. It is doubtful if the elevated temperature environment contributed to any acceleration of the corrosion initiated by the salt fog environment.

It was earlier concluded that the 6951 alloy brazed surfaces exhibited self healing during the 500 F elevated temperature soaking. This phenomena could not be explained, unless there was a considerable change in the electrode potentials of the material present at these locations, therefore, these specimen were carefully re-evaluated and by polishing and re-examining in increments of 0.005 of an inch further into the specimen, certain of the areas showing corrosion below the surface of the filler metal eventually were found to link up to corroded grain boundaries running up to the filler metal surface.

Differences in the corrosion resistance of the 4045 filler metal surface was related to the type of base metal alloy. Base metal alloys which are susceptible to silicon diffusion, leave a silicon depleted braze metal surface, which is more corrosion resistant than those surfaces which have retained a greater percentage of the silicon.

4.4.1 Metallographic Evaluation of Corrosive and Elevated Temperature Environment Effect on Brazed Aluminum Surfaces

A series of 6061, 6951 and 7005 aluminum alloy sheet specimen were spot brazed with 1/2 inch diameter 4045 (714) filler metal buttons, which were 3 mils thick. Brazed specimen are photographically illustrated in Figure 4-15.

A comparison of the cross sections of the 6061, 6951 and 7005 alloys and the 4045 aluminum silicon filler metal alloy shows differences in the filler metal microstructures when brazed to each of the three base metal alloys. This comparison was performed on specimen in the T6 condition prior to environment testing.

Typical Spot Brazed Specimen Prior to Environment Testing

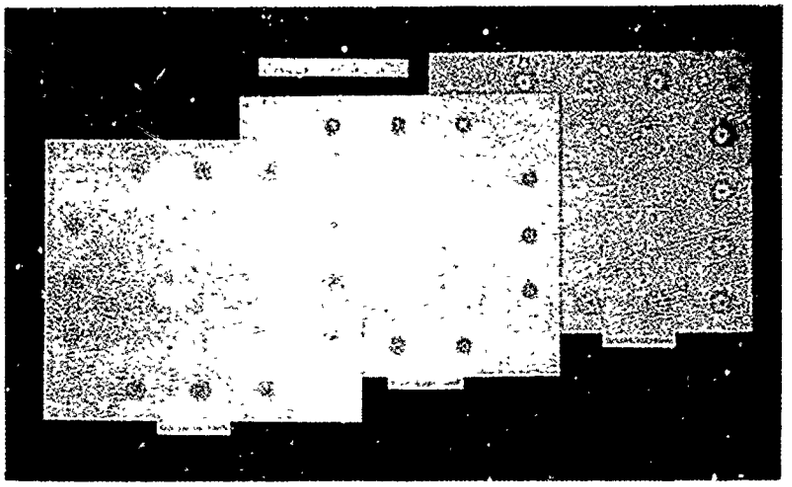

Figure 4-15

The 6951-4045 system showed more of the major alloying constituents present in and at the brazed surface, than that of the 7005-4045 system, whereas the 6061-4045 system showed little, if any, constituent retention, but exhibited a more grained surface. The microstructure of the brazed surface of the 6061 base metal alloy was essentially aluminum.

Typical microstructures of as-brazed specimen illustrating the differences in retained alloying constituents are presented in Figure 4-16.

Photomicrographs of As Brazed Surfaces

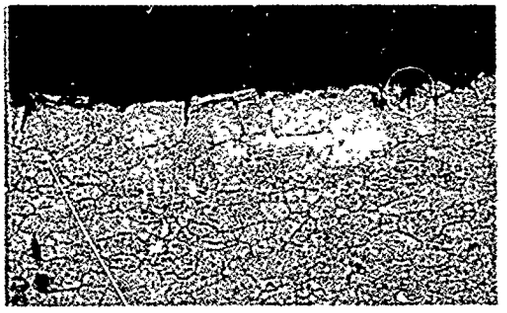

6951-4045 System--Microstructure

Mount # - - - - - - - - - - - - 436
Distance from button center - 0.4 in
Specimen condition - brazed - T6
Etchant - Boric Acid + HF- - (1 Min)
Magnification - - - - - - - - - 100X

7005-4045 System--Microstructure

Mount # - - - - - - - - - - - - 436
Distance from button center - 0.4 in
Specimen condition - brazed - T6
Etchant - - Boric Acid + HF - (1 Min)
Magnification - - - - - - - - 100X

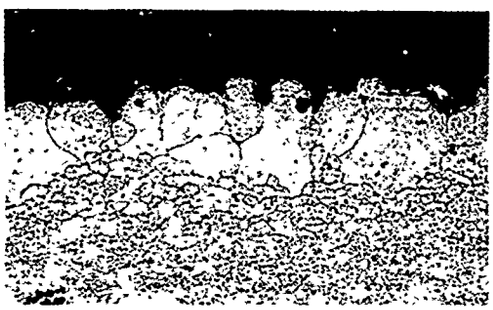

6061-4045 System--Microstructure

Mount # - - - - - - - - - - - - 436
Distance from button center - 0.4 in
Specimen condition - brazed - T6
Etchant - - Boric Acid + HF - (1 Min)
Magnification - - - - - - - - 100X

Figure 4-16

The following series of photomicrographs present the different corrosion modes of the three brazed material systems investigated. The top exhibit in each case is of the specimen after salt fog environment testing only. The two subsequent exhibits of each series were selected at random from specimen which were sectioned after salt fog and elevated temperature environment testing.

Photomicrographs of Corrosion Mode. 6061-4045 System

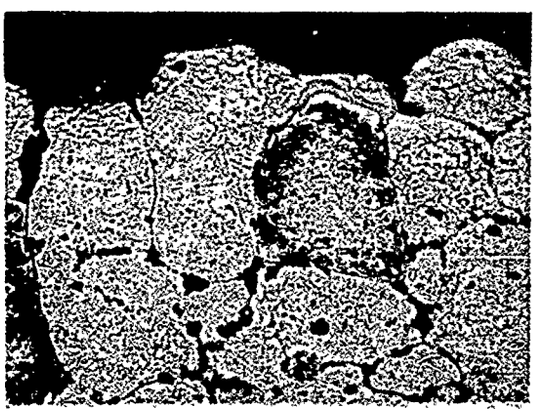

Mount # - - - - - - - - - - - - 437
Environment - -Salt Fog Only
Etchant - - Boric Acid + HF - (1 Min)
Magnification - - - - - - - - 250X

Photomicrographs of Corrosion Mode. 6061-4045 System (cont'd)

Mount # - - - - - - - - - - - - - 447
Environment - - Salt Fog - - 100 Hrs
350°F
Etchant - Boric Acid + HF - - (1 Min)
Magnification - - - - - - - - - 250X

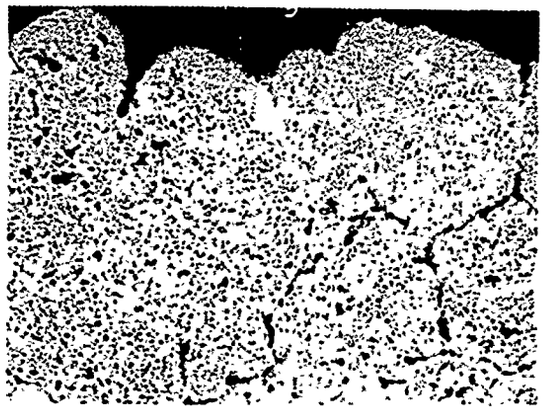

Mount # - - - - - - - - - - - - - 448
Environment - - Salt Fog - - 100 Hrs
500°F
Etchant - Boric Acid + HF - - (1 Min)
Magnification - - - - - - - - - 250X

Figure 4-17

Photomicrographs of Corrosion Mode. 7005-4045 System

Mount # - - - - - - - - - - - - - 437
Environment - - Salt Fog
Etchant - Boric Acid + HF - - (1 Min)
Magnification - - - - - - - - - 250X

Photomicrographs of Corrosion Mode. 7005-4045 System (cont'd)

Mount # - - - - - - - - - - - - - 446
Environment - - Salt Fog - - 100 Hrs at 300°F
Etchant - - Boric Acid + HF - (1 Min)
Magnification - - - - - - - - - 250X

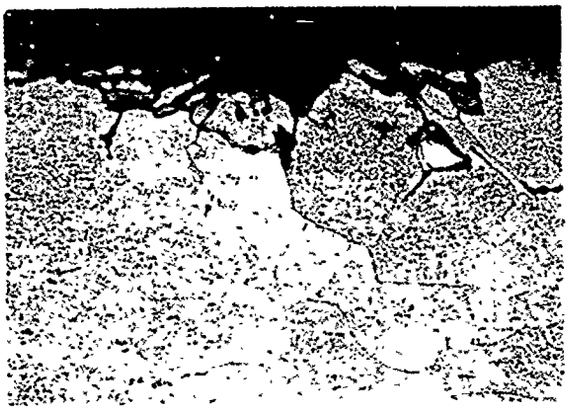

Mount # - - - - - - - - - - - - - 447
Environment - - Salt Fog - - 100 Hrs at 350°F
Etchart - Boric Acid + HF - - (1 Min)
Magnification - - - - - - - - - 250X

Figure 4-18

Photomicrographs of Corrosion Mode. 6951-4045 System

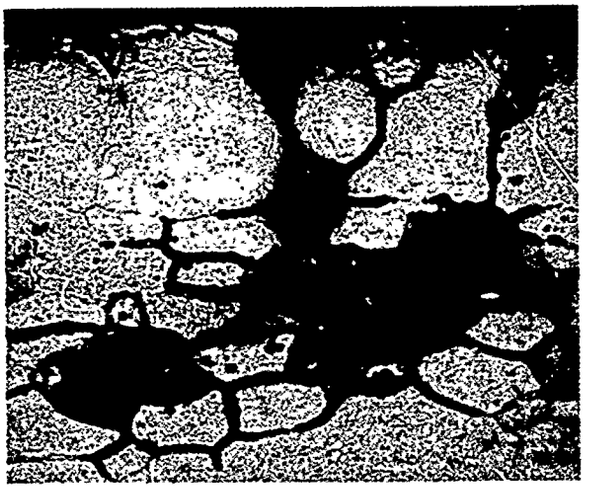

Mount # - - - - - - - - - - - - - 437
Environment - - - - - - - -Salt Fog
Etchant - Boric Acid + HF - - (1 Min)
Magnification - - - - - - - - - 250X

Photomicrographs of Corrosion Mode. 6951-4045 System (cont'd)

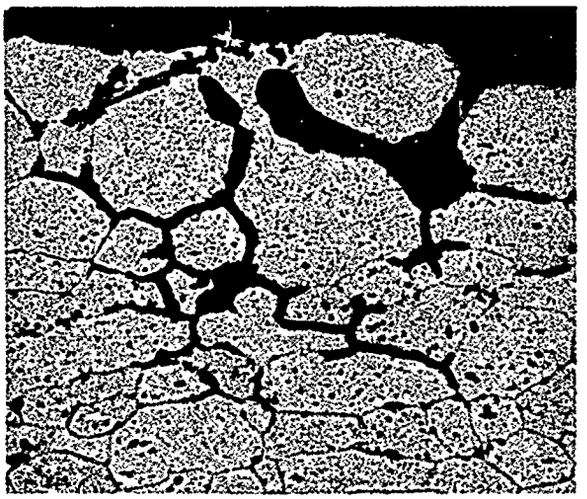

Mount # - - - - - - - - - - 443
Environment - - - - -Salt Fog
50 Hrs at 300°F
Etchant - Boric Acid + HF (1 Min)
Magnification - - - - - - 250X

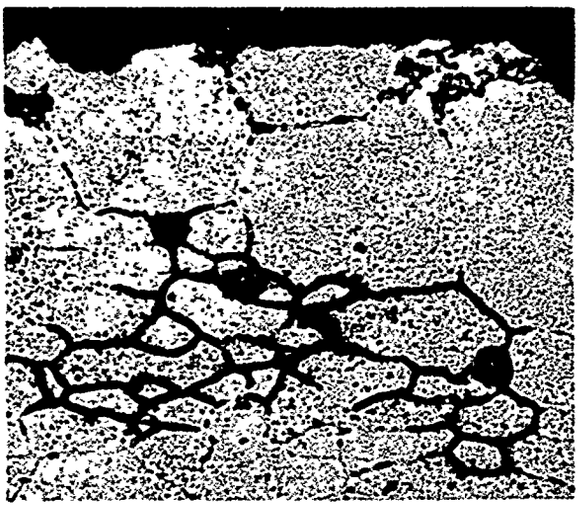

Mount # - - - - - - - - - - 445
Environment - - - - -Salt Fog
50 Hrs at 500°F
Etchant - Boric Acid + HF (1 Min)
Magnification - - - - - - 250X

Figure 4-19

4.5 Evaluation of Capillary Flow and Bridging of Two Commercially Available Aluminum Base Braze Filler Metals.

Two important aluminum braze filler metal characteristics were evaluated - horizontal gap bridging and vertical capillary flow.

At the incept of this program, while it was known that at least two commercially available aluminum base filler metals exhibited good wetting power, little was known about their ability to fill or bridge across interface gaps, or of their capillary rise power. Thus, more information in these areas was needed as a guide to filler metal placement and dimensional control of interfaces for planned complex hardware evaluations, of which three possible examples are:

- o Brazing of thin wall tube bundles to close out passage end header plates, if performed in the vertical position would prevent axial tube sagging, but may present a braze filler metal joint filling problem.
- o Brazing of honeycomb core nodes during sandwich panel composite joining by capillary flow along the core ribbon cell node junctions which might be angled at 90 degrees or less.
- o Core ribbon edge to skin gaps by bridging may off set need for impractical core blanket thickness tolerance requirements.

It was also realized that the degree of flow and capillary rise of any specific braze filler metal in the liquid state was dependent upon a time and temperature relationship, and to the amount of filler metal available. It was considered desirable to confine these factors to ones which had been applied successfully in the preceding brazing tasks. Preparation of details and brazing was therefore performed per Subsection 4.2.1.2 of this report.

Bridge and capillary test specimen base metal alloy was 6061. The two braze filler metal alloys were 4045 (714) and 718.

The 718 braze filler metal alloy exhibited a slightly higher capillary rise power than did the 4045. However, both fillers gave an effective capillary rise of 0.8 inches. There appeared to be no fractionating effect, as no microstructure differences were evident in sections removed at various heights from the capillary column.

A (horizontal) gap bridging investigation demonstrated that the 718 filler metal alloy gave a more effective bridging than did the 4045 alloy. The 718 alloy bridged effectively up to 0.0147 inches with minor porosity only, while the 4045 alloy bridged up to 0.009 inches.

As an observation, the following comment is appropriate:

> For brazing extremely thin members for optimum structural applications, the preceding data summary should be used conservatively, as the filler metal to base metal diffusion level ratio to thin member cross section thickness may be undesirable, unless the amount of available filler metal is controlled.

4.5.1 Effective Capillary Rise Power

6061 aluminum alloy capillary rise test blocks were machined to provide a rise of 0.8 inches, four angles (30°, 45°, 60°, and 90°) provided a broad coverage of possible vertical joints. The as machined specimen are photographically illustrated in Figure 4-20 below:

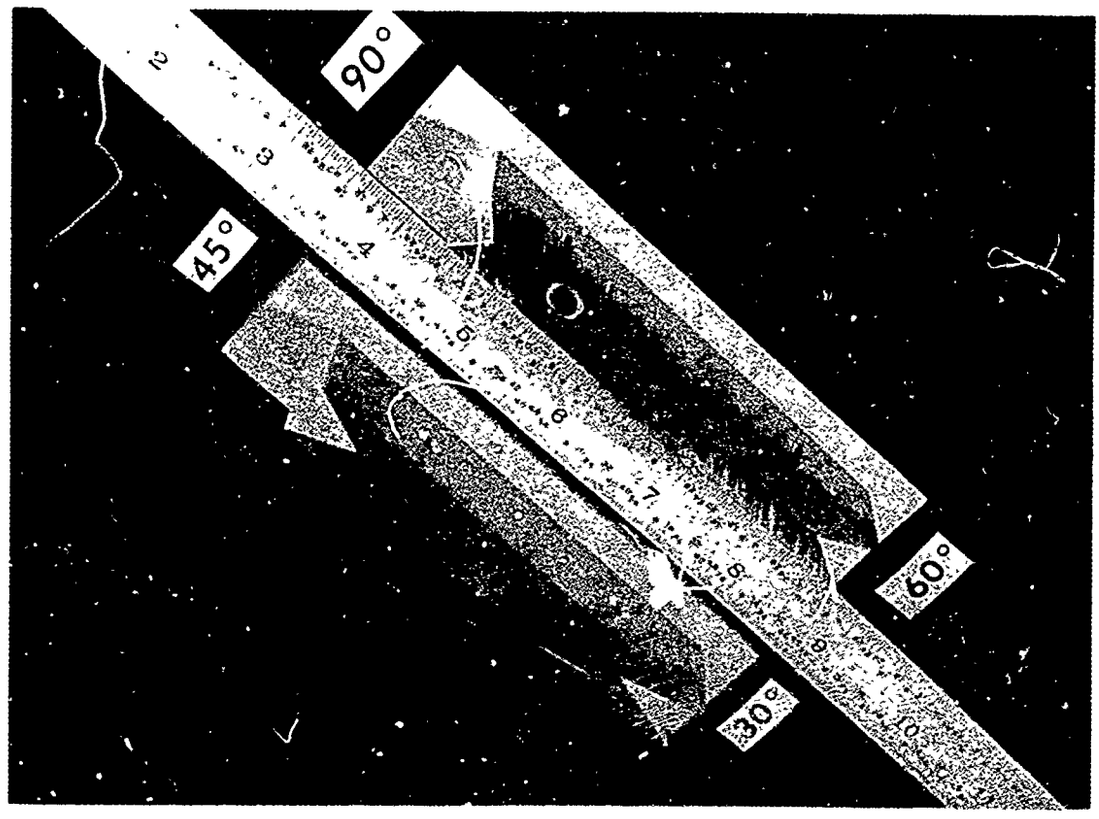

Figure 4-20

In each case an overlay of 0.003 inch braze foil covered the base plate on which the capillary rise test block was mounted as photographically shown in Figures 4-21 and 4-22 taken in the as-brazed condition.

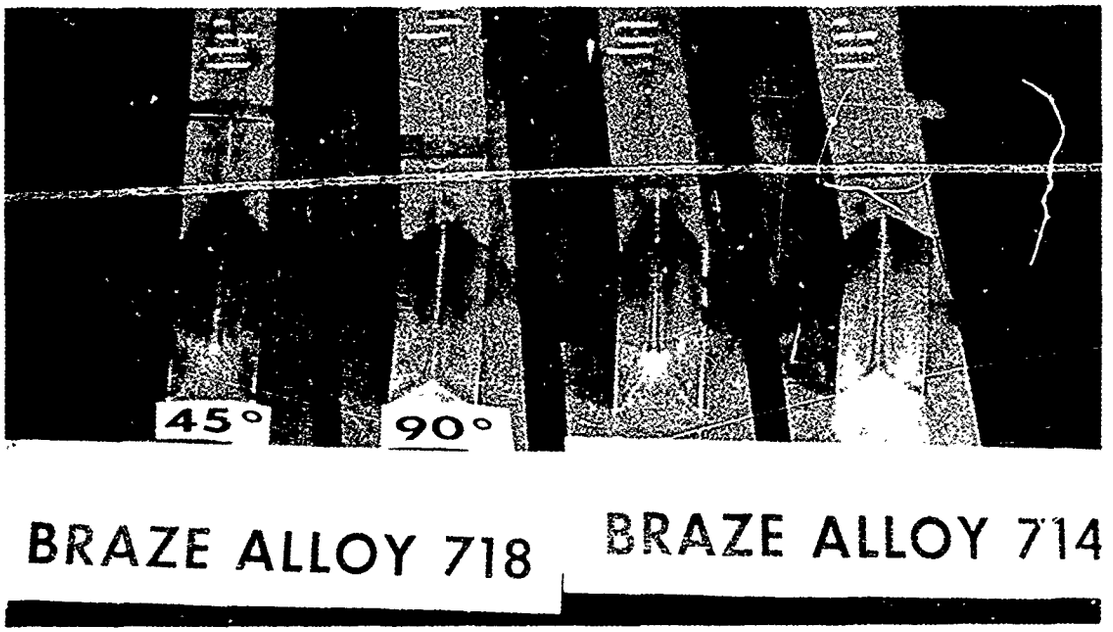

Figure 4- 21

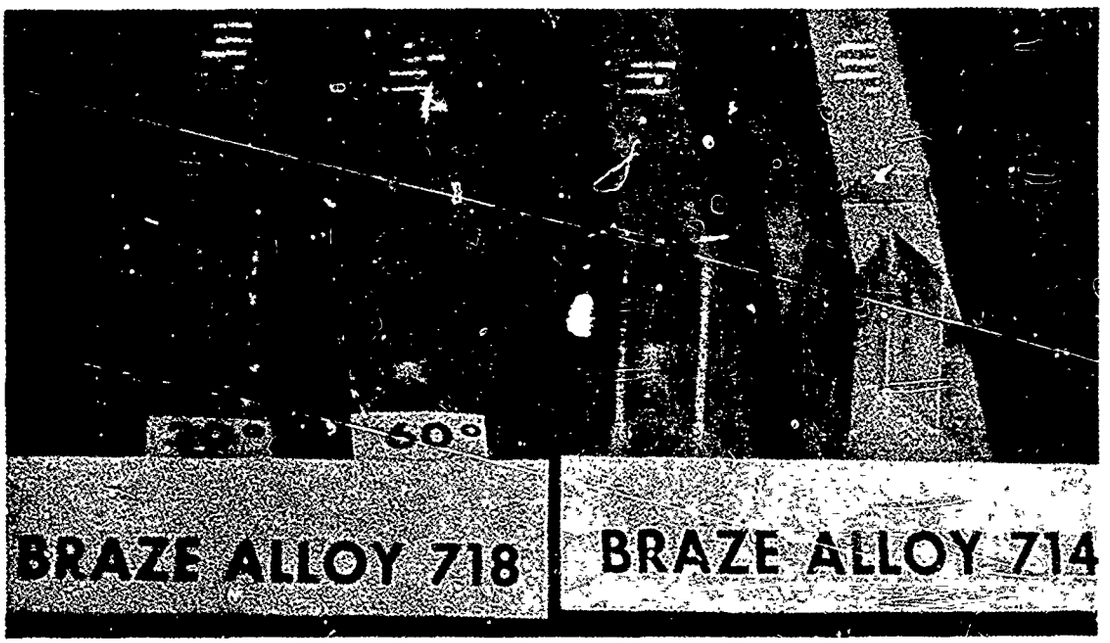

Figure 4-22

A series of closeup photographs (Figure 4-23) which illustrate four capillary columns for each filler metal alloy, were representative of the amount of material attracted into each capillary for the four angles (30°, 45°, 60°, and 90°). The difference in the performance of the two filler metals, with the 718 alloy exhibiting a slightly higher capillary rise power, can be attributed to its composition being essentially eutectic, with some added fluidity resulting from the copper constituent.

Each type of capillary column specimen were sectioned at four positions, and examined microscopically. The column fillet distance along each surface (leg) was recorded and plotted. The curves developed and presented in Figures 4-24 and 4-25 show that the 718 alloy column cross sections were greater than the 4045 (714) sections.

Photomicrographs of the four cross sections of the 718 alloy capillary column for the 60° angle specimen (Figure 4-26) show a considerable retention of the eutectic composition.

Table 4-5 is a tabulation of column sizes, and includes wetting out and filler metal diffusion data.

Macrograph of 30° included angle capillary column of 718 braze filler metal. Magnification-1.75X

Macrograph of 45° included angle capillary column of 718 braze filler metal. Magnification-1.75X

Macrograph of 30° included angle capillary column of 4045 braze filler metal. Magnification-1.75X

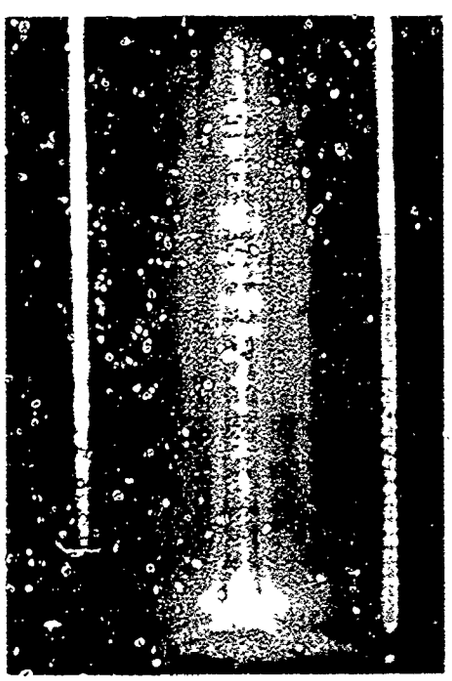

Macrograph of 45° included angle capillary column of 4045 braze filler metal. Magnification-1.75X

F

d angle
raze
ion-1.75X

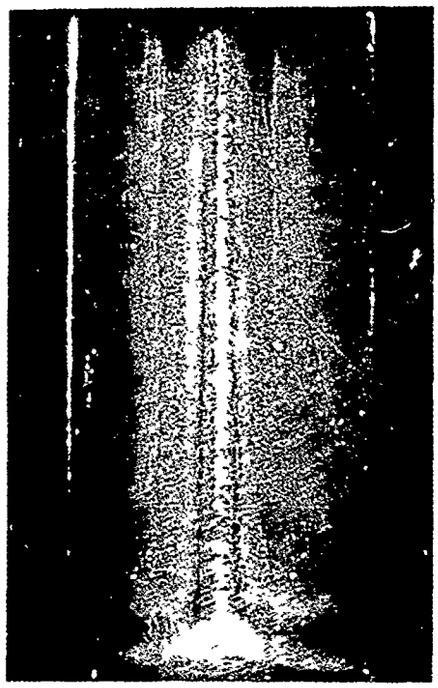

Macrograph of 60° included angle capillary column of 718 braze filler metal. Magnification-1.75X

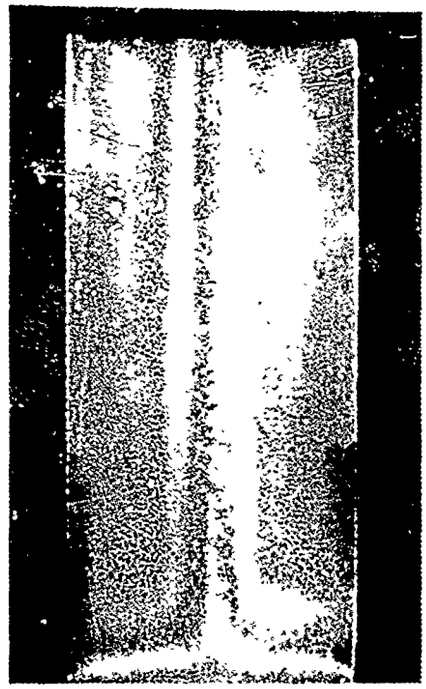

Macrograph of 90° included angle capillary column of 718 braze filler metal. Magnification-1.75X

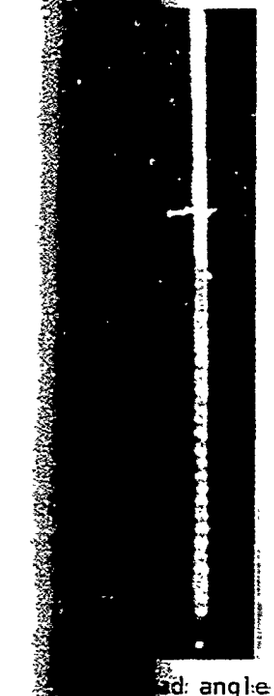

d angle
braze
ion-1..75X

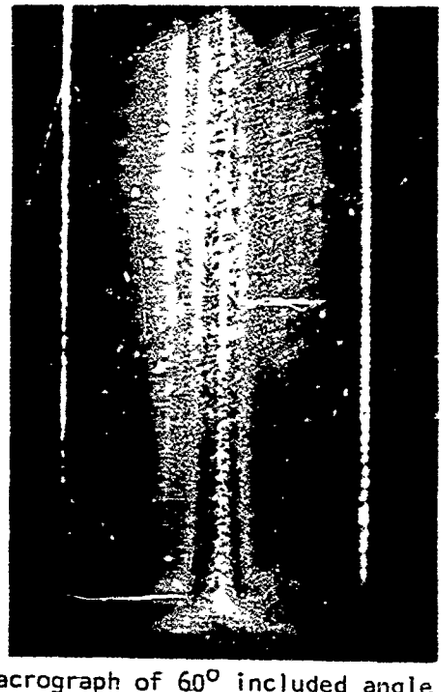

Macrograph of 60° included angle capillary column of 4045 braze filler metal. Magnification-1.75X

Macrograph of 90° included angle capillary column of 4045 braze filler metal. Magnification-1.75X

Figure 4-23

2

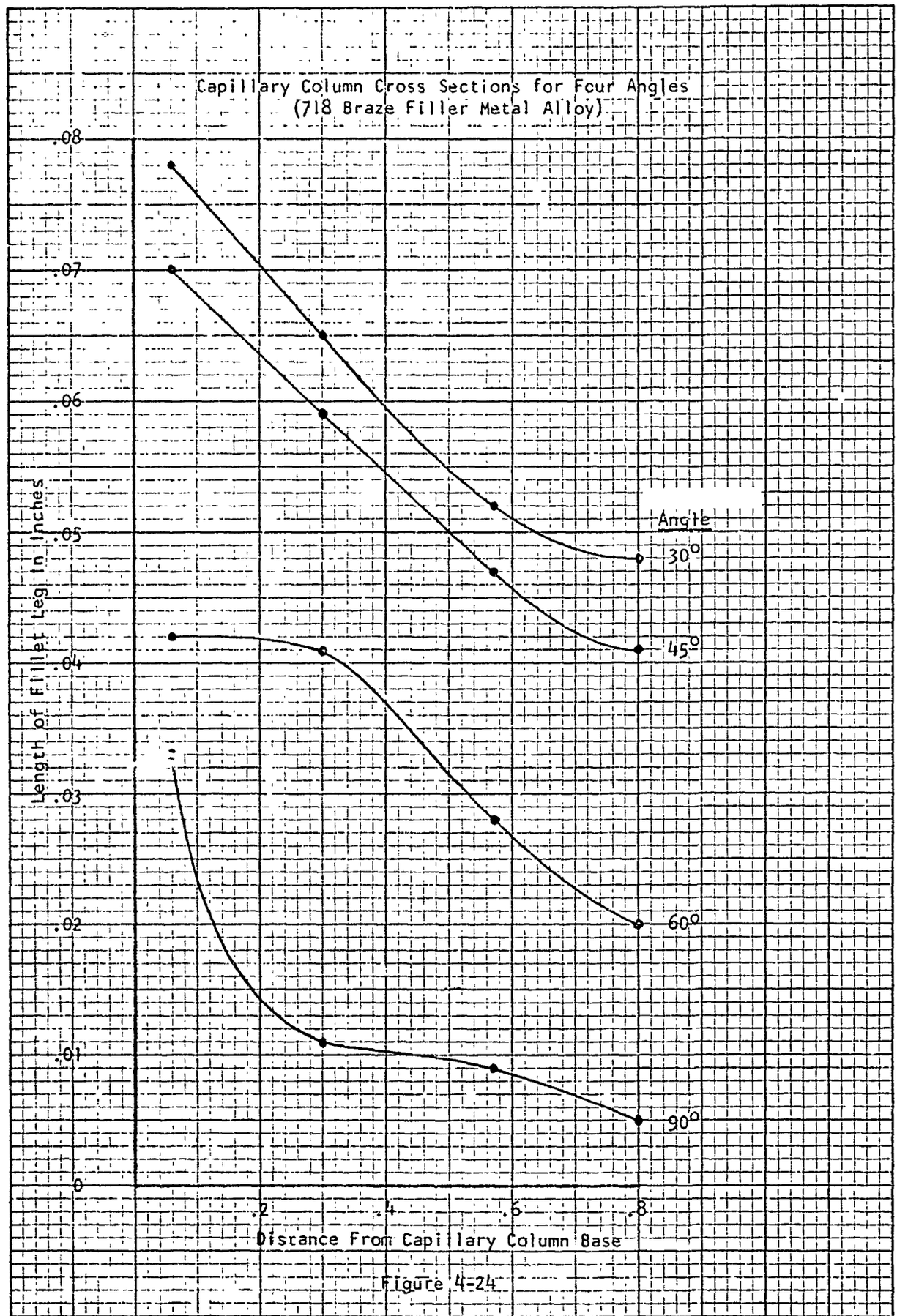
Capillary Column Cross Sections for Four Angles
(718 Braze Filler Metal Alloy)
.08
.07
.06
.05
.04
.03
.02
.01
0
Length of Fillet Leg in Inches
.2
.4
.6
.8
Distance From Capillary Column Base
Angle
30°
45°
60°
90°

Figure 4-24

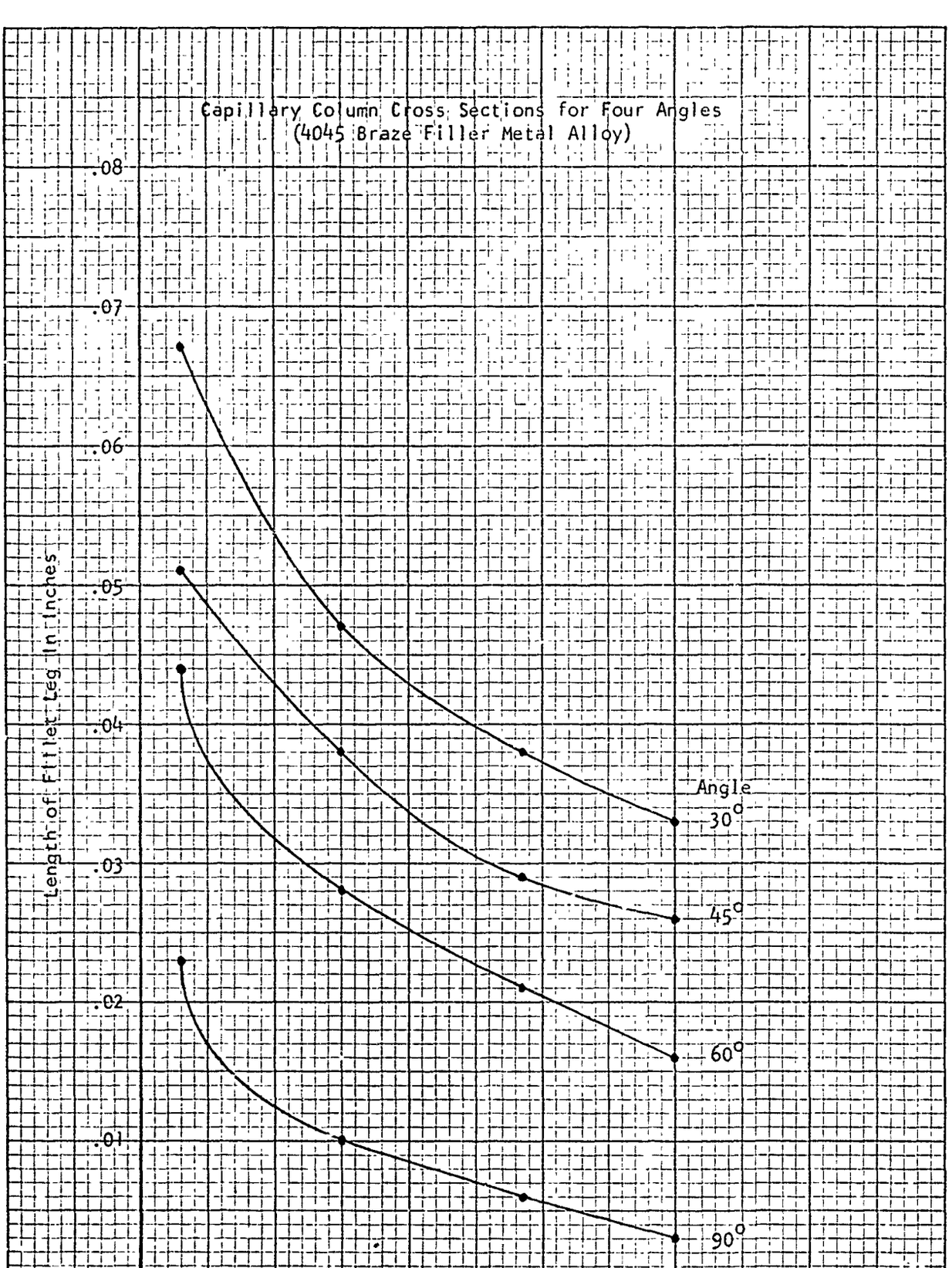
Capillary Column Cross Sections for Four Angles
(4045 Braze Filler Metal Alloy)
.08
.07
.06
.05
.04
.03
.02
.01
0
Length of Fillet Leg In Inches
Angle
30°
45°
60°
90°
.02
.04
.06
.08
Distance From Capillary Column Base

Figure 4-25

Photomicrographs of Cross Sections of Capillary Column
(60°included angle, 718 intermediate filler metal)

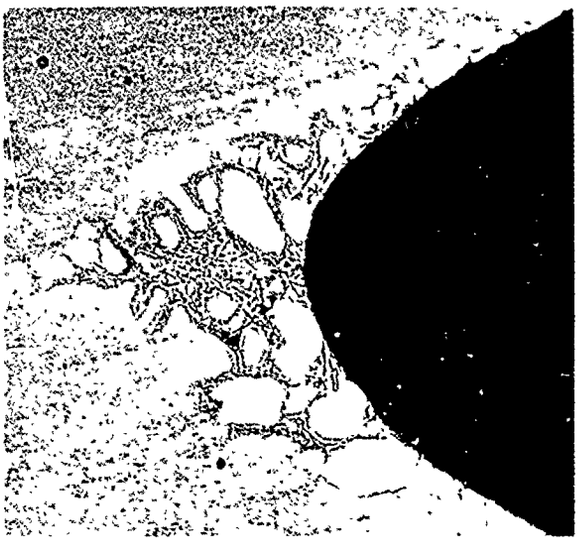

Mount #690 52X Boric HF
0.06 inches from braze surface

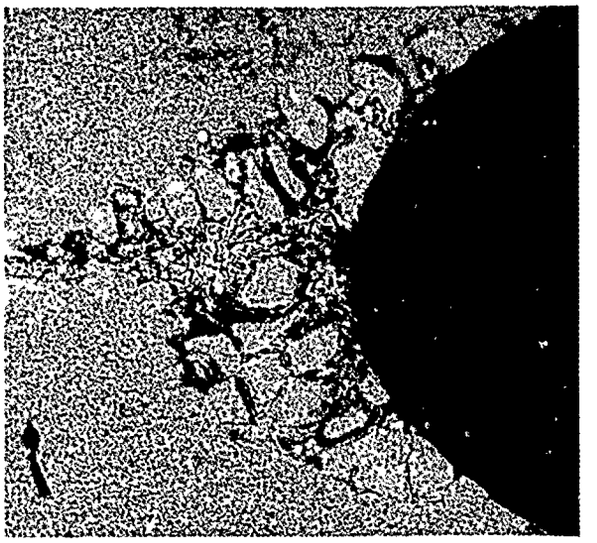

Mount #690 52X Boric HF
0.30 inches from braze surface

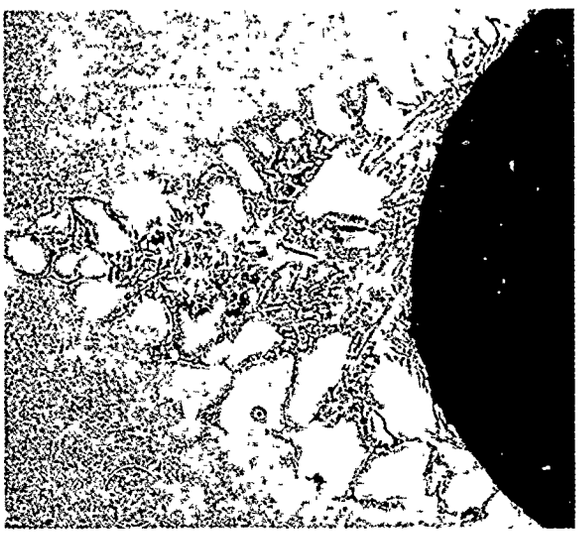

Mount #691 52X Boric HF
0.57 inches from braze surface

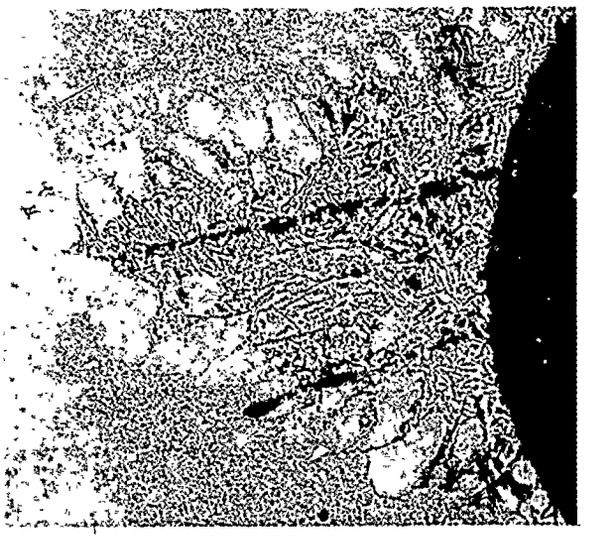

Mount #691 52X Boric HF
0.80 inches from braze surface

Figure 4-26

Intermediate Alloy	Included Angle In Degrees	"A" Location of Section	Fillet Dimensions "B" Leg	Fillet Dimensions "C" Face	Wetting of P.M.	Diffusion Into 6061
4045	30	.06	.067	.041	(1)	.0106
		.30	.047	.028	.339	.0041
		.57	.038	.023	.155	.0051
		.80	.033	.019	.166	.0041
718	30	.06	.078	.041	(1)	.0053
		.30	.065	.039	.171	.0054
		.57	.052	.031	.131	.0049
		.80	.048	.023	.087	.0045
4045	45	.06	.051	.049	(1)	.0074
		.30	.038	.036	.146	.0057
		.57	.029	.032	.182	.0059
		.80	.026	.018	.115	.0056
718	45	.06	.070	.078	(1)	.0066
		.30	.059	.070	.127	.0066
		.57	.047	.042	.092	.0066
		.80	.041	.033	.074	.0057
4045	60	.06	.044	.067	(1)	.0065
		.30	.028	.039	.187	.0056
		.57	.021	.036	.128	.0041
		.80	.016	.027	.096	.0037
718	60	.06	.042	.056	(1)	.0057
		.30	.041	.052	(1)	.0057
		.57	.028	.036	.123	.0074
		.80	.020	.035	.119	.0057
4045	90	.06	.023	.048	(1)	.0043
		.30	.010	.038	.180	.0065
		.57	.006	.011	.186	.0032
		.80	.003	.006	.159	.0037
718	90	.06	.033	.086	(1)	.0065
		.30	.011	.033	.153	.0082
		.57	.009	.028	.158	.0049
		.80	.005	--	.178	.0049

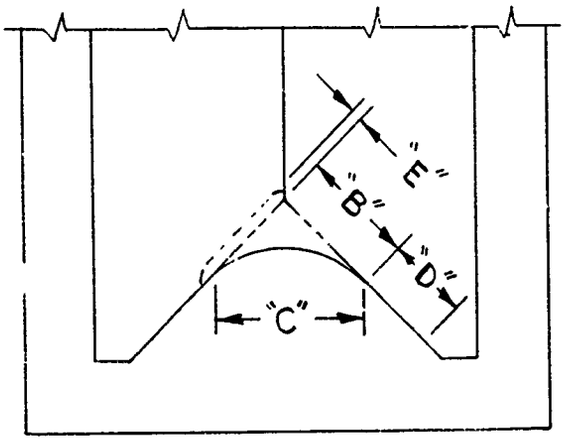

Definitions

"A" Vertical Distance From Capillary Base of Micro Section
"B" Length of Fillet Leg
"C" Width of Fillet Face
"D" Surface Wetting Beyond Termination of Fillet Leg
"E" Diffusion of Filler Metal Alloy Into 6061 Material
(1) 100% Wetting by Vertical Rise From Surface

Filler Metal Capillary Column - Cross Sections

Table 4-5

4.6 Effective Filler Metal Bridging

Two series of tests were conducted to determine the effective gap bridging of the 4045 (714) and 718 braze filler metal alloys. Horizontal gap 6061 aluminum specimen were machined per Figure 4-27.

Filler Metal Gap Bridging Test Specimen

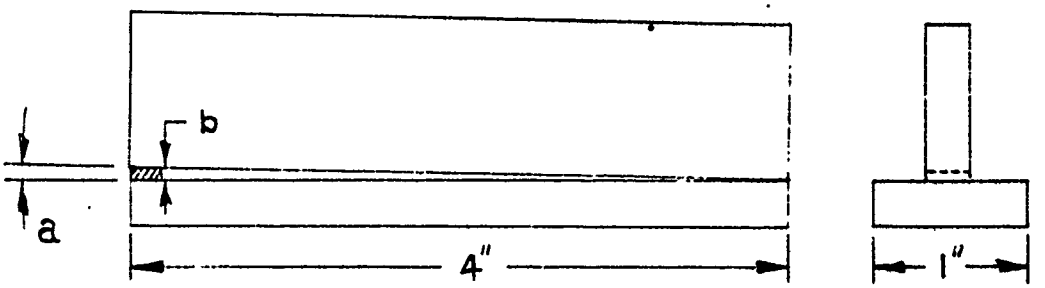

Angle a = 1°35' where b = 0.010" (Type A)
Angle a = 3°10' where b = 0.020" (Type B)

Figure 4-27

The Type A bridge was evaluated and found to be unsatisfactory. The filler metal foil (0.003" thick) distorted during heating making contact with the upper surface of the bridge. Thus the actual flow of the alloy could not be recorded.

The bridge configuration was modified by increasing the angle from 1°30" to 3°10'. The filler metal foil was retained flat against the base of the bridge by two CRES bars placed along the foil edges and parallel to the bridge.

The 718 alloy exhibited a higher bridging capability than that of the 4045 alloy. Actual gaps filled are tabulated in Table 4-6.

Table 4-6

Measurements of Filler Metal Bridging

Bridge Type	Filler Metal Alloy	Area of Measurements	Gap Bridged (Inches)
a	718	End of braze	0.0179
b	718	End of fillet formation	0.0147
a	4045	End of braze	0.0130
b	4045	End of fillet formation	0.0060

Bridging Test Specimen

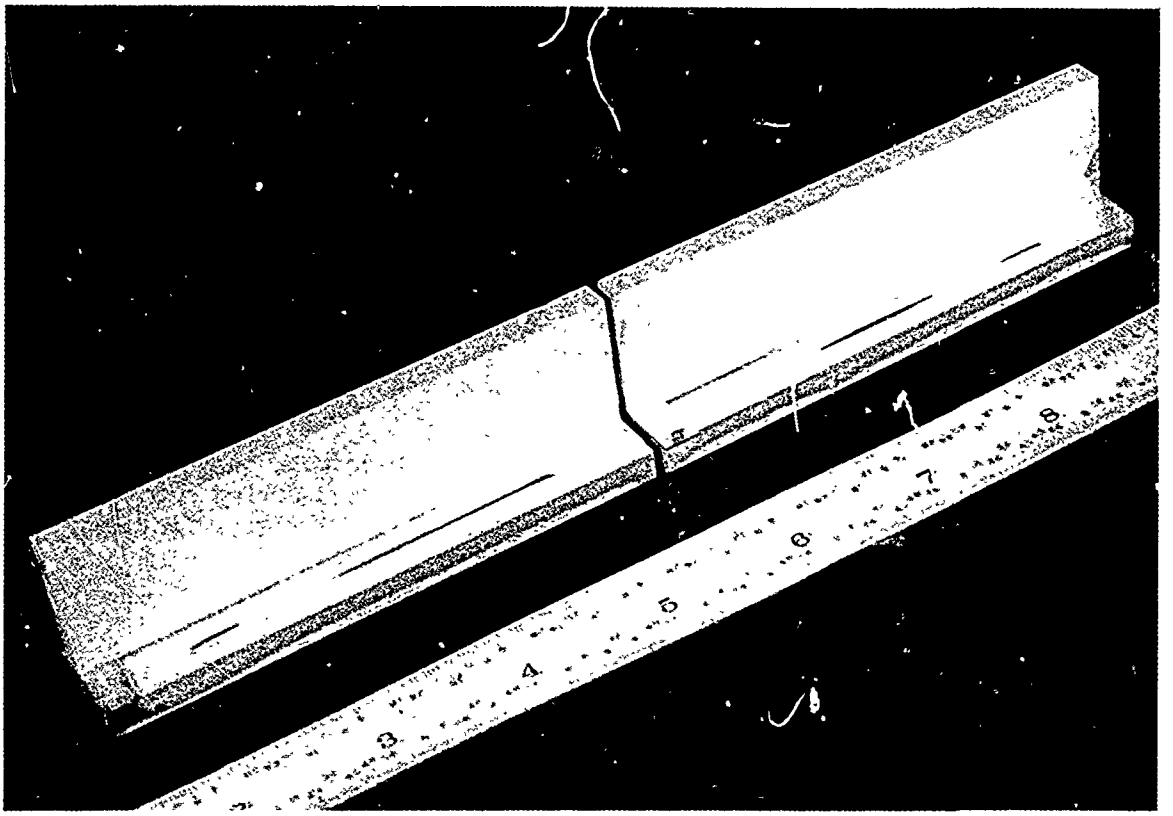

Bridging test specimen Type "B" after brazing with a gap varying from 0 at contact end to 0.020 at shim. 718 braze alloy specimen is shown to the right. 4045 alloy specimen is at the left.

Figure 4-28

SECTION 5.0

LOW PRESSURE DIFFUSION BONDING

5.1 Scope and Approach

This investigation concerned low pressure diffusion bonding as a possible alternate approach to fluxless brazing aluminum alloys. Base metal aluminum and filler metal alloys (interleaf) evaluated were commercially available. This section of the report covers the determination of optimum bonding cycles for simple lapped joints only.

Because aluminum alloys have critically low resistance to buckling at the state-of-the-art brazing temperatures, it was considered advisable to evaluate low pressure bonding only. Also, because of the need to restrict the bonding pressure, it was desirable to create an optimum thermodynamic interface, which was metallurgically compatible. Thus, the use of an interleaf alloy offering these properties was adjudged necessary.

Optimum control of diffusion when brazing thin members normally requires precise controlling of both time and temperature during the wetting and flow portion of the brazing cycle. This is especially critical for the state-of-the-art brazing of aluminum alloys. Thus, diffusion bonding, in this respect, offered a decided advantage inasmuch that the joining would be accomplished at temperatures below that of brazing.

Each material combination (system) was subjected to an ordered series of bonding cycle investigations, which determined the pressure-time bonding cycle having the optimum shear strength and microstructure. All investigations (bonding cycles) were conducted at 1040 F. Specimen (lap shear) bonded with selected cycles were subjected to lap shear testing at cryogenic, room, and elevated temperatures. Elevated temperature times were extended to 25, 50 and 100 hours. The affect of thermal environments was also determined microscopically.

Candidate materials evaluated:

Base metal aluminum alloys - - - - 3003, 6061, 6951, 7005
Interleaf alloys - - - - - - - - - 4045, 718

Each base metal aluminum alloy was investigated with both interleaf alloys, making a total of eight (8) material combination systems.

5.2 Summary of Results

The 3003 alloy is not suitable for low pressure metal to metal diffusion bonding with the 4045-718 interleaf alloys. However, the balance of the base metal alloy joints, with either both/or

one of the interleafs exhibited good structural lap shear strengths.

The 6061-718 base metal aluminum alloy and interleaf alloy system exhibited massive transcrystalline grain growth when subjected to extended elevated thermal environments at 350 F and above, and may be susceptible to a lowered fatigue endurance limit in this condition. The balance of the material combinations exhibited excellent shear strength between -300 F and 500 F, with good microstructure.

Surface preparation of interfaces for diffusion bonding is critical. The omission of a final overspray rinse on one batch of 6061 specimen resulted in a lowering of room temperature shear values of up to 35 percent. Excessive interface buffering was evident. (Reported in section 5.5)

Because of the high plasticity of aluminum at 1040 F, interface metal surface finishes between 20 RMS and 110 RMS had no significant effect on shear values of bonded joints.

5.3 Evaluation of Low Pressure Diffusion Bonding Cycles

A series of experimental diffusion bonding cycles for metal to metal lapped joints for eight material combinations were investigated. The method for enveloping the work and obtaining bonding pressures is illustrated in Figure 5-1.

Diffusion Bonding Work Package Layup

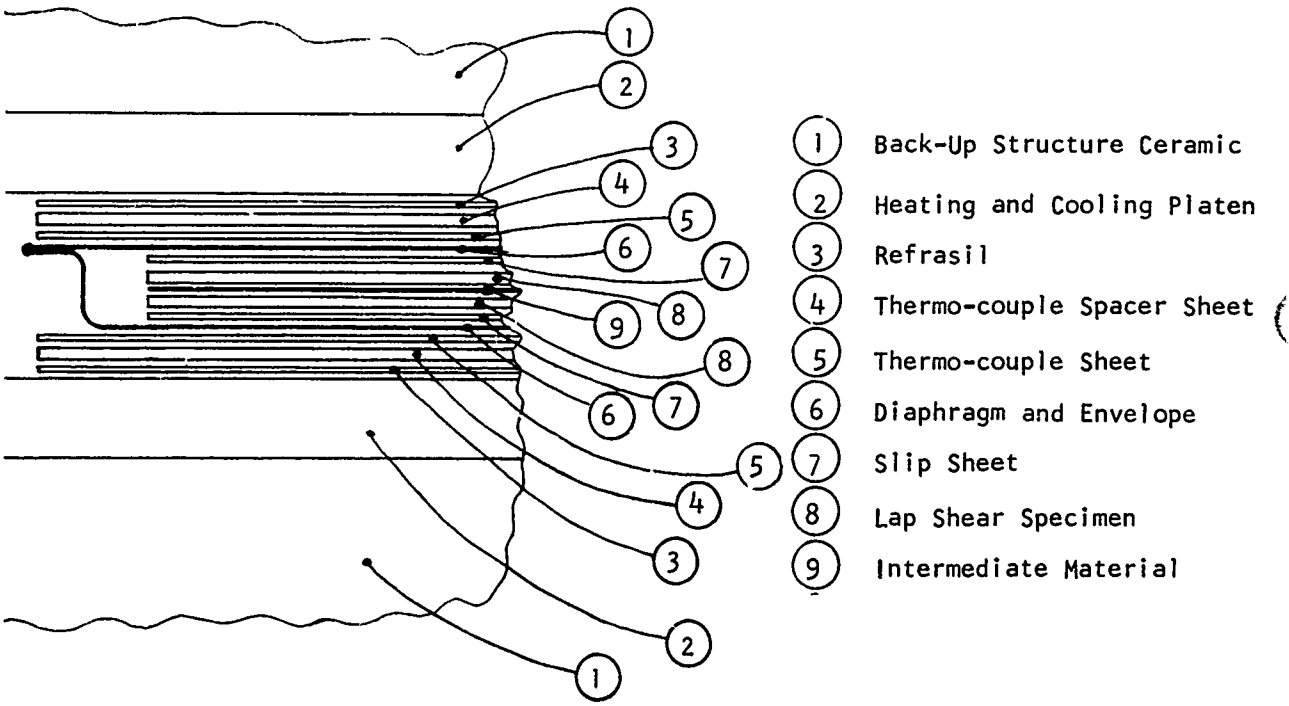

Figure 5-1

Bonding pressures were obtained by evacuating the envelope (Item 6), and using the differential pressure between the envelope interior and ambient, to react through the envelope diaphragms. Added pressure was obtained by allowing the dead weight of the upper portion of the unit tool (Items 1 and 2) to press on the top diaphragm. Work buildup height inside the envelope was approximately 0.010 inches greater than the inside height of the envelope. This assured that the dead weight would react against the work. By changing the area of work (lapped specimen) different pressures were calculated and used.

Initial screening of bonding cycles using a 1040 F constant temperature and varying the pressure time cycles included an evaluation of room temperature lap shear values and also investigations of each joint microstructure.

Room temperature shear values for the 6061, 6951, and 7005 base metal alloys using both interleaf alloys was found to equal that of brazed joints. The 3003 alloy exhibited low joint strengths, and poor metallurgical interface structures. This condition was only slightly improved by increasing both time and pressure beyond that required for the other material combinations.

Table 5-1 summarizes room temperature shear values obtained from the initial experimental bonding cycles used to screen each material system.

Experimental Shear Values[3] vs Varied Bonding Cycles

Mat'l. System No.	Base Al Alloy Type	Interleaf Alloy Type	Bonding Pressure (PSI)	Bonding Temp. (°F)	Bonding Time (Mins)	Average Shear (KSI)[1]	Interleaf Form
1	6951	4045	24	1040	60	10.4	Cladding
1	"	"	34	"	"	13.7	"
1	"	"	54	"	"	23.6	"
1	"	"	54	"	45	11.5	"
1	"	"	54	"	30	10.4	"
1a	"	718	24	"	60	12.2	Foil
1a	"	"	34	"	"	14.2	"
1a	"	"	54	"	"	17.1	"
1a	"	"	"	"	45	15.1	"
1a	"	"	"	"	30	15.1	"
2	7005	4045	24	"	60	20.0	Cladding
2	"	"	34	"	"	16.5	"
2	"	"	54	"	"	21.5	"
2	"	"	"	"	45	20.6	"
2	"	"	"	"	30	14.0	"
2a	"	718	24	"	60	11.5	Foil
2a	"	"	34	"	"	18.6	"
2a	"	"	54	"	"	17.9	"
2a	"	"	54	"	45	19.4	"
2a	"	"	54	"	30	20.8	"
3	6061	4045	54	"	30	-	Cladding
3	"	"	"	"	45	13.8	"
3	"	"	"	"	60	21.4	"
3a	"	718	"	"	30	17.4	Foil
3a	"	"	"	"	45	18.8	"
3a	"	"	"	"	60	23.0	"
4	3003	4045	"	"	30	5.7	Cladding
4	"	"	"	"	45	6.0	"
4	"	"	"	"	60	7.0	"
4	"	"	"	"	75	7.8	"
4	"	"	94	"	75	10.8	"
4a	"	718	54	"	30	(2)	Foil
4a	"	"	"	"	45	(2)	"
4a	"	"	"	"	60	(2)	"
4a	"	"	"	"	75	(2)	"
4a	"	"	94	"	"	2.9	"

(1) Average of three specimen except where noted
(2) Broke during machining of specimen
(3) Shear values at room temperature

Table 5-1

In reviewing the Table 5-1 results, it will be seen that the 6061 alloy was not evaluated at any joining pressure other than the 54 PSI. This alloy was the fourth to be evaluated. Based on the results obtained with the 6951 and 7005 alloys, it appeared necessary only to investigate the effect of varying the time at 1040 F.

The 718 interleaf exhibited poor compatability with the 3003 interface. Increasing the time 20 percent and the pressure 74 percent over and above that of the optimum cycles used for the balance of the candidate alloys produced only a slight improvement. The 3003-4045 system, with the increased pressure and time exhibited an improved joint, both in strength and metallurgical structure over that of the 3003-718 system, but fell well below the Type 1, 2, and 3 systems in both strength and interface microstructure quality. On this basis, the 3003 base metal alloy was rejected as a candidate material for low pressure diffusion bonding.

A review of the microstructures of each series of bonded joints provided significant data on the effect of varying the pressure and times. From this data it was possible to establish the optimum low pressure bonding cycles for each of the systems. Table 5-2 which was based on this review, and further confirmed under both cryogenic and elevated temperature environment testing summarizes the selected bonding cycles.

Optimum Diffusion Bonding Cycles

Material System Combination	Bonding Cycle		
	Temp. ^{o}F	Pressure (PSI)	Cycle Time (Mins)
6951-4045	1040	54	60
6951-718	1040	54	60
7005-4045	1040	54	45
7005-718	1040	54	30
6061-4045	1040	54	60
6061-718	1040	54	60

Table 5-2

In the event that a combination of the 7005 and 6061 alloys is considered, the above selected bonding cycles would not be applicable, however, a 45 minute cycle in lieu of either the 30 minute or 60 minute cycle would be suitable as a compromise, with only a slight lowering of the joint quality.

The following subsections provide a review of the diffusion bonded joint microstructures evaluated during the bonding cycle optimization investigation.

5.3.1 Effect of Varied Pressures and Times on Joint Microstructures System Number 1 (6951-4045)

Bonding at 24 PSI - 60 Minutes	35 percent voids existed at interface.
Bonding at 34 PSI - 60 Minutes	Minor porosity existed at interface with idiomorphic crystals shown buffered at interface.
Bonding at 54 PSI - 60 Minutes	No interface porosity with considerable reduction in buffer effect.
Bonding at 54 PSI - 45 Minutes	Intermittent hair line voids; buffer effect greater than above.
Bonding at 54 PSI - 30 Minutes	Intermittent hair line voids and severe buffer effect.

Original wrought structure of the intermediate material was effected more by increasing the bonding cycle time than by increasing the bonding pressure.

Grain sizes of the 4045 intermediate material were fine. Specimen required over etching to bring out grain boundaries.

Typical photomicrographs of joints bonded at 54 PSI, 30 and 60 minutes, are presented in Figure 5-2 which illustrates the minimization of buffer effect by increasing the cycle time.

Figure 5-2

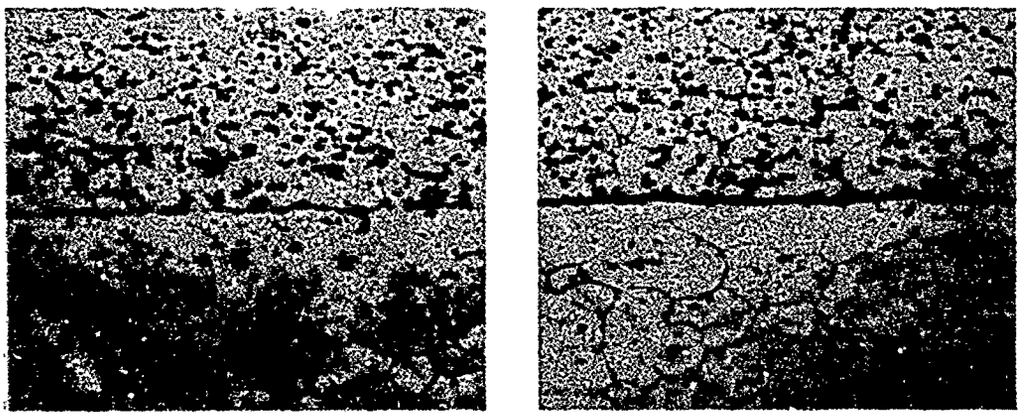

Boric Acid HF Etched - Mount #466
250X. Bonding Cycle-54 PSI, 60 Min

Boric Acid HF Etched - Mount #503
250X. Bonding Cycle-54 PSI, 30 Min

6951-4045 Bonded Joint System

5.3.2 Effect of Varied Pressures and Times on Joint Microstructures System Number 1a (6951-718)

Bonding at 24 PSI - 60 Minutes	14 percent voids existed at interface - severe buffer effect.
Bonding at 34 PSI - 60 Minutes	No interface porosity, initial transcrystalline growth across interfaces evident; slight buffer effect.
Bonding at 54 PSI - 60 Minutes	No apparent retention of original interfaces.
Bonding at 54 PSI - 45 Minutes	Considerable buffer effect.
Bonding at 54 PSI - 30 Minutes	Severe buffer effect.

The review of the 6951-718 material system results showed that the conditions for achieving a bonded joint, free of interface porosity and migratory constituents was less dependent on time, above 30 minutes, than of pressure.

Original wrought structure of the intermediate material was effected more by increasing the bonding cycle time than by increasing the bonding pressure.

Grain size of the 718 intermediate material was fine.

Specimen required over etching to bring out grain boundaries.

Figure 5-3

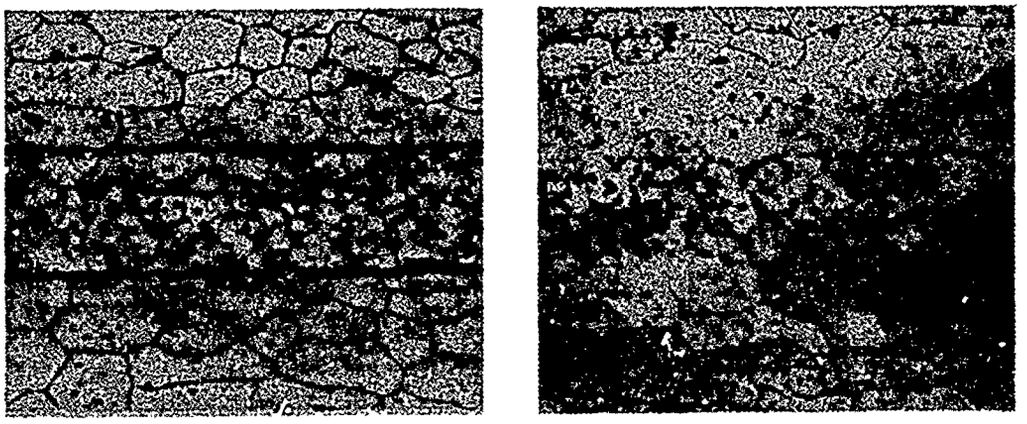

Boric Acid HF Etched - Mount #442
250X. Bonding Cycle-24 PSI-60 Mins.

Boric Acid HF Etched - Mount #466
250X. Bonding Cycle-54 PSI-60 Mins.

6951-718 Bonded Joint System

5.3.3 Effect of Varied Pressures and Times on Joint Microstructures System Number 2 (7005-4045)

Bonded at 24 PSI - 60 Minute Cycle	Slight trace of original interface with evidence of transcrystalline growth between components.
Bonded at 34 PSI - 60 Minute Cycle	Slight trace of original interface with large transcrystalline growth between components.
Bonded at 54 PSI - 60 Minute Cycle	Same as above.
Bonded at 54 PSI - 45 Minute Cycle	Same as above.
Bonded at 54 PSI - 30 Minute Cycle	Considerable retention of original interface with apparent coalescence; transcrystalline growth evident.

Idiomorphic crystals were mainly retained inter- and intragranually rather than at the component interface of the 4045 material. This is illustrated in Figures 5-4 through 5-4d.

Figure 5-4

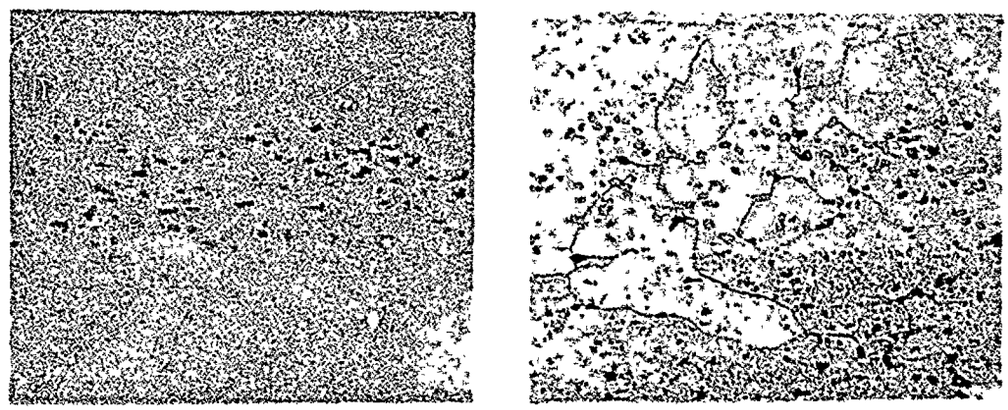

Bonding Cycle (24 PSI-60 Min.)
Unetched - Mount #458 - 250X

Bonding Cycle (24 PSI-60 Min.)
Keller Etched - 250X - Mount #458

7005-4045 Bonded Joint System

Boric Acid HF Etched - 250X
Mount #464 - Bonding Cycle
34 PSI - 60 Mins.

Figure 5-4a

Boric Acid HF Etched - 250X
Mount #467 - Bonding Cycle
54 PSI - 60 Mins.

Figure 5-4b

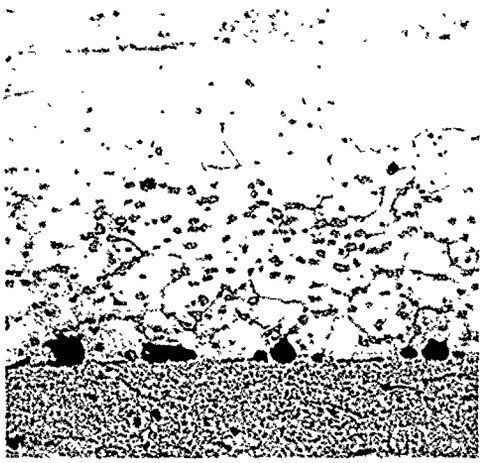

Boric Acid HF Etched - 250X
Mount #499 - Bonding Cycle
54 PSI - 45 Mins.

Figure 5-4c

Boric Acid HF Etched - 250X
Mount #503 - Bonding Cycle
54 PSI - 30 Mins.

Figure 5-4d

7005 - 4045 Bonded Joint System

5.3.4 Effect of Varied Pressures and Times on Joint Microstructures System Number 2a (7005-718)

Bonded at 24 PSI - 60 Minute Cycle	Considerable transcrystalline growth between components; grain size excessive.
Bonded at 34 PSI - 60 Minute Cycle	As above, with considerable idiomorphic crystals segregated to the center of the intermediate material.
Bonded at 54 PSI - 60 Minute Cycle	Very similar to above.
Bonded at 54 PSI - 45 Minute Cycle	As above.
Bonded at 54 PSI - 30 Minute Cycle	Metallurgical structure of complete joint superior to preceding. Grain size acceptable with uniformly dispersed alloying constituents.

Metallurgically, the joints bonded at 54 PSI with 30 minute cycle were superior to the balance of this series.

The heavy concentrations of idiomorphic (γ constituent) crystals located at grain boundaries generally through the center of the intermediate material show some pseudo coring effect, this is best illustrated in Figure 5-5c. This condition was overcome by reducing the bonding cycle to 30 minutes.

The coalescence of the major alloying constituent of the interleaf alloy increased with time.

Figure 5-5

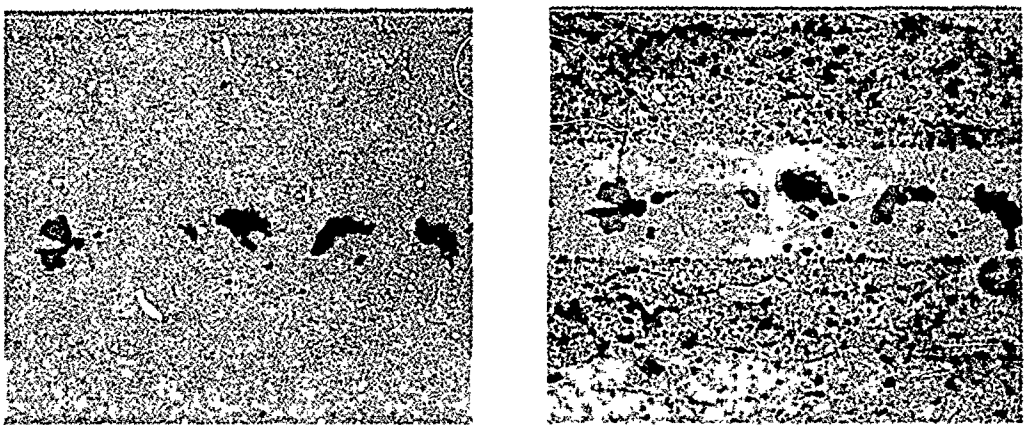

Unetched - Mount #458 - 250X

Keller Etched - Mount #458 -250X
Bonding Cycle - 24 PSI - 60 Mins.

7005 - 718 Bonded Joint System

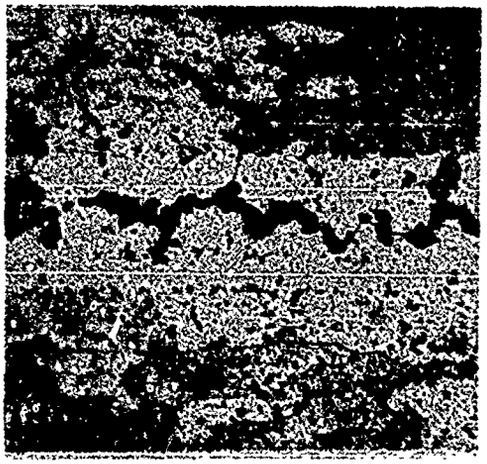

Boric Acid HF Etched - Mount #466
250X - Bonding Cycle - 34 PSI -
60 Mins.

Figure 5-5a

Boric Acid HF Etched - Mount #467
250X - Bonding Cycle - 54 PSI -
60 Mins.

Figure 5-5b

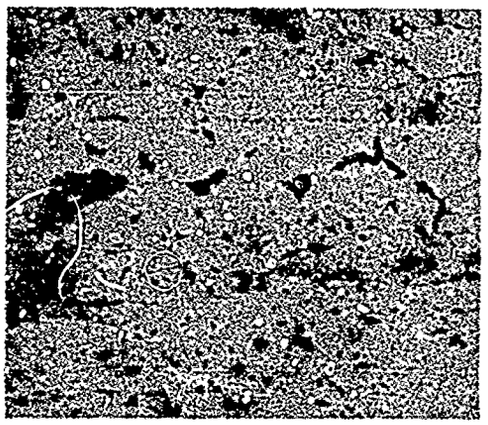

Boric Acid HF Etched - Mount #499
250X - Bonding Cycle - 54 PSI -
45 Mins.

Figure 5-5c

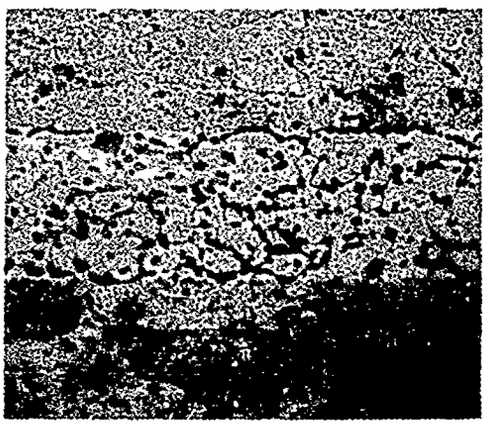

Boric Acid HF Etched - Mount #503
250 X - Bonding Cycle - 54 PSI -
30 Mins.

Figure 5-5d

7005 - 718 Bonded Joint System

5.3.5 Effect of Varied Pressures and Times on Joint Microstructures System Number 3 (6061-4045)

Bonded at 54 PSI - 30 Minute Cycle	Intermittent mass movement across interface with slight transcrystalline growth.
Bonded at 54 PSI - 45 Minute Cycle	Similar to preceding.
Bonded at 54 PSI - 60 Minute Cycle	Increased in original interface breakdown, with increased mass movement and coalescence of interleaf constituent. Transcrystalline growth essentially complete, boundary extensions into the interleaf material were difficult to etch.

Figure 5-6

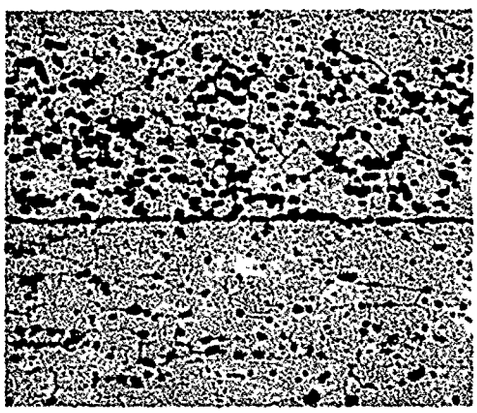

Typical microstructure of 6061-4045 bonded joint system bonded at 54 PSI and 30 minute time cycle.

Mount #552
Magnification 250X
Boric Acid HF Etched

Figure 5-6a

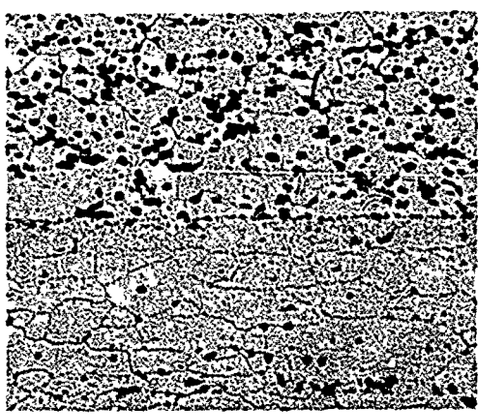

Typical microstructure of 6061-4045 bonded joint system bonded at 54 PSI and 60 minute time cycle.

Mount #552
Magnification 250X
Boric Acid HF Etched

6061 - 4045 Bonded Joint System

5.3.6 Effect of Varied Pressures and Times on Joint Microstructures System Number 3a (6061-718)

Bonded at 54 PSI - 30 Minute Cycle	Considerable breakdown of original interface with some transcrystalline growth.
Bonded at 54 PSI - 45 Minute Cycle	Increase in interface breakdown and transcrystalline growth over the 30 minute cycle. Slight coalescence of interleaf constituent.
Bonded at 54 PSI - 60 Minute Cycle	Essentially a complete interface breakdown with satisfactory transcrystalline growth. Slight increase of coalescence of constituents over the 45 minute cycle.

Figure 5-7

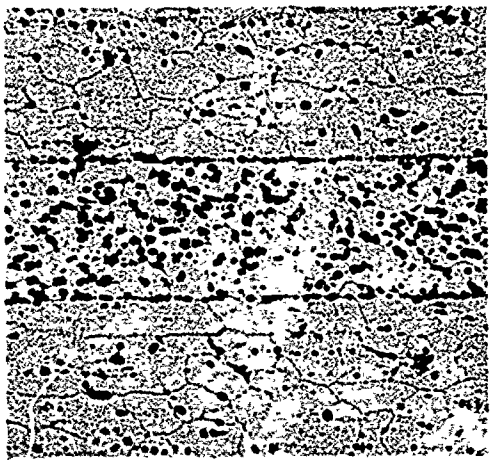

Typical microstructure of 6061 and 718 system bonded at 54 PSI and 30 minute time cycle.

Mount #552
Magnification 250X
Boric Acid HF Etched

Figure 5-7a

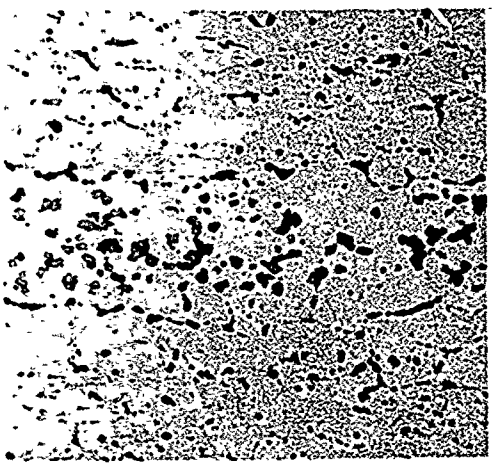

Typical microstructure of 6061 and 718 system bonded at 54 PSI and 60 minute time cycle.

Mount #553
Magnification 250X
Boric Acid HF Etched

6061 - 718 Bonded Joint System

5.3.7 Effect of Varied Pressures and Times on Joint Microstructures Sy tem Number 4 (3003-4045)

Bonded at 54 PSI - 30 Minute Cycle	Evidence of original interface breakdown with fair cohesive interface bonding.
Bonded at 54 PSI - 45 Minute Cycle	Very similar to preceding.
Bonded at 54 PSI - 60 Minute Cycle	Increase in original interface breakdown.
Bonded at 54 PSI - 75 Minute Cycle	Similar to preceding.
Bonded at 94 PSI - 75 Minute Cycle	Interface breakdown percent exceeded previous lower pressure and same time cycle.

Figure 5-8

Typical microstructure of 3003 and 4045 system bonded at 54 PSI and 30 minute time cycle.

Mount #554
Magnification 250X
Boric Acid HF Etched

Figure 5-8a

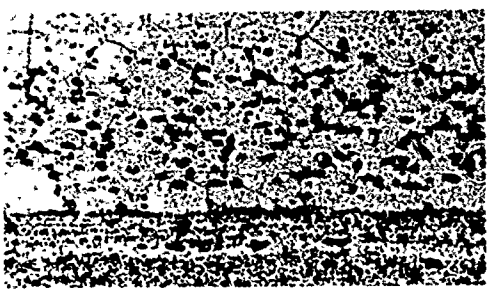

Typical microstructure of 3003 and 4045 system bonded at 54 PSI and 75 minute time cycle.

Mount #579
Magnification 250X
Boric Acid HF Etched

Figure 5-8b

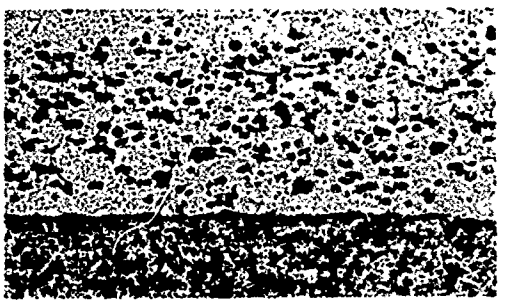

Typical microstructure of 3003 and 4045 system bonded at 94 PSI and 75 minute time cycle.

Mount #554
Magnification 250X
Boric Acid HF Etched

3003 - 4045 Bonded Joint System

5.3.8 Effect of Varied Pressures and Times on Joint Microstructures System Number 4a (3003-718)

Bonded at 54 PSI - 30 Minute Cycle - Retention of original interfaces with minor cohesive interface bonding.

Bonded at 54 PSI - 45 Minute Cycle - Same as Preceding.

Bonded at 54 PSI - 60 Minute Cycle - Same as Preceding.

Bonded at 54 PSI - 75 Minute Cycle - Evidence of initial breakdown of original interface with considerable cohesive interface bonding.

Bonded at 94 PSI - 75 Minute Cycle - Same as Preceding.

Figure 5-9

Typical microstructure of 3003 and 718 system bonded at 54 PSI with 75 minute time cycle.

Mount #549
Magnification 250X
Boric Acid HF Etched

Figure 5-9a

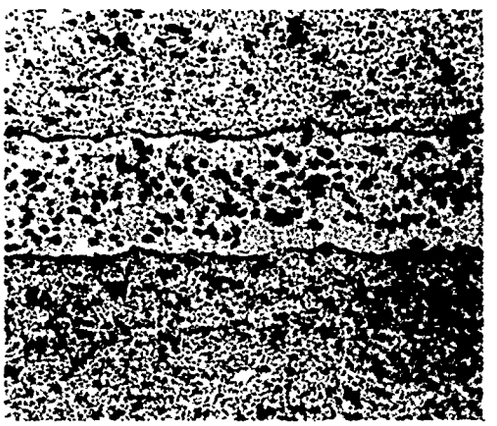

Typical microstructure of 3003 and 718 system bonded at 94 PSI with 75 minute time cycle.

Mount #579
Magnification 250X
Boric Acid HF Etched

3003 - 718 Bonded Joint System

5.4 Effect of Cryogenic and Elevated Temperatures on the 6951, 7005 and 6061 Aluminum Alloy Diffusion Bonded Joints

Lap shear bonded specimen were prepared and tested at -300 F, 300 F, 350 F, and 500 F. At each elevated temperature the specimen were held for 10 minutes, 25 hours, 50 hours, and 100 hours. Specimen base metal alloys were 7005, 6951, and 6061; each of which were joined with the 4045 and 718 interleaf alloys. Time-temperature-pressure cycles used were as selected in Table 5-2, Subsection 5.3.

Figures 5-10 and 5-11 photographically illustrate the universal testing facility with environmental chamber and specimen loaded for elevated temperature lap shear testing. Soaking at the various temperatures was performed prior to loading using a standard atmosphere convection oven.

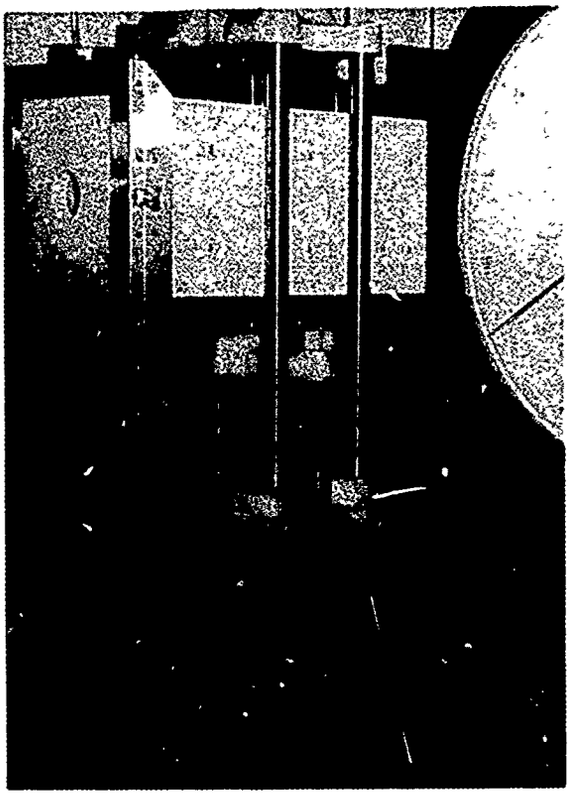

Universal Tester with Marshall Thermal Environment Oven Attached

Figure 5-10

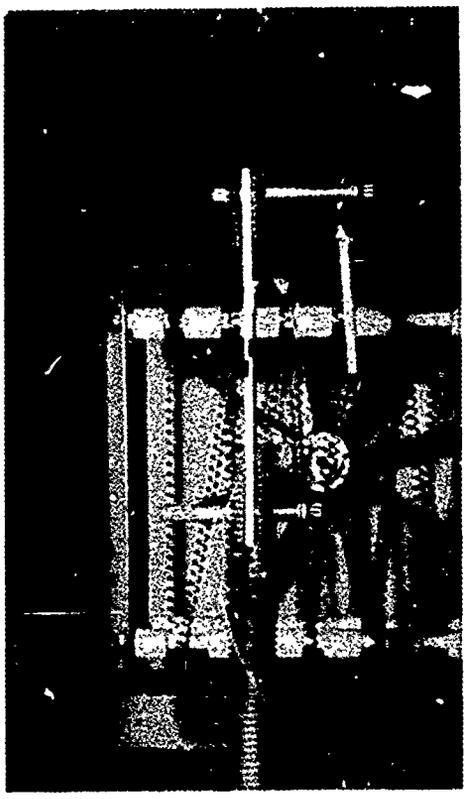

Setup for Lap Shear Testing at Elevated Temperature

Figure 5-11

5.4.1 Thermal Environment Effect on Diffusion Bonded Lapped Joints

Of the six systems evaluated the 6061-718 (Type 3a) system was the only system to exhibit any unusual thermal effects.

The 6061-718 system is extremely susceptible to extended elevated temperature environments. The resistance to temperature initiate breakdown is approximately after 50 hours at 350 F, at which point transcrystalline growth across the original interfaces increases. This growth, together with growth of the 718 grains approaches a massive state by extending the thermal environment period to 100 hours. Similar microstructure changes occur at approximately the same periods of time at 500 F. The microstructure change is considered as being caused by a serious γ' constituent depletion from the bonded areas to the base metal alloy.

All systems as tested exhibited good fracture toughness at -300 F.(1)

The 4045 interleaf generally exhibited the more superior properties, both in joint strength and in metallurgical stability, for the three base metal alloys evaluated.

In reviewing the microstructures of each series of joint specimen, the mechanical strength changes of the interleaf joint strength is seen to be related to precipitation reactions that influence the material's resistance to fracture. With considerable thermal aging, a coherent precipitate state was generally observed. When the thermal aging level was increased or extended, the structures showed noticeable loss in precipitate coherence and an increase in coalescence. This mechanism is associated with increased softness. Since dislocations are held up by internal stresses at the precipitated particles until sufficient stress is applied to force them between these particles, then the stress required to accomplish this dislocation movement, is less with an increase in coalescence, due to an increase in the spacing between particles.

5.4.1.1 Cryogenic and Elevated Temperature Lap Shear Values

The 4045 interleafed joints generally exhibited higher shear values than did the 718 interleafed joints. Specifically, the 1 and 2 Type series (6951-4045 and 7005-4045) shear values were higher at -300 F through 500 F, whereas the Type 3 (6061-4045) shear values were lower than the Type 3a (6061-718 at -300 F and room temperature, but were less susceptible to heat degradation, as their shear strength between 300 F and 500 F was higher than the Type 3a system.

The average shear values obtained are summarized in Table 5-3. Shear properties versus temperature curves are presented in Figures 5-12, 13, 14.

(1) Cryogenic shear test specimen were not subjected to elevated temperature soaking which may affect cryogenic fracture toughness.

5.4.1.2 Effects of Elevated Temperature Environment on Diffusion Bonded Joint Microstructures

Microscopic studies were conducted on diffusion bonded lap joint specimen, for each of the material combination systems having been subjected to elevated temperature environments as listed in Table 5-3.

For clarity, each system is discussed separately in the following:

Microstructure Analysis of the Effect of Elevated Temperatures on the 6951-4045 System

At 300 F, soaking for up to 100 hours caused no detectable microstructure changes which could be determined microscopically. The slight increase in strength after 25 hours and the subsequent loss in strength between 25 hours and 100 hours, must be attributed to an initial precipitation age hardening; continued precipitation out of the solutes produced an overaged effect which would not be detected other than by a loss in strength.

At 350 F overaging could be detected microscopically.

At 500 F, significant overaging precipitation progressively increased up to 100 hours, and loss of grain boundary definiation by constituent depletion and intergranular precipitates were predominate.

No significant coalescence of the interleaf alloying constituent was evident.

Figures 5-15 through 5-17 inclusive, illustrate the progressive affect of heat and time on the microstructure.

Thermal Environment - Lap Shear Values

Mat'l System Number	Base Al Alloy Type	Interleaf Alloy Type	Soak Time (Hrs)	Shear (KSI) vs Temperature(2) -300	RT	300	350	500
1	6951	4045	(1)	28.9	23.6	20.5	13.6	11.7
1	"	"	25	-	-	21.0	13.3	10.1
1	"	"	50	-	-	18.5	12.9	6.7
1	"	"	100	-	-	17.7	13.3	6.9
1a	"	718	(1)	23.3	17.1	14.4	11.5	8.6
1a	"	"	25	-	-	14.3	11.3	7.3
1a	"	"	50	-	-	12.7	10.7	6.8
1a	"	"	100	-	-	13.7	8.9	7.1
2	7005	4045	(1)	31.5	21.5	17.9	16.5	9.9
2	"	"	25	-	-	18.6	16.2	8.0
2	"	"	50	-	-	19.0	12.7	5.7
2	"	"	100	-	-	17.8	11.7	5.5
2a	"	718	(1)	27.6	20.8	16.2	13.0	7.6
2a	"	"	25	-	-	16.1	11.9	6.0
2a	"	"	50	-	-	16.2	11.1	5.9
2a	"	"	100	-	-	15.4	11.2	5.6
3	6061	4045	(1)	29.7	22.4(3)	18.2	17.8	10.5
3	"	"	25	-	-	19.0	16.6	10.4
3	"	"	50	-	-	18.3	14.4	9.2
3	"	"	100	-	-	17.4	13.4	7.0
3a	"	718	(1)	32.2	26.0(3)	17.9	16.4	10.0
3a	"	"	25	-	-	18.3	16.2	10.3
3a	"	"	50	-	-	17.7	14.6	9.8
3a	"	"	100	-	-	15.4	14.2	6.1

(1) Short time at temperature
(2) Average of three specimen
(3) Reinvestigated for nonrepeatable result - problem determined, resolved, and reported in Section 5.5.

Table 5-3

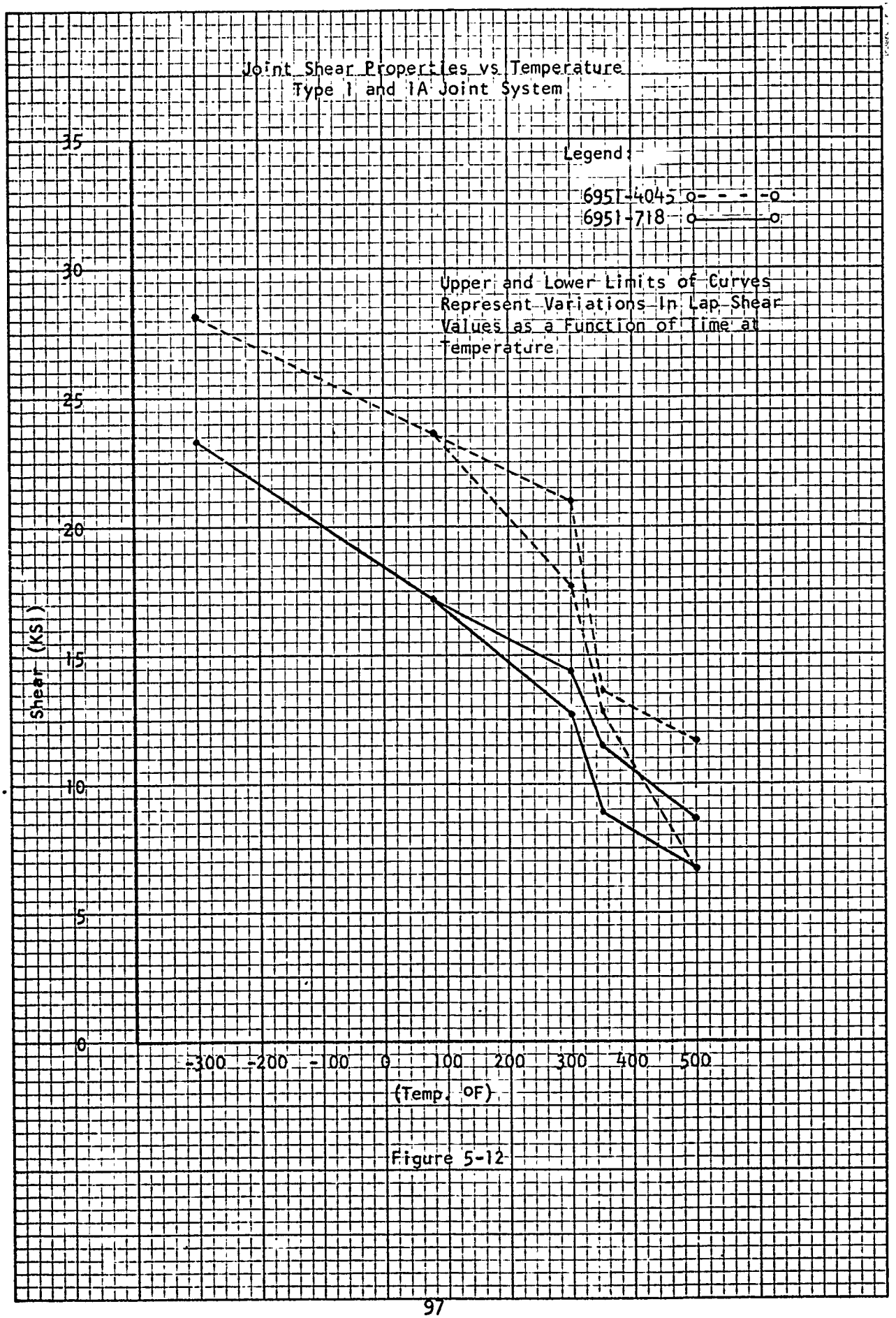
Joint Shear Properties vs Temperature
Type 1 and 1A Joint System
Legend:
6951-4045 o- - - -o
6951-718 o———o
Upper and Lower Limits of Curves Represent Variations In Lap Shear Values as a Function of Time at Temperature
Shear (KSI)
35
30
25
20
15
10
5
0
-300 -200 -100 0 100 200 300 400 500
(Temp. oF)

Figure 5-12

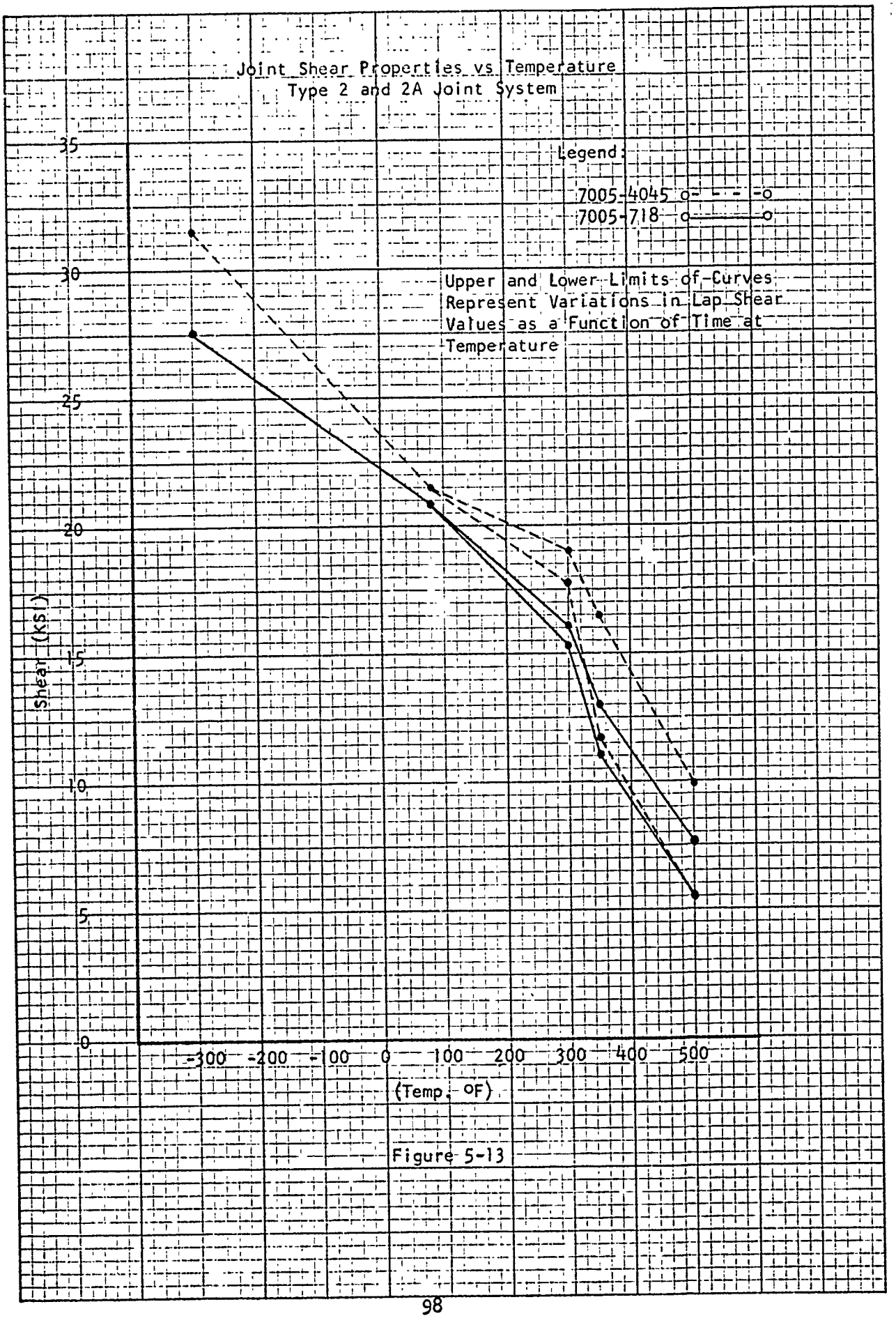
Joint Shear Properties vs Temperature
Type 2 and 2A Joint System
Legend:
7005-4045 o- - - -o
7005-718 o——o
Upper and Lower Limits of Curves Represent Variations in Lap Shear Values as a Function of Time at Temperature
Shear (KSI)
35
30
25
20
15
10
5
0
-300
-200
-100
0
100
200
300
400
500
(Temp. °F)

Figure 5-13

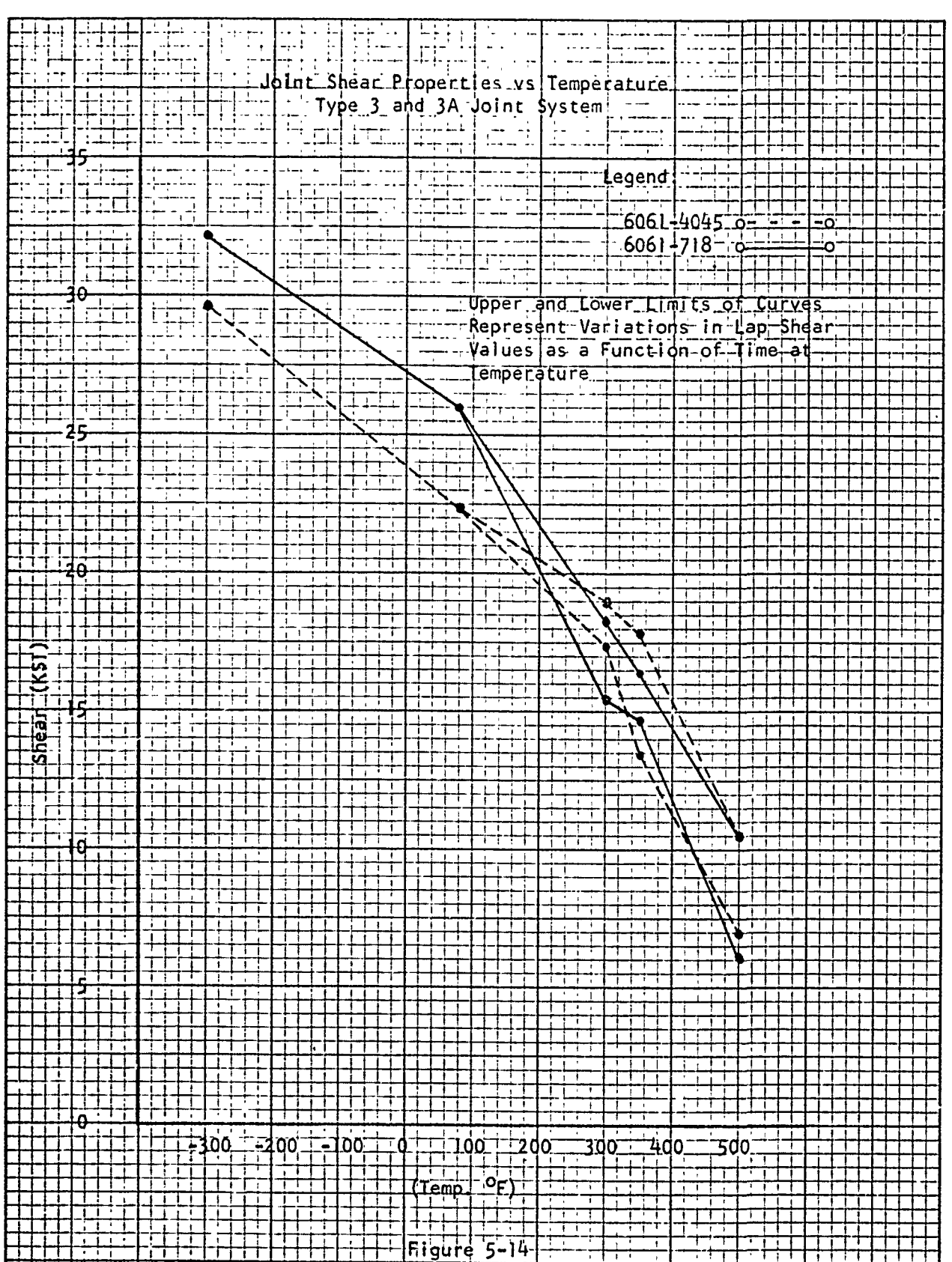
Joint Shear Properties vs Temperature
Type 3 and 3A Joint System
Legend
6061-4045 o- - - -o
6061-718 o——o
Upper and Lower Limits of Curves Represent Variations in Lap Shear Values as a Function of Time at Temperature
Shear (KST)
35
30
25
20
15
10
5
0
-300
-200
-100
0
100
200
300
400
500
(Temp °F)

Figure 5-14

Mount #559
Magnification - 250X
Soak Time - 10 Minutes

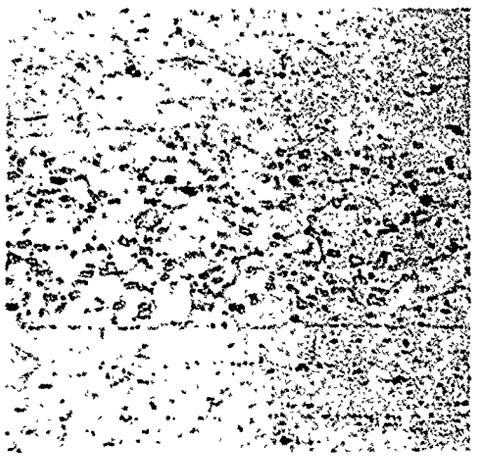

Mount #563
Magnification - 250X
Soak Time - 25 Hours

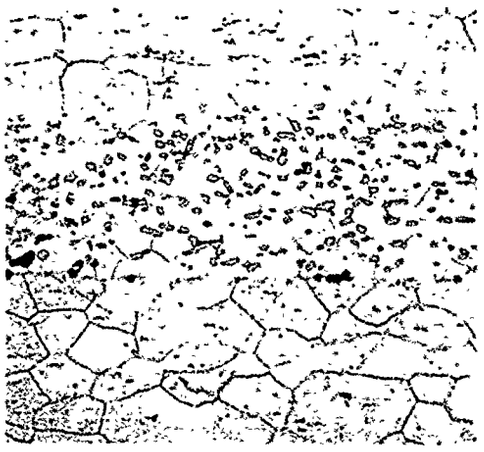

Mount #569
Magnification - 250X
Soak Time - 50 Hours

Mount #573
Magnification - 250X
Soak Time - 100 Hours

Microstructures of 6951-4045 System Showing Short Time Through 100 Hours at 300 F Environment Effect

Figure 5-15

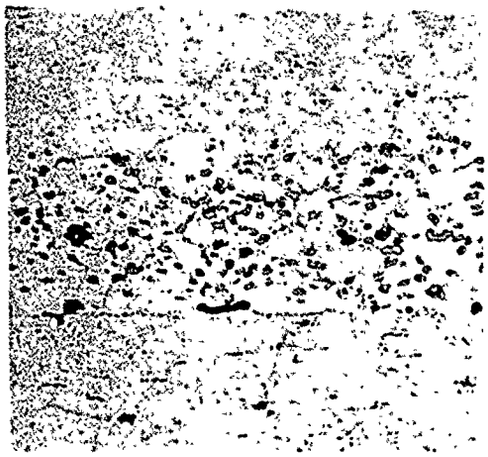

Mount #560
Magnification - 250X
Soak Time - 10 Minutes

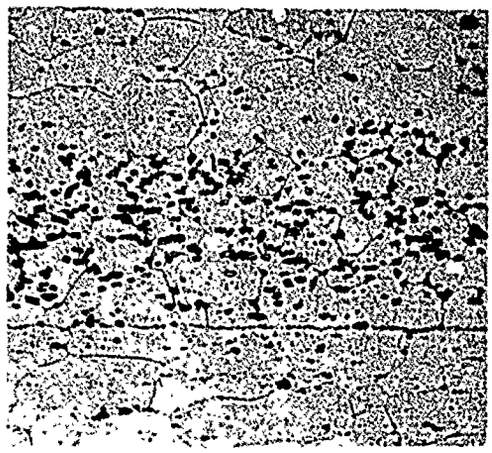

Mount #564
Magnification - 250X
Soak Time - 25 Hours

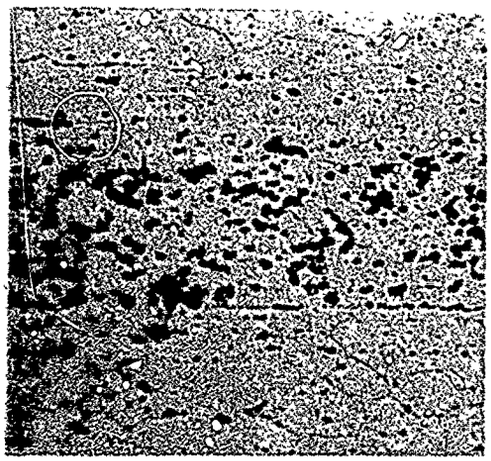

Mount #570
Magnification - 250X
Soak Time - 50 Hours

Mount #574
Magnification-250X
Soak Time - 100 Hours

Microstructure of 6951-4045 System Showing Short Time Through 100 Hours at 350 F Environment Effect

Figure 5-16

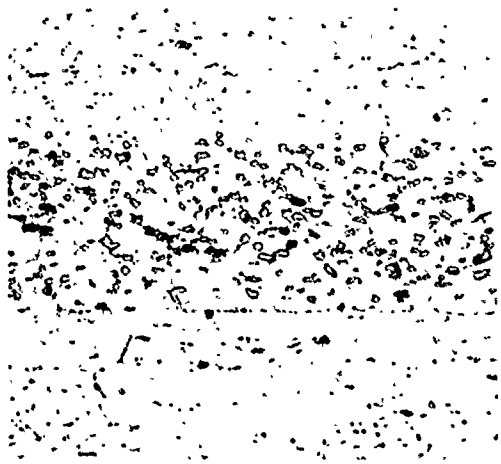

Mount #562
Magnification - 250X
Soak Time - 10 Minutes

Mount #565
Magnification - 250X
Soak Time - 25 Hours

Mount #572
Magnification - 250X
Soak Time - 50 Hours

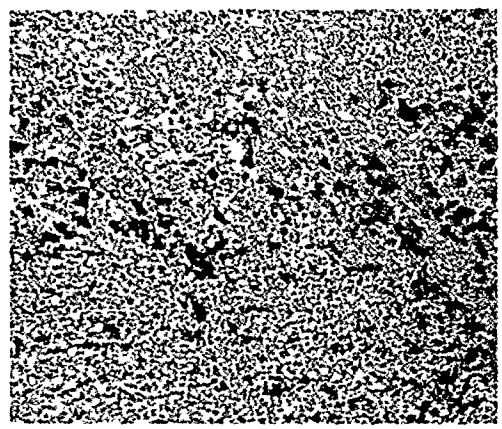

Mount #577
Magnification-250X
Soak Time - 100 Hours

Microstructure of 6951-4045 System Showing Short Time Through 100 Hours at 500 F Environment Effect

Figure 5-17

Microscopic Analysis of Elevated Temperature Environment Effect on the 6951-718 System

No pronounced microstructure changes were observed on the 6951-718 diffusion bonded joints having been subjected to 300 F and 350 F thermal environments of 10 minutes, 25 hours, 50 hours, and 100 hours. However, the 500 F thermal environment soaking showed considerable fine matrix solid solution precipitates throughout both interleaf and parent metal alloy after 25 hours. This mechanism increased through the 50 hour and 100 hour environments. No apparent interleaf constituent coalescence was evident. Figure 5-18 illustrates the precipitation mode discussed in the above.

Mount #559 - Mag 250X
300 F - 10 Minutes
Boric Acid HF Etched

Mount #573 - Mag 250X
500 F - 25 Hours
Boric Acid HF Etched

Mount #565 - Mag 250X
500 F - 50 Hours
Boric Acid HF Etched

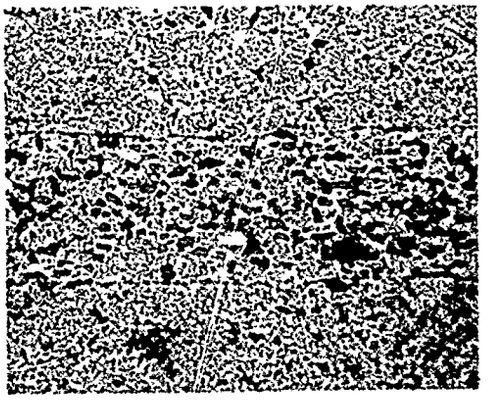

Mount #577 - Mag 250X
500 F - 100 Hours
Boric Acid HF Etched

Microstructure of 6951-718 System Showing Effect of 300 F - 10 Mins., 500 F - 25 Hours, 500 F - 50 Hours, 500 F - 100 Hours Thermal Environment

Figure 5-18

Microscopic Analysis of Elevated Temperature Environment Effect on the 7005-4045 System

No microscopic changes were observed as a result of subjecting the bond joint specimen to 300 F and 350 F thermal environment. The bonded joint specimen subjected to 25 hours, 50 hours, and 100 hours at 500 F, however, showed fine matrix solid solution precipitates throughout the interleaf alloy (4045) matrix. The interleaf alloy grain boundaries showed progressive depletion of material as a function of time, and an increase in coalescence of major precipitates. Figure 5-19 illustrates the joint microstructure with no thermal environment effects vs joints subjected to 500 F for 25 hours, 50 hours, and 100 hours.

Mount #559 - Mag 250X
300 F - 10 Minutes
Boric Acid HF Etched

Mount #565 - Mag 250X
500 F - 25 Hours
Boric Acid HF Etched

Mount #572 - Mag 250X
500 F - 50 Hours
Boric Acid HF Etched

Mount #577 - Mag 250X
500 F - 100 Hours
Boric Acid HF Etched

Microstructure of 7005-4045 System Showing Effect of 300 F-10 Minutes, 500 F-25 Hours, 500 F-50 Hours, 500 F-100 Hours Thermal Environment

Figure 5-19

Microscopic Analysis of Elevated Temperature Environment Effect on the 7005-718 System

Observation of the 7005-718 bonded joint system followed the same trend as did the preceding 7005-4045 system.

Mount #559 - Mag 250X
300 F - 10 Minutes
Boric Acid HF Etched

Mount #565 - Mag 250X
500 F - 25 Hours
Boric Acid HF Etched

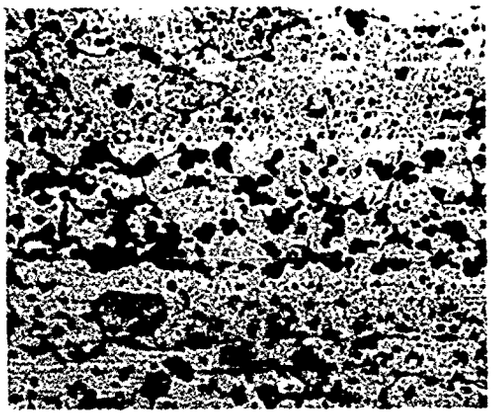

Mount #572 - Mag 250X
500 F - 50 Hours
Boric Acid HF Etched

Mount #577 - Mag 250X
500 F - 100 Hours
Boric Acid HF Etched

Microstructure of 7005-718 System Showing Effect of 300 F for Short Time, and 500 F for 25, 50 and 100 Hours.

Figure 5-20

Microstructure Analysis of Elevated Temperature Environment Effect on the 6061-4045 System

At 300 F and 350 F no significant microstructure changes were detected.

The 500 F environment caused considerable interleaf grain boundary depletion, with typical overaging of the 6061 alloy.

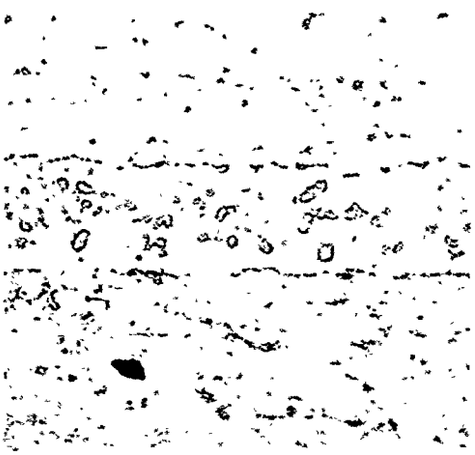

Mount #666
Magnification-250X
Soak Time - 10 Minutes

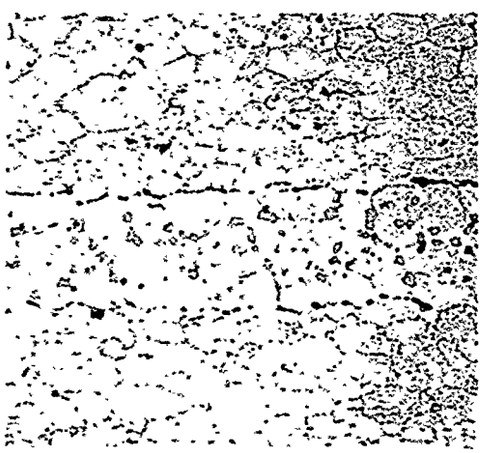

Mount #670
Magnification-250X
Soak Time - 25 Hours

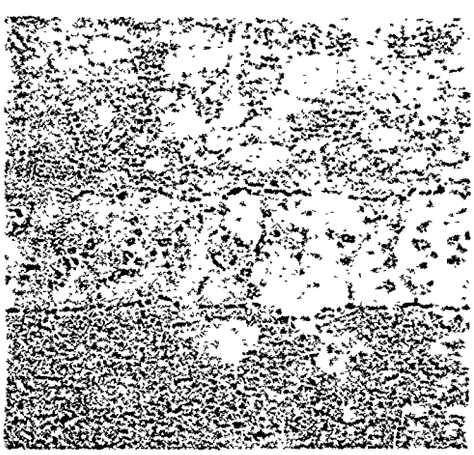

Mount #670
Magnification-250X
Soak Time - 50 Hours

Mount #672
Magnification-250X
Soak Time - 100 Hours

Microstructure of 6061-4045 System Showing Effect of Short Time Through 100 Hours at 300 F Environment.

Figure 5-21

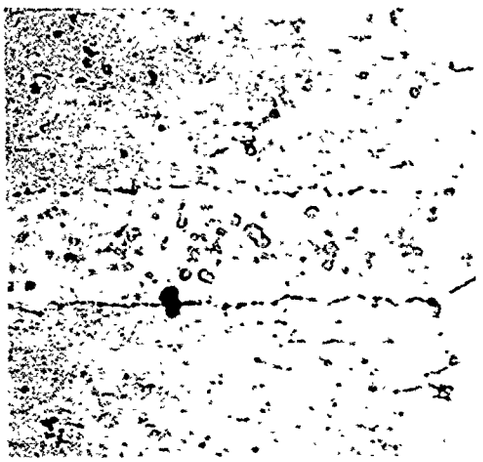

Mount #666
Magnification - 250X
Soak Time - 10 Minutes

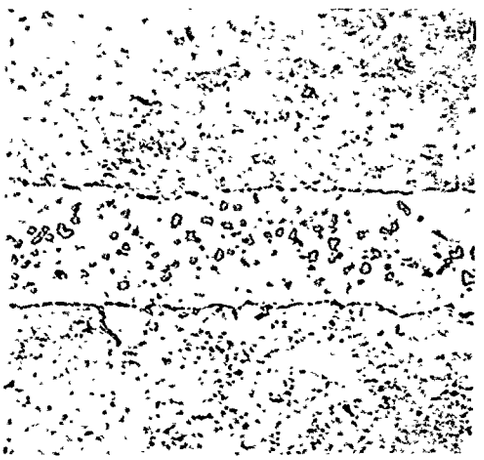

Mount #671
Magnification-250X
Soak Time - 25 Hours

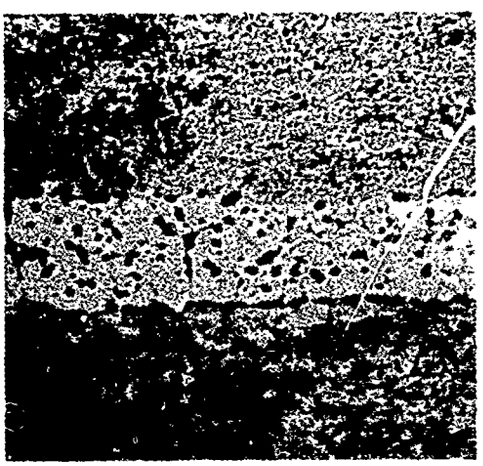

Mount #671
Magnification - 250X
Soak Time - 50 Hours

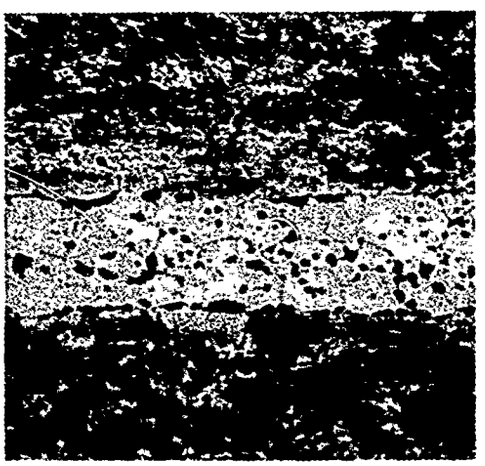

Mount #672
Magnification - 250X
Soak Time - 100 Hours

Microstructure of 6061-4045 System Showing Effect of Short Time Through 100 Hours at 350 F Environment.

Figure 5-21

Mount #668
Magnification-250X
Soak Time - 10 Minutes

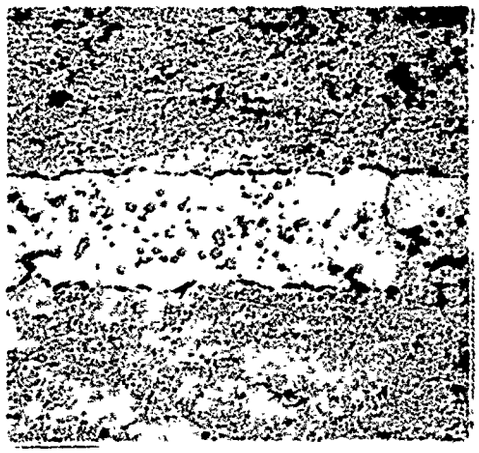

Mount #668
Magnification-250X
Soak Time - 25 Hours

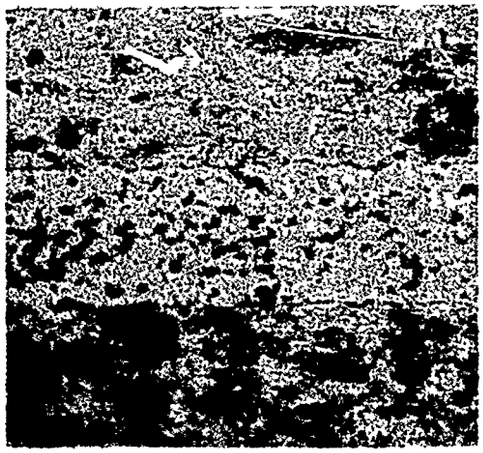

Mount #669
Magnification-250X
Soak Time - 50 Hours

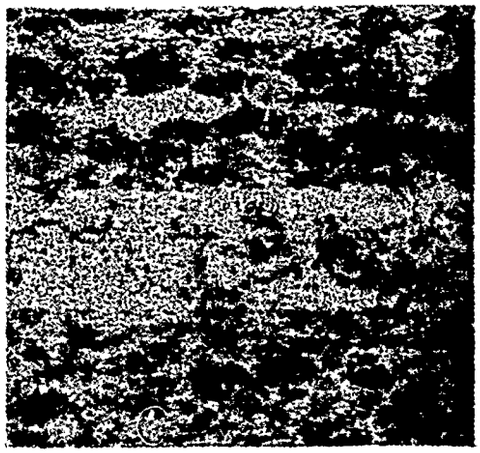

Mount #669
Magnification-250X
Soak Time - 100 Hours

Microstructure of 6061-4045 System Showing Effect of Short Time Through 100 Hours at 500 F Environment.

Figure 5-21

Microstructure Analysis of Elevated Temperature Environment Effect on the 6061-718 System

The 6061-718 system is not suitable for extended thermal environment at 350 F or above.

At 350 F, evidence of transcrystalline growth initiation between grains of both alloys local to original interface was detected after 50 hours. This transformation was massive after 100 hours.

At 500 F, similar microstructure changes were caused by the extended thermal environment between 50 and 100 hours.

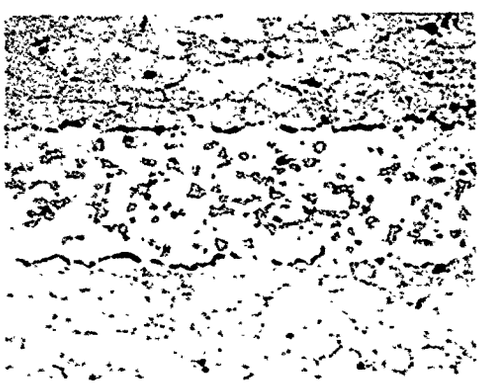

Mount #666
Magnification - 250X
Soak Time - 10 Minutes

Mount #670
Magnification - 250X
Soak Time - 25 Hours

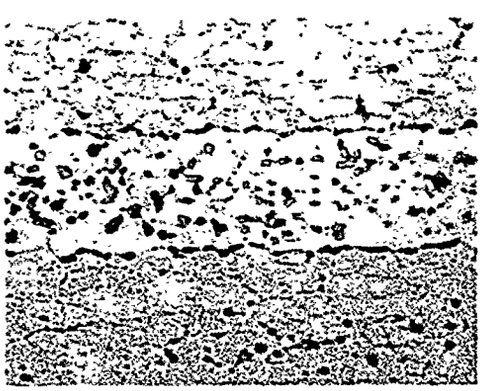

Mount #670
Magnification - 250X
Soak Time - 50 Hours

Mount #670
Magnification - 250X
Soak Time - 100 Hours

Microstructure of 6061-718 System Showing Effect of Short Time Through 100 Hours at 300 F Environment

Figure 5-22

Mount #666
Magnification-250X
Soak Time - 10 Minutes

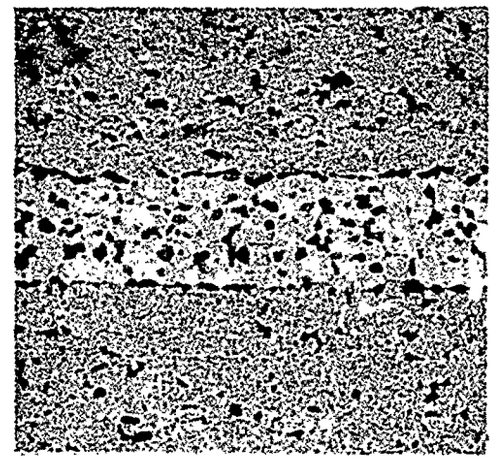

Mount #671
Magnification-250X
Soak Time - 25 Hours

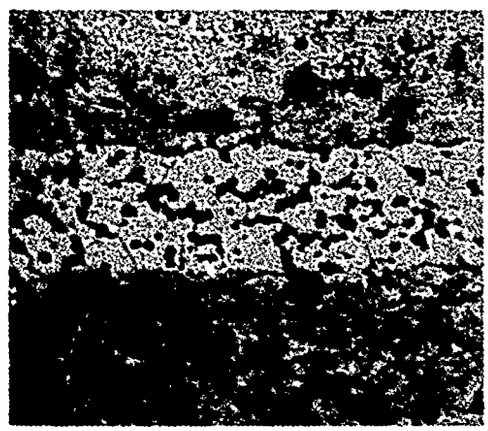

Mount #671
Magnification-250X
Soak Time-50 Hours

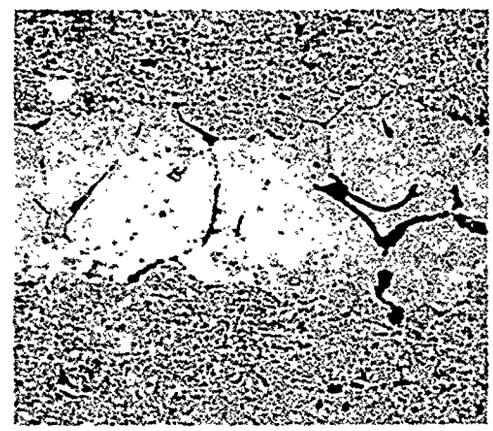

Mount #672
Magnification-250X
Soak Time - 100 Hours

Microstructure of 6061-718 System Showing Effect of Short Time Through 100 Hours at 350 F Environment

Figure 5-22

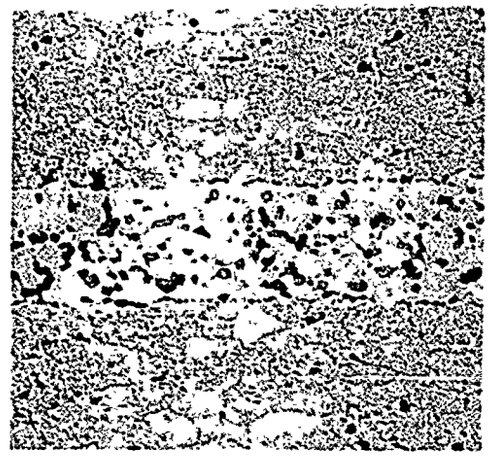

Mount #668
Magnification - 250X
Soak Time - 10 Minutes

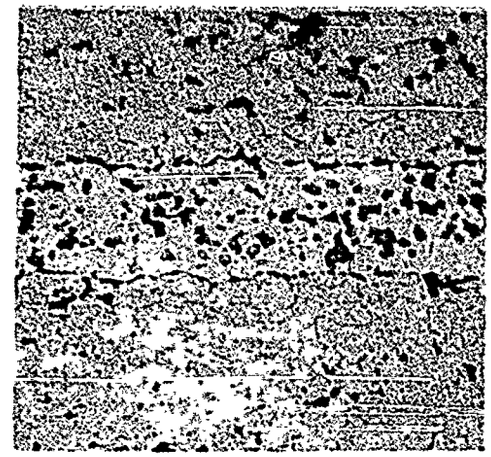

Mount #668
Magnification - 250X
Soak Time - 25 Hours

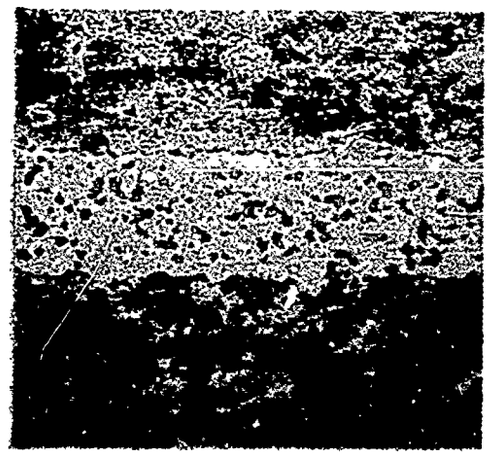

Mount #669
Magnification - 250X
Soak Time - 50 Hours

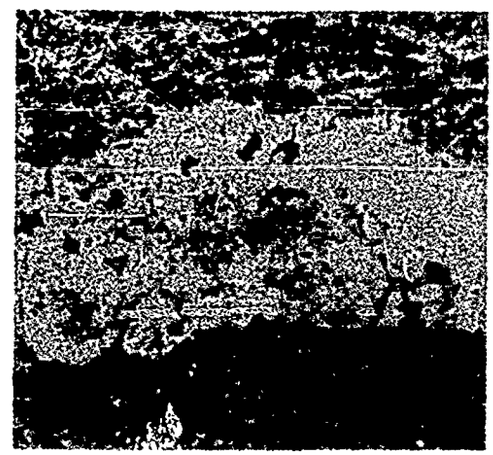

Mount #669
Magnification - 250X
Soak Time - 100 Hours

Microstructure of 6061-718 System Showing Effect of Short Time Through 100 Hours at 500 F Environment

Figure 5-22

5.5 Investigation of Non-Repeatable Joint Strength

All batches of specimen bonded for thermal tests were subjected to random shear tests at room temperature for repeatability of original batch (Number 1) quality.

Specimen for the 6061 base alloy with 4045 and 718 alloy interleaf systems were diffusion bonded at 54 PSI at 1040 F for 60 minutes. Random specimen, heat treated to condition T6, were evaluated at room temperature as a precautionary procedure, to ensure that the joint characteristics were reproducible (equal to that of Batch #1 used to establish the bonding schedule). The interface microstructures showed evidence of excessive buffering. The shear average value differences were as below:

System	Batch #1	Batch #2
6061-4045	21,400 PSI	17,946 PSI
6061-718	23,036 PSI	15,271 PSI

The two areas reviewed for the cause of the low joint quality were: 1) bonding time being inadequate for sufficient mass transfer, and 2) unsatisfactory surface preparation.

It was discovered, after a review of the laboratory notes and records maintained on bonding processes for Batch #2 specimen, that the final demineralized water spray scrubbing rinse had been omitted.

The mechanism involved in diffusion bonding is one of mass interface transfer (atomic migration). Mass transfer as a function of the sum of the mechanical energy plus kinetic energy, is relative to factors such as surface roughness and also buffer films at the interface which do not fall within the general solubility parameters. Therefore, bonding methods based on low mechanical force are logically highly susceptible to buffering of mass transfer by improperly prepared surfaces. In the case of light weight aluminum composites, the forces are necessarily low to avoid undesirable crushing of members.

Figures 5-23 and 5-24 photographically illustrate the final demineralized water immersion and spray scrubbing rinse.

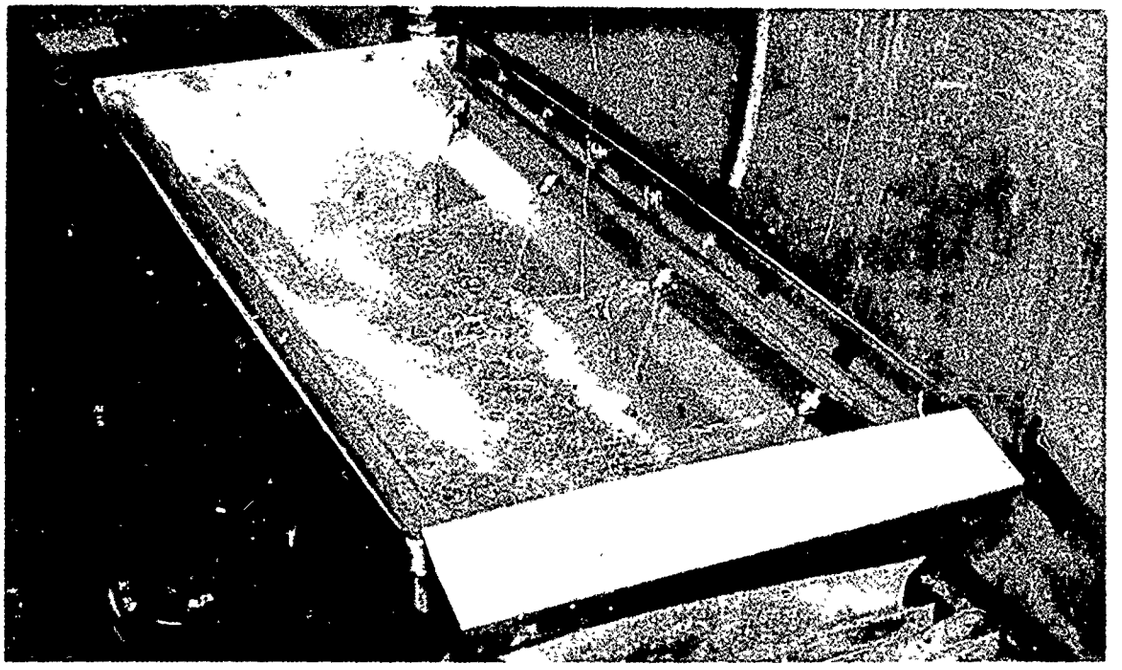

Demineralized Water Spray Rinse System
Figure 5-23

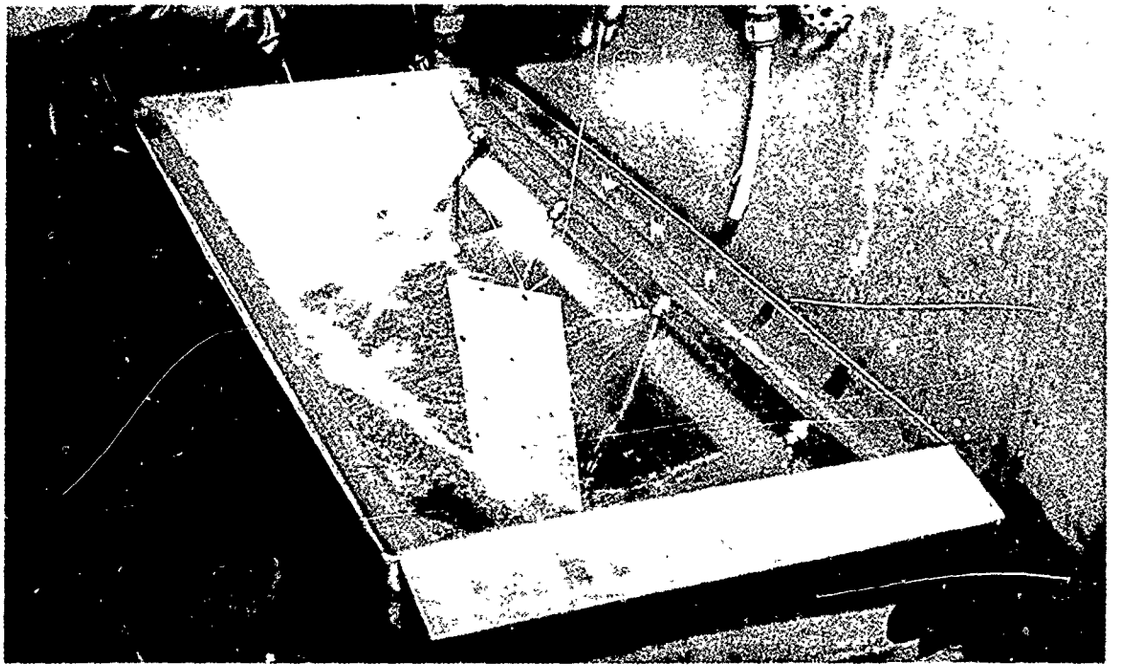

Final Spray Rinsing of 6061 Al Sheet
Figure 5-24

New specimen, Batch #3, were prepared with a final two (2) minute water rinse scrubbing included in the metal preparation. Random tests confirmed the preceding conclusion since average shear values increased to 22,421 PSI for the 6061-4045(1) system, and 26,030 PSI(1) for the 6061-718 system. The microstructure of interfaces was improved. Figure 5-25 illustrates the typical interface differences.

Contaminated Interface Microstructure

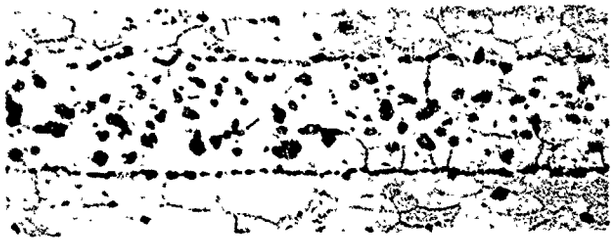

Mount #619 - Mag 250X
Boric Acid HF Etched
Shear Value-17,946 PSI
Excessive Interface
Bounding Buffer Effect
Minor Transcrystalline
Growth Only

6061-4045 System - Over Spray Scrubbing Omitted

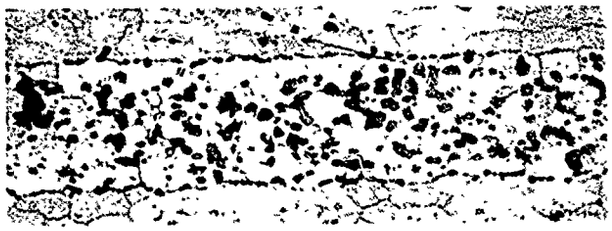

Mount #619 - Mag 250X
Boric Acid HF Etched
Shear Value-15,271 PSI
Excessive Interface
Bounding Buffer Effect
Minor Transcrystalline
Growth Only

6061-718 System - Over Spray Scrubbing Omitted

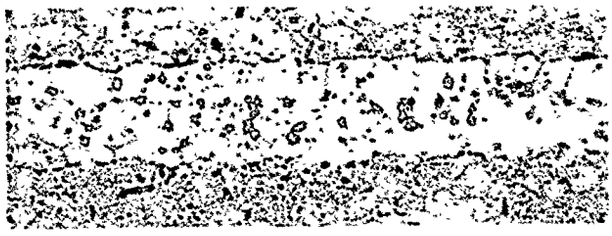

Mount #648 - Mag 250X
Boric Acid HF Etched
Shear Value-22,421 PSI
Good Transcrystalline
Interface Growth

6061-4045 System - Over Spray Scrubbing Added

Figure 5-25

(1) Shear strengths reported in Table 5-3.

Figure 5-25 (cont'd)

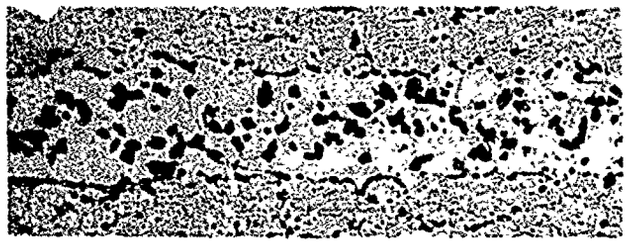

Mount #634 - Mag 250X
Boric Acid HF Etched
Shear Value-26,030 PSI
Good Transcrystalline
Interface Growth

6061-718 System - Over Spray Scrubbing Added

A parallel investigation was conducted to determine the effect of varied RMS finishes on joint quality. This effort was prompted by the low shear value problem. Table 5-4 shows typical finishes investigated vs shear strength of bonded joints tested at room temperature.

Table 5-4

Surface Roughness vs Room Temperature Lap Shear

Base Alloy	Interleaf Alloy	Chem. Prep.(3) RMS	Shear (KSI)	Mechanical Cleaned(4) RMS	Shear (KSI)	Chemical Milled(2) RMS	Shear (KSI)
6951	4045	20	23.6	50	22.4	65	22.0
6061	4045	15	22.4	40	22.0	100	21.0
7005	4045	20	21.5	45	22.0	110	20.0

(1) Equipment - Profilometer - Type LK Tracer
(2) Chemical Mill Rate 0.001"/Min.
(3) Chemical Mill Rate 0.0001"/Min.
(4) Sanded Parallel to Rolling with #320 Grit to Uniform Appearance and Repeated Normal to Rolling

5.6 Bonded Laminated Beam Fatigue

To determine the effect of diffusion bonding on the fatigue resistance of the candidate material system, homogeneous plate, and two ply bonded specimen were subjected to fixed cantilever constant amplitude reverse bend fatigue cycling. Material systems were 6061, 4045 and 718, 6951-4045 and 718, and 7005-4045 and 718. RR Moore type specimen 0.060" thick were used.

The curves shown in Figures 5-29, 5-30, and 5-31, developed from the test data indicated that the laminated specimen had a higher endurance limit than that of the homogeneous plate specimen. This is a similar finding to that for brazed laminates.

Figures 5-26, 5-27, and 5-28 photographically illustrate typical fractures of failed specimen.

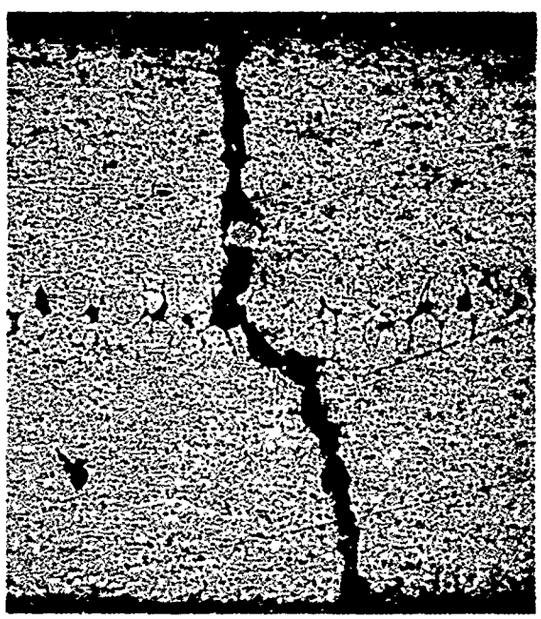

Mount #621 - Mag 45X
Etchant - Electrolytic
Nitric Methanol
6061 Base Alloy
4045 Interleaf Alloy
System

Figure 5-26

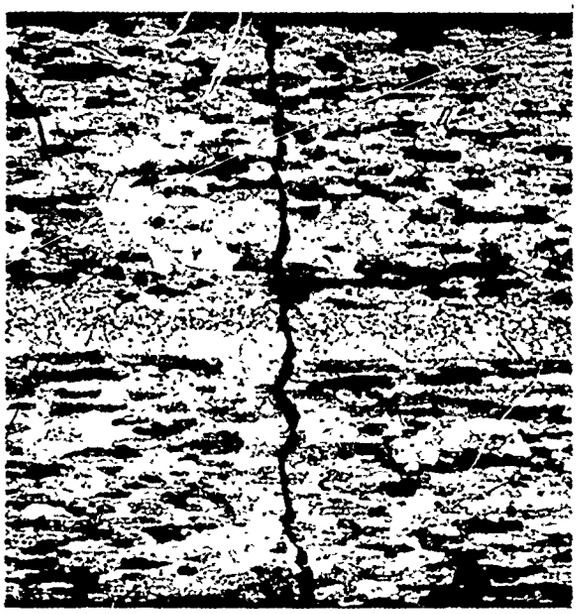

Mount #566
Magnification - 45X
Etchant - Boric Acid HF
7005 Base Alloy
4045 Interleaf Alloy

Figure 5-27

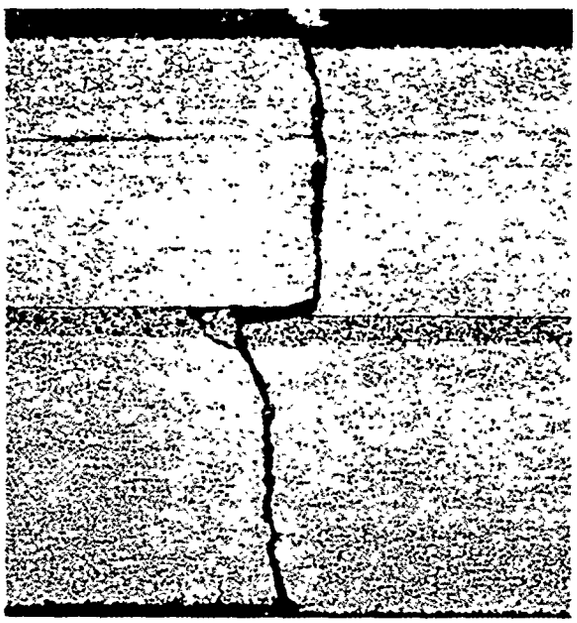

Mount #629
Magnification - 45X
Etchant - Boric Acid HF
6951 Base Alloy
4045 Interleaf Alloy System

Figure 5-28

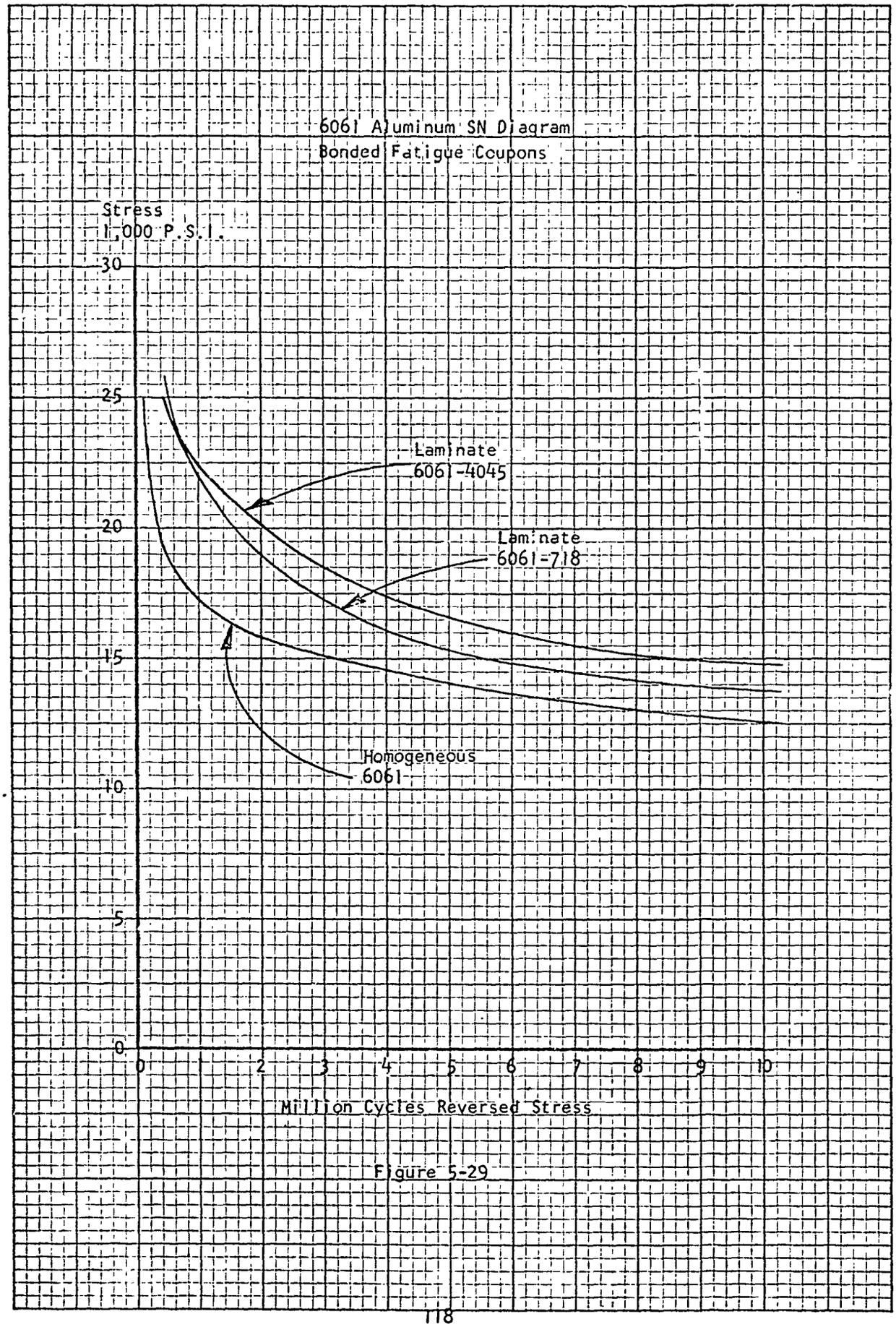
6061 Aluminum SN Diagram
Bonded Fatigue Coupons
Stress
1,000 P.S.I.
30
25
20
15
10
5
0
0
1
2
3
4
5
6
7
8
9
10
Laminate
6061-4045
Laminate
6061-718
Homogeneous
6061
Million Cycles Reversed Stress

Figure 5-29

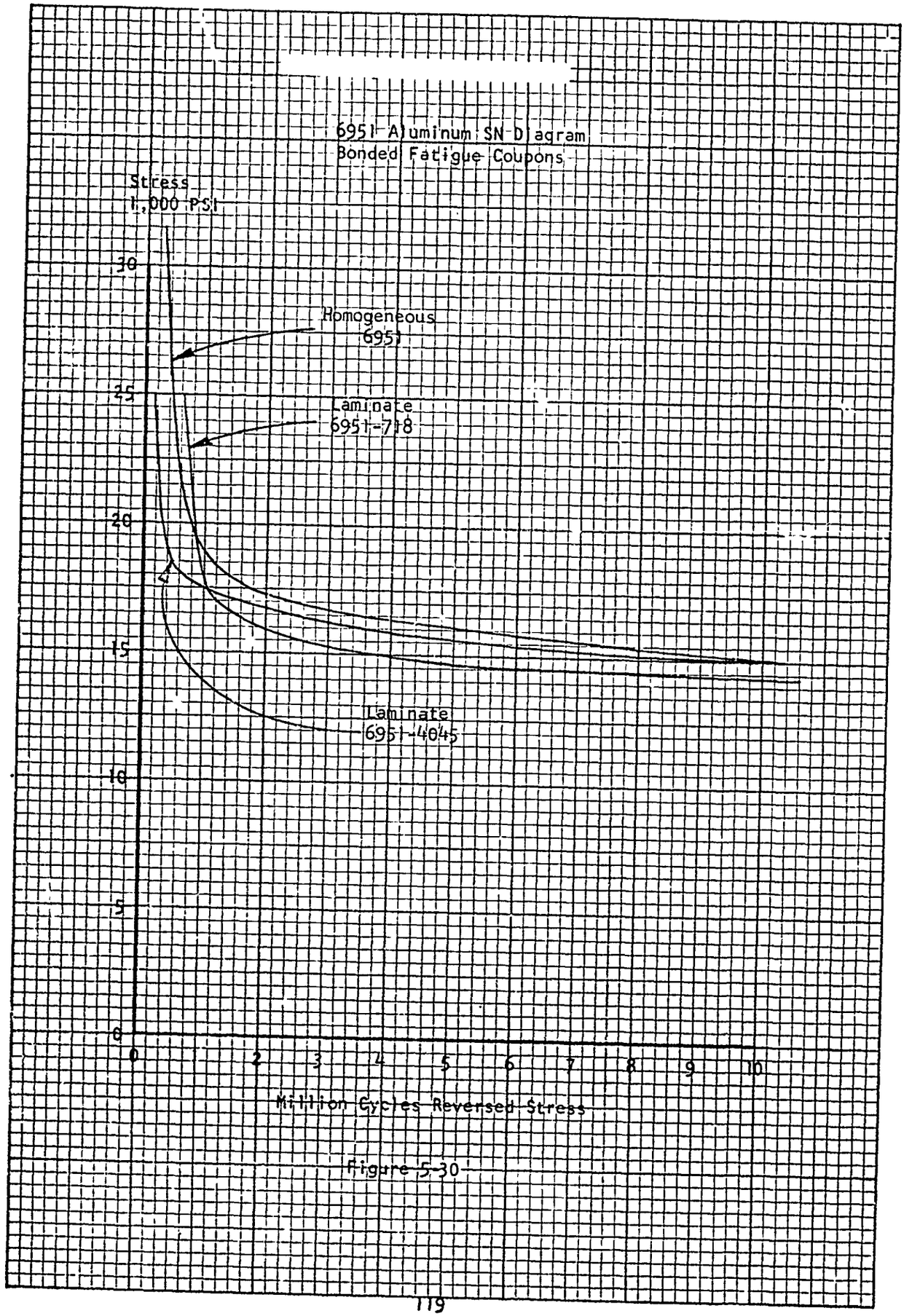
6951 Aluminum SN Diagram
Bonded Fatigue Coupons
Stress
1,000 PSI
30
25
20
15
10
5
0
Homogeneous
6951
Laminate
6951-718
Laminate
6951-4045
0
2
3
4
5
6
7
8
9
10
Million Cycles Reversed Stress

Figure 5-30

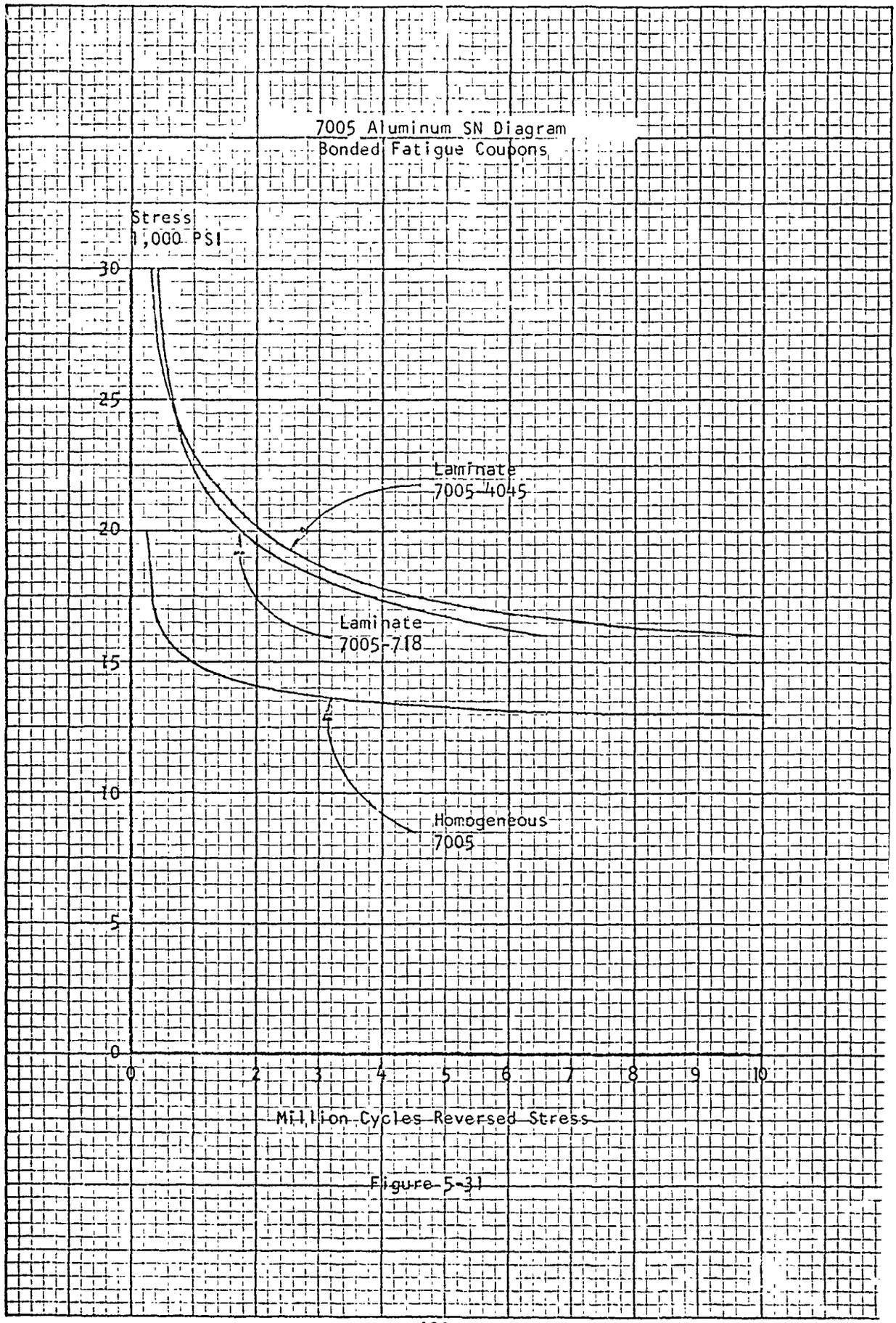
7005 Aluminum SN Diagram
Bonded Fatigue Coupons
Stress
1,000 PSI
30
25
20
15
10
5
0
Laminate
7005-4045
Laminate
7005-718
Homogeneous
7005
0
2
3
4
5
6
7
8
9
10
Million Cycles Reversed Stress

Figure 5-31

SECTION 6.0

EXPERIMENTAL BRAZE FILLER METAL INVESTIGATION

6.1 Scope and Approach

This investigation was concerned with establishing one or more new filler metal candidate systems, as possible alternates to the existing filler metal systems. Should the brazing of complex composite applications be limited due to the high flow temperatures of the existing systems or other characteristics, then new systems offering more advantageous properties would be desirable.

Investigations conducted demonstrated that five aluminum base ternary systems, which if refined with minor modifications, could be adjudged as candidate systems for brazing aluminum.

An approach for calculating the solidus-liquidus range theoretically was studied, and traded off against investigations conducted experimentally. The theoretical model approach was not feasible, and formulation of system was based on existing phase diagrams plus other related data. The reasoning for considering the theoretical model approach is discussed below:

Because of the limited information of melting range data which is available in binary and complex alloy phase diagram form, an apparent need existed in the area of aluminum braze alloy development, for some analytical criterion, by which liquidus temperatures could be estimated for complex alloys. For example, it might be necessary to know the effect of additions of copper and silver on the liquidus of a basic Al-Si binary alloy, in which it is almost certain that no equilibrium data exists. This approach was reviewed and, within the scope of the study, no theoretical model was established which included all the variables. One method for calculating the liquidus of a multi-component system was based upon the treatment for binary systems as presented in "Solubility of Nonelectrolytes" by Hildebrand and Scott. When assuming no solid solubility at equilibrium, the free energy of the solid must equal its partial molar free energy in solution.

The following equation is believed to represent the simplest application of solution theory to the problem of liquidus determination:

$$T = \frac{V_{Al}\left[(\delta_{Al} - \delta_2)X_2 + (\delta_{Al} - \delta_3)X_3 + \ldots + (\delta_{Al} - \delta_n)X_n\right]^2 + \Delta H^F_{Al}}{H^F_{Al}/T_m - R \ln (X_{Al})}$$

The appropriate constants are:

H^F_{Al} = 2480 cal/mol (heat of fusion)
V_{Al} = 10.7 cc (molar volume of liquid)
ζ_{Al} = 86 (solubility parameter)
T_m = 932°K (melting temperature)
X_n = mole fraction
R = gas constant

However, the preceding equation was found to lack sufficient concise parameters such as the omission of 1) variables of heat fusion with temperature, and 2) precise solid solubility parameters for three or more metals. It was concluded that a massive amount of empirical data would be necessary to support a theoretical model for obtaining melting points of complex alloys, which would closely approximate the actual solid-liquid co-existing state.

Assuming the soundness of the above statement, then new complex filler metal systems were best obtained by experiment, especially as those properties involving the electrochemical nature of metals, etc., could also be included.

A comprehensive study involving aluminum and its more common alloying elements was conducted. This study produced a limited number of binary and complex systems with theoretical solidus and liquidus points (and liquation) between 840 F (449 C) and 1070 F (560 C). Further reviews with respect to free energies, activity levels, and vapor pressures permitted the selection of potential metals for alloying. Selected metals were procured in the forms and grades below:

Metal	Form	Grade (%)
Al	Bar	99.9
Be	Flake	99.9
Cd	Rod	99.999
Cu	Bar	99.999
Ge	Ingot	99.999
Li	Lump	99.8
Mg	Ingot	99.999
Mn	Flake	99.9
Ni	Shot	99.8
Si	Powder	99.8
Sn	Shot	99.92
Zn	Shot	99.98

Forty nine (49) experimental induction melts were processed. Selected melts were evaluated in part for: 1) Differential thermal analysis (DTA), 2) Macro- and microscopic analysis of as-cast ingots and thermally homogenized ingots, 3) Minimum effective wetting temperature of 6061 Al surface, 4) Microstructure of brazed interfaces, 5) Room temperature lap shear strength of brazed 6061 Al lapped joints, 6) Roll reduction, and 7) Chemical and spectrographic analysis.

Due to the experimental nature of the melts, because of not having proven standards, the chemical compositions determined spectrographically were suspect. However, wet chemical analysis was also conducted for cross checking.

Initial melts were made to establish optimum processing steps and to obtain early data of the alloying effects. The maximum investigation concerned the effect of various temperature depressant metals on an aluminum-silicon binary. Temperature depressing additions were confined to not more than 4 parts by weight, in which the lowest minimum effective wetting temperature was obtained with the 95Al + 5Si + 4Mg ternary. The highest room temperature lap shear value was obtained with the 95Al + 5Si + 4In, however, the 95Al + 5Si + 4Cu system brazed at 1040 F (560 C) brazed lower than the Al + Si + In exhibited a shear strength which averaged only 0.1 KSI less.

Based on the investigations conducted, and with assumed ability to accomplish refinements, the Al + Si + Cu system offers the best combination of strength vs wetting temperature. The Al + Si + Mg system offers the lowest wetting temperature, while the Al + Si + In system based on the microstructure, is a potential candidate for corrosive environment applications, although in this area, the Al + Si + Mg system based on known data, should also exhibit good corrosion resistance.

6.2 Experimental Alloy Systems

Table 6-1 presents all melt formulations processed with summary data and comments. The initial melts were investigated mainly to obtain an overall understanding of the effect of alloying certain systems on the melting range, and to confirm the melt process. Subsequent formulations were confined to determining the effect of minor alloying additions to the AlSi binary system.

Melts as cast, in general, exhibited a heterogeneous macrostructure, subsequent thermal homogenization cycling was found to effectively minimize this condition, except for those alloys containing nickel. The nickel bearing alloys problem of segregation was resolved by changing the nickel from shot to flake, which improved the dissolution of the nickel into the alloy matrix, and by adding a homogenizing cycle of ten (10) hours at 950 F (510 C). The homogenizing cycle of 10 hours at 950 F was further found to be optimum for all melts.

The results presented in Table 6-1 demonstrate the feasibility of developing alloys potentially for brazing aluminum alloys below the existing state-of-the-art temperatures. Essentially, two categories exist--those with considerable braze temperature reductions but with inherent poor corrosion resistance, and those which exhibit somewhat higher flow temperatures but theoretically offered good corrosion resistance. However, each candidate

Melt No.	Nominal Alloy Composition (1)(2) (Expressed in Percent w/o)									
	Al	Be	Cd	Cu	Ge	In	Mg	Ni	Si	Sn
1 (1)	74						26			
2 (1)			64				36			
3 (1)	42									58
4 (1)	55	1		15						
5							76.4	24.6		
6 (1)	67			33						
7 (2)	78.8			4			5.4		11.8	
8 (2)	88.2							2.0	9.8	
9 (1)	77						13	10		
10 (1)	89							1	10	
11 (1)	87							3	10	
12 (1)	86							4	10	
13 (1)	84							4	12	
14 (2)	82.4						5.5		12.1	
15 (1)	90							1	10	
16 (2)	90.4							1.83	7.65	
17 (2)	88.2							2.86	8.85	
18 (2)	89.5							3.37	7.0	
19 (2)	90.5			0.51					10	
20 (2)	89.9			0.91					9.0	
21 (2)	88.0			3.02					8.8	
22 (2)	85.2			3.99					10.55	
23 (1)	90						1		10	
24 (1)	90						2		10	
25 (2)	88						2.0		9.7	
26 (1)	90						4		10	
27 (1)	95			1					5	
28 (1)	95			2					5	
29 (1)	95			3					5	
30 (1)	95			4					5	
31 (1)	95						1		5	
32 (1)	95						2		5	
33 (1)	95						3		5	
34 (1)	95						4		5	
35 (1)	90				1				10	
36 (1)	90				2				10	
37 (1)	90				3				10	
38 (2)	86			3.6					9.0	
39 (1)	90					1			10	
40 (1)	90					2			10	
41 (2)	86.7					3.21			9.8	
42 (1)	90					4			10	
43 (1)	90						2		10	
44 (2)	86.9						3		9.8	
45 (1)	90						4		10	
46 (2)	89.9	0.28					1		8.6	
47 (2)	89	0.28					1.9		8.6	
48 (2)	89.9	0.28					3		8.66	
49 (2)	86.7	0.28					4.1		8.68	

(1) Nominal Composition
(2) Composition by Analysis
NA Not Evaluated

RIMENTAL MELTS - COMPOSITION vs BRAZE RESPONSE

Sn	Zn	Fe	Wetting $^{-0}_{+10}$ Temp. (°F)	Diffusion (Inches)	Flow (Inches)	Average Shear (P.S.I.)	Comments
			977-1035		.05 - .08	6,525	
58							Lack of Wetting
	30						Excessive Diffusion
							Excessive Diffusion
			1010	N/A	N/A	10,758 --------	Brazed at 1030°F
			1020	N/A	N/A		
			1070	0.00497	.500	20,322 --------	Brazed at 1070°F
			1060				No Wetting
			1040	0.0038	1/16	N/A	
			1050	0.00489	0.050	N/A	
			1040	0.0039	3/64	13,471 --------	Brazed at 1050°F
			1040	0.003	5/64	12,496 --------	Brazed at 1050°F
			1040	N/A	N/A	10,206 --------	Brazed at 1050°F
			1050	N/A	1/8	N/A	
			1045	N/A	5/64	N/A	
			1040	N/A	1/32	N/A	
			1045	N/A	1/32	N/A	
			1055	0.00530	3/64	N/A	
			1055	0.00290	9/64	N/A	
			1045	0.00250	1/16	N/A	
			1035	0.00370	9/64	N/A	
			1040	0.00160	1/16	N/A	
		1/2	1035	0.00160	1/4	N/A	
		1/2	1025	N/M	1/32	N/A	
		0.1					
			1030	0.00120	5/64	N/A	
		1/2	1050	0.00214	1/16	N/A	
			1040	0.00214	3/64	N/A	
			1040	0.00214	3/32	N/A	
			1030	0.00161	5/32	16,328 --------	Brazed at 1040°F
			1020	N/M	3/64	N/A	
			1025	0.0033	13/64	N/A	
			1030	0.0033	23/64	N/A	
			1025		1/16	11,273 --------	Brazed at 1035°F
			1035	0.00410	3/64	N/A	
			1035	0.00620	3/64	N/A	
			1030	0.00570	5/128	N/A	
			1030	0.00450	1/16	13,317 --------	Brazed at 1040°F
			1060	0.00330	1/16	N/A	
			1055	N/A	1/16	N/A	
			1050	0.00120	5/64	N/A	
			1045	0.00410	1/8	16,646 --------	Brazed at 1055°F
			1030	0.00160	7/64	N/A	
			1030	0.00490	21/64	N/A	
			1030	0.0041	26/64	16,960 --------	Brazed at 1040°F
			1030	N/M	Small Area	N/A	
			1025	0.00164	3/16	N/A	
			1030	0.00246	21/64	N/A	
			1030	0.00287	5/16	12,005 --------	Brazed at 1040°F

TABLE 6-1

2

system requires refinement and their behavior under extreme environments must be determined.

The pertinent characteristics of five basic ternary systems are discussed in the following.

6.2.1 Aluminum - Silicon - Nickel System

Nickel acts as a melting range temperature depressant for the 90Al + 10Si binary. Additions of two (2) parts of nickel reduced the AlSi wetting temperature to 1040 F (560C), this wetting temperature was not lowered farther by increasing the nickel content from two (2) to four (4) parts.

The system exhibits reasonable ductility and can be cold worked up to 40 percent. Three (3) mil foil was produced from 1/2 inch ingot bar. Nickel infiltration is considered critical and must be added as fine particles for best dissolution into the AlSi matrix.

Shear strength of lapped 6061 alloy joints brazed at 1050 F (566 C) averaged 12 KSI which is considered marginal, but no doubt it can be improved by refinement directed toward an increase in surface activity.

The AlSi + Ni ternary alloys exhibited micro- and macro-segregation of nickel with an uneven dispersion of the segregates throughout each melt. Homogenization times, up to 48 hours, were ineffectual in eliminating the macrosegregation of nickel. This problem was primarily resolved by modifying the introduction of the nickel's form into the melt. Initially, the nickel was added in the form of 1/16 inch diameter pellets. By rolling the pellets to a foil thickness and subsequently reducing the size of the flakes, the dissolution of the nickel into the binary was made possible. Although the uniformity of the ternary melts was greatly improved over previous melts, there were still signs of massive segregation in the 3 percent and 4 percent melts. Thermal conditioning (homogenizing) the melts at 950 F for ten (10) hours reduced the heterogeneous condition, decreased coring effects, and produced a uniform macrostructure.

The general approach used in the homogenization studies was: Sections from each melt were subjected to 5 hours, 7 hours, 10 hours, and 48 hours at 950 F. Sections were examined by optical metallography before and after each heat treatment. Although some anomalies existed, the best results were obtained by thermal conditioning at 950 F for ten hours. Detailed results are given in Table 6-2. Figures 6-1, 6-2, and 6-3 show typical structures for each of the alloys before and subsequent to thermal conditioning.

Table 6-2

Summary of Effect of Thermal Treatment on Al+Si+Ni Alloys[1]

Composition	Time @ 950 F (Hours)	Observations of Effect
99(90Al-10Si)-1Ni	As Cast	Center section (#3) showed slightly more coalescence of constituents than that of balance. All sections exhibited good macroscopic uniformity.
	5	Similar to as cast.
	7	Similar to as cast.
	10	Less evidence of eutectic alloy phase. Coalescence form of constituents similar to as cast.
	48	Increase in fine precipitates in matrix.
97(90Al-10Si)-3Ni	As Cast	Sections 3, 4, and 5 showed slightly more coalescence of precipitates. Generally all sections showed massive uniform nickel silicon to matrix segregation.
	7	Considerable improvement in dispersion of precipitates.
	10	Fine uniform segregation of precipitates.
	48	Increase in random coalesced particles, with noticeable fine matrix precipitates.
96(90Al-10Si)-4Ni	As Cast	Sections 3, 4, and 5 showed considerably more nickel in coarse segregated phases.
	7	Considerable refinement in all sections.
	10	Sections very similar and uniform. Majority of precipitates were fine, with random coalesced particles.
	48	All sections exhibited pronounced breakdown of larger alloying pnases into fine matrix precipitates.

(1) Ingots were seperated equally into five (5) sections. Number one (1) being the top section.

Figure 6-1

Illustration of Homogenizing 1% Nickel Alloy Addition at 950 F(1)

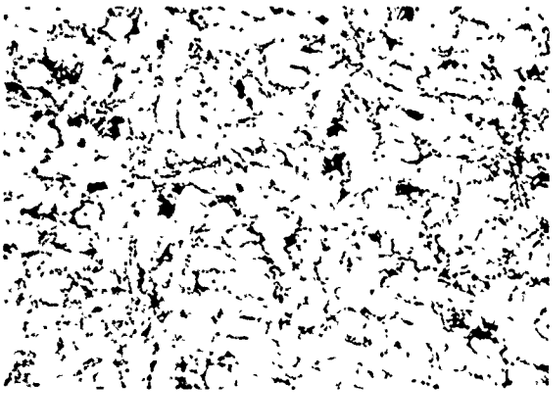

Section 2. Magnification 200X
Boric Acid-HF Etched-As Cast

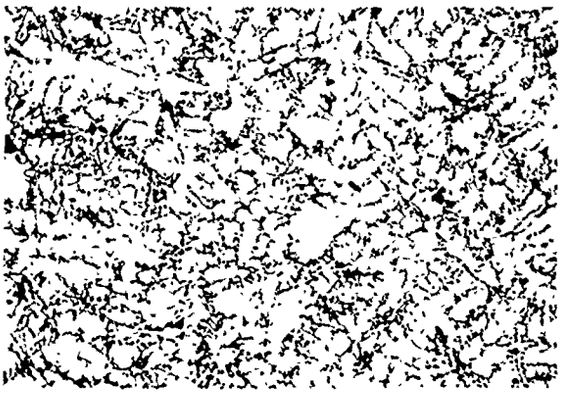

Section 5. Magnification 200X
Boric Acid-HF Etched-As Cast

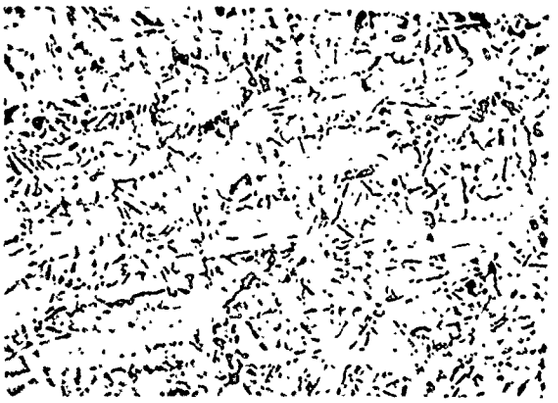

Section 2. Magnification 200X
Boric Acid-HF Etched
Heat Treated 10 Hours at 950 F

Section 5. Magnification 200X
Boric Acid-HF Etched
Heat Treated 10 Hours at 950 F

(1) Nickel added as fine chopped flake.

Figure 6-2

Illustration of Homogenizing 3% Nickel Alloy Addition at 950 F(1)

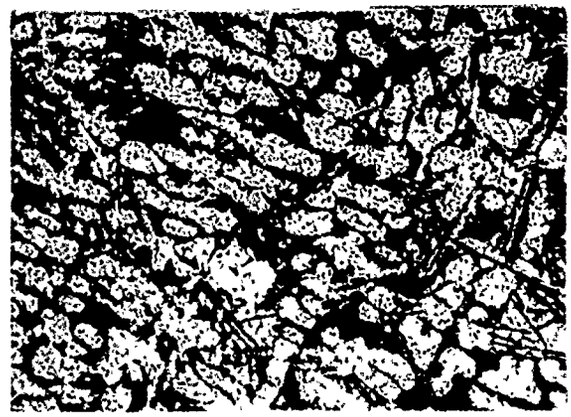

Section 3. Magnification 200X
Boric Acid-HF Etched-As Cast

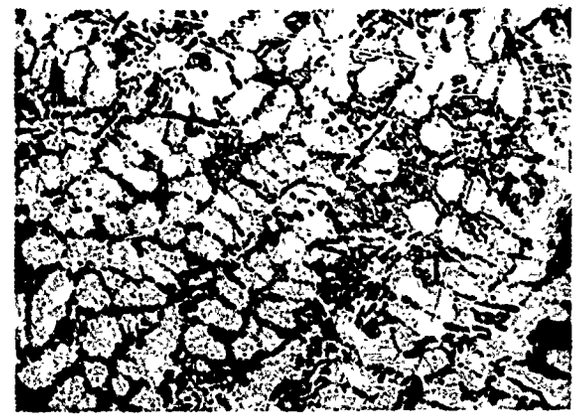

Section 5. Magnification 200X
Boric Acid-HF Etched-As Cast

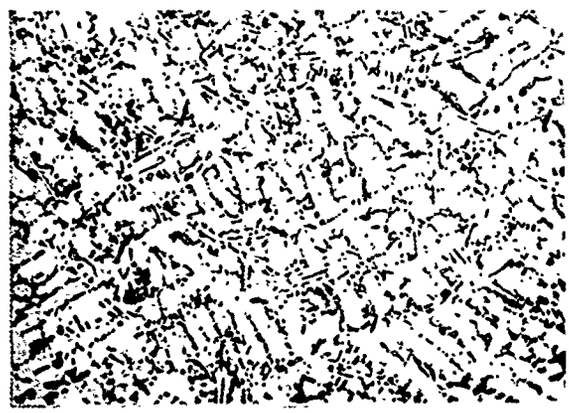

Section 3. Magnification 200X
Boric Acid-HF Etched
Heat Treated 10 Hours at 950 F

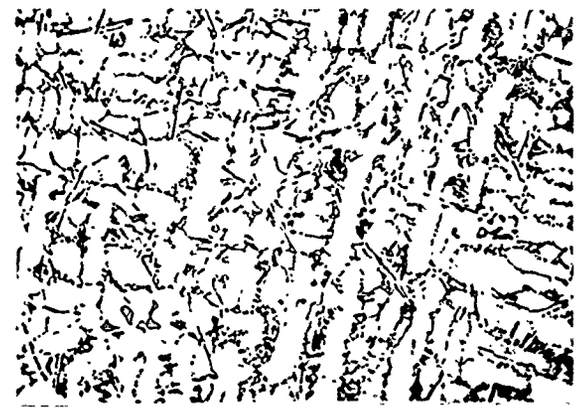

Section 5. Magnification 200X
Boric Acid-HF Etched
Heat Treated 10 Hours at 950 F

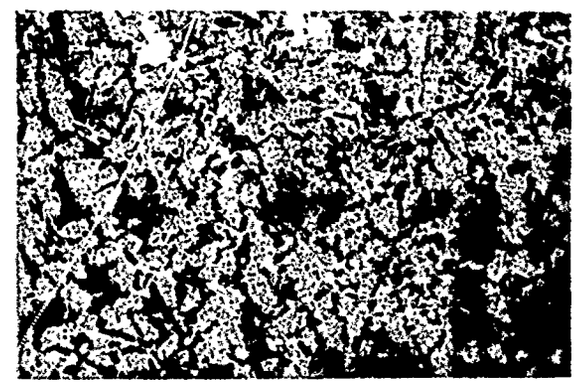

Section 5. Magnification 200X
Boric Acid-HF Etched
Heat Treated 48 Hours at 950 F

(1) Nickel added as fine chopped flake.

Figure 6-3

Illustration of Homogenizing 4% Nickel Alloy Addition at 950 F(1)

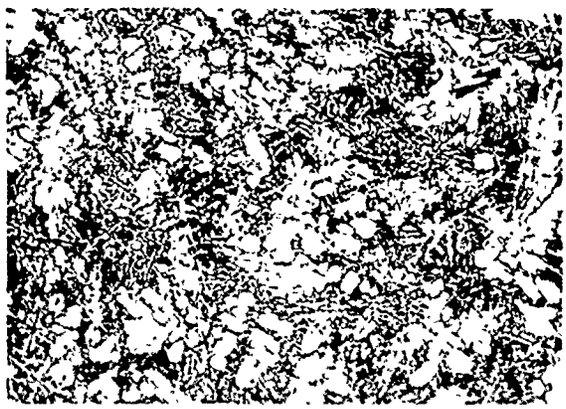

Section 2. Magnification 200X
Boric Acid-HF Etched-As Cast

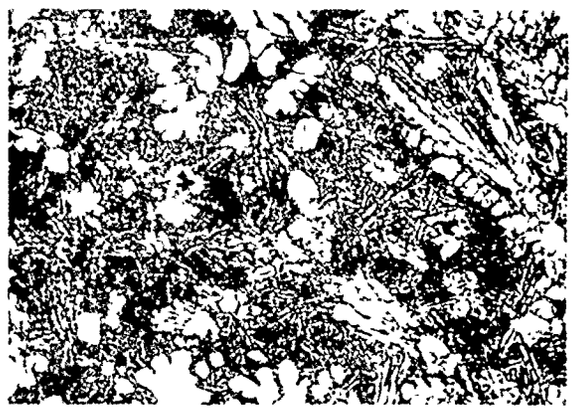

Section 4. Magnification 200X
Boric Acid-HF Etched-As Cast

Section 2. Magnification 200X
Boric Acid-HF Etched
Heat Treated 10 Hours at 950 F

Section 4. Magnification 200X
Boric Acid-HF Etched
Heat Treated 10 Hours at 950 F

Section 4. Magnification 200X
Boric Acid-HF Etched
Heat Treated 48 Hours at 950 F

(1) Nickel added as fine chopped flake.

6.2.2 Aluminum - Silicon - Magnesium System

Both silicon and magnesium can be formulated with aluminum to eutectic compositions. Magnesium is higher in the oxidization scale than aluminum and will depress the liquidus of aluminum to 844 F (451 C). A 74Al + 26Mg binary was found to wet 6061 Al at 980 F (471 C). However, the wetting power (flow) was poor, increasing the test temperature to 1030 F (554 C) did not produce any significant increase in flow.

The aluminum-silicon eutectic temperature is considerable higher than that of the Al-Mg binary eutectic. However, silicon increases the fluidity of the system.(1) Additions of 1, 2, 3 and 4 parts of magnesium to the 90Al + 10Si and 95 Al + 5Si binary alloys were evaluated. The lowest minimum effective wetting temperature of 6061 Al was obtained with the (95 Al + 5Si) + 4Mg ternary. This temperature, by repeated tests averaged 1025 F. Room temperature lap shear strengths of 6061 Al brazed at 1035 F for 5 minutes averaged 11.3 KSI.

Other characteristics of importance were:

- Good roll reduction of the (90-95 Al + 10 -5Si) + 1 - 4Mg ternary from 1/2 bar to foil.
- Short brazing cycles reduced the idiomorphic crystals to a minimum. Increased brazing times caused an increase in silicon and magnesium silicide dendrite structure, additions of 0.28 Be and 0.1 Fe did not provide any measurable dendrite refinement. However, it is possible that increasing the Be amount above 0.28 percent that some refinement could be obtained. The Be should also help in activating the base metal interface.

6.2.3 Aluminum - Silicon - Copper System

The Al-Cu eutectic alloy was evaluated, and found to wet 6061 Al at 1020 F (549 C).

Additions of 1 to 4 parts of copper to the (90-95 Al + 5 - 10Si) binary systems were evaluated, of these the (95Al + 5Si) + 4Cu ternary exhibited the lowest minimum wetting temperature on 6061 Al, the average temperature for this was 1030 F (554 C).

The 6061 Al lap joints brazed with the (95Al + 5Si) + 4Cu (5 minutes at 1040 F) produced a room temperature average shear value of 16.3 KSI.

It is assumed that liquation occurs in the AlSi + Cu ternary at the temperatures investigated as the liquidus temperature is higher than those producing wetting.

(1) Increase in fluidity refers to flow on aluminum base, not viscosity per se.

Characteristics of importance:

- o System effectively wets by liquation
- o No dendrite ℘ silicon structure.
- o Brazed interfaces exhibit continuous interface boundary coalescence of Al-Cu eutectic cored with ℘ silicon, this condition is suspected as being susceptible to corrosion. The system should exhibit higher shear strength but tended to premature failure at this interface. Refinement of this condition is desirable.

Photomicrograph Figure 6-4 illustrates the Al - Si - Cu and 6061 Al interface boundary condition.

Al-Si-Cu to 6061 Al Brazed Interface

Figure 6-4

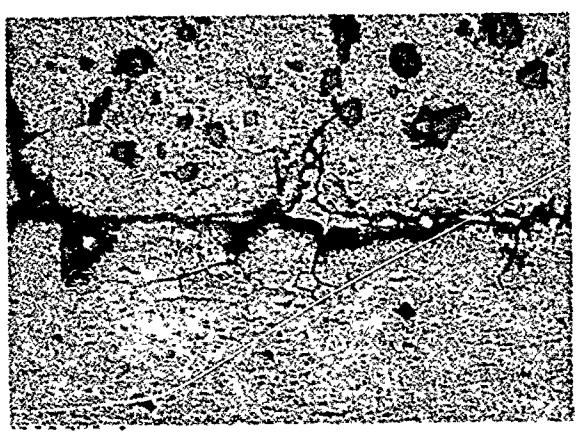

Mount #635
Boric Acid + HF Etched
Magnification - 250X
Spot brazed - 1040 F

6.2.4 Aluminum - Silicon - Germanium System

Germanium is reported to exhibit brittle phases in aiuminum. However, this is believed to be applicable to systems which approach the eutectic composition.

Additions of 1 to 4 parts by weight of Ge to the 90Al + 10Si binary were investigated for the minimum effective wetting temperature, and found to compare to that of the (90Al + 10Si) + 4Mg ternary. The room temperature shear strength of 6061 Al brazed with the (90 Al + 10Si) + 4Ge at 1040 F was 13.3 KSI.

The Al-Si-Ge to 6061 Al interface boundary exhibited less coalescence of alloying constituents than the Al-Si-Cu ternary system, but exceeded that of the Al-Si-Mg system.

Al-Si-Ge to 6061 Al Brazed Interface

Figure 6-5

Mount #698
Boric Acid + HF Etched
Magnification - 250X
Spot Brazed - 1040 F

6.2.5 Aluminum - Silicon - Indium System

Additions of 1 to 4 parts by weight of indium were made to the 90Al - 10Si binary system. The indium additions had less effect on wetting temperature depression than did copper, magnesium or germanium. The Al + In liquid phase apparently does not activate the base metal aluminum surface to any appreciable degree even though a liquid phase occurs at low temperatures. Indium additions for the 1, 2, 3, and 4 parts evaluated, progressively reduced the minimum effective wetting temperature from 1060 F (571 C) to 1045 F (563 C).

Room temperature shear strength of 6061 Al brazed with the (90Al + 10Si) + 4In at 1055 F (568 C) for 5 minutes averaged 16.6 KSI.

Because of the high quality appearance of the brazed interface and the shear value obtained, this system should be evaluated with increased indium content.

Figure 6-6 photographically illustrates the excellent joint microstructure.

Al+Si+In to 6061 Al Brazed Interface

Mount #704
Boric Acid + HF Etched
Magnification - 250X
90Al+10Si+4In
6061 Al Base Alloy
Braze Temperature - 1055 F
Braze Time - 5 Minutes

6.3 Foil Rolling Study

Melts Number 12 and 13 were homogenized at 875 F for 30 minutes and subsequently cold rolled from 0.5 inches thick bar to 0.42 inches thick. At this point the hardness was R_B 61.5 for Number 12 and R_B 80.0 for Number 13. Further progressive thermal treatment and rolling operations produced 0.003 inch and 0.004 inch foil for the two melts respectively. The rolling schedule is detailed in Table 6-3.

TABLE 6-3

Rolling Schedule of New Filler Metals

Melt #12			Melt #13		
R_B(1)	Thickness in Inches	Comments	R_B(1)	Thickness in Inches	Comments
	0.500			0.500	
	0.488			0.490	
	0.465			0.467	
	0.432			0.432	
61.5	0.419	30 Min. at	80.3	0.420	30 Min. at
	0.410	875°F		0.413	875°F
	0.390			0.395	
	0.369			0.373	
	0.353			0.352	
	0.330			0.331	
	0.313			0.313	
	0.273		76.3	0.292	30 Min. at
72.5	0.253	30 Min. at		0.280	875°F
	0.249	875°F		0.259	
	0.232		75.0	0.240	30 Min. at
71.0	0.214	30 Min. at		0.240	875°F
	0.204	875°F		0.231	
	0.190			0.213	
	0.178			0.200	
75.0	0.165	30 Min. at	77.0	0.188	30 Min. at
	0.165	875°F		0.173	875°F
	0.165			0.156	
	0.162			0.143	
	0.149			0.134	
	0.140			0.127	
	0.128			0.112	
	0.119			0.107	
	0.110			0.100	
	0.094			0.093	
	0.093			0.092	
	0.093			0.085	
	0.080			0.076	
	0.069			0.074	
	0.068			0.070	
75.0	0.050	30 Min. at		0.066	
	0.047	875°F		0.062	
	0.039		72.0	0.051	30 Min. at
	0.026			0.044	875°F
	0.019			0.040	
	0.009			0.037	
	0.004			0.028	
				0.018	
				0.011	
				0.0008	
				0.0006	
				0.0004	
				0.0003	

(1) Hardness prior to thermal treatment.

SECTION 7.0

APPLICATION OF BRAZING TO HARDWARE COMPOSITES
STATE-OF-THE-ART MATERIAL SYSTEMS

This investigation concerned the applicability of the state-of-the-art brazing processes and materials for small complex hardware composites, utilizing thin wall tubing, foil and/or thin sheet.

7.1 Criteria, Scope, and Approach

A series of structural and thermal functional composites were fabricated and tested to demonstrate the versatility and capability of the state-of-the-art fluxless brazing processes. The types of composites evaluated were:

- o Tube-shell heat exchanger matrix. Axial flow tubes were staggered on a horizontal and transverse pitch to tube diameter ratio of 1.07 and 1.25 respectively. Basic concept is illustrated in Figure 7-1.
- o Plate fin multi-layer (40 elements) heat exchanger matrix approximately 8" wide by 8" long by 4" high. Surface extended fin height was 0.08". Figure 7-2 illustrates the basic concept.
- o Honeycomb sandwich flat composites. Panel size was 12" wide by 12" long by 0.4" thick. Cell size was 1/4" with 0.004" thick ribbon. Basic concept is illustrated in Figure 7-3.
- o Thermal conditioning and mounting panel. Envelope size was 10.5" by 10.5". Panel incorporated a turbulent split fin with 6.8 inch pitch. Basic concept is illustrated in Figure 7-4.

TUBE SHELL HEAT EXCHANGER

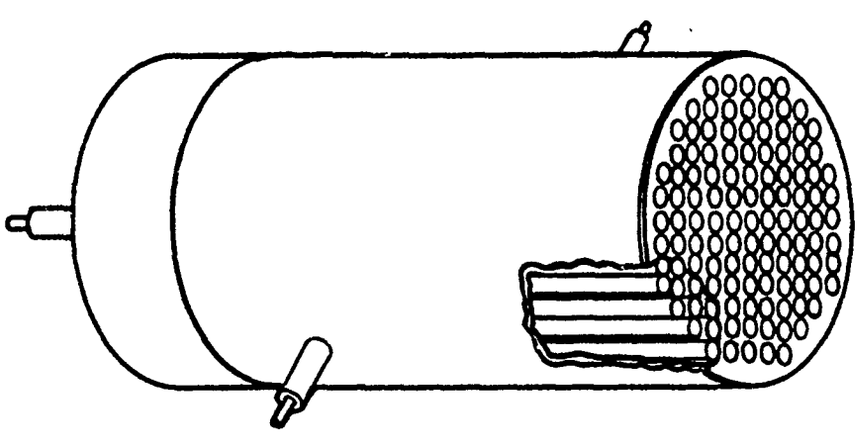

1) Fluxless brazed.
2) Matrix comprises 25 to 100 1/8" O.D. tubes with wall thickness of 0.002" to 0.006". Tube transverse pitch to tube dia. ratio of 1.25 tube longitudinal pitch to tube dia. of 1.07.
3) Header plates 0.015" thick maximum.

Figure 7-1

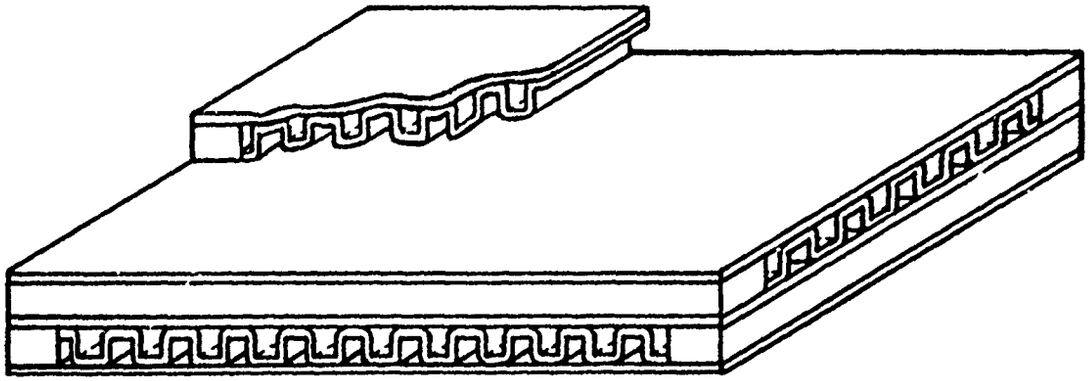

1) Fluxless brazed
2) Matrix comprises 40 elements with surface extended corrugated fin pitch and height approx. 0.080". Headers are not shown
3) Separator sheets max. thickness 0.02"

BASIC PLATE FIN MULTI LAYER HEAT EXCHANGER

Figure 7-2

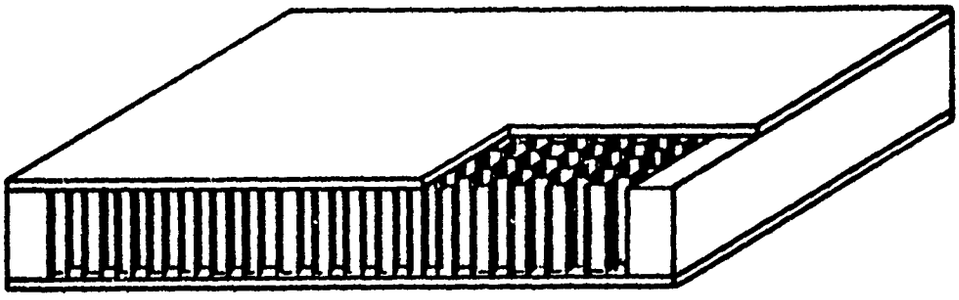

1) Fluxless brazed
2) Core cell $\frac{1}{4}$".
3) Face sheets 0.008 maximum thickness

STRUCTURAL HONEYCOMB SANDWICH COMPOSITE

Figure 7-3

THERMAL CONDITIONING AND MOUNTING PANEL

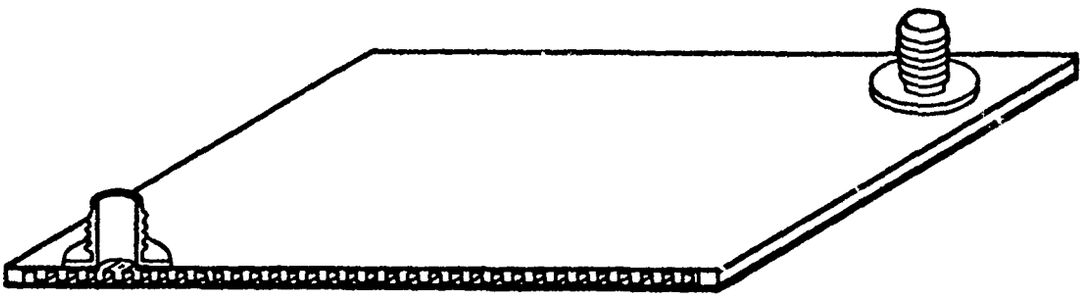

1) Fluxless brazed
2) Turbulent extended surface fin. Pitch 5 to 7 per inch. Height 0.090" approx.
3) Face sheets 0.008"
4) Fittings for proof pressure leak testing.

Figure 7-4

7.2 Summary of Results

A summary of results of investigations conducted on the composites fabricated and tested is presented in the following:

Thin wall tube Shell Heat Exchange

An analysis of the overall results determined that fluxless brazing is a suitable method for manufacturing multi tube-shell (thin wall) heat exchangers. Possibly a size limitation could be encountered. The complexity of the multitude of close packed axial flow tubes presents no serious handling or assembly problems. From a design aspect, the unsupported length of the axial tubes could be termed the critical factor and would require adequate structural dampening. Thin walled extruded tubing quality presents a material problem. Hydraulic quality tubing was investigated and found to include foreign matter inclusions and porosity. Most of these defects can not be detected prior to brazing.

Multi-Layer Plate Fin Heat Exchanger

An analysis of the overall results determined that fluxless brazing is a suitable method for manufacturing multi-layer plate fin heat exchangers. The number of elements which could be stack brazed is obviously not unlimited. A pressure analysis showed that the large unstiffened manifold walls were pressure critical and would require stiffening for pressures over 22 psig at room temperature.

Honeycomb Sandwich Composite

An analysis of the overall results determined that fluxless brazing is a suitable method for fabricating honeycomb sandwich composites. A probable size limitation would be encountered with heat treatable alloys due to rapid handling required by critical quench rates from solution heat treat temperatures. No major manufacturing problems were encountered.

Ultra-Light Thermal Conditioning And Mounting Panel

An analysis of the overall results determined that fluxless brazing is a suitable method for fabricating ultra-light thermal conditioning and mounting panels. No manufacturing problems were encountered in fabricating this structure.

7.3 Tube-Shell Heat Exchanger

This investigation was essentially conducted in two parts--first, an evaluation of thin wall tube to header joint concepts; second, a series (12) of tube shell heat exchanger matrices were fabricated and evaluated. The matrix brazements incorporated the most promising tube plate joint design.

7.3.1 Development of Tube-Plate Joints

A series of tube-plate brazed joint concepts were reviewed and based on the following criteria, two joints were selected for evaluation.

- Joints to be self-indexing during assembly to avoid unnecessary braze tooling mass which may adversely affect the braze temperature uniformity.
- It was desirable that the thin walled tube elements, being susceptible to buckling under non-uniform thermal stresses, have incorporated a convolute (bellows) form at some point or points along the tube between the fixed ends.
- Joint design should cater for a practical method of filler metal placement. Ideally - the filler should be pre-clad to at least one of the joint interfaces. Foil or formed wire rings could be considered.
- A plate-tube brazed flanged joint, with the joint interfaces positioned outward and accessible, would offer the possibility that brazed joint leaks could be reworked.

Figure 7-5 illustrates the two initial basic tube-plate designs selected for evaluation.

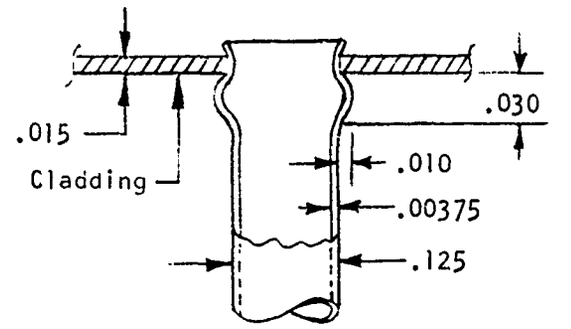

Type A

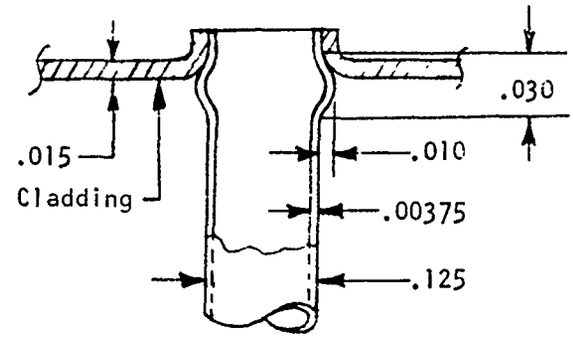

Type B

Tube Plate Joint Configurations

Figure 7-5

7.3 i.1 Evaluation Of Tube Plate Joints

Single Tube elements incorporating the type "A" and "B" joints were subjected to tensile shear tests at -300 F, room temperature, 300 F, 350 F, and 500 F. Included were extended elevated temperature soakings of 25 hours, 50 hours, and 100 hours.

Recognizing the need for filler metal diffusion control because of the thin tube walls, a brazing time of 3.5 minutes was adopted. The significant difference in each test, was that the effect of different thicknesses of (1, 2, and 3 mils) filler metal were evaluated. An analysis of the microstructures showed that the Type B joint provided more filler metal than did the Type A joint. The type B joint as shown in Figure 7-5 had cladding at the plate flange to tube O.D. surface interface, whereas the Type A joint relied on filler flow and filleting.

The 6061 alloy tubes were more susceptable to filler metal diffusion than the 3003 alloy tubes. The 1 and 2 mils cladding series were found acceptible for the 6061 alloy, whereas all three thicknesses of cladding produced no excessive diffusion of the 3003 alloy tubes.

For both types of joints investigated and all three filler metal thicknesses, no filler metal joint starved conditions were observed.

Type B joints were selected for tensile shear testing based on the filler metal at the joint interfaces providing improved integrity. The 6061 alloy was used for the thin wall tubes, as it provided a more severe test on the joint and offered a higher tube stiffness for the unsupported length.

Table 7-1 presents the tube stress at failure of Type B joints tested under tensile shear loads at -300°F through 500°F and subsequent to elevated temperature soaks. In all tests, the failure occurred in the tube element section, either adjacent to joint transition or at random distances along the tube section.

High failing load of tubes tested at 500 F after soaking for 10 minutes was assumed to be related to a form of precipitation of alloying constituents in the parent metal, which occurred during the early stages of over aging. However, no actual investigation was conducted to confirm this statement.

Tube-plate test elements were batch brazed (42 per batch). Method of braze indexing is illustrated in Figure 7-15. All braze tooling was made from 321 stainless steel. Each tube to plate element was laid unrestrained between the CRES positioning bars. CRES foil strips, poke welded to a glide sheet, held the work package during assembly into the braze envelope and subsequent brazing.

Tensile Stress of Tube Elements at Failure

-300°F	RT	300°F				350°F				500°F			
10 Min.	-	10 Min.	25 Hrs.	50 Hrs.	100 Hrs.	10 Min.	25 Hrs.	50 Hrs.	100 Hrs.	10 Min.	25 Hrs.	50 Hrs.	100 Hrs.
37,333 (3)	35,333 (3)	21,333 (1)	30,660 (3)	30,666 (3)	32,000 (3)	26,666 (1)	18,666 (2)	22,666 (2)	22,666 (2)	28,000 (3)	12,667 (2)	12,000 (1)	11,333 (2)
36,000 (3)	28,000 (1)	30,666 (3)	31,333 (3)	24,666 (1)	31,333 (3)	26,000 (2)	22,666 (1)	21,333 (1)	22,000 (1)	29,333 (3)	12,667 (2)	9,333 (2)	12,000 (3)
38,666 (1)	38,000 (3)	32,666 (3)	20,000 (1)	30,000 (3)	30,000 (3)	27,333 (2)	30,000 (3)	21,333 (1)	22,666 (1)	24,000 (1)	12,667 (2)	8,667 (2)	10,667 (2)
37,333	36,500	31,666	31,000	30,333	31,111	26,666	26,333	21,777	22,440	27,111	12,667	10,000	11,333

(1) Failed in tube near to joint transition. (2) Failed in tube adjacent to transition. (3) Failed mid-way in tube.

NOTES: 1) All specimens brazed at 1070 to 1080°F for 3 1/2 minutes with 4045 filler metal, solution heat treated at 970°F and air quenched, and aged at 350°F for 8 hours.
2) Joint configuration - B.
3) Plate Alloy -6951
4) Tube Alloy - 6061
5) Filler Thickness - 0.00123 Inches
6) All specimens tested at indicated environment temperature.

Table 7-1

Typical photomicrographs of each brazed joint test series are presented in Figures 7-6 through 7-14 inclusive.

Microstructure of Type "A" Brazed 6061 Al Tube Joints

Mount # - 392
Tube Alloy - 6061
Plate Alloy - 6951
Filler Metal - 4045
Braze Temp. - 1075°F
Braze Time - 3.5 Mins.
Filler Thickness - .001 In.
Joint Type - A
Magnification - 30

Comments: Tube wall filler diffusion was controlled.

Figure 7-6

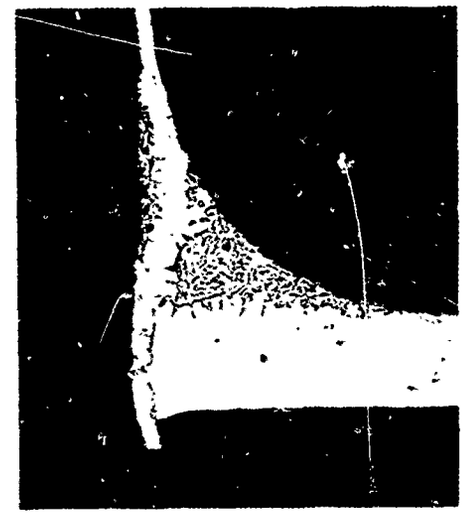

Mount # - 363
Tube Alloy - 6061
Plate Alloy - 6951
Filler Metal - 4045
Braze Temp. - 1077°F
Braze Time - 3.5 Mins.
Filler Metal Thk. - .002 In.
Joint Type - A
Magnification - 30

Comments: Filler metal is evident at ID surface of tube, believed due to damaged tube. This condition was not normal.

Figure 7-7

Microstructure of Type "A" Brazed 6061 Al Tube Joints (cont'd)

Mount # - 365
Tube Alloy - 6061
Plate Alloy - 6951
Filler Metal - 4045
Braze Temp. - 1077°F
Braze Time - 3.5 Mins.
Filler Thickness - .003 Inches
Joint Type - A
Magnification - 30

Comments: Severe metal diffusion of tube material is evident at root of fillet.

Figure 7-8

Microstructure of Type "A" Brazed 3003 Al Tube Joints

Mount # - 359
Tube Alloy - 3003
Plate Alloy - 6951
Filler Metal - 4045
Braze Temp. - 1077°F
Braze Time - 3.5 Mins.
Filler Thickness - .002 Inches
Joint Type - A
Magnification - 30

Comments: Well controlled tube wall diffusion.

Figure 7-9

Mount # - 361
Tube Alloy - 3003
Plate Alloy - 6951
Filler Metal - 4045
Braze Temp. - 1077°F
Braze Time - 3.5 Mins.
Filler Thickness - .003 Inches
Joint Type - A
Magnification - 30

Comments: Well controlled tube wall diffusion.

Figure 7-10

Microstructures of Type "B" Brazed 6061 Al Tube Joints

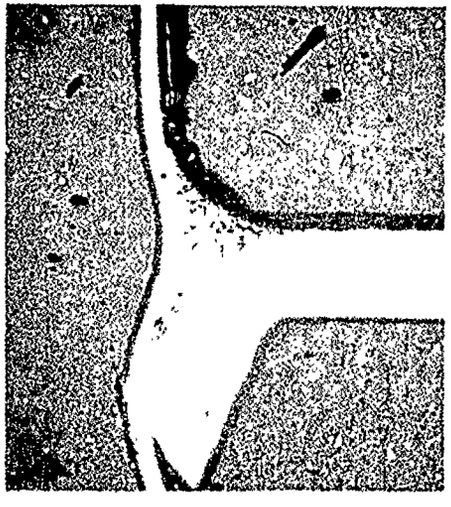

Mount # - 364
Tube Alloy - 6061
Plate Alloy - 6951
Filler Metal - 4045
Braze Temp. - 1077°F
Braze Time - 3.5 Mins.
Filler Thickness - .002 Inc.
Type Joint - B
Magnification - 30

Comments: Well controlled tube well diffusion.

Figure 7-11

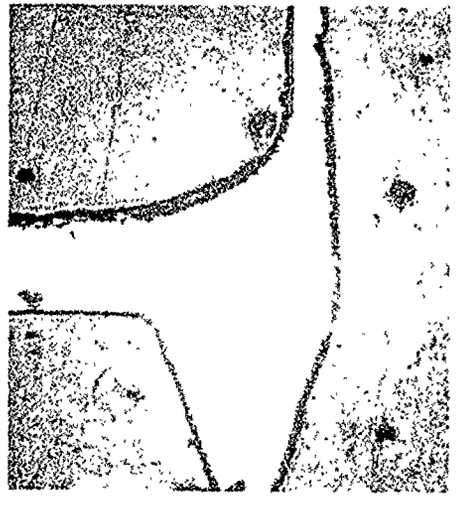

Mount # - 366
Tube Alloy - 6061
Plate Alloy - 6951
Filler Metal - 4045
Braze Temp. - 1077°F
Braze Time - 3.5 Mins.
Filler Thickness - .003 Inc.
Type Joint - B
Magnification - 30

Comments: Excessive diffusion at fillet fooc thin tube wall.

Figure 7-12

Microstructures of Type "B" Brazed 3003 Al Tube Joints

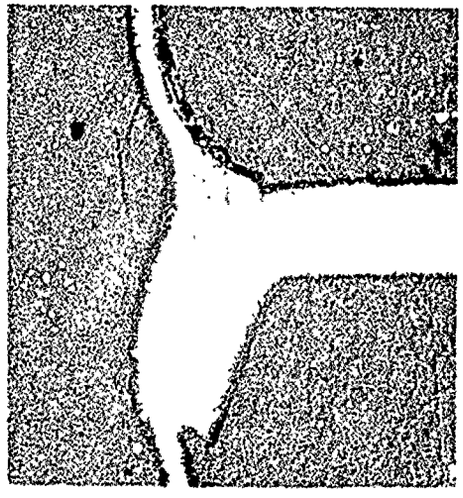

Mount #	-	360
Tube Alloy	-	3003
Plate Alloy	-	6951
Filler Metal	-	4045
Braze Temp.	-	1077°F
Braze Time	-	3.5 Mins.
Filler Thickness	-	.002 In.
Type Joint	-	B
Magnification	-	30

Comments: Well controlled tube wall diffusion.

Figure 7-13

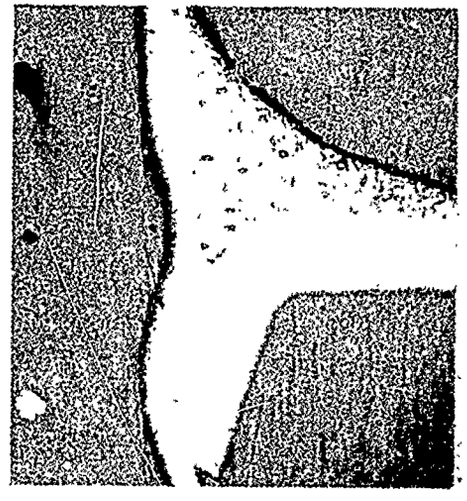

Mount #	-	362
Tube Alloy	-	3003
Plate Alloy	-	6951
Filler Metal	-	4045
Braze Temp.	-	1077°F
Braze Time	-	3.5 Mins.
Filler Thickness	-	.003 In.
Type Joint	-	B
Magnification	-	30

Comments: Well controlled tube wall diffusion.

Figure 7-14

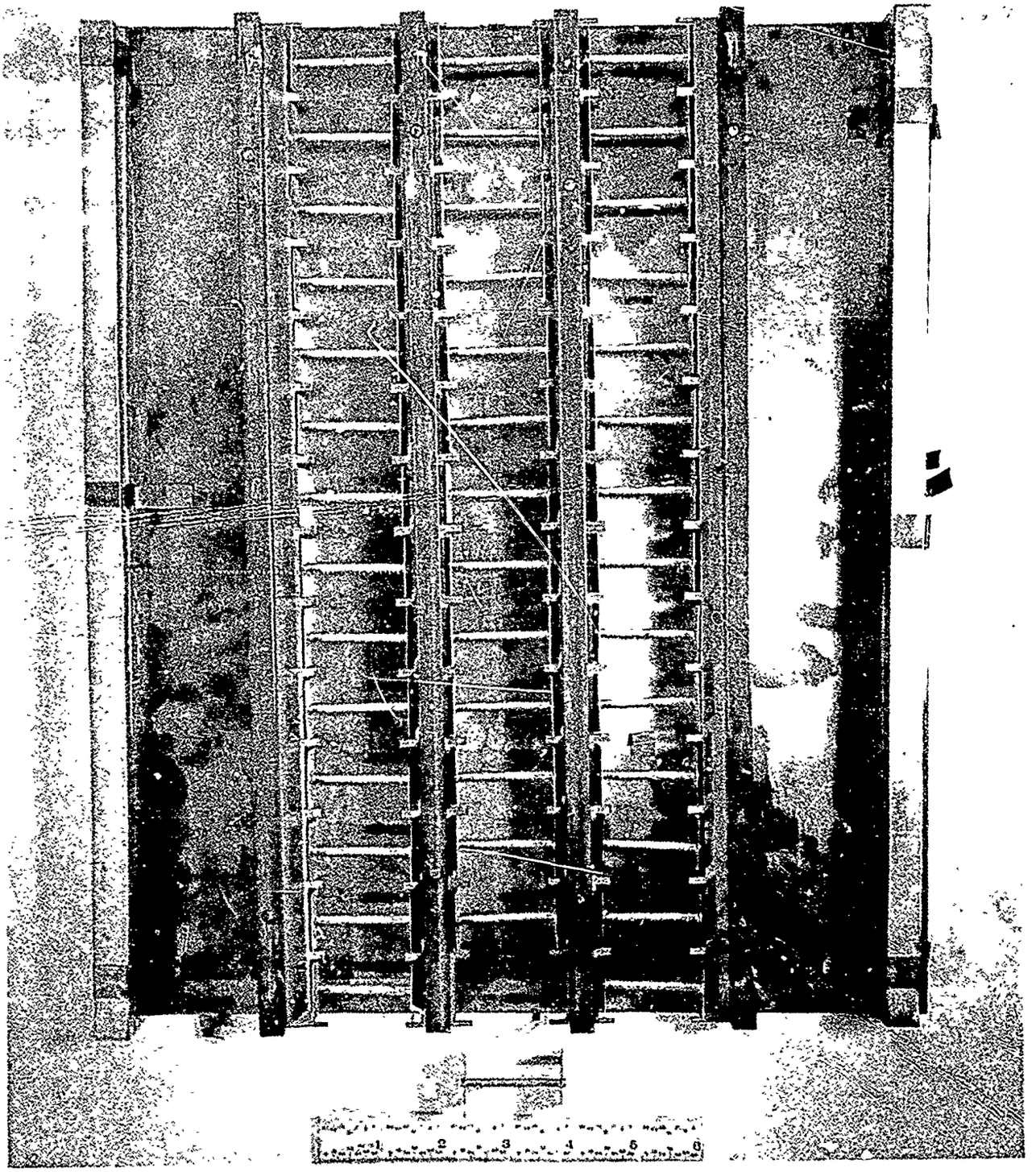

Figure 7-15

7.3.2 Development of Tube-Shell Heat Exchanger Matrix

A total of 12 tube shell matrices were evaluated for manufacturing feasibility and brazed quality.

Initially, a total of 10 units were fabricated as Type 1 and 1A as presented in the design per Figure 7-16. Type 1 and 1A designs were common, excepting that the header close outs differed. Type 1 header was designed for a minimum mass to simplify the vibration testing, Type 1A close outs were used for thermal cycling, and provided diverging and converging inlets and outlets for the axial gas flow. Also the No. 1 unit had Type A tube-plate joints, whereas units 2 through 10 inclusive were fabricated with the Type B joints.

The detail and assembly operations for the tube bundle to header plates and transverse flow wall (shell) presented no serious difficulties with complete self jigging achieved. A composite photograph (Figure 7-17) presents the details in various manufactured steps, and includes the total tooling used, less brazing envelope. The thin wall tube convolutes were formed by inserting an expandible mandrel to a predetermined depth into the tube end, expanding by forcing the tapered mandrel through a split tubular form using hand pressure, releasing the pressure and withdrawing the tool. Header end plates were a slip fit inside the shell. Shell O.D. was chemically milled for welding purposes.

The final two test units were fabricated to a modified tube-plate joint design as it was determined that the thermal expansion convolution form was incorrectly posotioned (not at the tube inflexion point), and as such, lowered the tube life under reverse deflections when subjected to a vibrating environment.

The details for the modified design are presented in Figure 7-18. Convolutions were deleted as form tooling limitation precluded location of the convolution at the inflection point. A press fit end plate retainer ring was incorporated to replace the end plate locating function of the convolutions. The tube to header flange was formed in the opposite direction of Units No. 2 through 10 to compensate for the braze joint contact area attributable to the convolutions. This in turn required the use of Number 24 braze sheet (clad both sides) for the end plates so that braze alloy would be located at the interfaces of both the tube to header joints and the header to shell joints.

TYPE 1

VIBRATION-TEST MATRIX

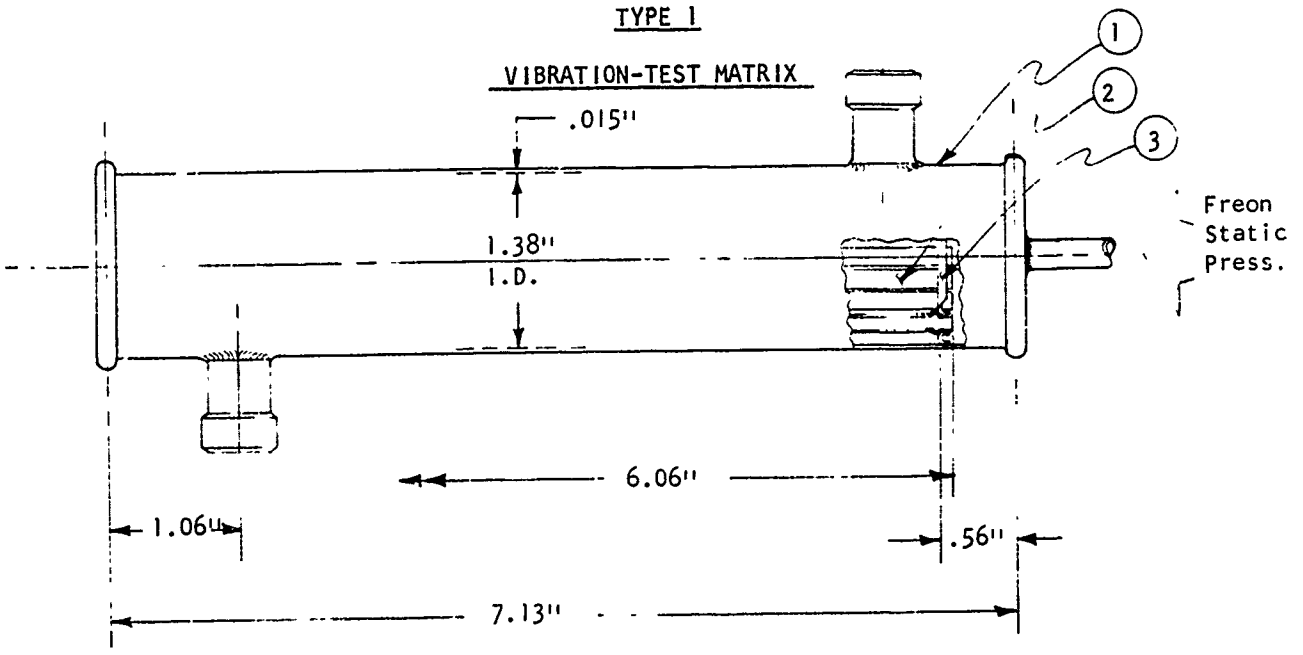

TYPE 1A

THERMAL CYCLING-TEST MATRIX

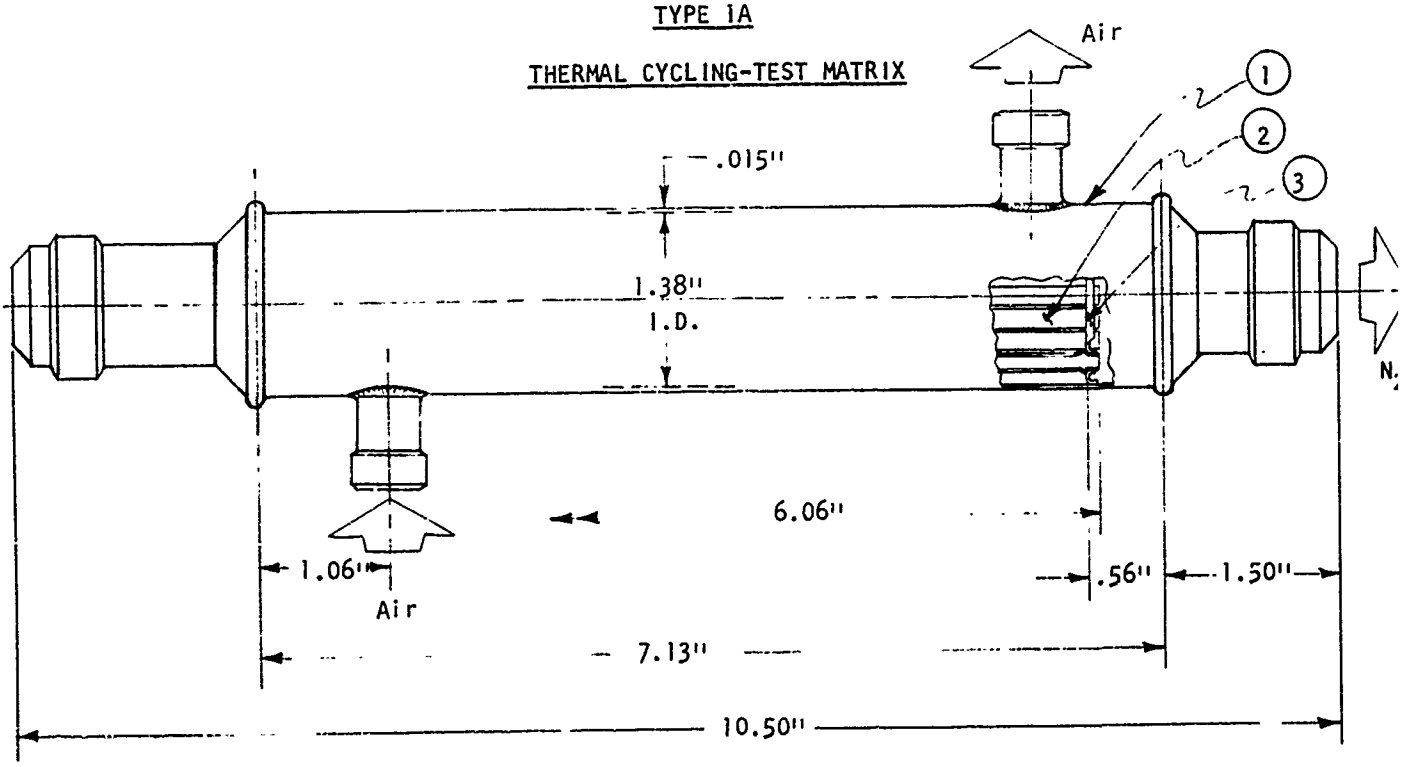

① SHELL 6061 ALUMINUM
② TUBE .125" O.D. x .0375" WALL THICKNESS 6061 ALUMINUM
③ HEADER PLATE .015" 6061 ALUMINUM

Figure 7-16

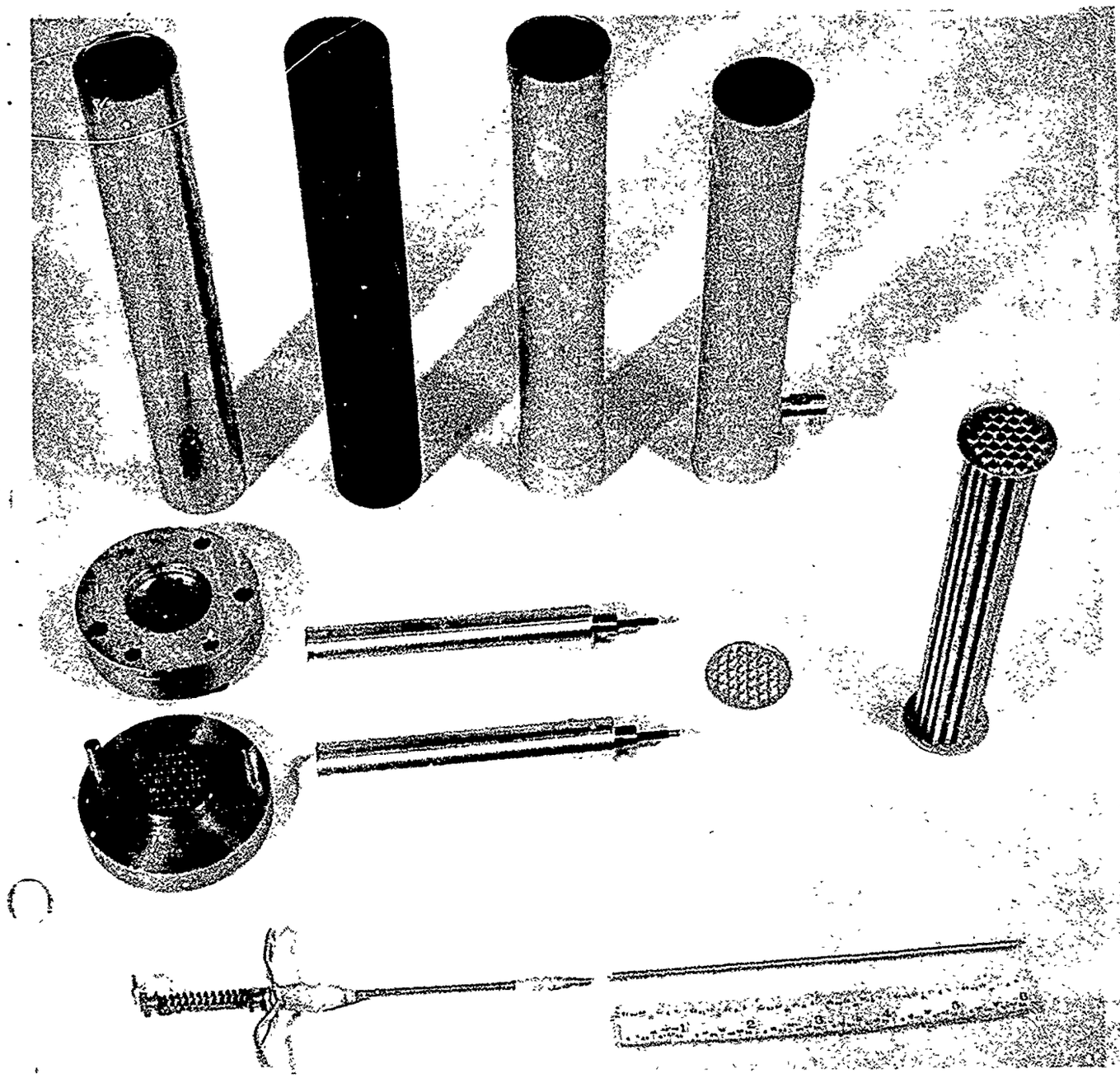

- Tube Shell Heat Exchanger Matrix Details and Tooling

Figure 7-17

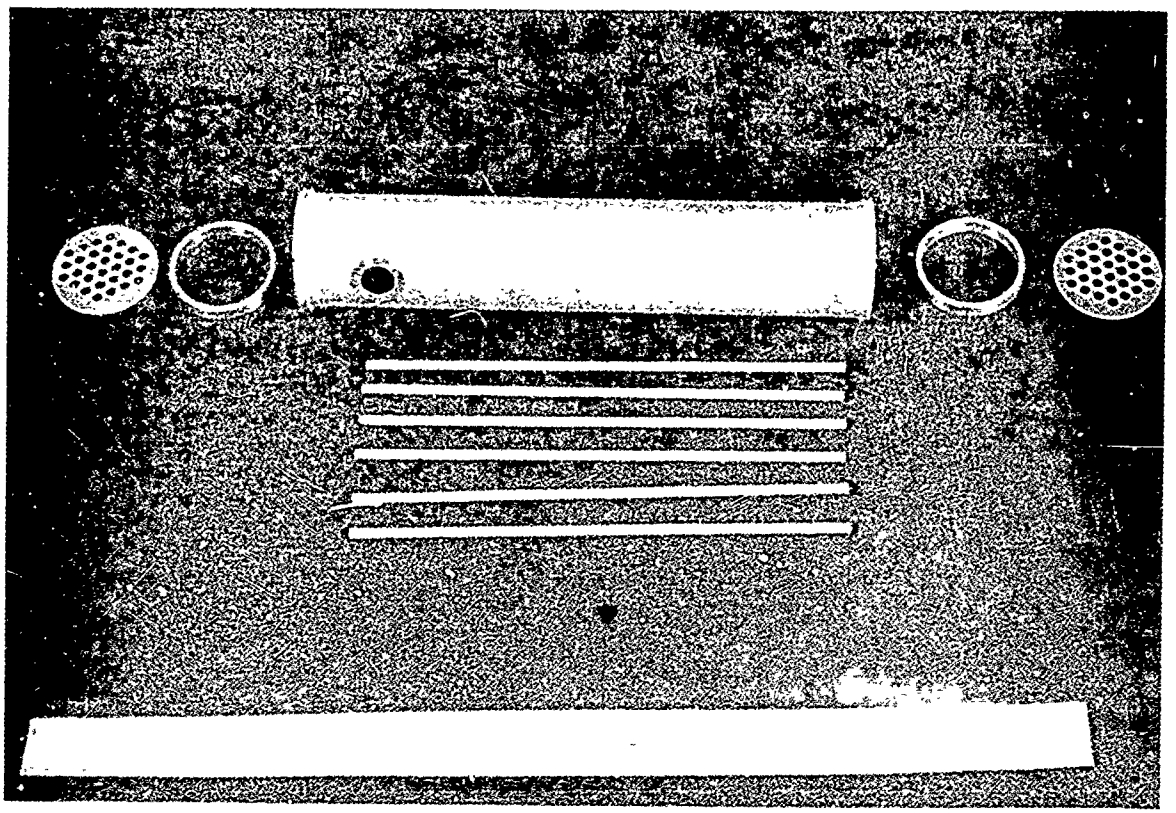

Modified Tube Shell Heat Exchanger Matrix Details

(Only six tubes shown for clarity)

Figure 7-18

7.3.2.1 Tube-Shell Brazed Matrix - Vibration Test

The objective of the vibration testing was to establish the integrity of the tube-to-header plate brazed joint when subjected to a dynamic environment. As the test units were to be pressurized with Freon during vibration, to permit detection of initial structural failure by loss in pressure, it was necessary to conduct an internal pressure stress analysis, to hold the resultant stresses from the gas pressure to a level that could be ignored as a factor during vibration.

The analysis showed the outer shell was the more critical structural element. However, this shell is partially removed prior to vibration to permit an optical measurement of the tube bundle element amplitudes during the actual vibration test and only the axial flow tubes are pressurized.

The following analysis provides the tube-to-plate joint shear stress and axial load on the tube elements and shows that a pressure of 30 psig induces stresses low enough that they can be ignored during vibration.

The stress is due to an internal pressure applied to the header plates and reacting on the tube bundle at the brazed joint. A pressure of 30 psig was used. Based on test results, a minimum ultimate shear stress (Fsu) of 12,000 PSI will be used.

Load = Area X Pressure

Area = Header Plate Surface Area Minus Tube Area

$$A = \frac{M}{4} (D^2 - N d^2)$$

A = Area, in^2

D = Diameter of Header Plate

d = Outside Diameter of Tube

N = Number of Tubes

$$A = \frac{M}{4} [1.375^2 - (30) (0.125)^2]$$

$$A = 1.117 \text{ in}^2$$

$$\text{Load} = (1.117 \text{ in}^2) (30 \frac{\text{lbs}}{\text{in}^2}) = 33.51 \text{ lbs.}$$

Load/Tube = 30 Tubes - 1.117 lbs/Tube

Circumference of 1/8 inch tube = $0.125\pi = 0.393$ in.

Shear Area = (0.393) (0.016) = 0.00628 in^2

(Header Thickness = 0.016 in.)

$$\text{Shear Stress, } Fs = \frac{P}{A} = \frac{1.117 \text{ lbs}}{0.00628 \text{ in}^2} = 1{,}775 \text{ lbs/in}^2$$

$$\text{Margin of Safety, M.S.} = \frac{12000}{1775} - 1 = \underline{\underline{5.76}}$$

The stress in the tube produced by the pressure is a resultant of the hoop tension and the axial tension and is as follows:

$$\text{Hoop Stress, } f_{t_h} = \frac{P\,d}{2t}$$

Where: f_{t_h} = Hoop Stress, lbs/in^2

P = Pressure, lbs/in^2 (30 lbs/in^2 for test)
t = Wall Thickness of Tube, Inch
d = Inside Diameter, Inch

$$f_{t_h} = \frac{30\ [0.125 - 2(0.00375)]}{2(0.00375)} = 470 \text{ lbs/in}^2$$

$$\text{Axial Stress, } f_{t_a} = \frac{P}{A}$$

Where: f_{t_a} = Axial Stress, lbs/in^2

P = Axial Load,
A = Cross Section Area of Tube in^2

$$A = \frac{\pi}{4}\left\{0.125^2 - \left[0.125 - 2(0.00375^2)\right]\right\}$$

$A = 0.00144$ in^2/Tube
$P = 1.117$ lbs/Tube

$$f_{t_a} = \frac{1.117}{0.00144} = 775 \text{ lbs/in}^2$$

$$f_{total} = \sqrt{(f_{t_h})^2 + (f_{t_a})^2}$$

$$f_{total} = 904 \text{ lbs/in}^2$$

MIL-HDBK-5 Allowables for 6061-T6: Ftu = 38,000 lbs/in^2
Fty = 35,000 lbs/in^2
Fsu = 24,000 lbs/in^2

$$\text{Margin of Safety, M.S.} = \frac{38000}{904} - 1 = \underline{\underline{41.0}}$$

It is noted that the stresses produced by 30 psig are small and the effect on the vibration from this pressure will be small.

A preliminary structural analysis was performed to predict a stress level in the brazed joint and to determine the natural frequency of the heat exchanger tubes. To perform this analysis, it was assumed

1. The tube-to-header plate joints were fixed.
2. The tubes would be loaded by a uniform input "g" level acceleration of 20 g.
3. The assembly would experience a magnification of six times the input load during the test.

The analysis predicted that the static 1g stress in the brazed joint was 10.65 PSI with a deflection of 1.83×10^{-5} inches at the center. The lowest natural frequency (normal to the axis of the tubes) was 734 HZ. The stress at 120 gs would then be 1228 PSI.

The preparation of the test specimens was as follows:

The ends of the shell were welded closed with 0.080 inch thick aluminum plates. A 1/4 inch I.D. pipe was welded to the center of one end close out plate so that the two headers and tube bundle could be pressurized with freon gas. The freon gas source line included a pressure gage, and was valved such that during vibration, any damage to joints or tubes would be indicated by a drop in pressure. A 90° segment of the outer shell extending to 1/2 inch from each end plate was removed, so as to permit measurement of any tube motion during vibration. The matrix was clamped into a vibration fixture by circular pads; one at each header plate position. The header and tube passage was proof tested for leaks at 60 PSI, all exterior joint surfaces were sniffed with a probe attached to a mass-spectrometer. The matrix as prepared and mounted is illustrated in Figure 7-19. The complete equipment set-up is illustrated in Figure 7-20.

Vibration equipment capacity and type used was as follows:

Ling Vibrator - 1500 Force Pounds
X-Y Plotter
Optron - Model 680 - Optical Tracker
Log Amplifier
Oscilloscope

Vibration Test

Two tube shell heat exchangers were subjected to a sinusoidal vibration environment until failure. Failure was indicated by a loss in gas pressure in the 1/8 inch O.D. tubes and/or header passage.

The No. 1 exchanger (first part tested) had a Type A tube-to-end plate joint while the No. 2 exchanger had Type B joints.

A frequency sweep at 6g input level was performed on Unit No. 1, to determine the resonant frequencies.

The measured resonant frequency was 760 HZ, close agreement with the calculated 734 HZ. The measured magnification factor was 322. This represented an output level of 1932 g.

The part lost pressure during the frequency sweep test while in the first resonant frequency. The tubes maintained structural integrity and the unit was used to obtain other basic vibration data. The data obtained included the "g" level distribution along the length of the tubes vs. input "g" level. It was determined that the tubes were vibrating in the first mode of resonance by use of a strobe light; also, each tube was resonating at a slightly different frequency and that the plane of vibration of some tubes was not always in the same plane as the driving force.

An analysis was performed to include the measured "g" level distribution across the length of the tubes. The mass or weight of the tube times the "g" level at each point was used as the load. The ends of the tubes were assumed to be fixed. A 1g input stress level at the brazed tube-to-header plate joint was calculated to be 1222 PSI.

A change in the test procedure was made to prevent the second part from failing in the frequency search. The test was to be performed at resonant frequency and in ten minute increments, the first to be performed at 0.75g and each increment to be increased by 0.25 g.

Unit No. 2 was subjected to a sinusoidal frequency sweep to determine the resonances and magnification factors. The lowest natural frequency was 760 HZ and the magnification factor was 722.

Table 7-2 shows the input "g" level and time for each level of load input together with a monitored read out of pressure losses. Table 7-3 shows the input "g" level, the applied stress, time at "g" input, number of applied cycles, allowable number of cycles, and summation of minor fatigue damage $\Sigma\text{-}(n_i/N_i)$.

The allowable number of cycles (N_i) was determined from an SN curve of 6061-T6 material. The applied number of cycles (n_i) was the applied frequency (resonant frequency, 760 HZ) times the test period in seconds for each of the load inputs. The sum of the ratios of n_i to N_i, $\Sigma = (n_i/N_i)$ gives the percent of fatigue damage. When this sum is equal to one (1), a failure is predicted.

Table 7-2 shows a pressure drop during the 3.00 g level input. Table 7-3 predicts a failure after 29 minutes at 3.25 g input.

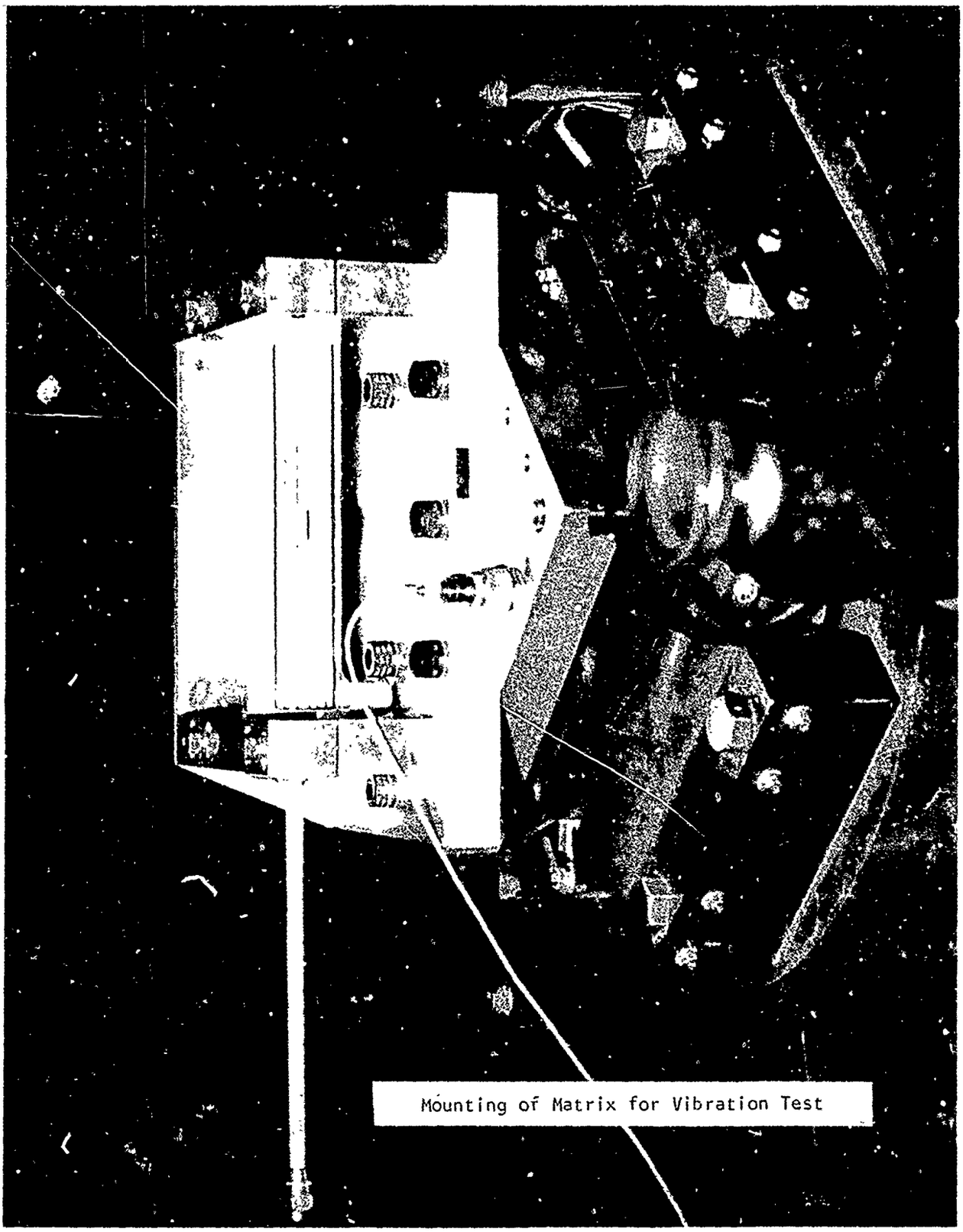

Figure 7-19

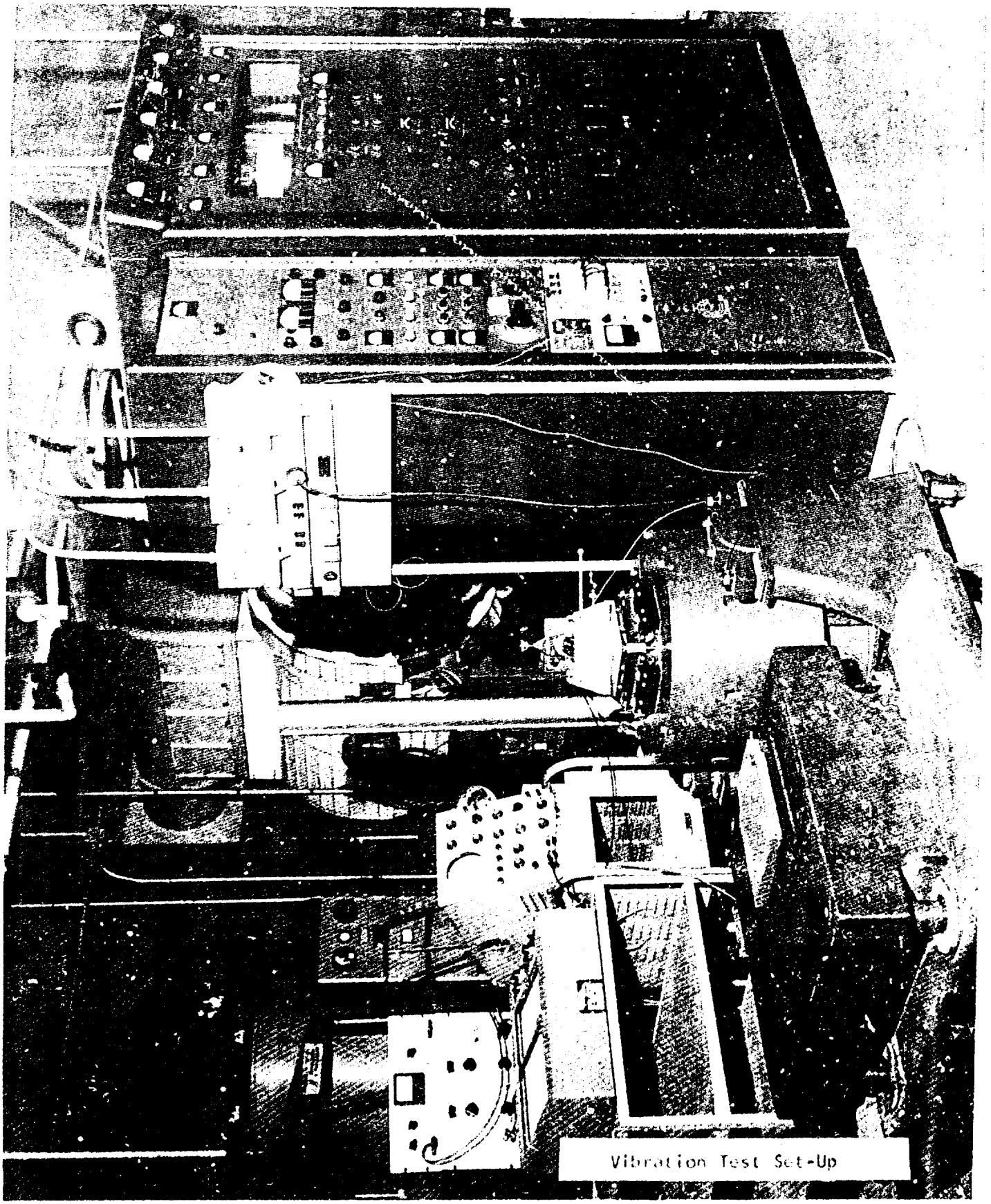

Figure 7-20

Tube-Shell "g" Level - Cycling - Vibration vs Pressure Loss

Input "g" Level	Time of "g" in Mins.	Pressure PSIG
1.00	10	30
1.25	10	30
1.50	10	30
1.75	10	30
2.00	10	30
2.25	10	30
2.50	10	30
2.75	10	30
3.00	10	29
3.25	3	22.5
3.25	5	21.5
3.25	6	18
3.25	7	16
3.25	8	12.5
3.25	9	11
3.25	10	8

Table 7-2

Tube-Shell Vibration Endurance Limit

Input "g" Level	Applied Stress (PSI)	Time of "g" Input In Minutes	No. of Applied Cycles (ni)	Ni	ni	ni/Ni
1.00	2740	10				
1.25	3420	10				
1.50	4110	10				
1.75	4790	10				
2.00	5480	10				
2.25	6170	10	456000	1.0×10^8	.004560	.004560
2.50	6850	10	456000	1.2×10^7	.038040	.042600
2.75	7530	10	456000	5.8×10^6	.078600	.121200
3.00	8220	10	456000	3.3×10^6	.136500	.257700
3.25	8900	3	136800	2.1×10^6	.065160	.322860
3.25	8900	5	218000		.108600	.431460
3.25	8900	6	273600		.130260	.561720
3.25	8900	7	392000		.151980	.713700
3.25	8900	8	364800		.173700	.887400
3.25	8900	9	410400		.195420	1.082820
3.25	8900	10	456000	2.1×10^6	.217140	1.299960

Table 7-3

Vibration Failure Analysis

Unit No. 2 was vibration tested and developed a minor gas leak during the 3g level input. It was subjected to between 2,000,000 and 2,600,000 cycles at this level during which the static pressure dropped from 30 psig to 8 psig. This unit was tested and the leak rate was measured at 1.37×10^{-7} std. cc/sec. of helium at 30 psig, which equals 1.22×10^{-9} std. ft^3/year. This rate in terms of quantity was insignificant. In order that the cause of the pressure loss could be located, the unit was subjected to a further 2,736,000 cycles at 2.25 "g" load input. Since no apparent increase in damage occurred, the load input level was increased to 4 "g" which immediately (not more than 60 seconds at 760 HZ) caused propagation of the defect resulting in a complete loss in the axial flow passage pressure. This damage was investigated.

The ends of each axial thin wall tube prior to brazing had two beads (convolutions) formed, one at each end adjacent to the header plates. The purpose of these convolutions was two-fold. The primary purpose was to provide a thermal expansion joint; the other purpose was to index the position of the two (2) header plates. In reviewing the tube design the best location structurally for convolutions would be at the inflection points.

These inflection points, having no bending stresses due to vibration or "g" loading, occur at 21.13% of the length of the tube. With the convolution at the 21.13% location, the only load to be transferred through the convolution is the shear load. The Number 2 unit was disassembled for visual inspection by cutting away the outer shell. An examination showed the leak defect to be located at the major diameter of one of the convolutions, and found to be a crack propagating radially around the circumference as shown in Figure 7-21. An electron fractography study was conducted on the fracture surface, however, due to the thinness of the wall (0.00375"), the fracture surface replica could not be produced for the total wall surface edge; consequently, the type of fracture initiation could not be determined. About 70% of the fracture surface was reproduced and the failure mechanism of that portion of the fracture area studied was of the type to cause a quasi-cleavage (over-stressed) rupture as illustrated in Figure 7-22.

Fracture replicas were obtained by a two-step replicating technique, using a mylar film and carbon deposition followed by platinum shadowing of the carbon interface prior to dissolving of the plastic film.

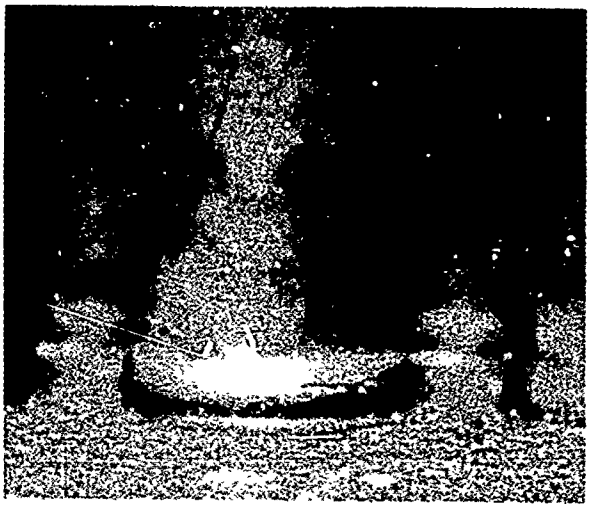

Fractured Convolution - Tube Shell Test Unit Number 2

Figure 7-21

Electron Fractograph - Quasi-Cleavage and
Dimpled Ruptured

Magnification - 29,400X

Figure 7-22

7.3.2.2 Tube-Shell Brazed Matrix-Thermal Cyclic Tests

Objective of the thermal cyclic tests was to demonstrate the practical aspects of the application of fluxless brazed thin walled aluminum tube shell heat exchangers for possible service requiring 500 F hot air to be cooled with super cooled counter flowing gas.

As differential expansion would occur during thermal cycling, a study of the effect of the worst temperature condition was made. In order to conduct this study it was assumed that the shell did not deflect, also, because of the complex configuration of the two header end plates, a four-spoke configuration was used with an equivalent total cross section of that of the plates. On this basis, it was calculated that the end plates (due to contraction) were in tension and a strain of 0.006 inches could have been applied across the diameter of the plate. Should the plate have sufficient resistance to elastic yield, the circumferentially brazed joint would come under a damaging stress and if as previously assumed the shell did not deflect, the joint could have been overstressed and have failed. All of which required that the end plates be designed sufficiently weak so as to yield elastically in order to prevent damaging stresses reacting at the plate-to-shell joint.

A series of induced thermal stress tests were conducted on Type 1A heat exchanger units conforming to the drawing shown in Figure 7-16 (Section 7.3.2). Thermal testing was so arranged that the hot gas would flow into one side and end of the shell passage, over the surface of the cooled tube bundle, and exit out at the opposite side and end of the passage, while super-saturated cold gas was forced into the divergent header at the same end as the hot gas inlet and passed through the tube bundle and exited through a converging header at the opposite end.

Figure 7-23 illustrates the thermocouple positions used to measure gas stream and component surface temperatures. Figure 7-24 shows Unit No. 3 heat exchanger matrix and Figure 7-25 shows the matrix installed and ready for thermal cycling. The test procedures used are described in the following:

- The tube shell heat exchanger matrix unit was proof pressure leak tested with helium at a 60 PSIG positive pressure in the header and tube bundle passage. With shell passage (hot passage) connected to a mass-spectrometer leak detector calibrated to 0.1 X 10^{-9} std. cc/sec. minimum leak rate, measureable leak rates were recorded.

  Hot air was forced through the shell inlet port at 500 F with temperature control obtained by measuring the hot air stream at the inlet and manually correcting the power input to the electrical heating source. The hot air temperature and flow was

maintained at a steady state until all eleven (11) thermocouples were reasonable stable, at which point cold supersaturated N2 gas was forced through the inlet header and tube bundle at -300 F to -320 F. The cold gas stream temperature was measured with the #10 thermocouple at the inlet header and by the #11 thermocouple at the outlet. Both hot air and cold N_2 gas flows were maintained until the nine (9) remaining thermocouples showed a steady EMF. Both air and N_2 gas flows were then cut off and the heat exchanger matrix unit brought back to ambient temperature, this completed one (1) thermal stress cycle. This cycle was then repeated eleven (11) times making a total of twelve (12) . The matrix was then proof pressure leak tested. Seven (7) further cyclic series were conducted.

Table 7-4 shows a typical series of twelve thermal stress cycles. Based on the low differential between the supercooled nitrogen inlet and outlet temperatures, the minimum part temperature during the hot air /N_2 cycle was assumed to be -300 F at the inside surface of the tubes. The outer shell temperatures (T.C. 3 through 8 averaged 105 F which indicates the minimum total temperature differential between tubes and shell was 405 F. The inlet fitting temperature (T.C. No. 2) averaged 278 F indicating maximum total temperature differential to be 578 F. However, local areas directly under the inlet fitting could have been subjected to temperature differentials up to 800 F due to direct impingement of the hot air stream. The efficiency of the unit is demonstrated by the difference of 453 F between the inlet air temperature and the outlet fitting temperature (assumed to equal the outlet air temperature).

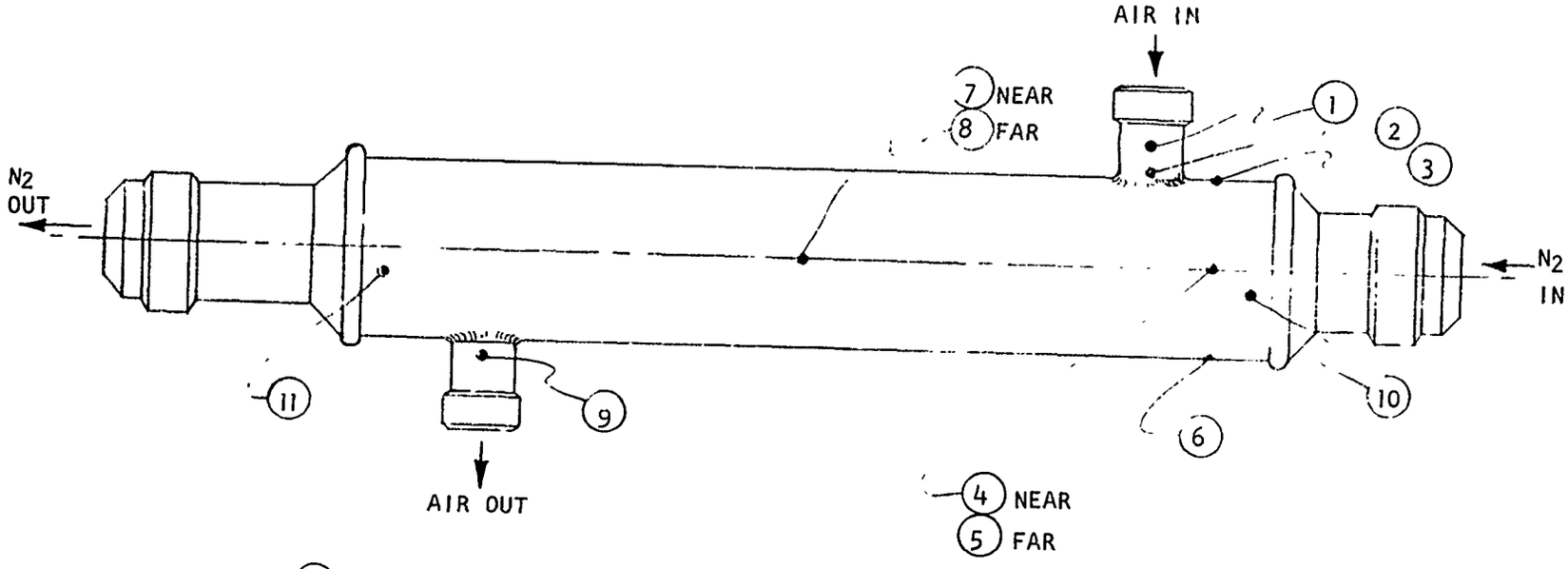

(1) HOT AIR STREAM

(2)(9) FITTING SURFACE

(3)(4)(5)(6)(7)(8) SHELL SURFACE

(10)(11) N_2 STREAM

INDICATES THERMAL-COUPLE NUMBER AND LOCATION

Figure 7-23

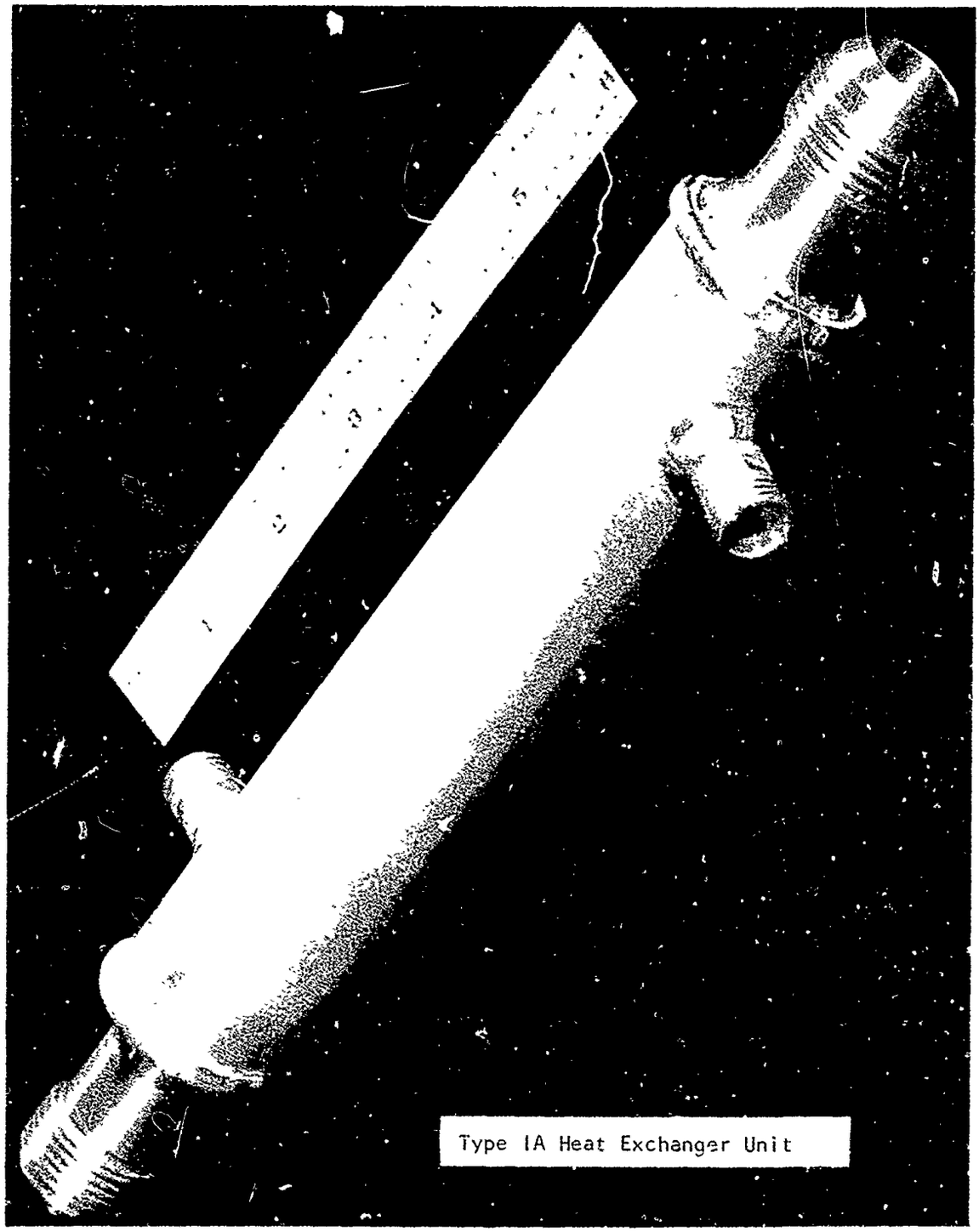

Figure 7-24

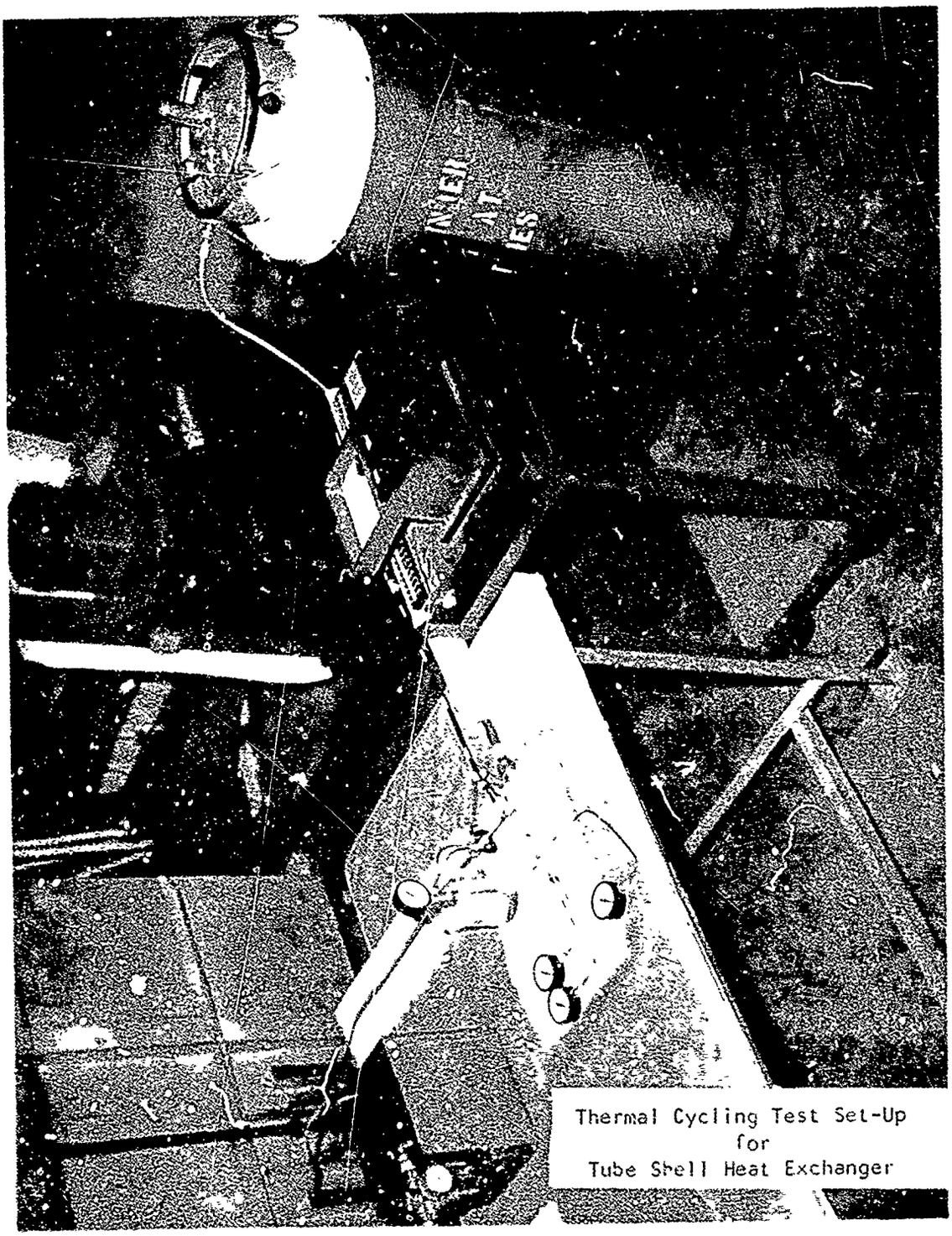

Thermal Cycling Test Set-Up
for
Tube Shell Heat Exchanger

Figure 7-25

TYPICAL TUBE-SHELL THERMAL STRESS TEST SERIES

TABLE 7-4

	Cycle #	STEADY STATE TEMPERATURE °F - EACH T. C. POSITION										
		1	2	3	4	5	6	7	8	9	10	11
Hot Air	1	505	448	412	412	398	398	392	390	397	496	329
Hot Air/N_2		509	290	120	20	66	60	162	146	44	-300	-300
Hot Air	2	500	445	411	408	393	393	389	385	388	496	307
Hot Air/N_2		500	307	156	68	114	104	194	181	85	-304	-304
Hot Air	3	502	434	396	392	382	380	378	372	375	488	300
Hot Air/N_2		503	262	88	-20	30	24	142	128	8	-300	-300
Hot Air	4	508	442	410	404	384	384	384	376	377	485	302
Hot Air/N_2		500	273	120	12	72	55	152	138	34	-300	-300
Hot Air	5	503	416	366	358	355	358	373	362	362	492	248
Hot Air/N_2		504	270	112	4	60	46	158	140	12	-300	-300
Hot Air	6	501	416	368	362	354	356	369	359	360	488	258
Hot Air/N_2		504	282	128	28	80	68	164	154	46	-300	-308
Hot Air	7	500	420	384	378	370	370	373	365	368	490	285
Hot Air/N_2		500	270	110	20	64	48	160	140	44	-300	-300
Hot Air	8	502	416	380	373	363	365	375	365	367	492	288
Hot Air/N_2		500	275	125	40	84	70	168	155	50	-310	-310
Hot Air	9	500	400	368	358	348	350	367	355	357	488	255
Hot Air/N_2		501	280	138	45	88	80	176	163	58	-300	-305
Hot Air	10	503	412	375	368	360	362	376	364	366	490	274
Hot Air/N_2		500	276	128	36	76	68	170	156	48	-300	-305
Hot Air	11	501	400	362	353	343	345	364	352	350	488	242
Hot Air/N_2		500	278	132	46	88	84	186	165	86	-300	-304
Hot Air	12	504	416	384	376	366	368	375	366	370	488	283
Hot Air/N_2		498	278	132	40	78	74	172	160	55	-295	-301

Table 7-5 presents the thermal cycling versus leak rate results of tests performed on Units No. 3, 4 and 5. Unit No. 3 had a leak rate of 3.11×10^{-8} std. cc/sec. prior to the start of thermal cycling tests and a leak rate of 1.72×10^{-5} std. cc/sec. at the completion of 96 thermal stress cycles. The last 36 cycles showed no significant increase in leak rate and the final leak rate is considered acceptable for most service applications. Unit No. 4 had no detectable leak prior to the start of the thermal cycling test but had leaks in the wall of six (6) tubes after 12 thermal stress cycles and had leaks in the wall of 29 tubes after 24 thermal cycles. Unit No. 5 had a 7.36×10^{-8} leak prior to start of thermal stress cycling. This leak exceeded the maximum range of the leak detector after 12 thermal stress cycles while after 24 thermal stress 26 leaks were found in tube walls.

Tube-Shell Thermal Cycle vs Leak Rate

Table 7-5

Cum. Thermal Cycles	Unit No. 3 Helium Leak Rate Std. cc/sec.	Unit No. 4 Helium Leak Rate Std. cc/sec.	Unit No. 5 Helium Leak Rate Std. cc/sec.
None	3.11×10^{-8}	None	7.36×10^{-8}
12	3.30×10^{-8}	6 Tubes (1)	1 Tube (1)
24	6.25×10^{-8}	29 Tubes (1)	26 Tubes (1)
36	2.40×10^{-6}	(2)	(2)
48	2.45×10^{-6}		
60	1.61×10^{-5}		
72	1.28×10^{-5}		
84	1.53×10^{-5}		
96	1.72×10^{-5}		

(1) Leak Rate Exceeded Equipment Range
(2) Test Discontinued

Visual observation of the point of departure of bubbles with the unit pressurized to 60 psig with helium and submerged in water, indicated the leak in Unit No. 3 was located in the area of a tube-to-header braze joint, while Units No. 4 and 5 leaks were in the side wall of the 1/8" O.D. tubing some distance away from the braze joint. Stereoscopic examination prior to sectioning revealed no indication of defects in the leak areas. Results of microscopic examination on cross sections from typical defective areas are included in the overall braze quality analysis.

7.3.2.3 Tube-Shell Brazed Matrix-Braze Quality Evaluation

All brazed matrices were subjected to both visual and stereoscopic examinations. Header plates to shell brazed joints showed a solid braze line with well formed fillets. All axial flow tubes also showed a solid braze line.

Six of the first as brazed and welded units are photographically illustrated in Figure 7-26. Figure 7-27 presents the modified header plate version as brazed.

No header plate to shell joints were found defective either visually or by leak tests, or by damage from thermal or vibration testing.

Out of 720 axial tube to end plate joints, 9 were found to leak of which 7 were extremely low and acceptable while 2 were marginal; also it should be considered that these leaks were located and rated with helium, and the rates would be less for other gases or air. Also it is believed that this problem was eliminated in units 11 and 12, with the improved header plate to type joint configuration. All gross leaks were located in the axial flow tubing walls, and found to originate from defects in the as received extruded tubing. Table 7-6 presents a summary of the leaks per unit and type plus the affect of thermal stresses.

Tube-Shell Heat Exchanger Brazements

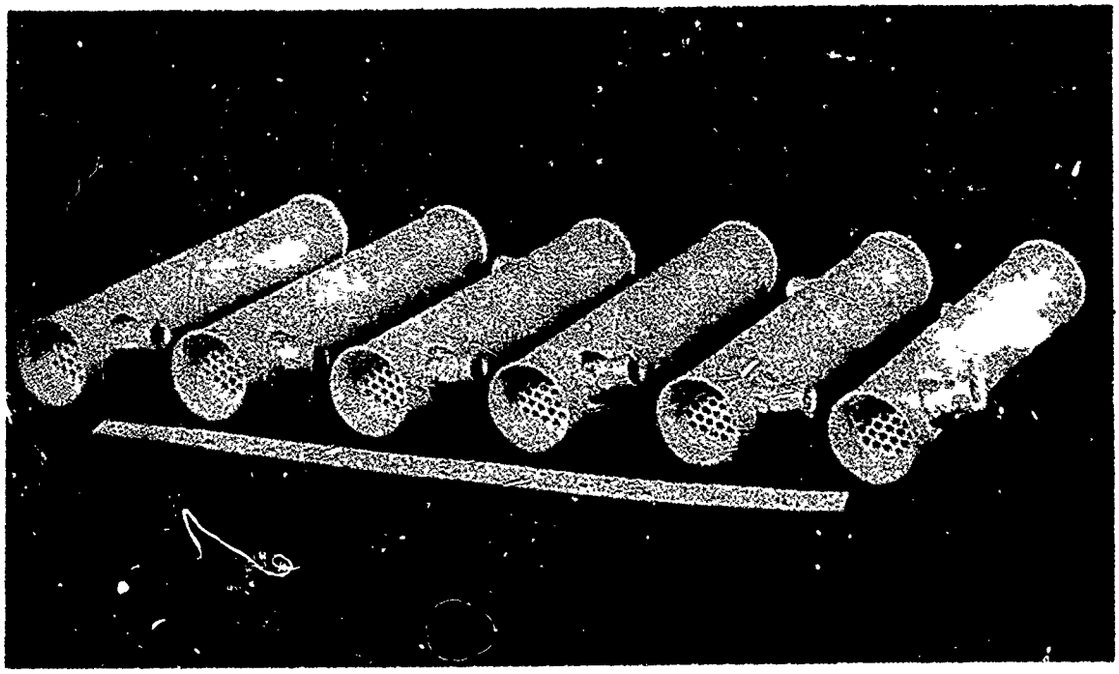

Figure 7-26

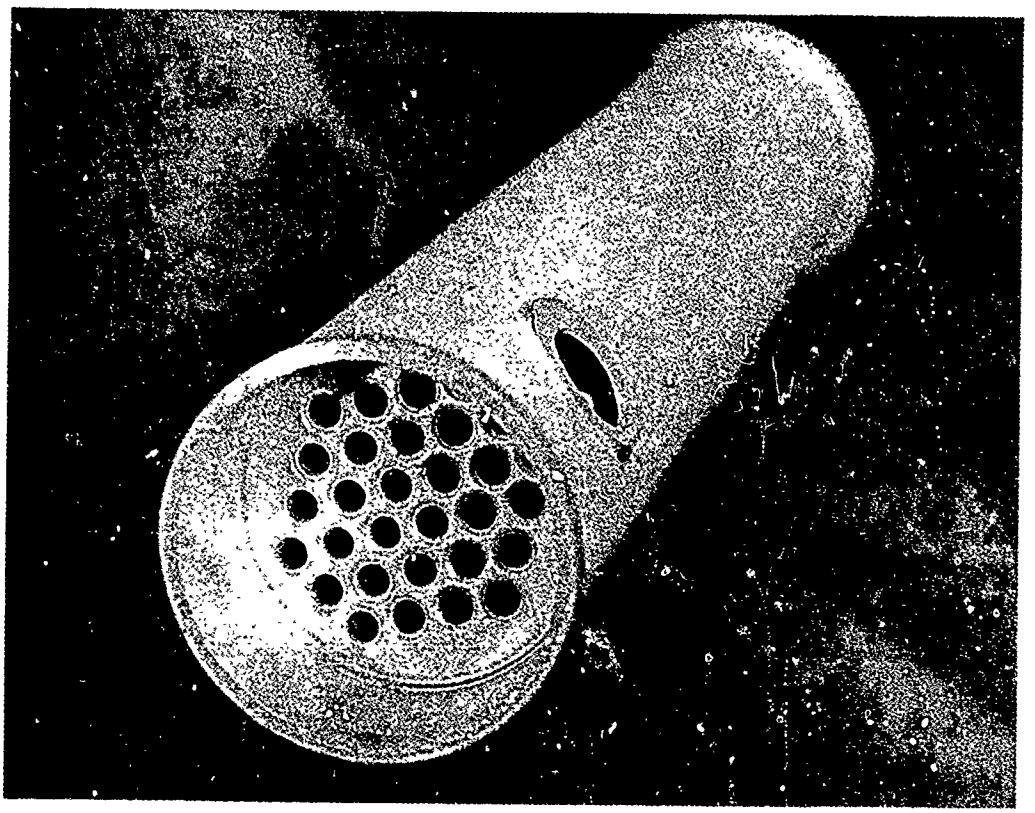

Tube Shell Heat Exchanger Matrix Erazed of Modified Design

Figure 7-27

Tube Shell Matrix - Leak Test Results Summary (1)

TABLE 7-6

Unit No.	Condition of Specimen As Leak Tested			
No.	As-Brazed	Cond. T-6	After Thermal Cycling	No. of Thermal Cycles
1	(2)	4 Tube Joints Rate 8.0×10^{-8}	(2)	None
2	(2)	None	(2)	None
3	(2)	1 Tube Joint Rate 3.11×10^{-8}	1 Tube Joint Rate 1.72×10^{-5}	96
4	None	None	29 Tubes - Rate Exceeded Equip. Range	24
5	None	1 Tube - Rate 7.36×10^{-8}	26 Tubes - Rate	24
6	1 Tube Joint Rate 1.23×10^{-6} 1 Tube - Rate 2.85×10^{-6}	1 Tube Joint Rate 2.85×10^{-5} 1 Tube - Rate 3.5×10^{-6}	(2)	None
7	4 Tubes - Total Rate 3.85×10^{-6}	Rate Exceeded Equipment Range	(2)	None
8	1 Tube Rate 2.38×10^{-6}	Rate Exceeded Equipment Range	(2)	None
9	1 Tube Rate 1.64×10^{-8}	Rate Exceeded Equipment Range	(2)	None
10	2 Tube Joints Total Rate 4.37×10^{-6}	Rate Exceeded Equipment Range	(2)	None
11 (4)	(2)	1 Tube - Rate 1.02×10^{-6}	(2)	None
12 (4)	(2)	1 Tube - Rate Exceeded Equip. Range	(2)	None

(1) Leak rate is shown in std. cc/sec. of helium at 60 psig.
(2) Indicates no leak test in this condition.
(3) Reworked by plug welding ends of axial tubes.
(4) Fabricated from tubing supplied as hydraulic grade.

Microscopic studies of defective areas showed that the brazed joint leaks were due to localized porosity in the braze filler metal. Figure 7- 28 illustrates a defective joint which was sectioned normal to the tube axis.

Axial Flow Tube To Header Plate Joint Defect

Mount # - 510
Magnification - 200X
Boric Acid HF Etched

Figure 7-28

Tube elements with known leaks were removed from one of the heat treated tube shell brazements, and leaks were traced to voids which extended to each wall surface as fine porosity Figure 7-29, 7-30 and 7-31 provide good examples of this type of defect. The porosity condition may also have had an affect on the brazed joints. Foreign matter could have been trapped in the void areas and, if located in a joint area, could cause local contamination.

Tube Wall Defect

Figure 7-29

Tube Wall Surface Defect

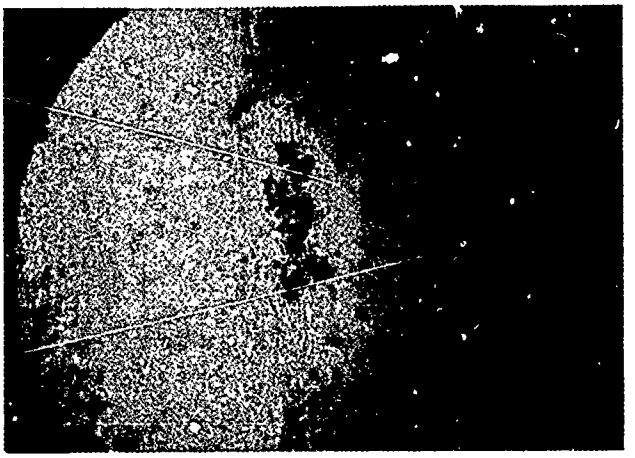

Figure 7-30

Tube Wall Defect

Figure 7-31

The defects occurring in the 1/8" OD thin wall tubes were identified as being in the as-received material occurring as porosity and inclusions. Random lengths of the as-received tubing were inspected under a stereomicroscope; this inspection revealed numerous surface defects. The majority of these defects showed up as surface porosity. Selected defective areas were sectioned and progressively polished through the defect; this investigation revealed gross voids under the porous surface which continued through to the inner wall surface. A number of surface imbedded inclusions were detected in which traces of copper were found. Figure 7-32 illustrates a surface inclusion. The cross sections of this area are shown in Figure 7-33. Figure 7-34 shows a large surface void with an inclusion at one end. The wall is deformed inward which suggests that the inclusion was forced into the tube wall after the extrusion operation.

Tube Surface Defect and Inclusion

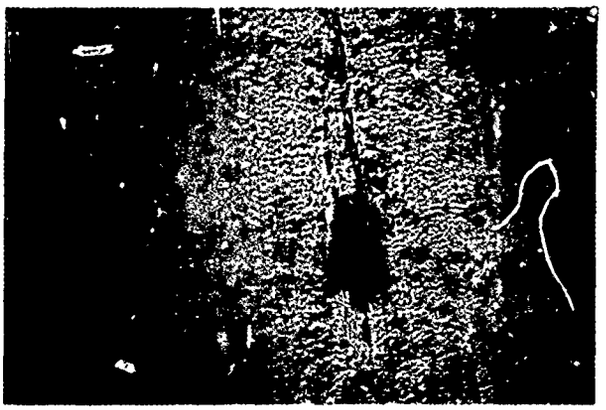

Figure 7-32

Tube Cross Section-Illustrates Inclusion at End of Defect

Figure 7-33

Tube Cross Section-Illustrates Opposite End to Figure 7-33

Figure 7-34

Hydraulic grade 1/8 inch O.D. 6061 tubing was procured having been hydrostatically tested at 300 psig by the vendor. Visual and microscopic examination of the tubing as received revealed no apparent inclusions. A few light longitudinal marks were detected visually, but had no apparent depth when cross sectioned and examined microscopically. A residue of an undetermined nature was observed on the inside surface of the tubing (Figure 7-35) which when subjected to normal cleaning and a simulated braze and heat treat cycle became a black tenacious coating (Figure 7-36). Precleaning in concentrated nitric acid at 200 F for 2 minutes removed all visual signs of contamination when followed by normal cleaning and a simulated braze and heat treatment cycle (Figure 7-37).

Tube Surface Contamination- As Received

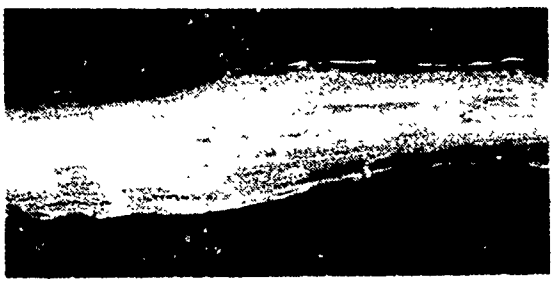

Magnification $2\frac{1}{2}$X
Etchant None
Figure Number 7-35

Tube Surface Contamination-After Brazing

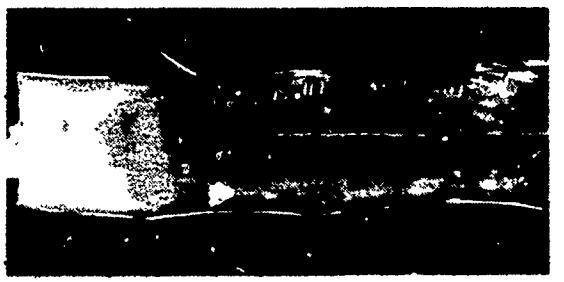

Magnification $2\frac{1}{2}$X
Etchant None
Figure Number 7-36

Contaminate Removed by Acid Cleaning

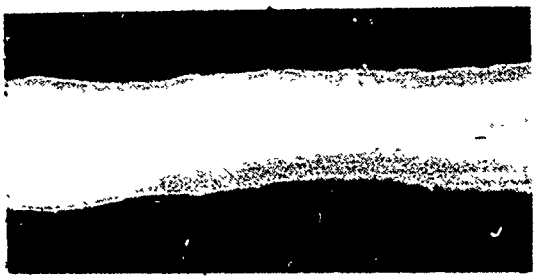

Magnification $2\frac{1}{2}$X
Etchant None
Figure Number 7-37

Unit Number 11 was brazed with the improved quality tubing and incorporated the nitric acid preclean of the detail tubes. A 1.02×10^{-6} leak was detected in one tube (Table 1-6) approximately 0.19 inches from the tube to header plate joint transition.

Unit Number 12 was also brazed with the improved quality tubing except all tube O.D. surfaces were examined microscopically after final cleaning for lay up, and tubes with surface defects were discarded. A leak in excess of the leak detector range was found about midway of tube length in one of the outermost tubes after braze and heat treatment (Table 7-6). The outer shell was removed between header plates and the leak precisely located as shown in Figure 7-38. Figure 7-39 is a close up of the defect and shows the defect to be porosity.

Sections for microscopic examination were prepared from the defect shown in Figure 7-39 and from other dark spots and corrosion patterns seen in Figure 7-38, and from tube to header joints. Figure 7-40 shows the cross section of the leak area. The general rectangular shape of the defect would suggest an inclusion in the material as received. Some porosity at the outer surface was noted. These defects are similar in appearance to those shown in Figures 7-30 and 7-32, indicating that the tube wall quality was not significantly improved. Other defects noted in Figure 7-38 were found to have a maximum of depth of 0.0003 inches.

Tube Surface Leak as Located by Leak

Figure 7-38

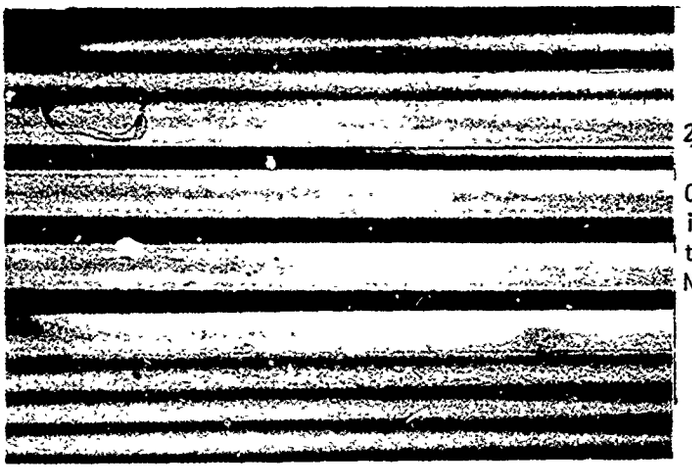

$2\frac{1}{4}$X No Etch

Circles area on tube indicates leak location tube shell heat exchanger Number 12.

Figure 7-39

15X No Etch

Close up view of leak location shown above. Note typical corrosion pattern.

Section of Defective Tube Wall Removed For Brazement

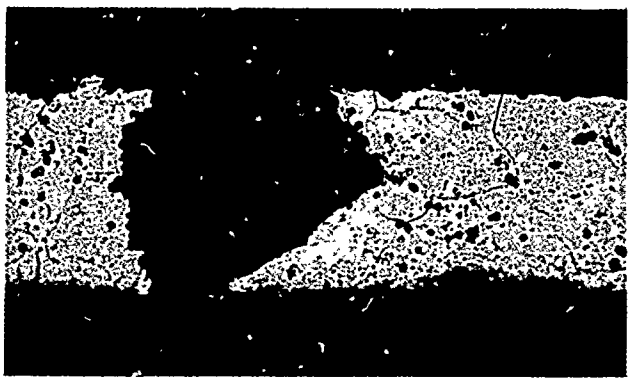

Mount No. - 641
Magnification- 250X
Boric HF Etchant

Figure 7-40

In an attempt to segregate defective tubes prior to fabrication of a tube shell matrix, forty two (42) detail tubes were subjected to a simulated braze and heat treat cycle. These tubes when examined microscopically prior to the simulated cycle, appeared free of defects but all forty two (42) tubes appeared defective after the simulated cycle. Typical defects are shown in Figures 7-41 and 7-42 with the cross section of each shown in Figures 7-43 and 7-44 respectively. The wall deformed inward suggesting that the defect occurred after extrusion and appears to have been caused by embedding of inclusions and/or mechanical damage in handling.

Tube Wall Defects Located by Simulated Braze Cycle Tests

Figure 7-41

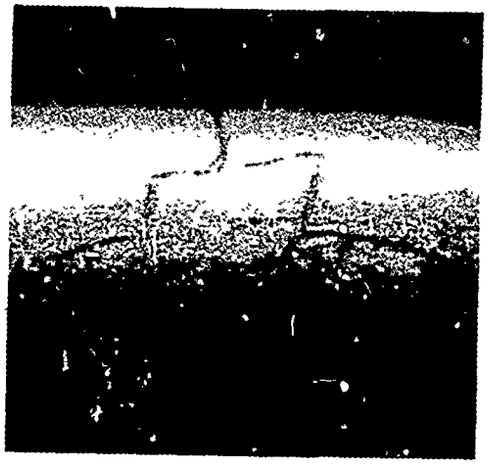

Figure 7-42

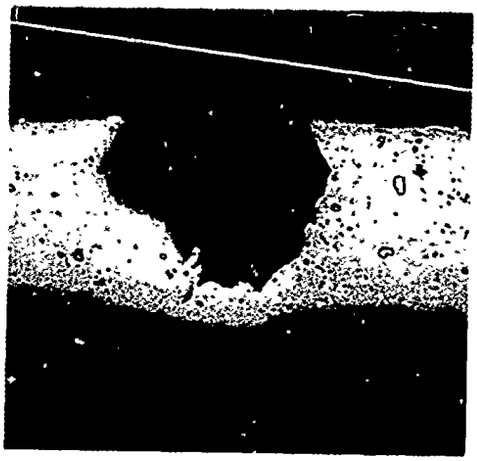

Mount No. - 694
Magnification 250X
Electrant Boric HF Acids

Figure 7-43

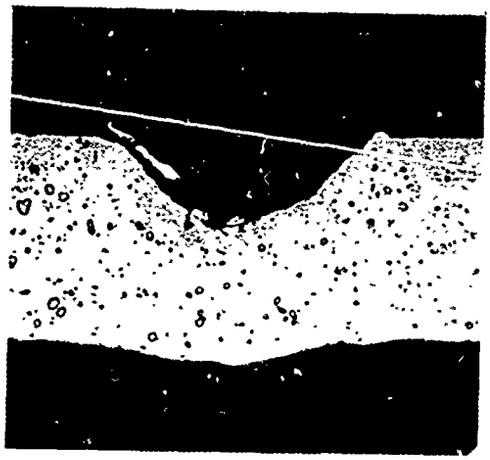

Mount No. - 694
Magnification 250X
Electrant Boric HF Acids

Figure 7-44

7.4 Multi-Layer Plate Fin Heat Exchanger

This investigation covered the application of brazing to fabrication of multi-layer plate fin heat exchangers. The evaluation was concerned only with the brazing problem, thus the configuration evaluated was not designed to a specific performance requirement. However, the brazements were subjected to maximum imposed thermal stress cycling and progressive pressure leak testing as part of the joining reliability study.

A total of three (3) multi-layer plate fin heat exchangers were evaluated for manufacturing feasibility and braze quality. The detail and assembly operations presented no difficulties. The three (3) units were fabricated to the design shown in Figure 7-45. Figure 7-46 shows the details manufactured for the typical unit. The separator plates were machined from 6951 clad with 4045 intermediate alloy on both surfaces. The separator bars were machined from 6061 sheet stock and chem-milled to close tolerance thickness requirements. Pins were used in the 1/4 inch corner mounting holes to index details during braze. The top and bottom face sheets were masked and the 4045 clad intermediate alloy removed from the manifold area by chemical milling to aid welding of manifolds subsequent to brazing.

The first unit fabricated was used for confirmation of the brazing cycle. The matrix build up was thermocoupled at three (3) positions, each of which were recorded and monitored throughout the heat up and initial cool down portion of the braze cycle. Heating rate was programmed at 15 F/min. for the initial heating, and progressively slowed to reduce the ΔT of the work. Actual heating rates and work temperatures are shown in Table 7-7.

During brazing, the surface extended fins apparently provided good heat paths, thus, permitting the heat to conduct sufficiently through the matrix, as substantiated by the final 2F temperature spread experienced. Four progressive heat rate reductions were used during the first 80 minutes; no further changes were needed during the final 14 minutes of heating to the brazing peak out temperature. Units Number 2 and 3 were brazed under similar braze cycle programming.

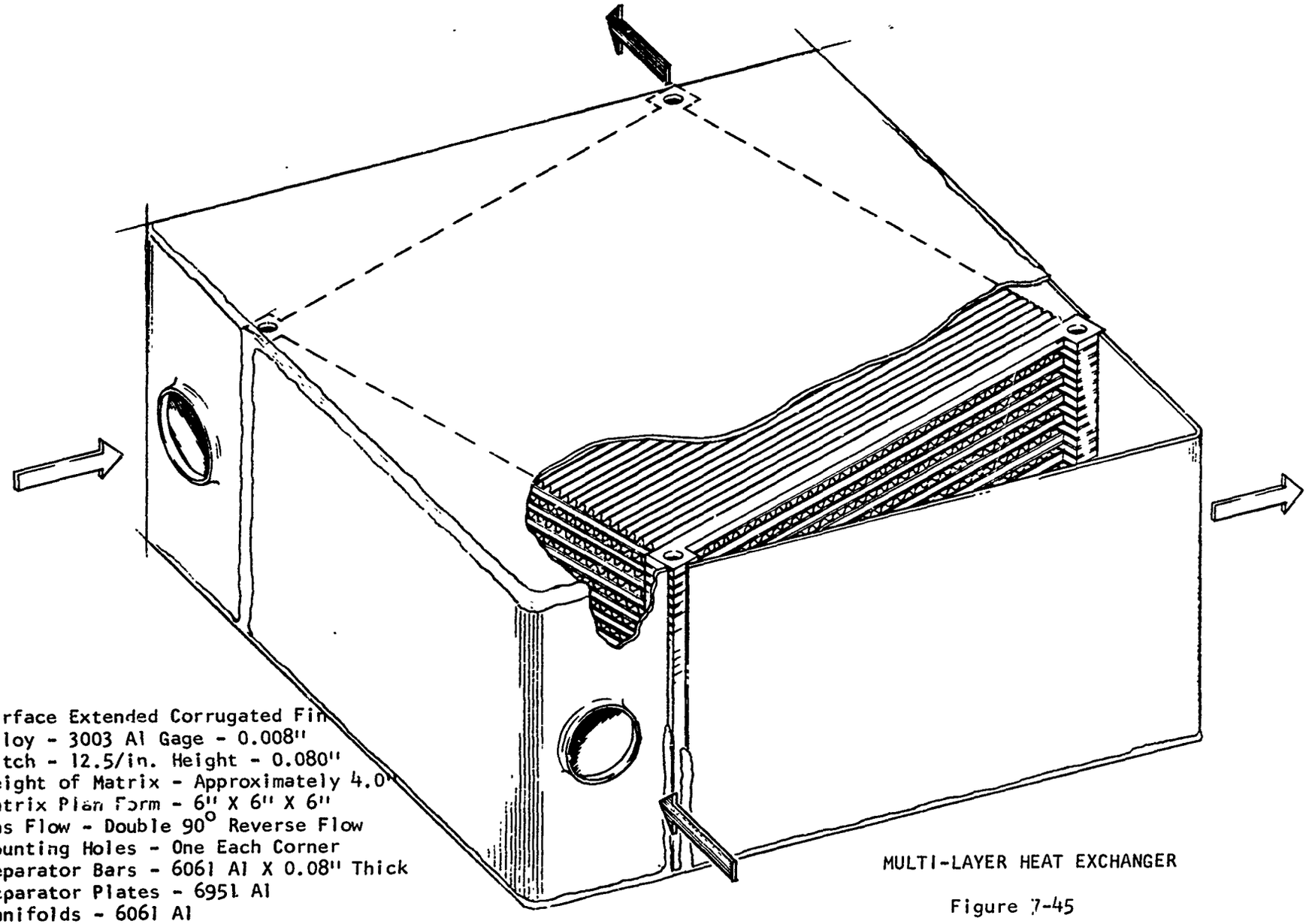

- o Surface Extended Corrugated Fin
  Alloy - 3003 Al Gage - 0.008"
  Pitch - 12.5/in. Height - 0.080"
- o Height of Matrix - Approximately 4.0"
- o Matrix Plan Form - 6" X 6" X 6"
- o Gas Flow - Double 90° Reverse Flow
- o Mounting Holes - One Each Corner
- o Separator Bars - 6061 Al X 0.08" Thick
- o Separator Plates - 6951 Al
- o Manifolds - 6061 Al

MULTI-LAYER HEAT EXCHANGER

Figure 7-45

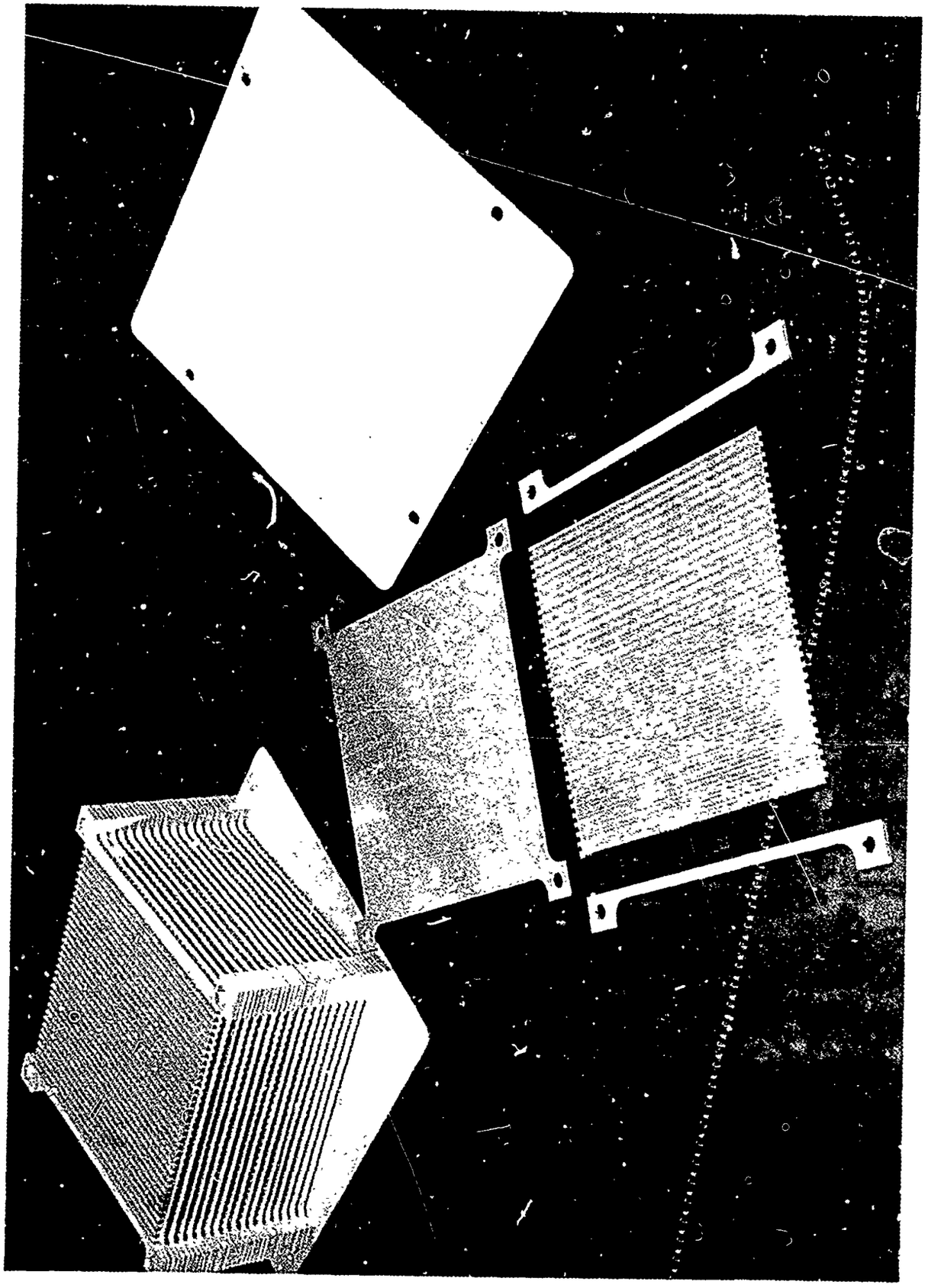

Details for Multi-Layer Brazement Matrix
Figure 7-46

Braze Cycle Heating Rates vs. Work Temperature

TABLE 7-7

Time in Min.	Rate in °F/Min.	Aver Work Temp. °F	TC #1 (1) Temp. °F	TC #2 (3) Temp. °F	TC #3 (4) Temp. °F	ΔT of Work °F
20	14	348	365	330	350	35
40	11	632	640	625	630	15
60	8.5	855	857	648	860	12
80	3.4	1023	1023	1020	1025	5
90	3.4	1059	1060	1058	1060	2
94	Power Off	1075	1075	1073	1077	4
99	Coolant On	1081 (1)	1081	1080	1082	2
100		1060				

(1) Temperature increase due to lag between heating source and work.
(2) Top Center
(3) Center
(4) Bottom Center

7.4.1. Multi-Layer Plate Fin Weldment - Pressure Analysis

The objective of the pressure analysis was to establish safe working limits for proof pressure leak and thermal cyclic testing subsequent to assembly operations. The initial test plan included vibration testing but a prediction failure analysis showed the failure would occur in the external manifolding and not in the brazed matrix. Therefore vibration testing was deleted.

From observation of the configuration, the large unstiffened outer chamber walls of the heat exchanger were pressure critical. The walls were analyzed for the combination of bending and membrane deflection and stresses by subjecting them to a pressure and temperature simultaneously. Maximum pressures were determined for the various temperature extremes from -300 to 500 F and pressures for the various temperature conditions were a function of the ultimate stress.

The formulas used in the following analysis are taken from R. J. Roark, "Formulas for Stress and Strain". For analysis purposes, the edges of the plates (walls) were considered to be simply supported. Plate dimensions were: t = 0.060 in.
a = 6.625 in.
b = 3.900 in.

Where t = plate thickness, a = plate length, b = plate width.

The 6061-T6 alloy properties for the three temperature conditions were taken from MIL-HDBK-5 and are given below:

Room Temperature - $F_{tu} = 42{,}000\ lbs/in^2$
$F_{ty} = 36{,}000\ lbs/in^2$
$F_{su} = 27{,}000\ lbs/in^2$
$E = 9.9 \times 10^{-6}\ lbs/in^2$

500°F - $F_{tu} = 16{,}800\ lbs/in^2$
$F_{ty} = 15{,}800\ lbs/in^2$
$F_{su} = 10{,}800\ lbs/in^2$
$E = 7.9 \times 10^{-6}\ lbs/in^2$

-300°F - $F_{tu} = 52{,}900\ lbs/in^2$
$F_{ty} = 42{,}800\ lbs/in^2$
$F_{su} = 34{,}000\ lbs/in^2$
$E = 10.9 \times 10^{-6}\ lbs/in^2$

The maximum stress and deflection occur at the center. The material is in the T-6 condition at the center, but is in the as-welded condition around the periphery. For this reason the allowable stress is reduced by 50%, therefore, the room temperature values were:

$F_{tu} = 21{,}000\ lbs/in^2$
$F_{ty} = 18{,}000\ lbs/in^2$
$F_{su} = 13{,}500\ lbs/in^2$
$E = 9.9 \times 10^{-6}\ lbs/in^2$

When the deflection of a plate exceeds approximately half of the thickness, the diaphragm or membrane stress becomes of prime importance. The total pressure the plate will accept, will be the superposition of the pressure which causes a deflection by bending up to 1/2t and the deflection produced by membrane action up to the allowabel Ftu.

W = Pressure, lbs/in^2
E = Modules of Elasticity lbs/in^2
t = Thickness of Skin, Inches
a & b = Dimensions of panel, Inches
S = Stress due to pressure, W, lbs/in^2

Membrane Deflection

From the table in Roark, page 222, "Rectangular Plates Under Uniform Load Producing Large Deflection", the values of wb^4/Et^4 can be found.

Solve for Pressure

$$a/b = \frac{6.625}{3.90} = 1.70$$

Temperature = RT

$S = 21,000 \text{ lbs/in}^2$
$b = 3.90 \text{ in.}$
$E = 9.90 \times 10^{-6} \text{ lbs/in}^2$
$t = 0.060 \text{ in.}$

$$\frac{S\,b^2}{E\,t^2} = \frac{(21,000)(3.9)^2}{(9.9 \times 10^{-6})(0.06)^2} = 8.96$$

$$\frac{w\,b^4}{E\,t^4} = 40$$

$$W = \frac{(40)(0.06^4)(9.9 \times 10^{-6})}{(3.9)^4} = \underline{\underline{22.2}} \text{ lbs/in}^2$$

Temperature = -300 F

$$S = \frac{21,000 \times 52,900}{42,000} = 26,500 \text{ lbs/in}^2$$

$E = 10.9 \times 10^{-6} \text{ lbs/in}^2$

$$\frac{S\,b^2}{E\,t^2} = \frac{(8.96)(26,500)(9.9)}{(21,000)(10.9)} = 10.27$$

$$\frac{w\,b^4}{E\,t^4} = 52 \; ; \; \frac{b^4}{t^4} \quad \frac{0.06^4}{3.94} = 5.62 \times 10^{-8}$$

$$W = (52)(10.9 \times 10^{-6})(5.62 \times 10^{-8}) = \underline{\underline{31.7}} \text{ lbs/in}^2$$

Temperature - 500°F

$S = 16,800 \text{ lbs/in}^2$

$E = 7.9 \times 10^{-6} \text{ lbs/in}^2$

$$\frac{S\,b^2}{E\,t^2} = \frac{(16,800)(3.9)^2}{(7.9 \times 10^{-6})(0.06)^2} = 9.0$$

$$\frac{w\,b^4}{E\,t^4} = 40$$

$$W = (40)(7.9 \times 10^{-6})(5.62 \times 10^{-8}) = \underline{\underline{17.7}} \text{ lbs/in}^2$$

It is noted that the pressures, W, will stress the plate to the maximum allowable stress at these temperatures.

Table 7-8 summarizes the established safe internal working pressures for the multi-layer plate fin heat exchanger as designed for this investigation.

Multi Layer (Weldment) Heat Exchanger Proof Pressures

TABLE 7-8

Temperature	Maximum Pressure	Allowable Stress
RT	22.2 PSI	21,000 PSI
-300°F	31.7 PSI	26,500 PSI
+500°F	17.7 PSI	16,800 PSI

7.4.2 Multi-Layer Plate Fin Weldment Proof Pressure Test

All three units fabricated were proof tested at room temperature and 22 psig gas pressure. Figure 7-47 shows a typical pressure test set up. Interpassage leak tests were performed by pressurizing one passage of the heat exchanger with helium and connecting the leak detector to the other passage. Leak tests of the welds and the 1/4 inch mounting holes were performed by pressurizing both passages of the heat exchanger with helium and sniffing external surfaces with a vacuum probe.

No external or interpassage leaks were detected in the three (3) heat exchanger weldments. Header side walls did not permanently deform during proof pressure leak test.

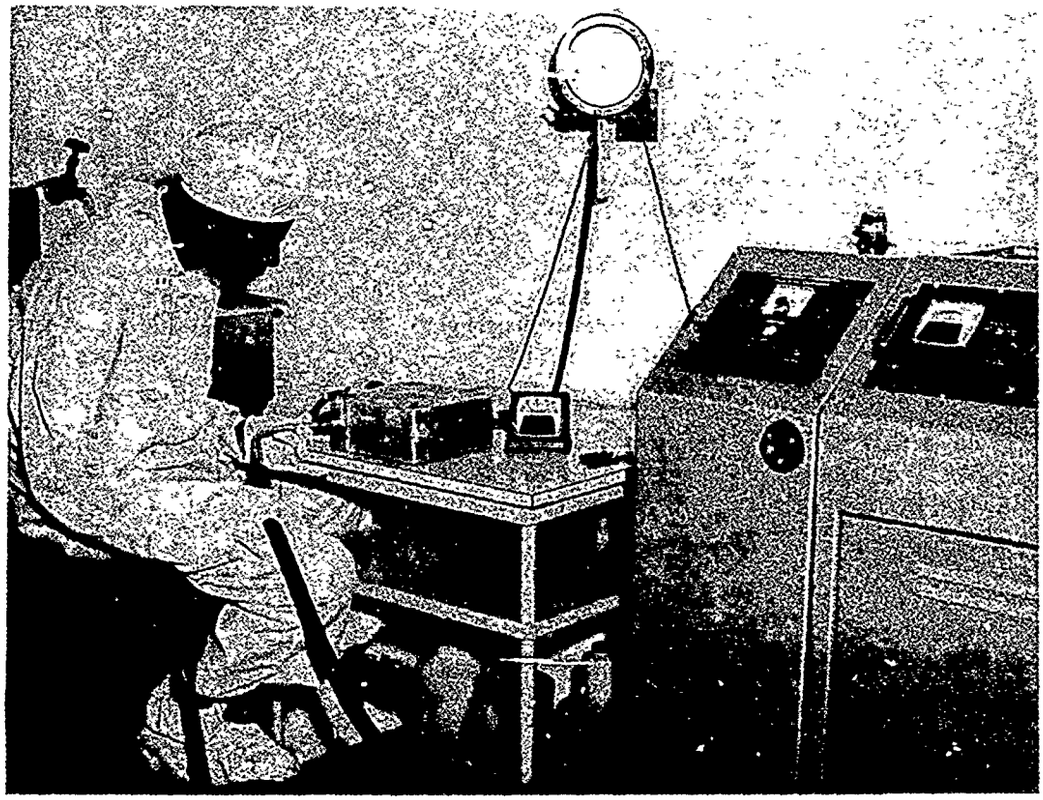

Helium Mass Spectrometer Leak Detection of
Multi-Layer Plate Fin Heat Exchanger

Figure 7-47

7.4.3 Multi-Layer Plate Fin Heat Exchanger - Thermal Cyclic Tests

The objective of the thermal cyclic tests was to demonstrate the integrity of fluxless brazed joints under thermal stress conditions created by heating with 500 F hot air, and counter flowing super cooled gas.

Thermal testing was so arranged that the hot gas would flow into one of the side manifolds, over alternate layers of surface extended corrogated fin, and exit out of the opposite manifold. The super saturated cold gas flowed into one of the side manifolds 90° from the hot gas, over alternate layers of surface extended corrugated fin, and exited out of the opposite manifold. This resulted in laminated layers 0.080" high of hot air and cold gas flowing at 90 degrees to each other and presenting a maximum surface area for heat transfer.

Thermocouple positions used to measure gas stream and component part temperatures are shown in Figure 7-48. Figure 7-49 shows the Number 2 multi-layer plate fin heat exchanger weldment and Figure 7-50 shows the weldment installed and ready for thermal cycling. The test procedures used are described in the following:

a) The weldment was proof pressure tested at 22 psig for external and interpassage leaks.

b) Hot air was forced through the hot passage inlet at 500 F and flow was maintained until all six (6) thermocouples were reasonably stable. Then cold super saturated nitrogen gas was forced through the cold passage inlet and both hot air and cold gas flows were maintained until all thermocouples showed a steady EMF. Both hot air and cold gas flows were then cut off and the weldment was brought back to ambient temperatures. This completed one (1) thermal stress cycle, which was then repeated eleven (11) times making a total of twelve (12). The weldment was then pressure proof leak tested. Eight further cyclic series were conducted.

Table 7-9 shows typical temperatures recorded through one (1) complete series of thermal cycles, and that steady state conditions were achieved during the hot air only and the hot air cold gas cycles which is substantiated by the relative uniformity of thermocouple Number 3 (outer skin adjacent to hot air passage) and Number 4 (outer skin adjacent to cold gas passage). The temperature differential between hot and cold stabilized passages ranged from 784 F to 812 F. The efficiency of the unit is demonstrated by the average difference of 456 F between the hot air inlet and outlet temperatures. This is further illustrated by comparing the average decrease in hot air temperature of 456 F with the average increase of cold gas temperature of 401 F.

Table 7-10 summarizes thermal cycling versus leak rate results of tests performed on units Number 2 and 3. Both units were leak free before thermal cycling and unit Number 3 remained leak free throughout 108 thermal cycles. Unit Number 2 showed an inter-passage leak with the hot passage pressurized with helium at 22 PSI, and the helium trace being detected in the coolant passage which was at ambient pressure. As shown in Table 7-10, the leak was one way only which indicated that the hot air manifold close-out applied a peeling force at one or more of the brazed joints. Assuming the peeling force caused the leak, then a manifold close-out sufficiently stiffened so as to resist any diaphragm yielding of the upper and/or lower close out plates, would prevent this type of damage. In reviewing the Table 7-10 temperatures, it would appear that the maximum thermal stress occurred local to the N_2 inlet (TC #6), and the hot passage local to the air outlet.

An investigation was conducted attempting to locate the leak detected during the thermal cyclic testing of the Number 2 multi-layer plate fin heat exchanger. The hot passage manifold close outs were removed, the cold passage was then pressurized to 22 PSI with helium, and all exposed brazed joints were tested with a leak detector probe. with no leaks being detected. A yoke was constructed which gripped the edges of the upper and lower skins adjacent to the plate fin matrix and a tension load was applied thereby imparting a peeling action to the brazed joints. The maximum applied load was 43 pounds per linear inch of skin edge which equaled approximately 230 PSI peeling force on the braze joint. No leaks were detected when the cold passage was pressurized to 22 PSI with helium while the peeling force was applied. In view of the small size of the leak (1.3×10^{-9}) which is well under the generally accepted maximum leak rate of 1.0×10^{-5} cc/sec. for heat exchanger applications, no further effort was made to locate the leak.

Multi-Layer Heat Exchanger Thermal Cyclic Test
Temperature Sensing Positions

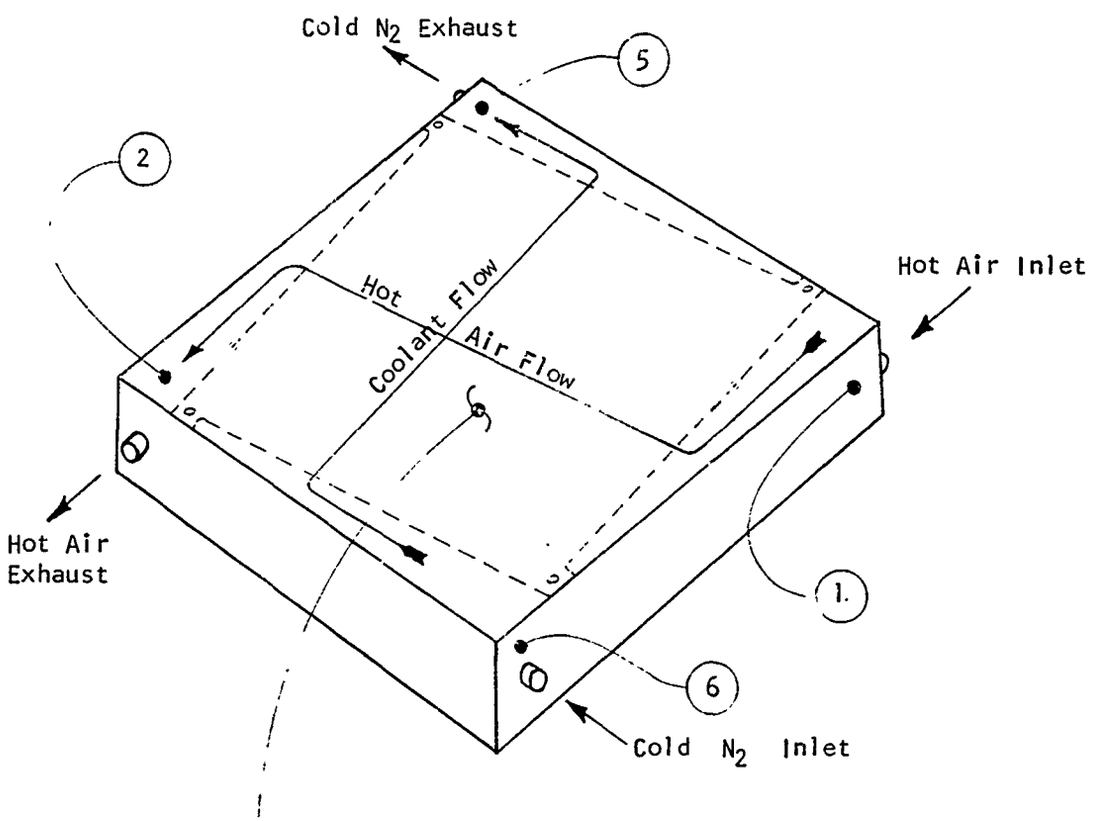

(4) Skin - Upper Outer Surface

(3) Skin - Lower Outer Surface

(○) Denotes Thermocouple Number

● Denotes Thermocouple Location

Figure 7-48

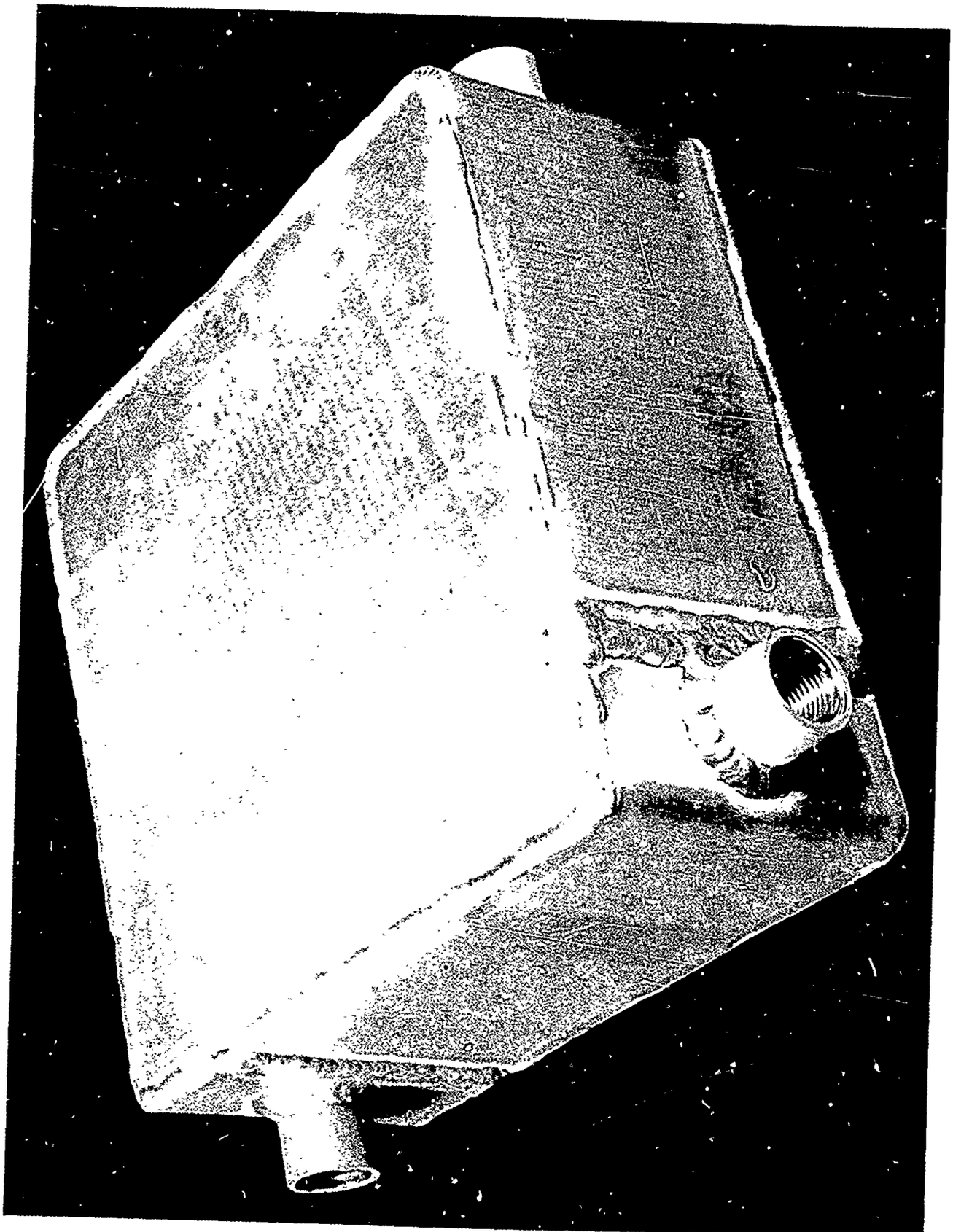

Multi-Layer Weldment
Figure 7-49

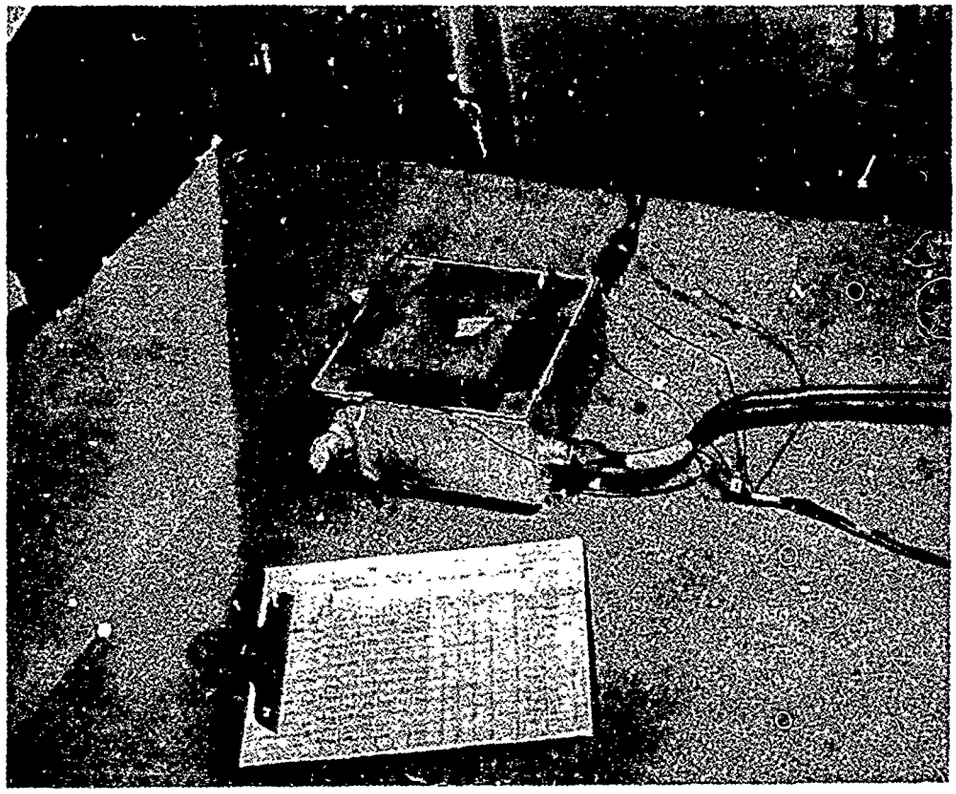

Multi-Layer Plate Fin Heat Exchanger Prepared for Thermal Cycling

Figure 7-50

Typical Thermal Cyclic Steady State Temperatures

TABLE 7-9

		Location of Thermocouple Hot Junctions					
Condition	Cycle No.	Air Inlet 1	Air Outlet 2	Lower Face 3	Upper Face 4	Nitrogen Outlet 5	Nitrogen Inlet 6
Hot Air	1	494	310	318	312	245	308
Hot Air/N_2		488	60	164	156	120	-300
Hot Air	2	488	295	304	396	217	297
Hot Air/N_2		484	74	178	160	124	-300
Hot Air	3	504	292	304	298	214	295
Hot Air/N_2		512	64	166	160	156	-300
Hot Air	4	512	274	292	284	198	280
Hot Air/N_2		512	34	124	120	72	-300
Hot Air	5	512	300	312	304	217	300
Hot Air/N_2		512	46	150	140	76	-300
Hot Air	6	512	288	308	298	214	298
Hot Air/N_2		512	88	172	168	158	-300
Hot Air	7	512	292	306	300	212	297
Hot Air/N_2		512	60	158	145	106	-300
Hot Air	8	512	288	304	294	210	292
Hot Air/N_2		512	64	164	160	174	-300
Hot Air	9	512	300	306	300	235	300
Hot Air/N_2		512	23	110	110	60	-300
Hot Air	10	512	300	306	300	235	300
Hot Air/N_2		512	23	110	110	60	-300
Hot Air	11	508	319	318	315	245	310
Hot Air/N_2		508	11	104	104	42	-300
Hot Air	12	508	299	307	298	225	300
Hot Air/N_2		508	60	126	126	59	300

Multi-Layer Plate Fin Heat Exchanger Leak Test Data

TABLE 7-10

	Unit No. 2 Leak Test Results Summary		Unit No. 3 L.T. Results	
	Hot Passage Pressurized	Coolant Passage Pressurized	Hot Passage Pressurized	Coolant Pressurized
Before Thermal Shock	None	None	None	None
After 1st Series	None	None	None	None
After 2nd Series	None	None	None	None
After 3rd Series	None	None	None	None
After 4th Series	None	None	None	None
After 5th Series	None	None	None	None
After 6th Series	None	None	None	None
After 7th Series	None	None	None	None
After 8th Series	None	None	None	None
After 9th Series	1.30×10^{-9}(1)	None	None	None

(1) Inter passage leak, measured in Std. cc/sec. at 22 PSI.

7.4.4. Multi-Layer Plate Fin Heat Exchanger - Braze Quality Evaluation

Braze quality evaluations included visual and microscopic examination, flatwise tension, and burst test. No braze deficiencies were noted and strengths were as expected for the materials used in fabrication.

All brazed multi-layer plate fin heat exchangers were examined visually and with a stereomicroscope. All brazed joints showed a complete line of braze with well formed fillets at the face to separator bar joints. Figure 7-51 shows a typical brazed and heat treated multi-layer plate fin matrix. The four tubular pins were used to index the details during brazing.

Figure 7-52 shows Unit Number 1 weldment as sectioned to permit removal of small sections for microscopic evaluation. Approximately one hundred (100) joint locations were selected and examined under a stereomicroscope showing that all fillets were well rounded and substantious. Various sections were mounted and polished and found to be satisfactory.

The flat interface of the fin stock in contact with the separator plates showed filler metal diffusion up to 0.003 inches as illustrated in Figure 7-53. This condition uniformly decreased to zero at the fillet-to-fin member transition. Structurally and metallurgically, this condition is not considered to be detrimental to the function or life of the joint. Various separator-to-passage close out edge members were microscopically examined and found free of porosity. The filler metal diffusion level into the separator plates did not exceed 0.0015 inches as illustrated in Figure 7-54.

Three (3) coupons approximately 2 inches by 2 inches square of the full matrix thickness were cut from the Number 2 multi-layer plate fin heat exchanger to determinate the flatwise tensile strength of the brazed matrix. Figure 7-55 shows a typical flatwise tension coupon with test attachment blocks bonded to upper and lower skins. Figure 7-56 shows a typical flatwise tension test set up. Tests were performed at 0.055 inches per minute cross head movement. Figure 7-57 shows a typical flatwise tension test failure. Failure of all coupons occurred in the upstanding members (3003 Al) of the fin. Results of the flatwise tension tests are shown in Table 7-11.

Brazed Matrix Flatwise Tensile Strength

TABLE 7-11

Coupon Number	Break Load in Pounds	Coupon Surface Area Inch^2	Pounds/In^2 of Matrix Surface	Cross Sectional Area of Fin(1)	Ultimate Tensile Strength of Fin, PSI
1	3535	3.73	948	0.0648	14,630
2	3615	3.73	969	0.0648	14,954
3	3445	3.73	924	0.0648	14,259

(1) Cross sectional area of fin was computed as follows:

a) 3003 fin stock thickness = 0.0054 inches actual measurement
b) number of fin uprights per inch of matrix = 12 actual count
c) therefore, fin cross sectional area per square inch of matrix = 0.0054" x 12 x 1"=0.0648 inch^2.

The 14,614 PSI average ultimate strength of the 3003 fin is within the 14,000 to 19,000 PSI range specified in Alcoa's Aluminum Handbook for 3003 in the 'O' condition. Failure occurring in the upstanding member of the fin demonstrates integrity of the braze joints.

The low bursting strength of the unsupported manifold close outs precluded an actual burst test of the complete weldment. Figure 7-58 shows details of a manifold close out support structure designed and built to allow a burst test to be performed on the Number 3 multi-layer fin heat exchanger brazed matrix.

Figure 7-59 shows the burst test set up used in testing the Number 3 multi-layer plate fin heat exchanger. The upper plate deformed at 990 PSIG and this point of failure was confirmed by measurable permanent deformation up to 0.038 inches under no load conditions for both upper and lower end plates.

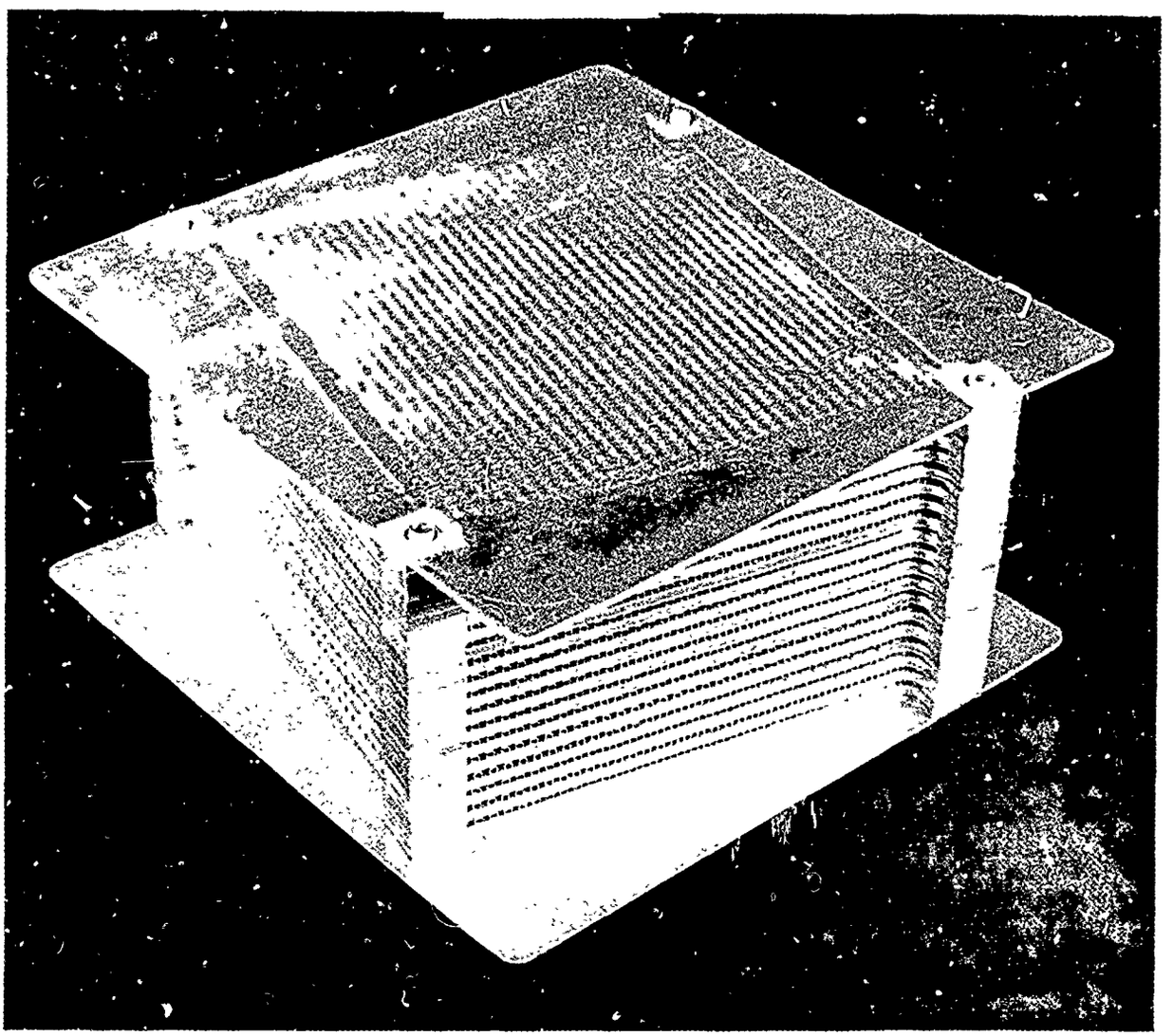

Multi-Layer Brazed and Heat Treated Matrix

Figure 7-51

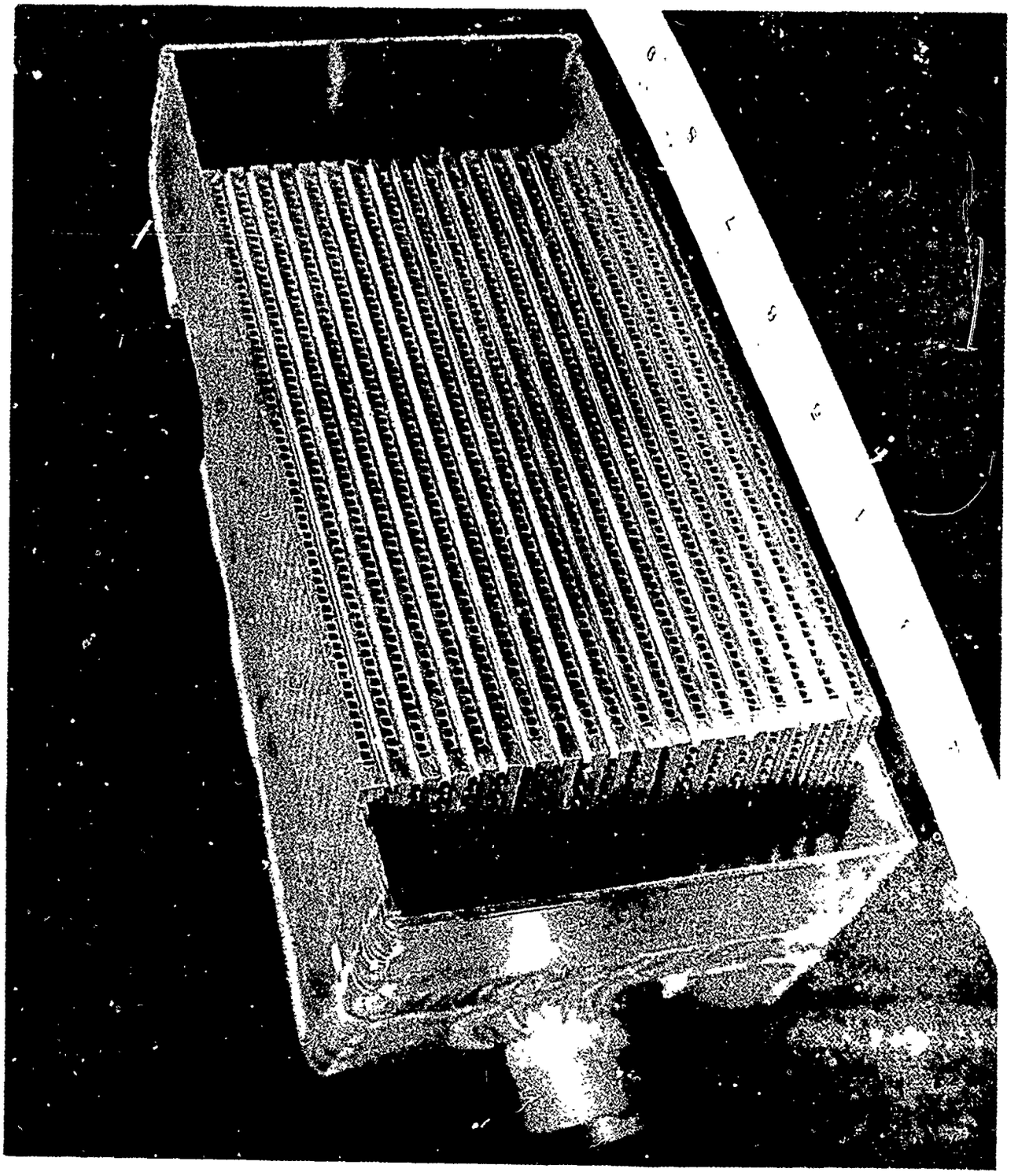

Multi-Layer Sectioned Through Weldment and Brazed Matrix

Figure 7-52

Typical Fin to Separator Plate Joint

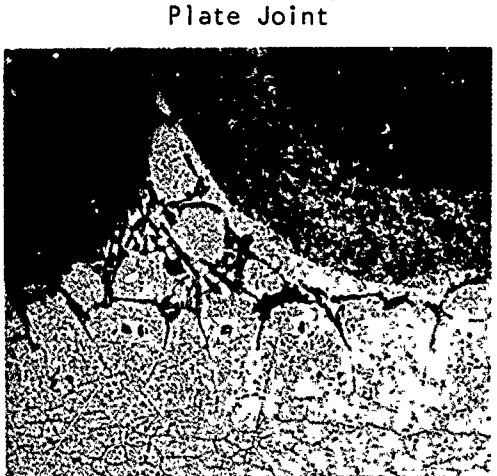

Mount No. - 506
Magnification - 80X
Etchant - Boric Acid, HF

Figure 7-53

Typical Separator Bar to Separator Plate Joint

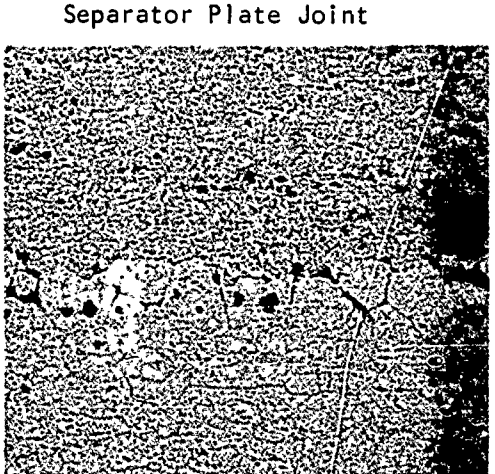

Mount No. - 509
Magnification - 80 X
Etchant - Boric Acid, HF

Figure 7-54

Flatwise Tension Coupon With Test Attachment Block Bonded to Upper and Lower Skins

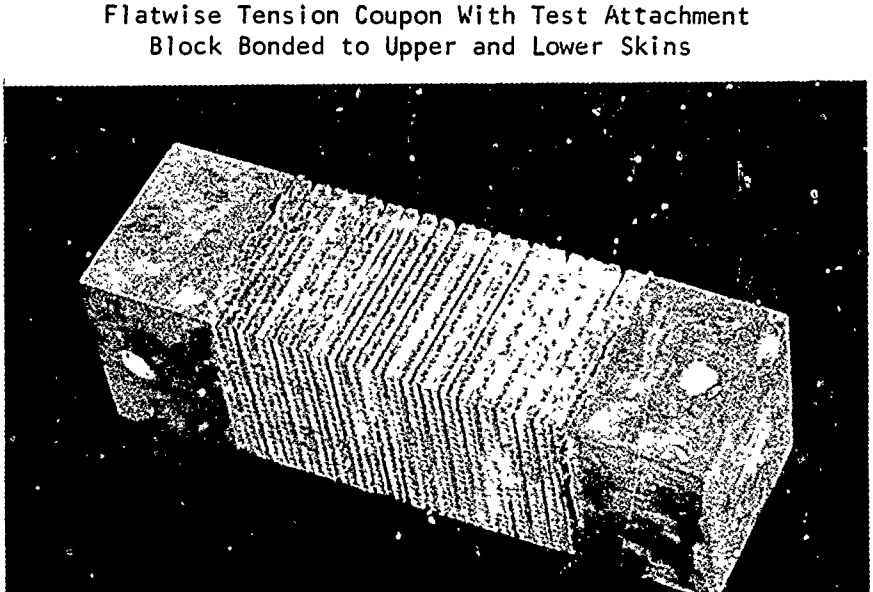

Figure 7-55

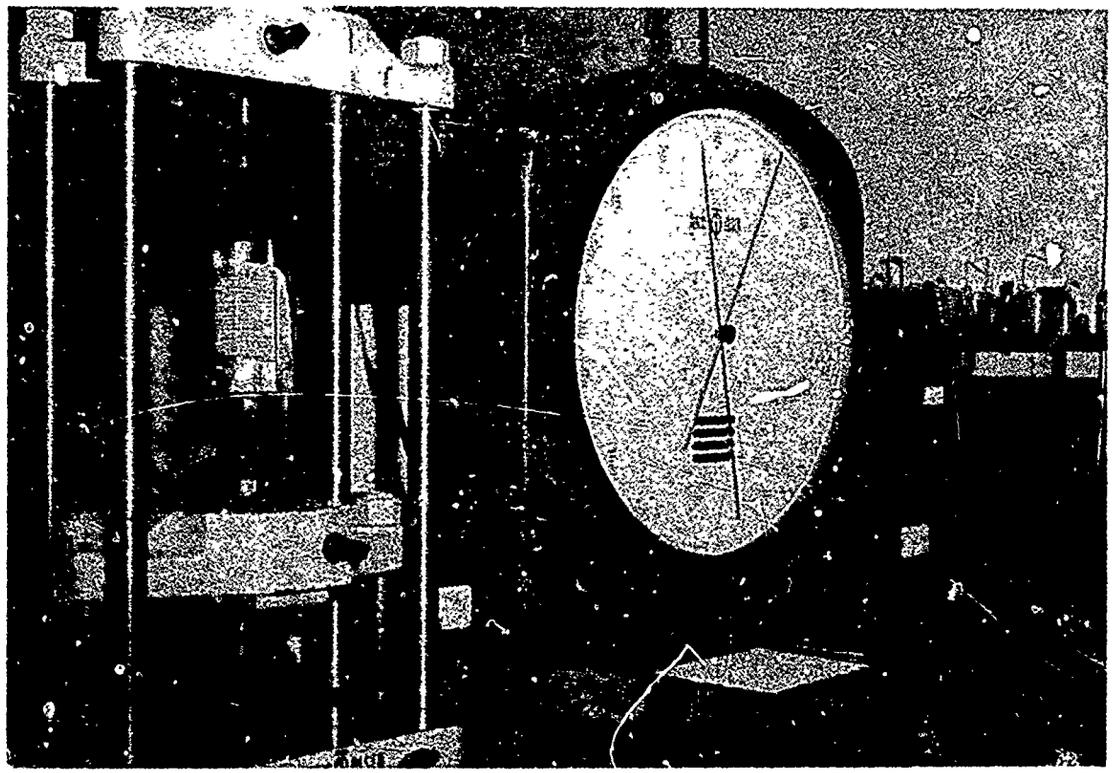

Typical Flatwise Tension Test Set Up. Photograph Taken Just After Start of Failure of Coupon

Figure 7-56

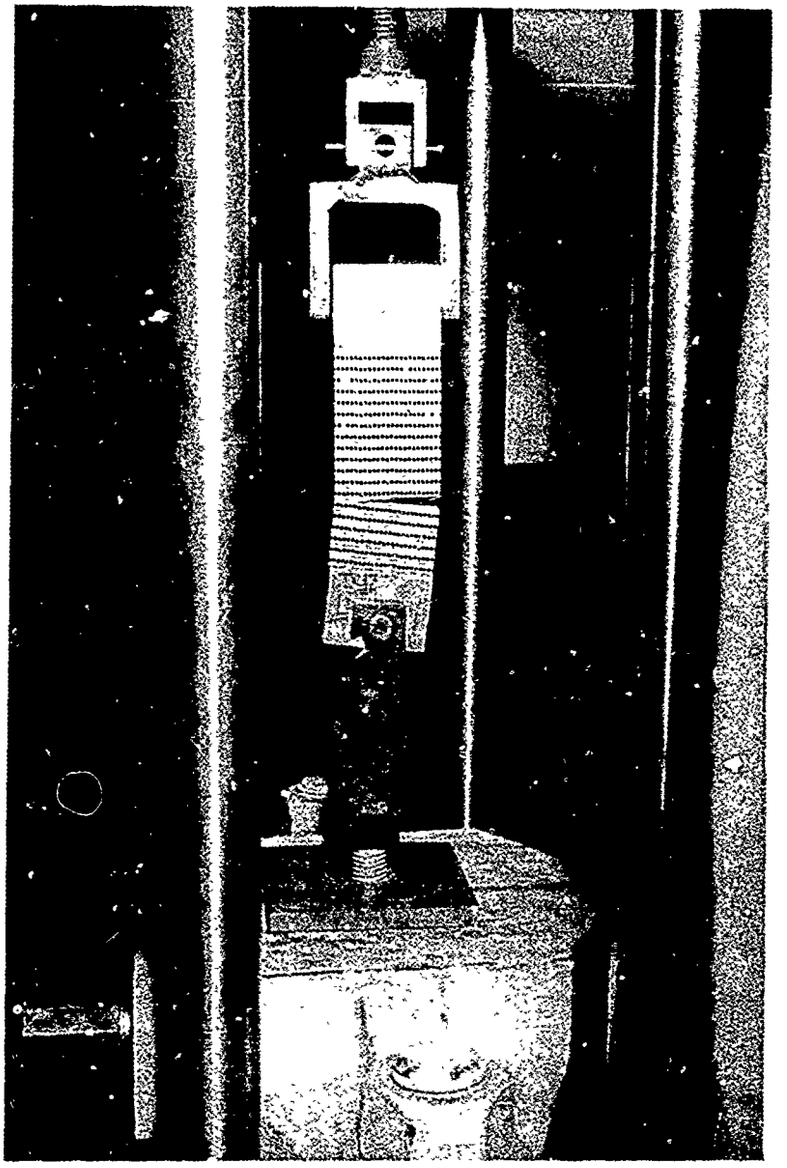

Typical Flatwise Tension Test Failure

(Note that failure occurred in the upstanding members of the fin).

Figure 7-57

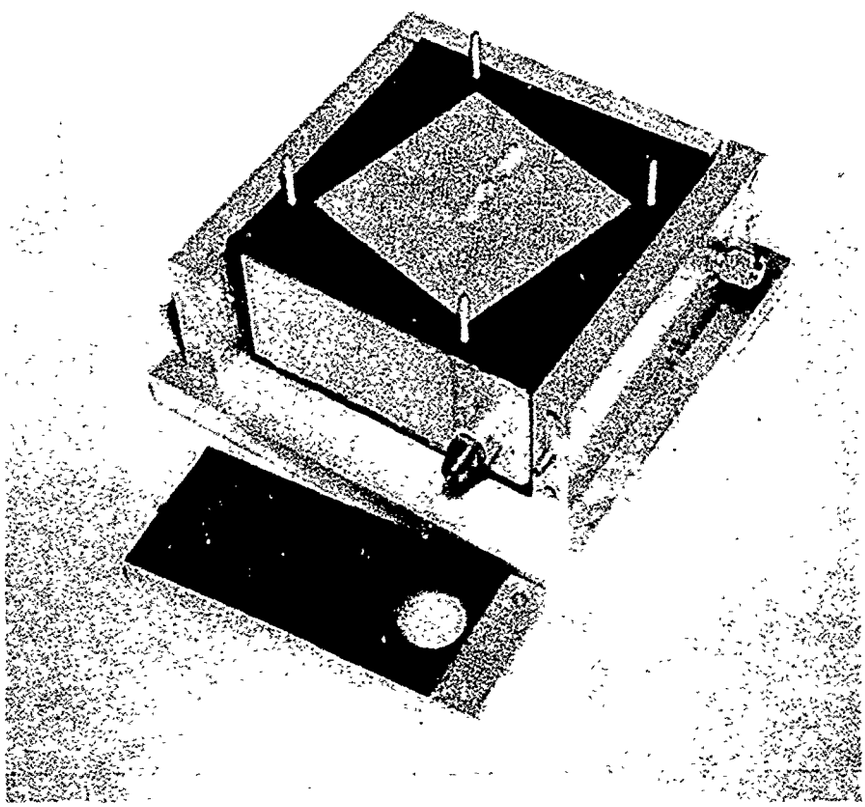

Details of Manifold Close Out Support Structure

(Rubber pads were used between the back up structure and the part to compensate for surface irregularities.)

Figure 7-58

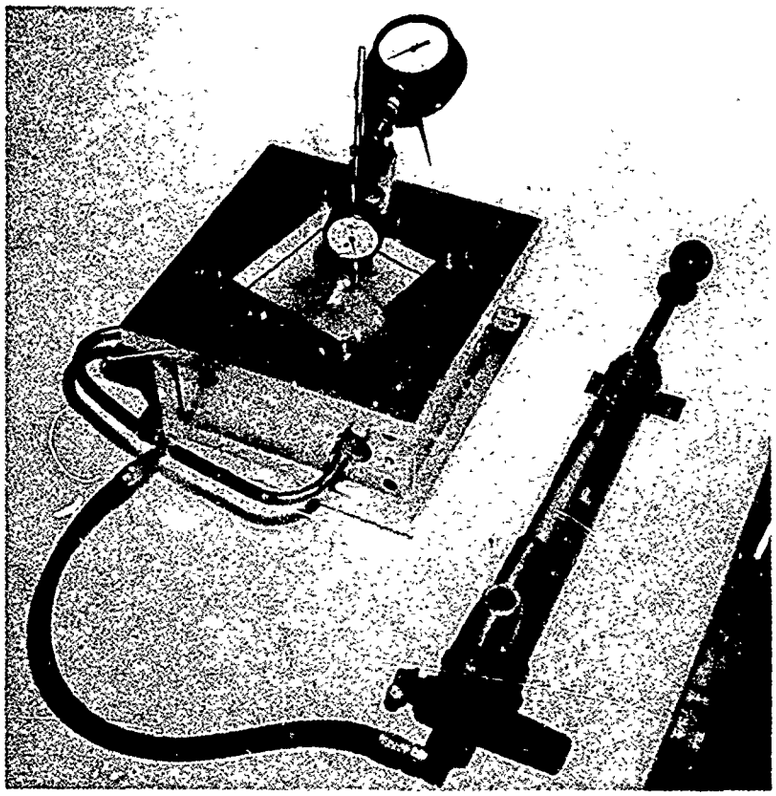

Burst Test Set Up Used in Testing the Number 3
Multi-Layer Plate Fin Heat Exchanger

(Test was performed hydrostatically with water at ambient room temperature. Dimension of window in picture frame on top surface was 5.625 inches which confined failure to brazed fin to plate matrix).

Figure 7-59

7.5 Honeycomb Sandwich Composite

The investigation was directed toward establishing the feasibility of applying the fluxless brazing processes and techniques as a manufacturing approach for producing honeycomb sandwich structural composites. The objectives included establishing basic materials and structural data for possible use in future applications.

7.5.1 Development of Honeycomb Sandwich Brazed Composites

One (1) initial 6"x 6" panel was fabricated for confirmation of the brazing cycle. Four (4) 12" x 12" and one (1) 24" x 24" panels were fabricated and tested for establishing basic mechanical data.

Initial tasks were delayed because the indexing method, used to locate the core ribbons during ultrasonic welding of the core blanket nodes, allowed mis-matching up to 0.011 inches. This condition would not allow proper contact between the core ribbon edges and face sheet. The cause for mis-matching was attributed to a deflection of the lower welding pin (anvil) during welding. As the first twelve (12) core blankets were produced with this mis-matched condition, it was considered more economical to rework the blanket surfaces. The rework was accomplished by machining as summarized below:

Initial Blanket Thickness 0.381" - 0.370"

Step 1 - Place 12" x 12" blanket in flat CRES pan.

Step 2 - Blanket cells and surrounding area filled with flaked polyglycol and dead weighted to hold blankets flat.

Step 3 - Work heated to 150°F, polyglycol added until blankets were immersed in molten polyglycol, then cooled to room temperature, as illustrated in Figures 7-60 and 7-61.

Step 4 - Stabilized blankets were removed and machined as shown in Figure 7-62.

Step 5 - Blankets were then placed in pan, heated, and the polyglycol was drained.

Step 6 - Blankets were steam jet cleaned to remove all residue.

Final blanket thickness - 0.34".

Stabilizing of Honeycomb Core With Polyglycol

Figure 7-60

Stabilized Honeycomb Core

Figure 7-61

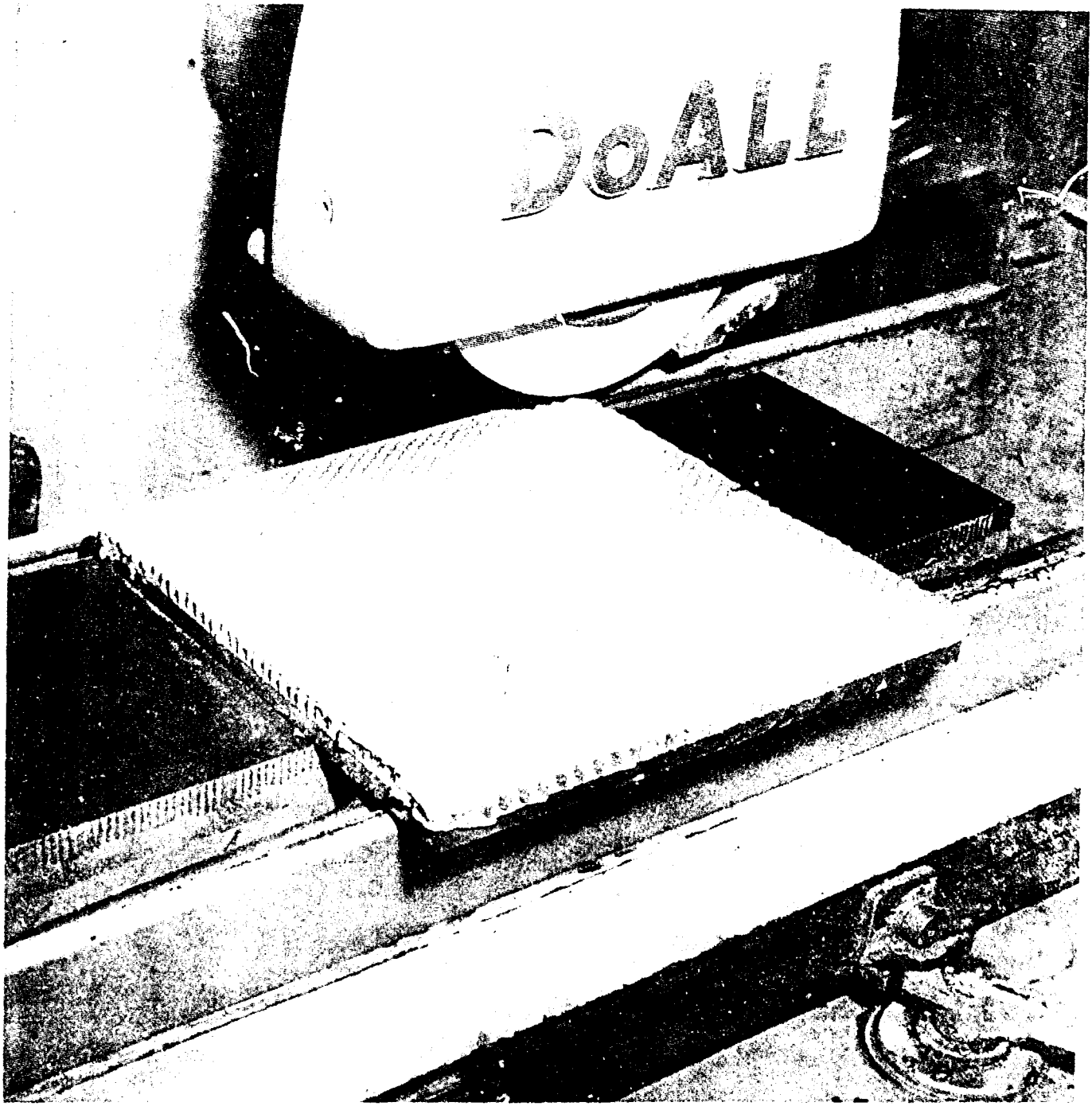

Machining of Stabilized Honeycomb Core

Figure 7-62

The initial 6" x 6" panel was brazed at 1082 F ± 4 F, using a five (5) minute hold at the brazing temperature. A pressure of 1" Hg per square inch of face sheet was applied during the final brazing period. Kiss blocks were used outside of each of the four panel edges to prevent any additional pressures being applied to the panel. The 1" Hg pressure was the differential between the envelope environment pressure and ambient.

A review of the ribbon-to-face sheet joints showed the ribbon joint transition to be free of any damaging diffusion or grain growth, as illustrated in Figures 7-63 and 7-64. The two grains, shown in the left hand fillet of Figure 7-64, illustrate the effect of burrs left on the ribbon edges. A visual inspection of all accessible nodes showed complete node flow had been achieved at each side of the ultrasonic welded joints. Evidence of this can be seen in Figure 7-68.

Microphotograph - Core Ribbon to Face Sheet Joint

Mount No. - 488
Magnification - 100X
Etchant - None

Figure 7-63

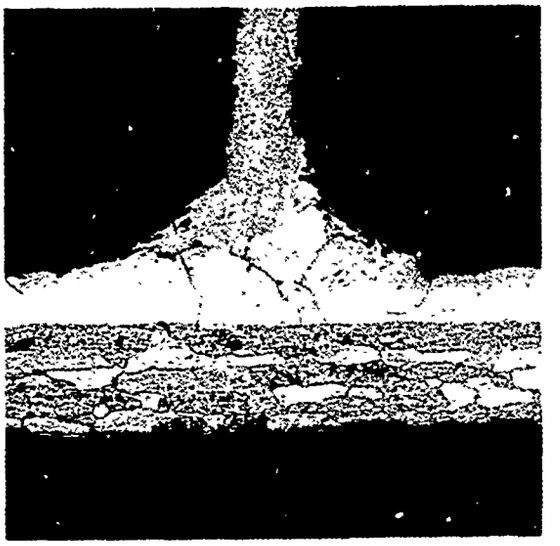

Mount No. - 488
Magnification - 100X
Etchant - Boric Acid, HR

Figure 7-64

The initial test panel and subsequent panels were constructed from materials as below:

Face St. Alloy	Face Shet. Thickness	Filler Metal	Core Alloy	Cell Size
7005	0.008"	4045	6061	4-40P-.004

The 7005 alloy use in face sheets was selected as being less sensitive to solution heat treatment quenching rates, as rapid quenching was considered impractical for large panel sizes. However, 6061 aluminum was used for the core components for economical reasons since fifteen (15) lbs. of foil was required and the 7005 alloy was procureable only as a minimum mill run of 2000 lbs. The test panels were heat treated to the thermal cycle recommended by Alcoa (1) for 7005 aluminum, because of this, the 6061 alloy heat treatment response is up to 10% below the T-6 condition. However, this is considered sufficient to obtain usable property data.

Four (4) 12" x 12" and one (1) 24" x 24" test panels were fabricated to be used for various test purposes. Figure 7-65 shows a typical prelayup assembly of panel details including a solid center bar to be used for canilever mounting of coupons for vibration testing. Details of the core splice joint between the four 12" x 12" core blanket used in the 24" x 24" panel are shown in Figure 7-66. Cell walls of joining edges were bent to form a nearly continuous flange with a 718 intermediate alloy filler strip between core blankets. Figure 7-67 shows the first 12" x 12" panel brazed and heat treated. Excess core was trimmed from the panel periphery.

7.5.1.1 Honeycomb Sandwich Composite - Initial Inspection

Initial inspection of honeycomb sandwich composites showed a satisfactory braze was accomplished.

Visual and stereomicroscopic examination of joints around the periphery of the panels and along cut edge of coupons prepared for testing showed 100 percent node flow and complete core to face joint filleting. Figure 7-68 shows typical filleting and node flow.

Radiographic examination of these panels showed 100 percent node flow and fillets ranging from 0.010 inches to 0.015 inches with an average of 0.012 inches. Splice joints were nearly 100 percent complete with some minor voiding at the ends of cell walls bent to form the splice flange. Equipment limitations precluded resistance spot tacking of the abutting core blanket splice joints as is normally done during layup for braze with stainless steel and similar materials. (Spot tacking serves as a means of ensuring intimate joint contact thereby improving splice joint quality).

(1) U.S. Patent No. 3,171,760. Thermal Treatment for X7005, 7039, X7106 and X7139 Aluminum Alloys.

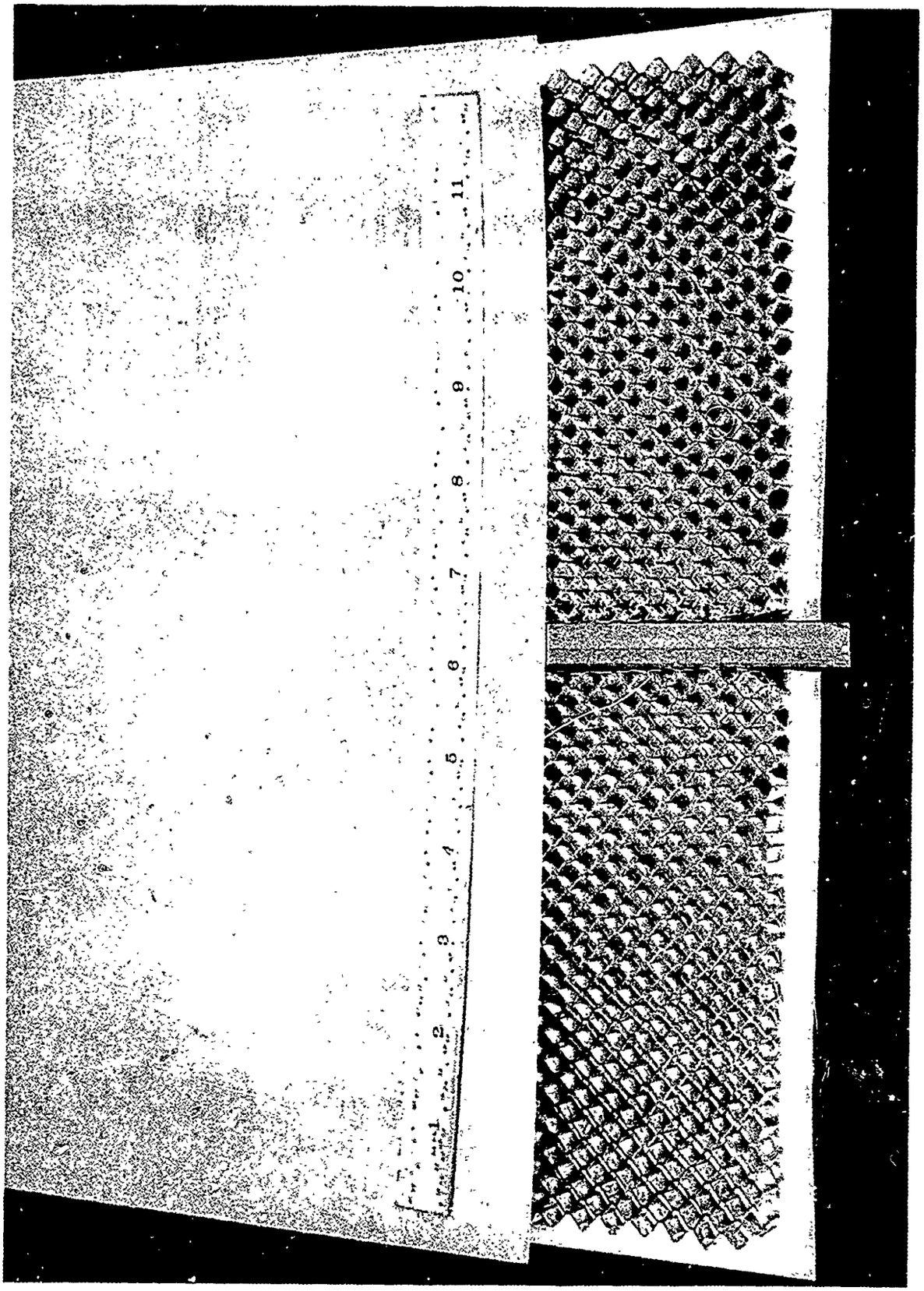

Figure 7-65

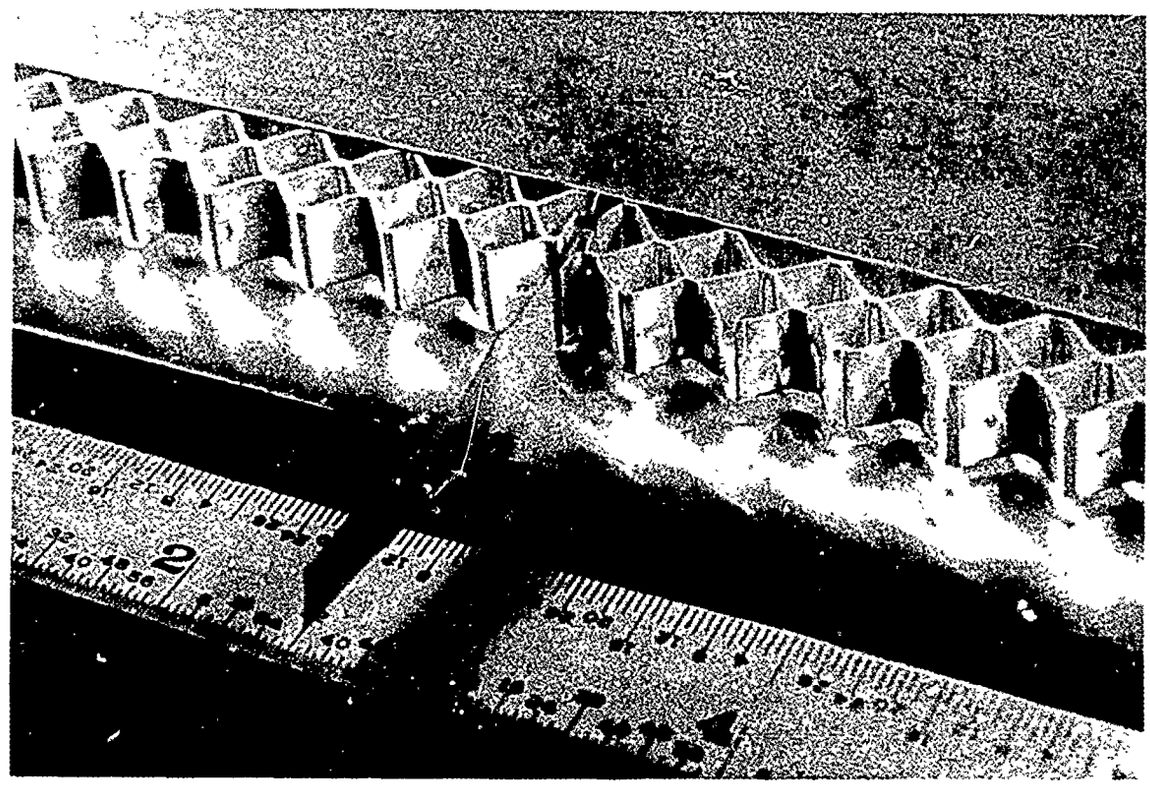

Details of Core Blanket Splice Joint

Figure 7-66

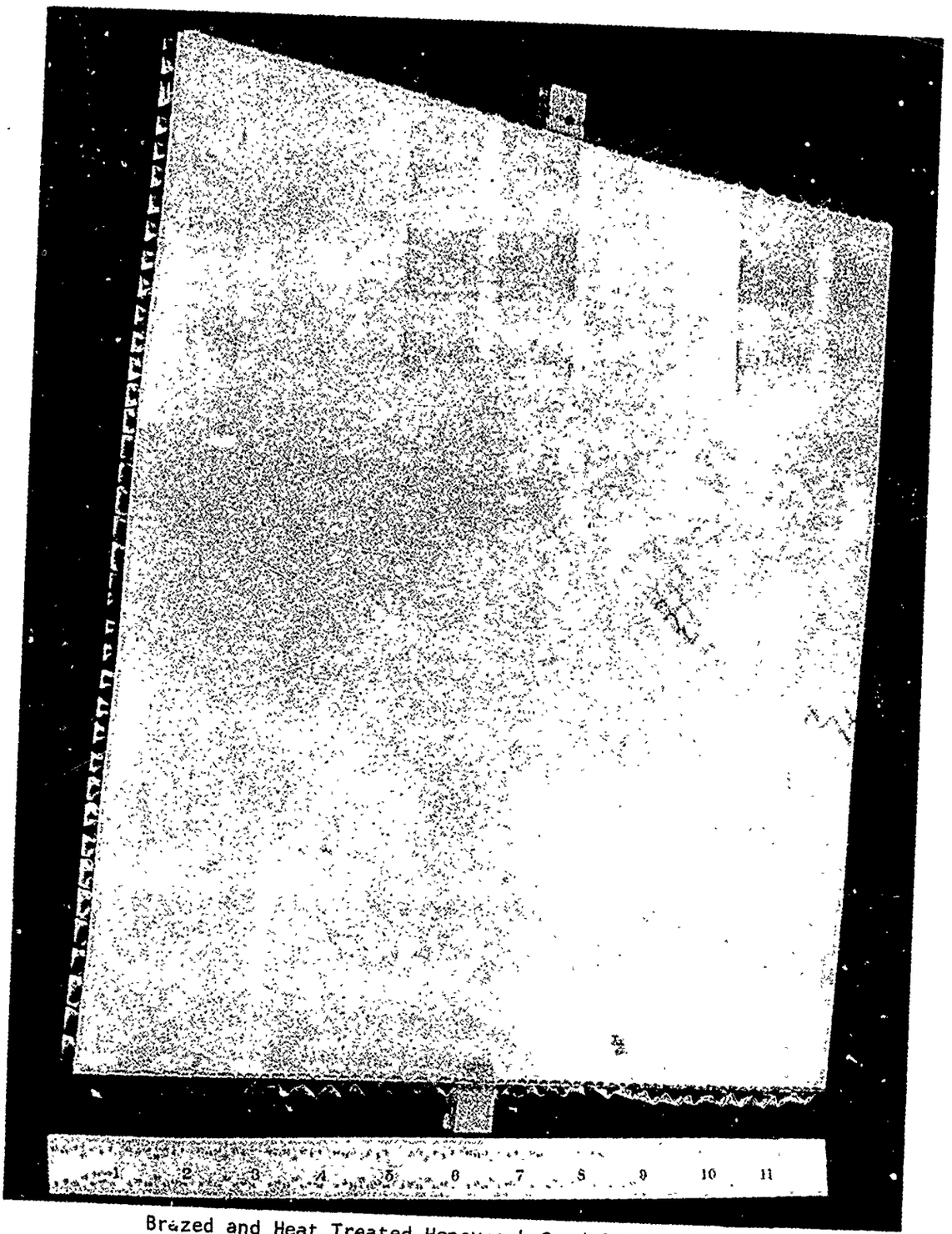

Brazed and Heat Treated Honeycomb Sandwich Test Panel

Figure 7-67

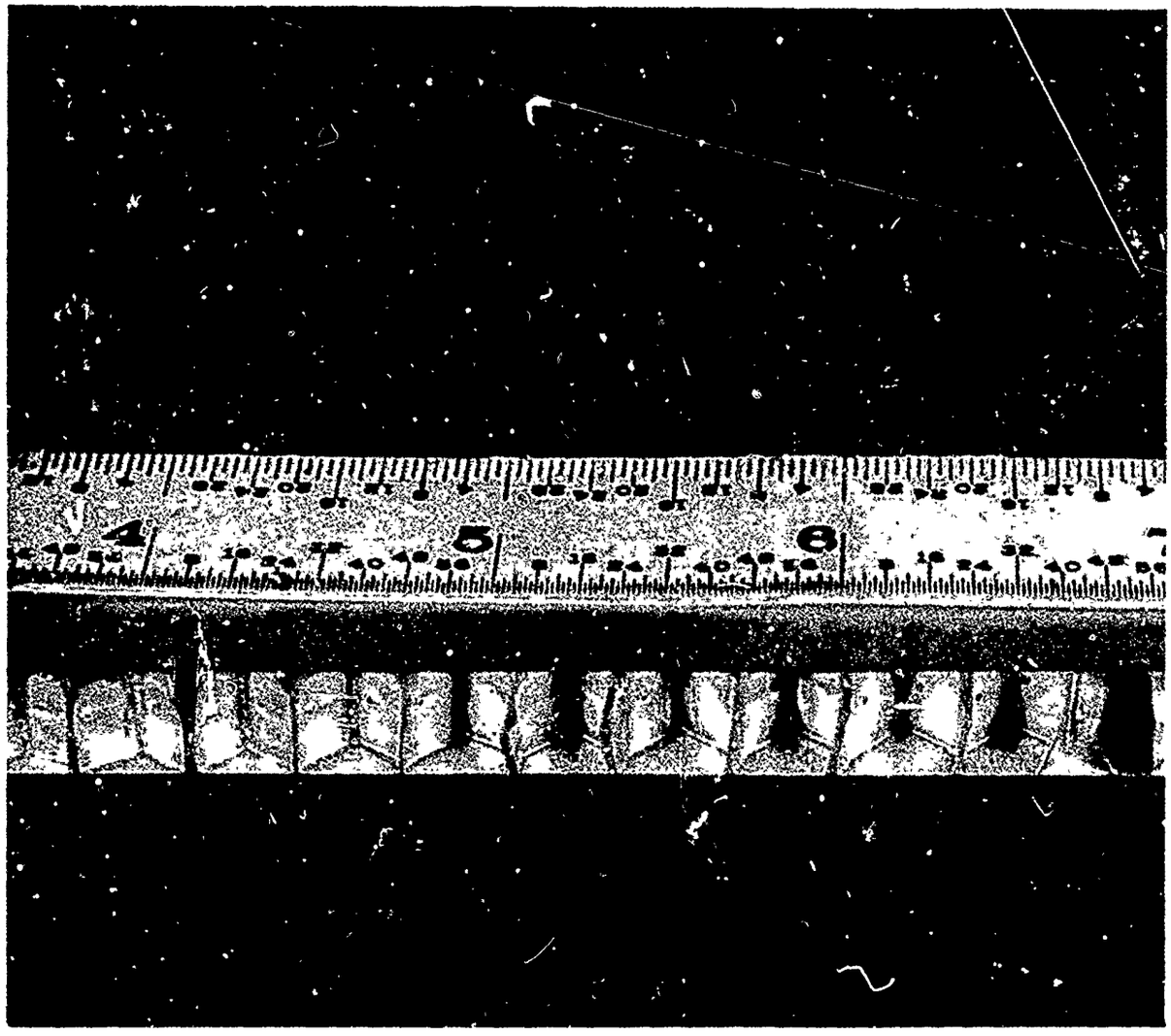

Illustration of Honeycomb Sandwich Panel
Fillet and Node Flow

Figure 7-68

7.5.1.2 Honeycomb Sandwich Composite - Structural Data Determinations

An analysis of three brazed and heat treated honeycomb sandwich coupons evaluated by vibration testing showed that the endurance limit of the failed members exceeded that of 7005-T6 sheet. All failures occurred in the skin local to the cantilevered end (fixed end) of the coupon and initial cracking mode was ductile fatigue.

The braze alloy having a lesser coefficient of thermal expansion than the skin resulted in a probable intercellular buckling of the skin and produced large unexpected variations of strain due to temperature differences. Therefore, thermal cyclic procedures were not established for brazed honeycomb sandwich composites.

Vibration and flatwise tension tests after thermal cyclic testing were not accomplished due to failure to establish a satisfactory thermal cyclic test procedure.

7.5.1.3 Honeycomb Sandwich Composite - Vibration Test

The objective of the vibration testing was to establish structural integrity of fluxless brazed honeycomb composites. Structural integrity was evaluated by vibrating in an axis normal to the sandwich skins.

Vibration Test Set-Up

Figure 7-69 illustrates a honeycomb sandwich test coupon mounted to the vibration test fixture; the coupon being mounted as a double cantilevered beam so that the center of the beam (test coupon) acted as a fixed end. The fixture incorporated a clamp for positioning an optical accelerometer probe (FoTonic KD45, with a 1/2 and 1/2 distribution probe) normal to the coupon skin surface. The probe measured the deflection amplitude during vibration. The output of the probe was fed into an oscilloscope and then to a recording oscillograph. A Strobe light was used to determine the vibration mode.

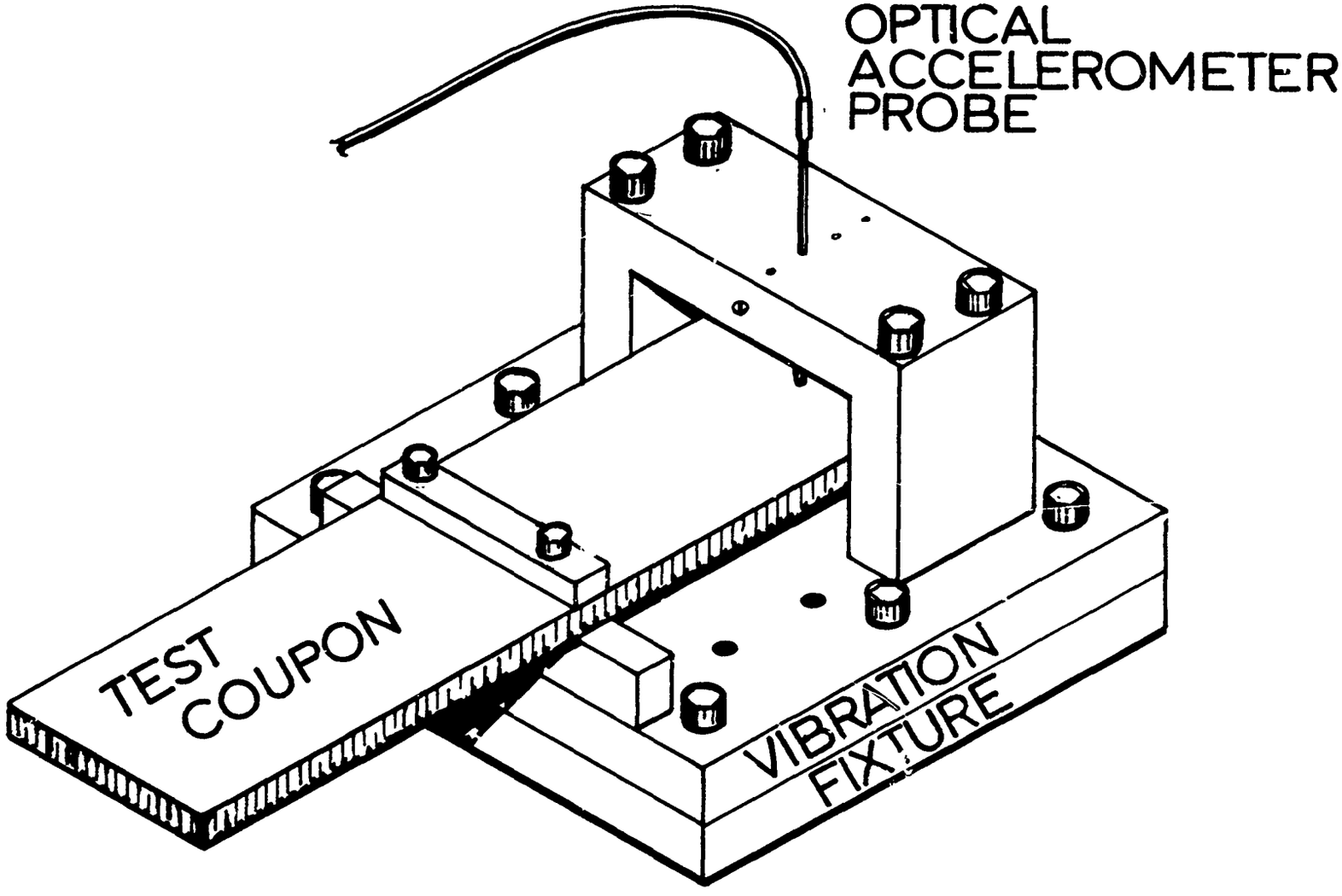

Vibration Test Set-Up For Sandwich Beam Test Coupon

Structural Analysis of Brazed Honeycomb Sandwich Composite

Figure 7-70 shows a typical cross section of the sandwich beam test coupon.

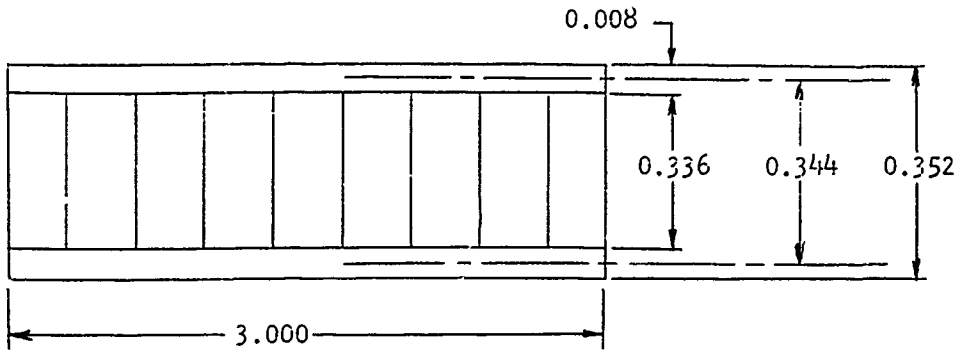

Typical Sandwich Beam Cross Section

Figure 7-70

Moment of Inertia (I) of Cross Section of Sandwich Beam

Area of Skins = $2(0.008 \text{ in})\ (3 \text{ in}) = 0.048 \text{ in}^2$

$I = (0.048 \text{ in}^2)\ (0.172 \text{ in})^2 = 0.00142 \text{ in}^4$

Weight Caluclations:

Wt. of Skin Per Inch = $(0.048 \text{ in}^2)\ (0.10 \text{ lbs/in}^3) = 0.0048$ PSI

Wt. of Core Per Inch = $(7.9 \text{ lbs/ft}^3)\ (0.336 \text{ in})\ (3 \text{ in}) = \underline{0.0046}$ PSI

Wt. of Specimen Per Inch = W = 0.0094 PSI

Mass of Specimen Per Inch = $M = \frac{W}{g}$

$$M = \frac{0.0094 \text{ lbs/in}}{386.4 \text{ in/sec}} = 2.44 \times 10^{-5} \text{ lbs/sec}^2$$

Calculated Static Deflection and Stress for one (1) "g" Input

Deflections are calculated at one (1) inch, two (2) inches, and three (3) inches, from the free end of the beam.

The equations used are as follows:

$\delta = \frac{Wl^4}{8EI}$ at Free End

$\delta = \frac{W}{24EI}(X^4 - 4l^3X + 3l^4)$ at X Distance From Free End

Where: δ = Deflection, Inches

E = Modulus of Elasticity, PSI

I = Moment of Inertia, in^4

ℓ = Length of Beam, Inches

W = Weight Per Inch of Length, lbs/in

X = Distance From Free End, Inches

Static Deflections for One (1) "g" Input:

Point (Inches)	Deflection (Inches)
X = 0.0	δ End = 0.0000882
X = 1.0	δ 1 = 0.0000676
X = 2.0	δ 2 = 0.0000478
X = 3.0	δ 3. = 0.0000290

Natural Frequency (f_n) of Specimen:

$$f_n = \frac{3.52}{2\pi\ell^2} \frac{(EI)^{\frac{1}{2}}}{(M)}$$

ℓ = 5.755 in.

E = 10.3×10^{-6} lbs/in^2

I = 1.422×10^{-3} in^4

M = 2.44×10^{-5} $\frac{lbs/sec^2}{in^2}$

f_n = 416 Hz

Material Properties X7005-T6 (KSI): (Ref. Alcoa, Green Letter)

F_{tu} - 45	F_{bru} (e/d = 1.5) - 67
F_{ty} - 36	F_{bry} (e/d = 1.5) - 50
F_{cy} L - 36	F_{bru} (e/d = 2.0) - 85
F_{cy} T - 38	F_{bry} (e/d = 2.0) - 58
F_{su} - 37	E - 10.3×10^3
G - 3.9×10^3	E_c - 10.5×10^3

The maximum stress will occur in the skins near the center support and will be the result of bending.

Stress Maximum = $f = \frac{m\ C}{I}$ Static Load for one (1) "g" Input

Where:

f = Stress (Tension or Compression), PSI

m = Moment, in-lbs

C = Distance from Centroid to Outer Fibers, Inch

I = Moment of Inertia, in^4

and

$m = \frac{W\ell^2}{2}$

ℓ = Length of Cantilever Beam, Inches

W = Weight of Beam per Inch, lbs/in

$m = \frac{(0.0094\ lbs/in)\ (5.755\ in)^2}{2} = 0.156$ in-lbs

$f = \frac{(0.156\ in/lbs\ (0.176m)}{(0.00142\ in^4)} = 19.3$ PSI

Vibration Test Results

A frequency search was performed on test coupon Number 1 to determine the resonant frequencies. The input load was 2.2 "g" and the sweep time was one (1) octave per half minute. The search swept from 20 Hz to 2,000 Hz.

A small resonance was indicated at 435 Hz. No other resonances were observed. This is in close agreement with the calculated lowest natural frequency of 416 Hz.

The use of a Strobe light indicated that the panel was vibrating in the first mode.

The deflections were measured with the optical accelerometer and are shown below:

Sx = 0.0 = Not Measured
Sx = 1.0 = 0.04175 inch double amplitude = 0.02087 inch
Sx = 2.0 = 0.02995 inch double amplitude - 0.01497 inch
Sx = 3.0 = 0.02032 inch double amplitude = 0.01016 inch

The magnification factors, Q, are determined by comparing the static deflections produced by the 1.0 "g" and 2.2 "g" inputs as follows:

Point X = 1.0 inch

$$Q_1 = \frac{0.02087 \text{ in.}}{(2.2)\ (0.0000676 \text{ in})} = 140.2$$

Point X = 2.0 inch

$$Q_2 = \frac{0.01497 \text{ in.}}{(2.2)\ (0.0000478 \text{ in})} = 142.1$$

Point X = 3.0 Inch

$$Q_3 = \frac{0.01016 \text{ in.}}{(2.2)\ (0.0000290 \text{ in})} = 159.2$$

This closely approximates a uniform loading. The stress produced from the dynamic condition at resonance will be a function of the input "g" level, the static 1.0 "g" stress level, and the magnification factor.

Dynamic Stress at Resonance

f = (140)(19.32 lbs/in) ("g" input) = g(2,710 PSI)

The Number 1 test coupon (2142-5C) was subjected to a 20 "g" input at resonant frequency, until failure.

$f = 20(2{,}710 \text{ lbs/in}^2) = 54{,}200 \text{ PSI}$

The time until failure was one (1) minute.

The total number of cycles was 60 Sec. x 435 Hz - 26,100 cycles.

Test coupon Number 2 (2142-5A) was subjected to a frequency search at an input level of 2.2g and at a rate of one octave per half minute. The resonant frequency was measured to be approximately 440 Hz and the magnification factor was the same as test coupon Number 1 (2142-5C). Test coupon Number 2 (2142-5A) was then subjected to a 15g input level at resonant frequency until failure. The time to failure was three (3) minutes, ten (10) seconds. The total number of cycles was 190 seconds x 440 Hz = 100,000 cycles.

The stress produced by a 15g input and magnification factor of 140 was:

f = 15(2,710 PSI) = 40,500 PSI

Test coupon Number 3 (2142-5B) was subjected to a frequency search at an input level of 2.2g and at a rate of one octave per half minute. The search was conducted from 100 Hz to 2000 Hz. The resonant frequency was measured to be approximately 440 Hz and the magnification factor was the same as test coupon Number 1 (2142-5C).

Test coupon Number 3 (2142-5B) was then subjected to a 10g input level at resonant frequency until failure. The time to failure was thirteen (13) minutes and thirty (30) seconds. The total number of cycles was as follows:

$$810 \text{ Seconds} \times 440 \text{ Hz} = 356{,}400 \text{ Cycles}$$

The stress produced by 10g input and a magnification factor of 140 was as follows:

$$f = 10(2{,}710 \text{ lbs/in}^2) = 27{,}050 \text{ PSI}$$

A Strobe light was used to observe the excursions during the vibration testing. No deformation or buckling of the core was observed, and no damage was noted to the braze filleting. In all three tests the skins cracked parallel and local to the fixed end.

An error in measurement of time was possible since the part was considered as failed when there was a drop in the amplitude of the beam. As a crack develops the stiffness of the beam decreases, causing the resonant frequency to decrease. The rate of change is directly proportional to the crack propagation rate and the failure time recorded is subject to the skill and interpretation of the test engineer. Any error would cause a shift in time on the stress vs cycles chart to a lower number of cycles. The change would be more apparent for the number of cycles experienced on coupon Number 1 (2.42-5C).

Figure 7-71 provides a comparison of the endurance limit of each of the three coupons to that of sheet 7005 aluminum in the T-63 condition, and shows that the endurance limit of each skin component exceeded that of the sheet.

Figure 7-72 shows deflected shape of coupons at resonant frequency and 2.2 "g" input.

Failure Analysis

Electron Microscope Fractography Study of Sandwich Composite Skin Failures

An electron fractography mechanism study was conducted on the face sheet fracture surfaces of three honeycomb sandwich test coupons, each of which had been vibrated to failure at resonant frequency with 20g, 15g, and 10g sustained load inputs. The two-step replicating technique was used to obtain full depth replicas of typical fracture surface areas. After observations of these areas were performed at magnifications up to 13,200X on a conventional, non-scanning electron microscope, the fracture modes were categorized.

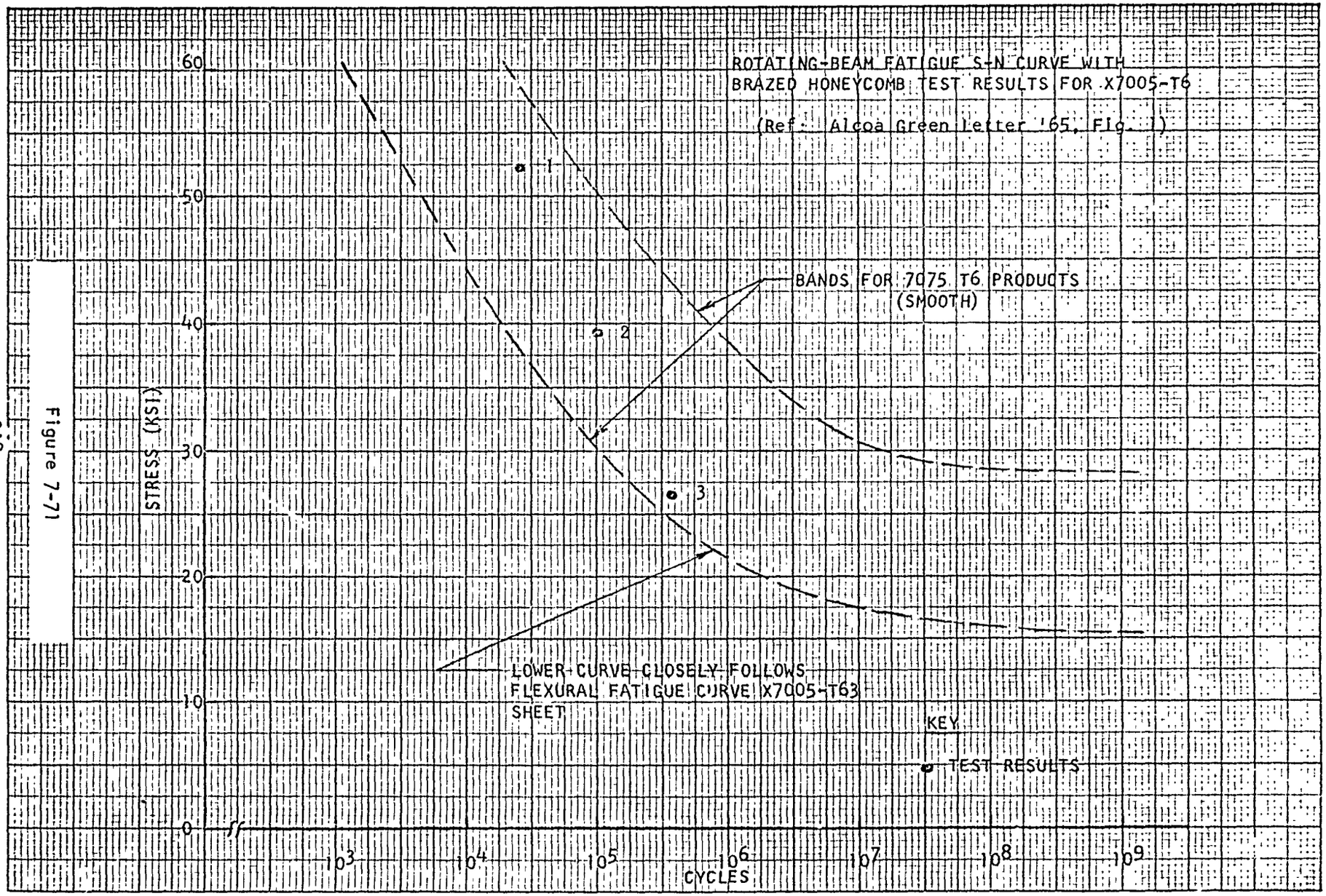
ROTATING-BEAM FATIGUE S-N CURVE WITH
BRAZED HONEYCOMB TEST RESULTS FOR X7005-T6
(Ref: Alcoa Green Letter '65, Fig. 1)
BANDS FOR 7075 T6 PRODUCTS
(SMOOTH)
LOWER CURVE CLOSELY FOLLOWS
FLEXURAL FATIGUE CURVE X7005-T63
SHEET
KEY
TEST RESULTS
STRESS (KSI)
60
50
40
30
20
10
0
1
2
3
10^3
10^4
10^5
10^6
10^7
10^8
10^9
CYCLES

Figure 7-71

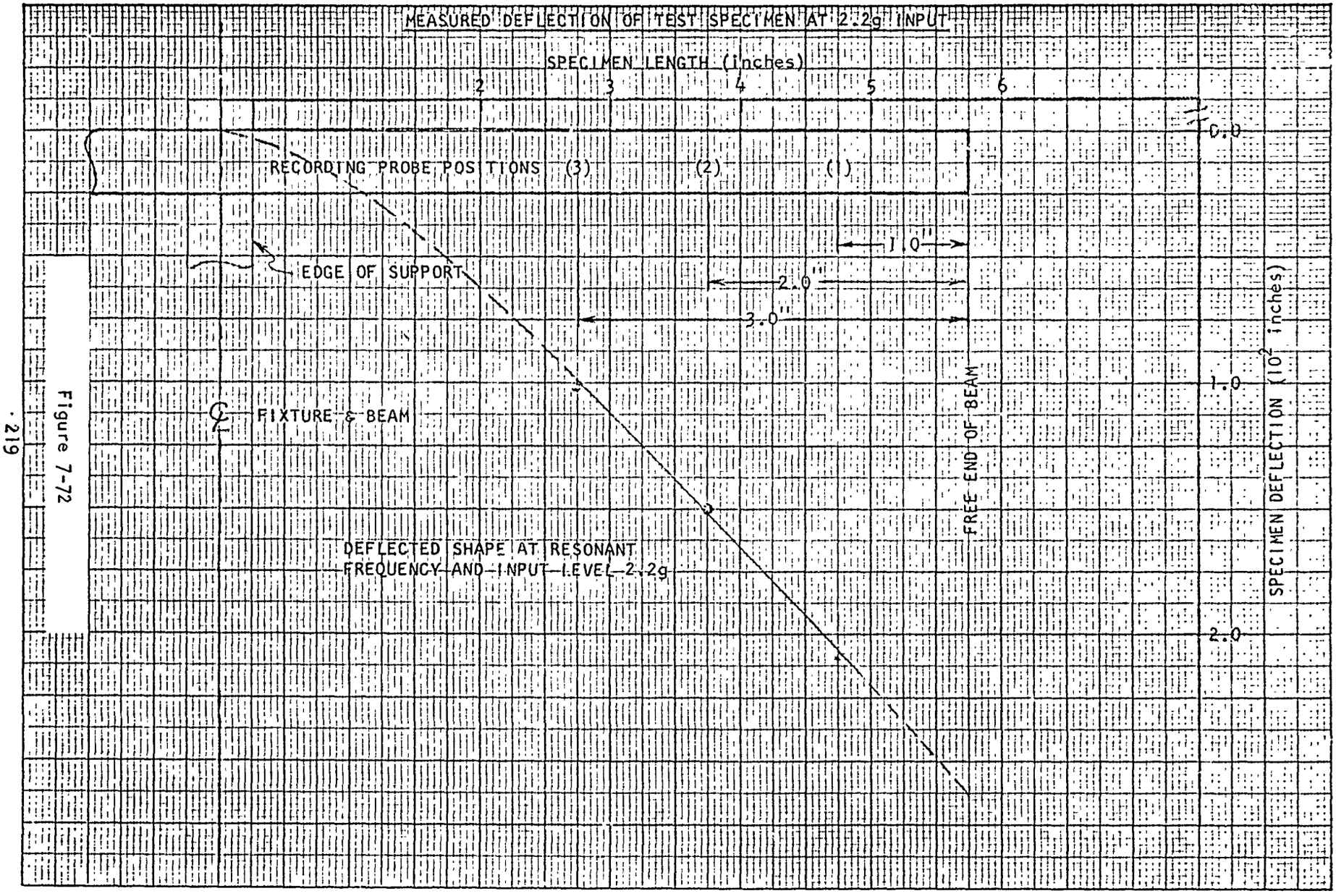
MEASURED DEFLECTION OF TEST SPECIMEN AT 2.2g INPUT
SPECIMEN LENGTH (inches)
2
3
4
5
6
0.0
RECORDING PROBE POSITIONS (3) (2) (1)
1.0"
EDGE OF SUPPORT
2.0"
3.0"
FIXTURE & BEAM
FREE END OF BEAM
DEFLECTED SHAPE AT RESONANT FREQUENCY AND INPUT LEVEL 2.2g
1.0
2.0
SPECIMEN DEFLECTION (10^2 inches)

Figure 7-72

Fractography study results are discussed below:

In all three tests the failure fracture mode was similar. In each case the initial fracture was a ductile fatigue mode which shifted to a typical quasi-cleavage, over-stressed, rupture as a result of the redistribution of stresses caused by the introduction of the crack. (Initial fracture surfaces, since they are stress-free boundaries, are the dominating influence on the distribution of stresses in the fracture path tip vicinity).

Fractography Study of Test Coupon Number 1 Fracture Surfaces

This coupon was stressed at 54,200 PSI (20g input) and failed in the face sheets after 261,000 cycles.

High magnification observation of the full depth fracture surface showed initial ductile fatigue striations with brittle fractures of second-phase particles as illustrated in Figures 7-73 and 7-74.

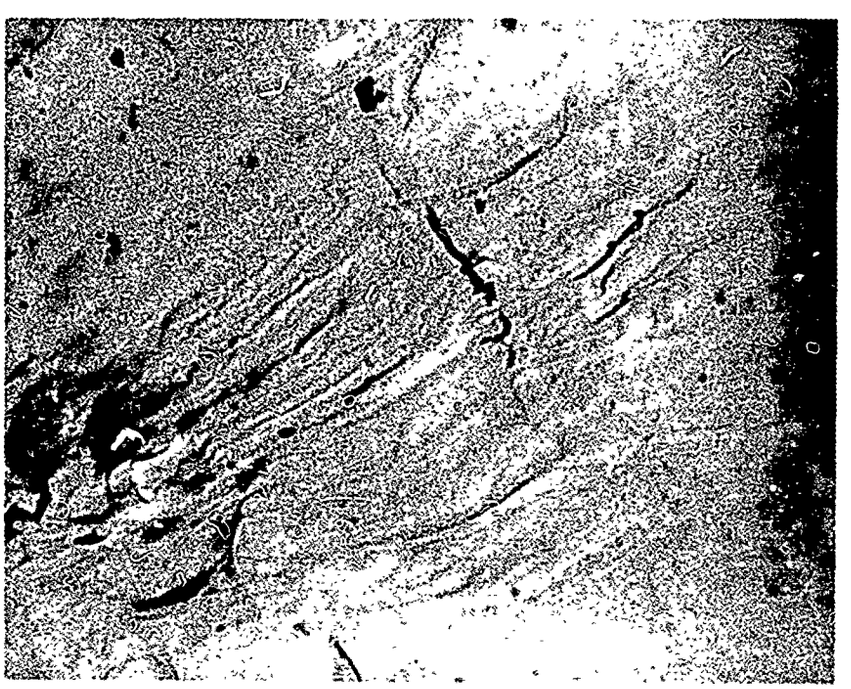

Electron Fractograph - Ductile Fatigue Striations

Magnification - 13,200X

Figure 7-73

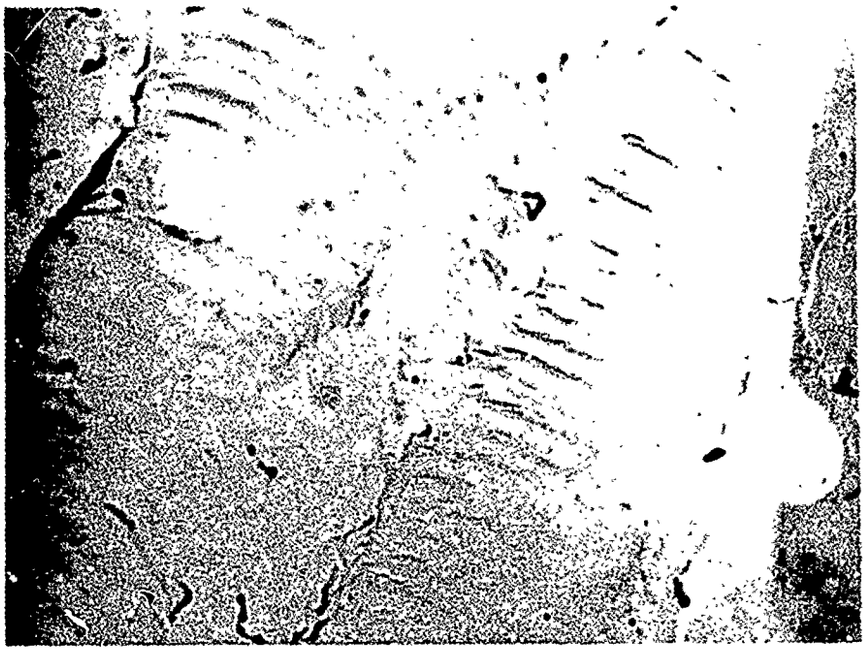

Electron Fractograph - Brittle Fracture of Second-Phase Particle in Ductile Matrix

Magnification - 10,400X

Figure 7-74

The remainder of the fracture path observed (approximately 90%) was a quasi-cleavage and dimple rupture separation typical of an over-load condition. No braze filler metal effect was evident at the lower end of the fracture (core-to-face sheet interface). The quasi-cleavage and dimple rupture is illustrated in Figure 7-75.

Fractography Study of Fracture Surfaces of Test Coupons Numbers 2 and 3.

The study results conducted on samples of the fractures removed from the test coupons vibrated with 15g and 10g load inputs were similar to the findings for the Number 1 test coupon tested with a 20g load input.

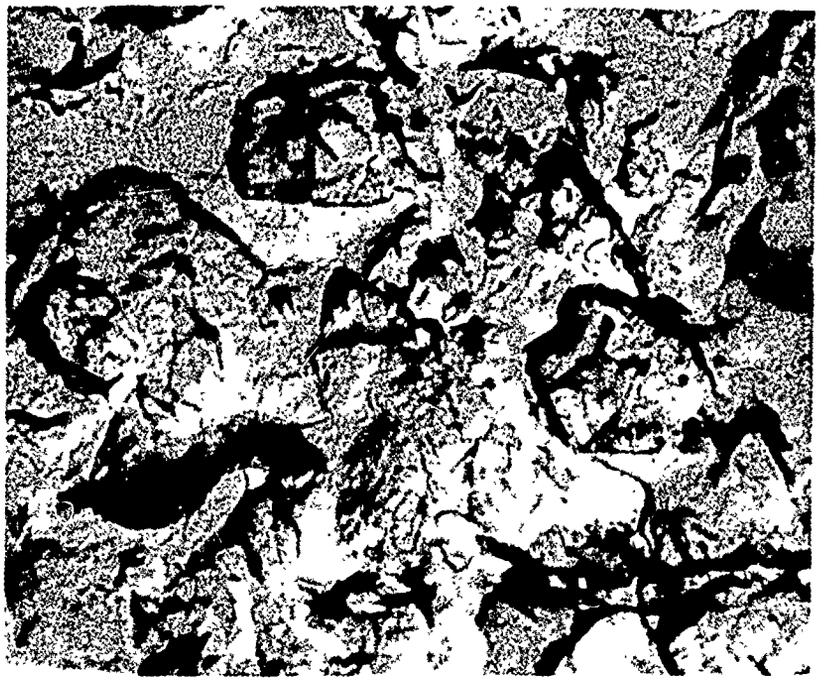

Electron Fractograph - Quasi-Cleavage and Dimple Ruptures

Magnification - 11,200X

Figure 7-75

Failure Analysis Summary

In all cases, each of the skins fractured local to the cantilevered end (fixed end) of the coupon. The analysis showed that the endurance limit of the failed members exceeded that of 7005-T6 sheet when stressed to 54,200 PSI, 40,500 PSI, and 27.050 PSI. An electron fractography study of each failed area showed that the initial cracking mode was ductile fatigue which shifted immediately to an over-stress failure in the test conducted. The fatigue mode appeared to have occurred in a larger percentage of the fracture paths for each of the two coupons which were subjected to a lesser stress. No damage was evident in the face sheet stiffening members (core ribbons) or face sheet-to-core brazed joints.

7.5.1.4 Honeycomb Sandwich Composites - Thermal Cyclic Tests

The objective of the thermal cyclic test was to demonstrate the structural integrity of fluxless brazed honeycomb composites when subjected to large temperature changes between surfaces.

The work on brazed structural honeycomb sandwich composites was confined to establishing a method for measuring the stress developed by the face sheets when a thermal gradient was imposed across the section.

A honeycomb brazement was subjected to a thermal test. One side of the panel was maintained at room temperature and the other side of the panel was subjected to an elevated temperature. Strain gages on each side spaced to give the thermal stress distribution indicated large unexpected variations of strain due to the temperature differences. Difficulty was also experienced in maintaining a uniform temperature distribution.

To calibrate the strain gages, an additional test was performed which was to record the strains due to a uniform temperature soak. Six gages and six thermocouples were installed (3) each on each side of a panel, one inch by five and a half ($5\frac{1}{2}$ inches). The temperature was raised and allowed to soak until the output of each thermocouple indicated the same temperature. The thermal strains were recorded. The gages at the center of the panel on each side indicated a higher tensile strain than those on the ends.

The braze alloy has a thermal coefficient of approximately 11.6×10^{-6} in/in F and the 7005 alloy has 12.9×10^{-6} in/in F. This difference should produce compression in the 7005 alloy and tension in the braze alloy with the magnitudes of tension and compression increasing to the center of the panel.

This difference from the test result is possibly caused by buckling within each cell produced by the tensile (inside) and compressive (outside) forces. This buckling would produce a tensile strain on the outer surface which is higher than the compressive strain from the differential expansion rates of the braze and 7005 alloys. This would further produce a higher tensile indication at the center of the panel than that at the ends.

Visual and stereomicroscopic examination of coupons used during attempts to establish thermal cyclic test procedures showed no indication of damage to the structure.

7.6 Ultra Light Thermal Conditioning and Mounting Panel

This investigation was conducted to demonstrate the feasibility of fluxless brazing and ultra light composite using aluminum foil skins. This investigation proved the feasibility of items of this description.

One (1) ultra light thermal conditioning and mounting panel was fabricated per the design shown in Figure 7-76. No manufacturing problems were encountered in detail fabrication, brazing, heat treating or assembly operations. Figure 7-77 shows the completed composite prior to burst testing.

7.6.1 Testing of Ultra Light Thermal Conditioning and Mounting Panel

Results of tests performed on the ultra light composite proved the integrity of fluxless brazing for ultra light composites.

The tests performed and results are summarized below:

- o Radiographic - No metal-to-metal joint porosity detected. All fin-to-face sheet node attachments well filleted. No crushing of fin members.
- o Flatness - Plate was within 0.008 inches TIR flatness in the unrestrained condition.
- o Face Sheet Surface - No face sheet sagging between fin nodes occurred (dimpling of face sheets of braze honeycomb is common). Lack of sagging (dimpling) was attributed to the controlled pressure cycle.
- o Proof Pressure and Leak Test - Plate was subjected to an internal pressure of 60 psig using helium. No deformation in excess of 0.001 inches was recorded. No measurable helium leak was detected at a sensitivity level of 1.0×10^{-9} cc/sec. at 60 psig.
- o Burst Test - Plate was hydrostatically pressurized to failure. Failure occurred at approximately 635 psig. Failure occurred in lower face sheet opposite the two coolant pressure fittings. This area was unsupported for a diameter of 0.375" and was the predicted failure point. The failing stresses exceeded that of a flat plate by some 300 percent. No stress analysis was performed as components of this nature are not normally subjected to pressures exceeding 60 psig. However, it was assumed that the stresses reacted as would that of a diaphragm with stress risers at the fin nodes at the periphery of the 0.375" diameter area.

Mode of failure showed that the 0.375" diameter area had a slight elastic deformation at 635 psig and permanent deformation at 641 psig. No leak was caused by this deformation.

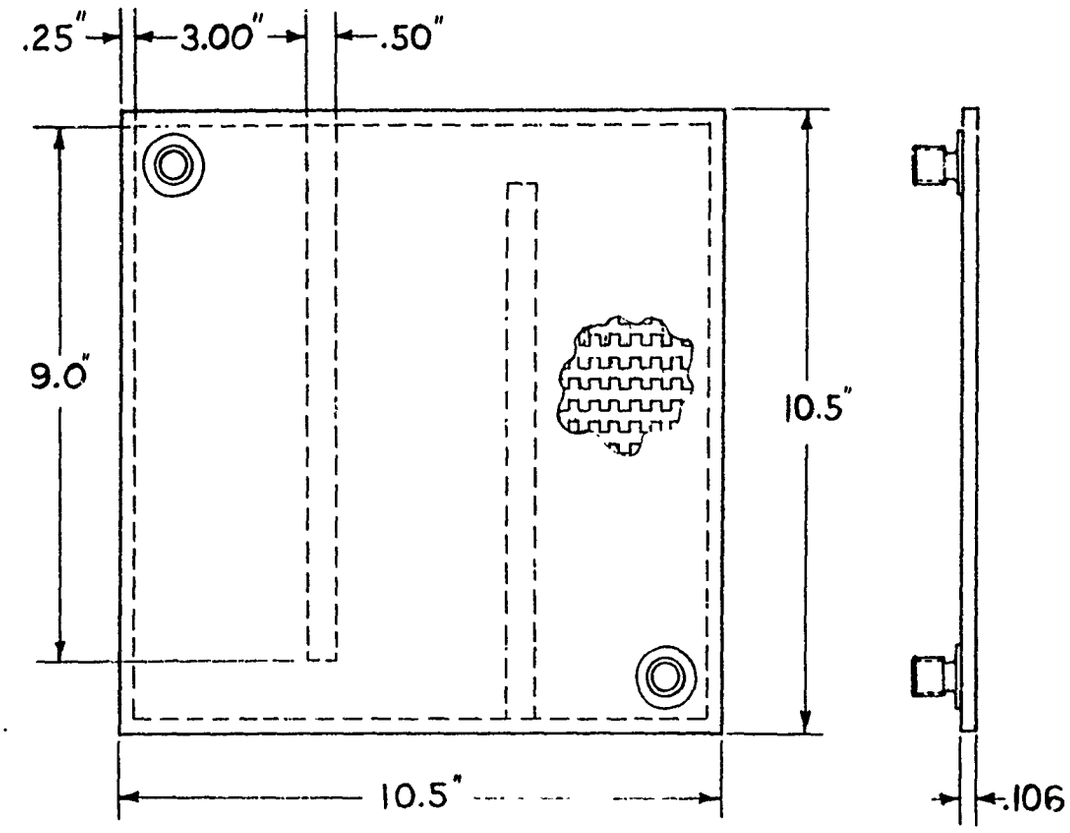

Face Sheet	- 7005 Al Alloy .006" Thk.
Edge Member	- 6006 Al Alloy .090" Thk.
Flow Separator	- 6061 Al Alloy .090" Thk.
Coolant Fittings	- 6061 Al Alloy
Filler Metal	- Type 4045
Surface Extended Fin Pitch	- 6.7 Inches
Surface Extended Fin Stock	- 6061 Al Alloy .008" Thk.

Thermal Conditioning Panel Configuration

Figure 7-76

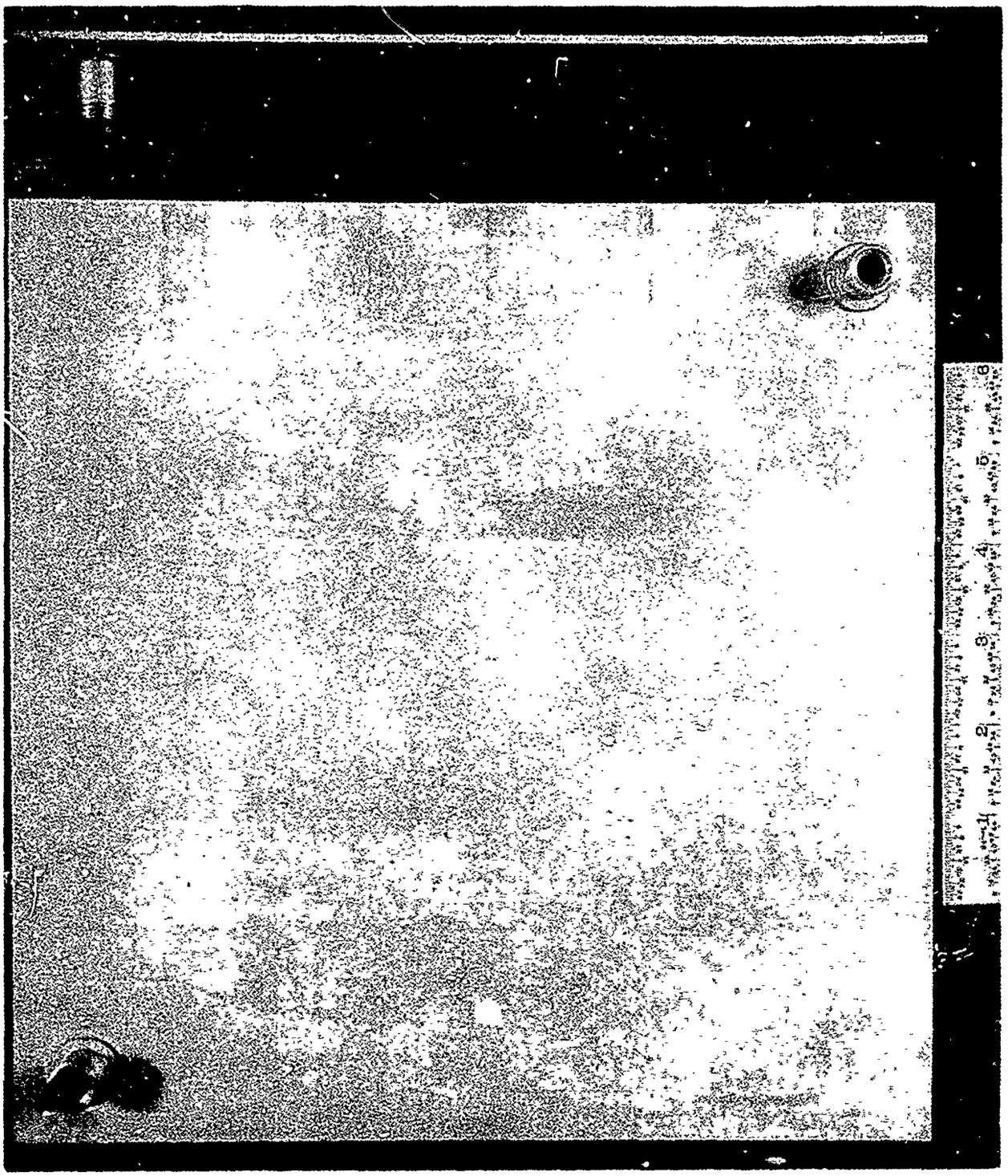

Thermal Conditioning Panel Prior To Burst Test

Figure 7-77

SECTION 8.0

HARDWARE FEASIBILITY APPLICATION - DIFFUSION BONDING

8.1 Scope, Approach, and Summary

This investigation concerned the feasibility of low pressure diffusion bonding complex lightweight aluminum composites. Specifically, three applications were selected; namely, honeycomb sandwich composites, multi-layer plate fin heat exchangers, and thermal conditioning panels. Tube shell heat exchanger applications were not considered, due to the complexity of achieving the necessary material contact at tube to head plate joint interfaces.

Two (2) base metal aluminum alloys (7005 and 6061) and one (1) interleaf alloy (4045) were selected. The bonding cycles successfully developed as reported in Section 5.0 were used.

In summary, this investigation (within the limits of the materials selected) demonstrated that low pressure diffusion bonding has a poor potential for lightweight composite applications. This is especially true when compared to the applicability of fluxless brazing.

Acceptable low pressure diffusion bonded structural joints are limited in multi-joint composite applications to where all critical joint members exhibit a high degree of column rigidity in the direction of bonding forces. This is an inherent problem which diffusion bonding of lightweight composites possess and which increases in magnitude with larger composite surface areas, as the ability to provide the necessary mating of critical interfaces and the applying of uniform pressures becomes increasingly difficult.

The structural honeycomb sandwich composite investigation was limited to 1/4 inch cell core; in this respect the core could be termed low density core. Using a higher density core, ie, 3/16 inch or 1/8 inch cell core, would increase the core wall stiffness and would offer an overall increase in the multi-joint quality. The application of high density core diffusion bonded sandwich composites, therefore cannot logically be ruled out.

Three honeycomb sandwich test panels were diffusion bonded and evaluated. Increasing the bonding pressure caused cell walls to deflect and resulted in loss of joint contacts. Reducing the pressure and increasing the bonding time improved the joints, however, the overall properties were sub-standard.

A series of multi-layer plate fin elements were evaluated in this investigation. The optimum pressure as developed in Section 5.0 was found to be too great. By reducing the pressure, which resulted in a lower deflection of the thin wall members, and by increasing the bonding time, a significant improvement was achieved.

Two ultra lightweight thermal conditioning panels were diffusion bonded and evaluated. The results were unsatisfactory, as edge member closeout to face sheet joints exhibited linear microporosity which leaked when pressurized with helium.

8.2 Honeycomb Sandwich Panel Evaluation

Three (3) low density honeycomb sandwich test panels were diffusion bonded and evaluated.

Test panel details were:

Face sheet.	6951 alloy	12" x 12" x 0.0098"
Core ribbon	6061 alloy	0.004" thick
Core blanket size . .	1/4" sq. cell. . . .	12" x 12" x 0.364"
Interleaf	4045 alloy foil. . .	0.003" thick

Test Panel Number 1

Panel Number 1 was diffusion bonded at 53.3 PSI at 1040 F for 60 minutes. Core blanket was stabilized with polyglycol and ground flat to ± 0.0005".

Calculated bonding pressure:

Using a pressure of 1.76 PSI, the force on 144 in^2 of face sheet is $F = P \times A = 1.76 \times 144 = 253.44$ lbs.

The theoretical pressure applied normal to core ribbon edge was $\frac{\text{Force}}{\text{Ribbon density}} = \frac{253.44}{144 \times 0.033} = 53.3$ PSI

Result

Four corners crushed from 0.004" to 0.010". Balance of panel thickness reduction varied up to 0.002". Core ribbon to face sheet interfaces contained up to 10 percent voids. (Figure 8-1)

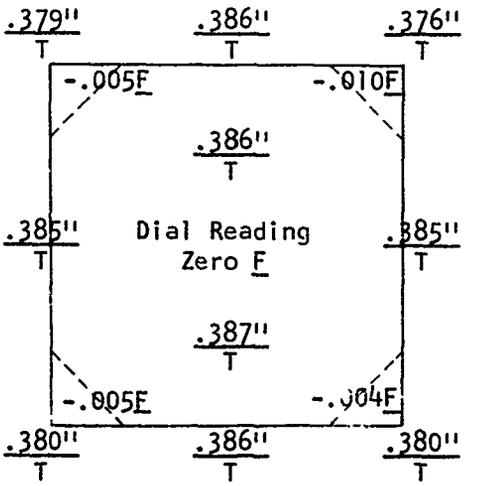

Figure 8-1

Joint interfaces exhibited buffering with insufficient transcrystalline growth.

Mount #625
Magnification - 250X
Boric Acid HF Etched

Figure 8-2

Test Panel Number 2

Panel Number 2 was diffusion bonded at 1040 F for 60 minutes at an increased pressure to that of Number 1, from 53.3 PSI to 70 PSI. Increased pressure caused severe buckling of core ribbon.

Test Panel Number 3

Panel Number 3 was cycled at the same pressure and temperature as was Number 1 (53.3 PSI at 1040 F). The holding time was increased to 90 minutes from the original 60 minutes to increase mass transfer and promote transcrystalline grain growth across joint interfaces.

Result

It was difficult to determine if the percent of voids was less than the Number 1 panel. It was estimated that not more than a two (2) percent improvement was achieved, however, this difference may well have been within the tolerance of repeated tests per the Number 1 panel bonding schedule.

Panel thickness reduction increased from 0.002 inches for the Number 1 test to 0.0035 inches for the Number 3 test as a result of slight deformation of the ribbons adjacent to the interfaces.

Mount #706 Mag. - 250X
Boric Acid + HF Etched

Figure 8-3

Typical joint interfaces showed bending of core ribbon local to interfaces.

Joint interfaces were reasonably free of buffering with initiation of transcrystalline interface grain growth.

Flatwise tensile tests failed at joint interfaces. Average stress on core ribbon at failure was 9.8 KSI. Areas tested were essentially free of gross voids.

Flexure testing was attempted - due to local skin distortion initiation at void areas - these tests were discontinued.

8.3 Multi-Layer Plate Fin Evaluation

Six (6) surface extended corrugated fin to plate test panel elements were diffusion bonded and evaluated.

The bonding schedule developed in Section 5.0 of this report was implemented on the first three (3) test elements. The second three (3) tests were conducted under modified schedules to improve the joint quality.

Pre-bonded details and bonded elements are illustrated in Figures 8-10 and 8-11.

Test element details were prepared per Figure 8-4 below.

Plate Fin Element Cross Section

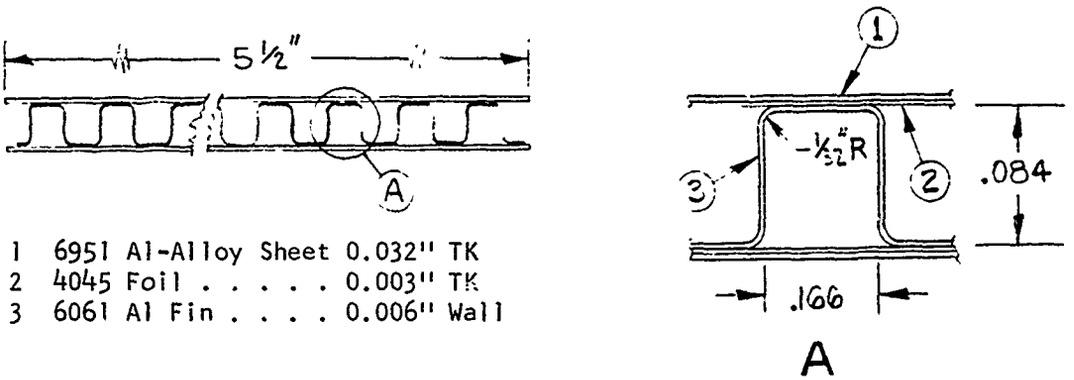

1 6951 Al-Alloy Sheet 0.032" TK
2 4045 Foil . . . . . 0.003" TK
3 6061 Al Fin . . . . 0.006" Wall

Figure 8-4

Unstable fin node to plate interfaces caused by a deflection of the fin vertical walls and flat node areas resulted in localized contact. This movement which was the resultant of the bonding force applied normal to the plate surface is illustrated in Figure 8-5.

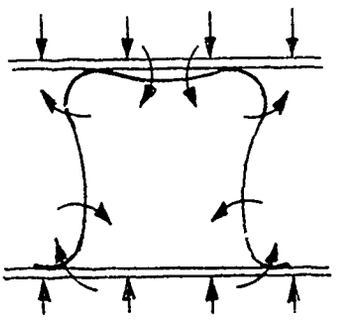

Figure 8-5

An increase in time at constant pressure and temperature (54 PSI at 1040 F) from 60 minutes to 120 minutes provided no improvement to joint quality.

By reducing the pressure to 30 PSI and holding bonding to 120 minutes, the fin deflection was reduced, while a general increase in bonded area was achieved.

The average bonded element flatwise tensile properties versus bonding schedule are presented in the following:

Bonding Pressure (PSI)	Bonding Time (Mins)	Bonding Temp. (°F)	Stress on Vertical Fin at Failure (KSI)
54	60	1040	9.7(1)
54	120	1040	9.0(1)
30	90	1040	9.0(1)
30	120	1040	11.0(1)

(1) Average of four specimen

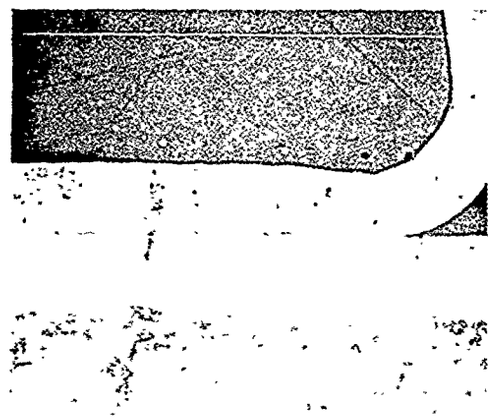

Section of fin node to plate joined at 54 PSI for 60 minutes at 1040 F.

Excessive void area between bonded areas below heels of fin member.

Mount #673
Magnification - 40X
Boric Acid + HF Etched

Figure 8-6

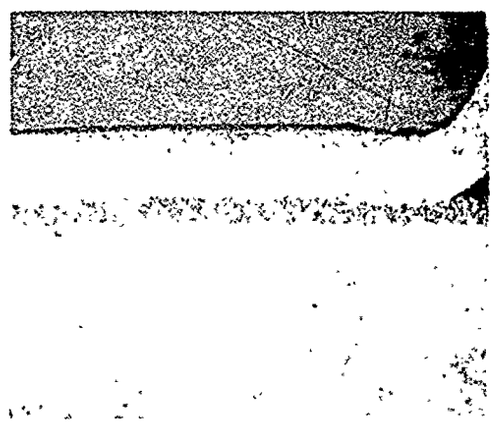

Section of fin node to plate joined at 30 PSI for 120 minutes at 1040 F.

Void length and gap decreased approximately 15 percent as compared to joints illustrated in Figure 8-6.

Mount #722
Magnification - 40X
Boric Acid + HF Etched

Figure 8-7

Photomicrographs below are of joints illustrated on preceding page which are increased in magnification to illustrate the differences in voided areas.

Bonded at 54 PSI for 60 Minutes at 1040 F
Mount #752 Mag. - 250X

Figure 8-8

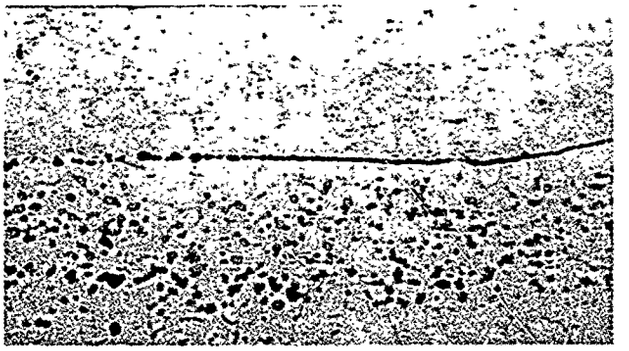

Bonded at 30 PSI for 120 Minutes at 1040 F
Mount #747 Mag. - 250X

Figure 8-9

Plate Fin Element Details

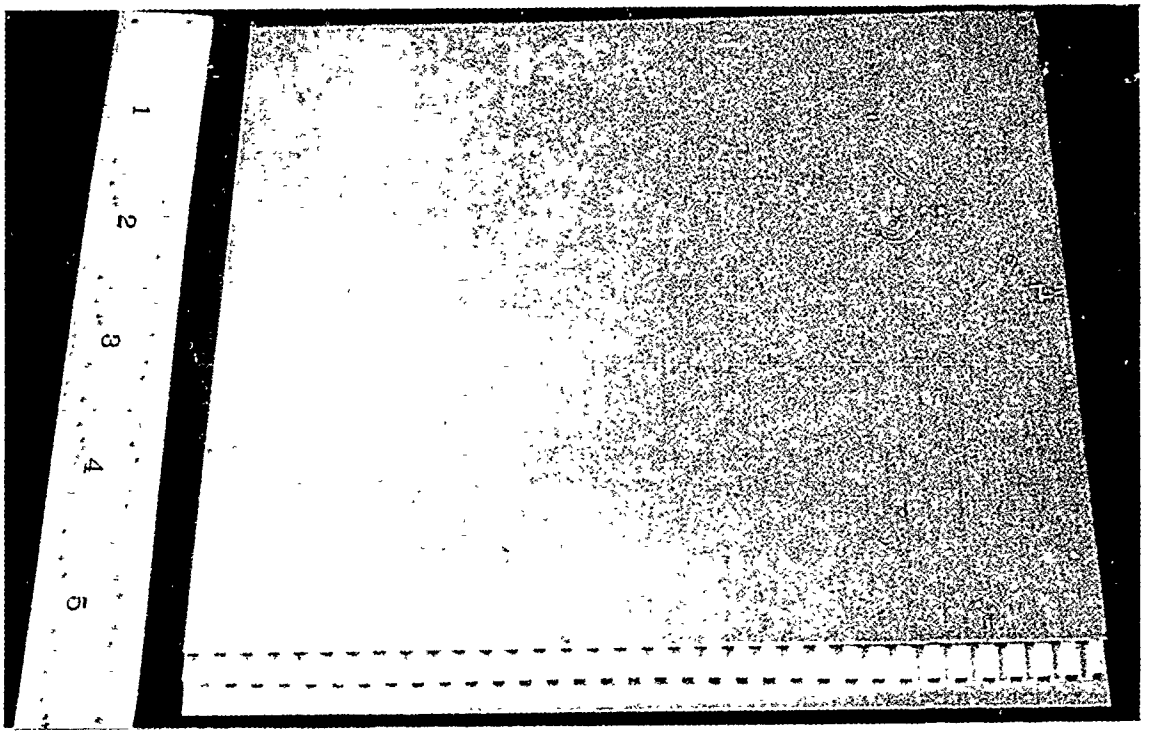

Figure 8-10

Plate Fin Bonded Test Element

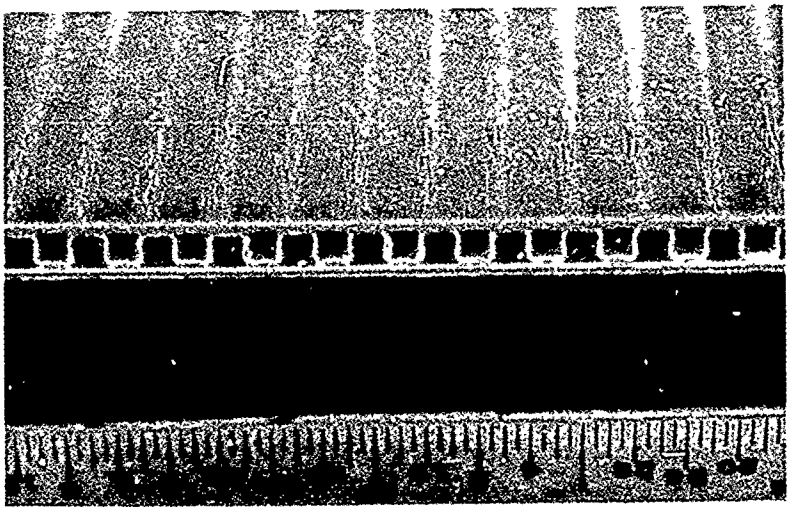

Vertical members of fin are shown to be deflected as illustrated in Figure 8-5

Figure 8-11

8.4 Ultra Lightweight Thermal Conditioning Panel - Hardware Feasibility Evaluation

Two (2) single passage thermal conditioning ultra lightweight composites were diffusion bonded and evaluated.

The 7005 alloy was selected for the thermal plates (face plates) as it is less sensitive to solid solutioning quenching rates than the other alloys evaluated in Phase I, a 90 second air quench was used, thus minimizing possible thermal shock.

Thermal plates were 6 mils thick, a surface extended split turbulent fin was used in the coolant passage which would provide a heat transfer rate of 200 to 300 BTU/ft^2/hr with a normal active system.

The Number I test panel was pressurized internally with helium and proof pressure leak tested, and found to have a total leak rate of 1.4×10^{-4} std cc/sec at 8 psig.

The Number 2 test panel was diffusion bonded with an extended cycle. Cycle was increased from 60 to 120 minutes; this modification to the bonding cycle resulted in an improved leak rate performance.

A microscopic review of joint interfaces local to detected helium leaks showed evidence of linear microscopic porosity. The 7005 Al to interleaf interfaces were superior to those of the 6061 Al to interleaf interfaces.

Test Panel Number I

Panel Number I was diffusion bonded at 54 PSI for 60 minutes at 1040 F.

Panel configuration was per Figure 8-12. Final composite envelope size was machined after bonding and heat treating to T6.

Panel was radiographically inspected - no detectable voids were found.

Panel was subjected to an internal pressure helium leak test, and found to have incipient leaks through the closeout member to thermal plate diffusion bonded interfaces. The total leak rate measured at 8 psig with a mass spectrometer was 1.4×10^{-4} std cc/sec.

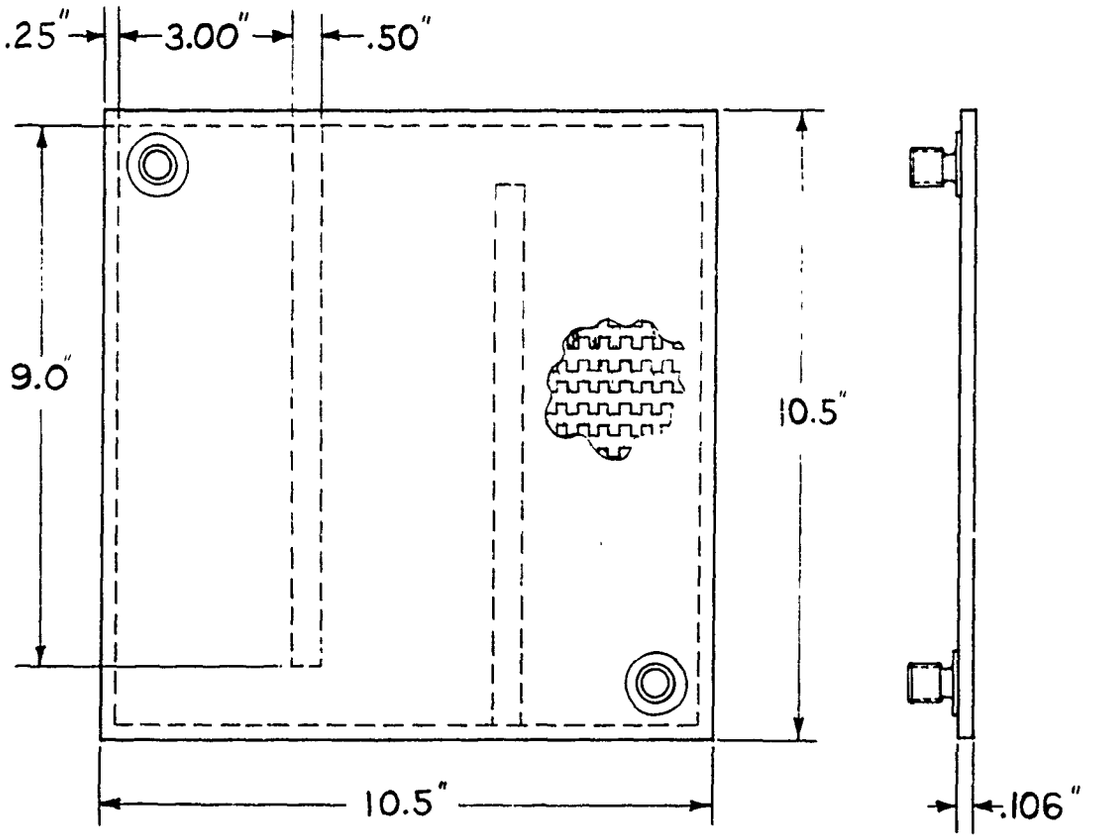

Face Sheet	- 7005 Al Alloy .006" Thk.
Edge Member	- 6006 Al Alloy .090" Thk.
Flow Separator	- 6061 Al Alloy .090" Thk.
Coolant Fittings	- 6061 Al Alloy
Filler Metal	- Type 4045
Surface Extended Fin Pitch	- 6.7 Inches
Surface Extended Fin Stock	- 6061 Al Alloy .008" Thk.

Thermal Conditioning Panel Configuration

Figure 8-12

Micro-lap shear specimen were removed from edge member trim, and lap joint average shear value was determined as being 16.2 KSI. This was approximately 30 percent less than the average of the original metal to metal evaluation (reference Section 5.0).

Figure 8-15 gives measured free state flatness and thickness of panel bonded and in the T6 condition.

Figures 8-16 and 8-17 photographically illustrate the panel details and bonded assembly respectively.

Test Panel Number 2

Bonding schedule was modified by increasing the bonding time from 60 minutes to 120 minutes, which resulted in an improved micro-structure of the critical joint interfaces and decreased the total measured leak rate at 8 psig to 1.34×10^{-5} std cc/sec.

Optimumly, the leak rate should not be greater than 1.0×10^{-7} std cc/sec of helium at 40 psig.

Micro-lap shear specimen were machined from edge member trim and also the flow separator bars to face sheet joints and tested. Average shear value was 20.1 KSI. From this standpoint, the structural quality of the metal to metal joints was acceptable.

Microscopic inspection of bonded metal to metal closeout interfaces revealed linear porosity in the 6061 to interleaf interface areas where helium traces were detected externally during leak testing. Areas where no helium was detected were found to be free of porosity and to have good metallurgical interfaces. Typical photomicrographs of these two conditions are presented below:

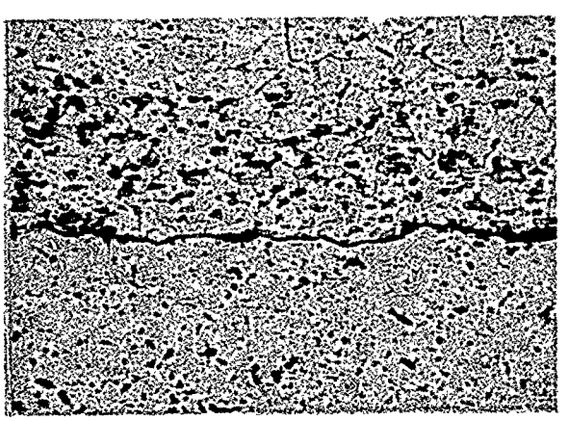

7005 Al to 6061 Al bonded interface

Linear micro porosity found at 4045 interleaf to 6061 Al

Mount #636
Boric Acid + HF Etched
Magnification - 250X

Sectioned From Leak Area of Number 2 Test Panel

Figure 8-13

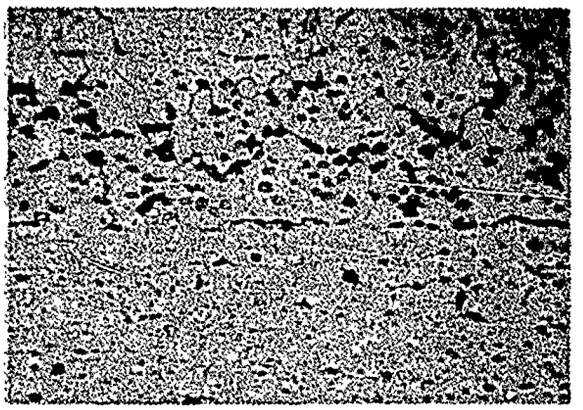

Micro Section - Non Leaking Area - Number 2 Panel

7005 Al to 6061 Al bonded interface.

Slight buffering effect at interleaf to 6061 alloy interface.

Mount #637
Boric Acid + HF Etched
Magnification - 250X

Figure 8-14

Thermal Conditioning Panel - Free State Flatness and Thickness (Bonded and Heat Treated to T6)

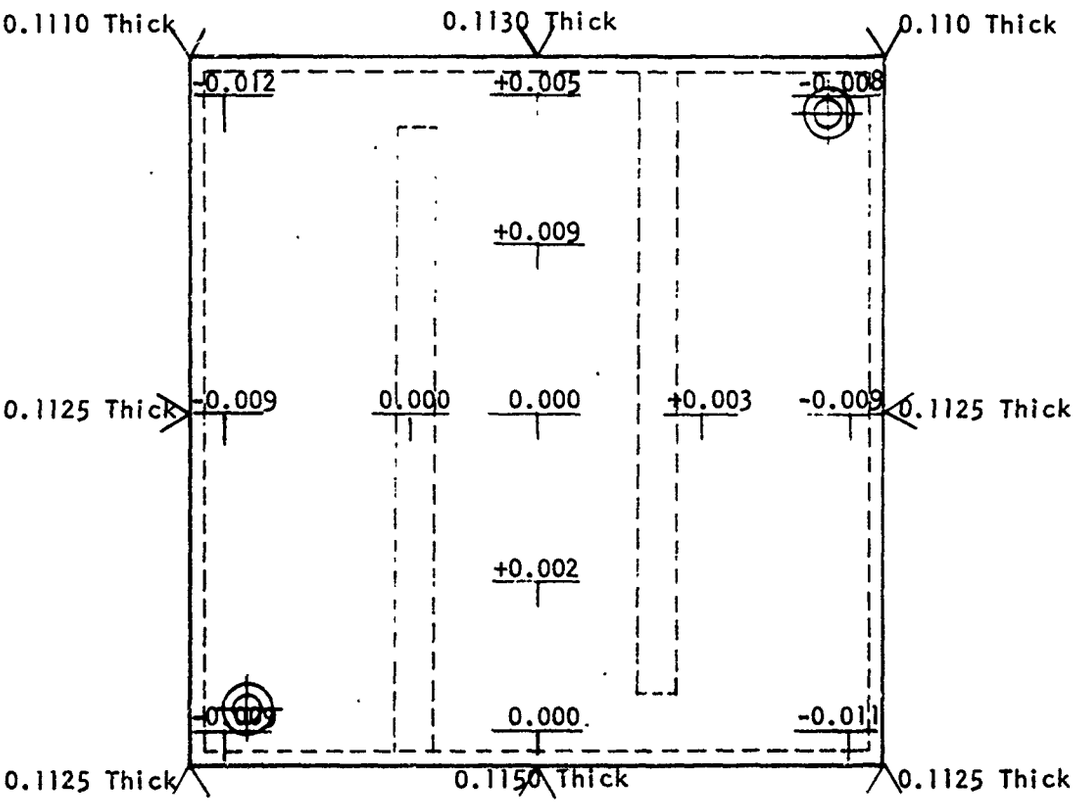

Figure 8-15

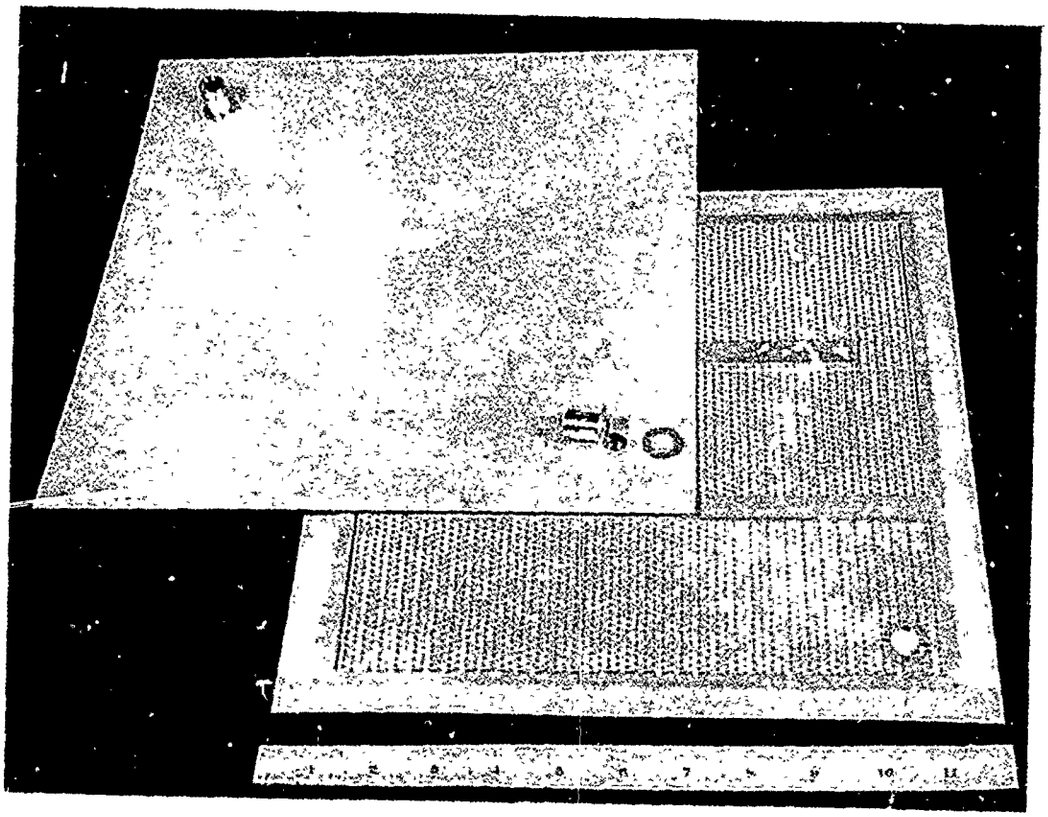

Diffusion Bonded Thermal Conditioning Panel - Details

Figure 8-16

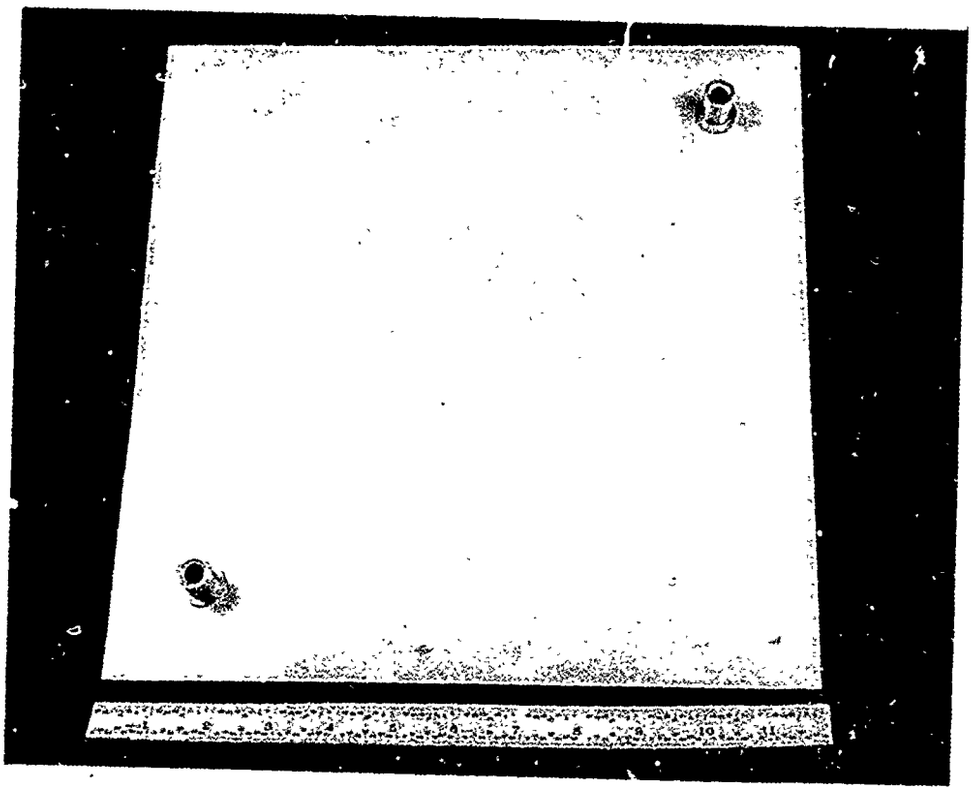

Thermal Conditioning Panel as Diffusion Bonded

and

Heat Treated

Figure 8-17

SECTION 9.0

APPLICATION OF EXPERIMENTAL BRAZE FILLER METAL SYSTEMS

9.1 Scope

Because of the advancements obtained in the state-of-the-art-materials brazing evaluation for complex hardware composite applications, this investigation was limited to a demonstration of the potential of brazing composites with one (1) experimental ternary system.

Early in the Section 6.0 investigation a AlSi + Ni experimental ingot had been successfully rolled to foil. This foil was used to evaluate the potential for brazing honeycomb core to face sheet composites. On the basis of the results obtained, a fair assumption is that other more promising AlSi modified ternary systems as reported in Section 6.0 could have been successfully used for brazing at temperatures below that used for this system (AlSi + Ni).

9.2 Evaluation of Brazing Honeycomb Sandwich Composites with the AlSi + Ni Ternary System

Melt #12 (reference Table 6-1, Section 6.0) as reduced to foil was evaluated to demonstrate the feasibility of brazing 6061 Al honeycomb core to 7005 Al face sheets.

Brazing was accomplished at 1055 F $\pm$ 5 F, the panel was held at the peak temperature for five (5) minutes. Panel size was restricted to 6" x 6". One edge of the brazement is photographically illustrated in Figure 9-1 after sectioning. Distorted ribbon edges were caused by sawing operation.

Radiographic inspection showed areas of excessive core ribbon to face sheet joint filleting, with other localized areas exhibiting no fillet formation.

Figures 9-2 and 9-3 illustrate micro-cross sections of filleted and nonfilleted joints.

Thin ribbon members in joint areas were free of undesirable diffusion and excessive transcrystalline grain growth.

The ingot, prior to rolling, had not been subjected to thermal homogenizing conditioning and was known to be heterogeneous with massive macrosegregation. A microscopic evaluation of both filleted and nonfilleted areas confirmed that the filleted areas were nickel bearing up to three (3) times greater than that present in the nonfilleted areas. Figure 9-2 shows massive flow and

filleting with an idiomorphic AlSi microstructure. The dispersion of silicon and nickel was adjudged excellent. Figure 9-3 shows considerable retention of the wrought effect indicating incomplete melting, however, the interfaces were metallurgically good.

It is considered that the non-uniform filleting would have been minimized had the AlSi + Ni ingot been subjected to the ten (10) hours of thermal homogenization at 970 F prior to rolling.

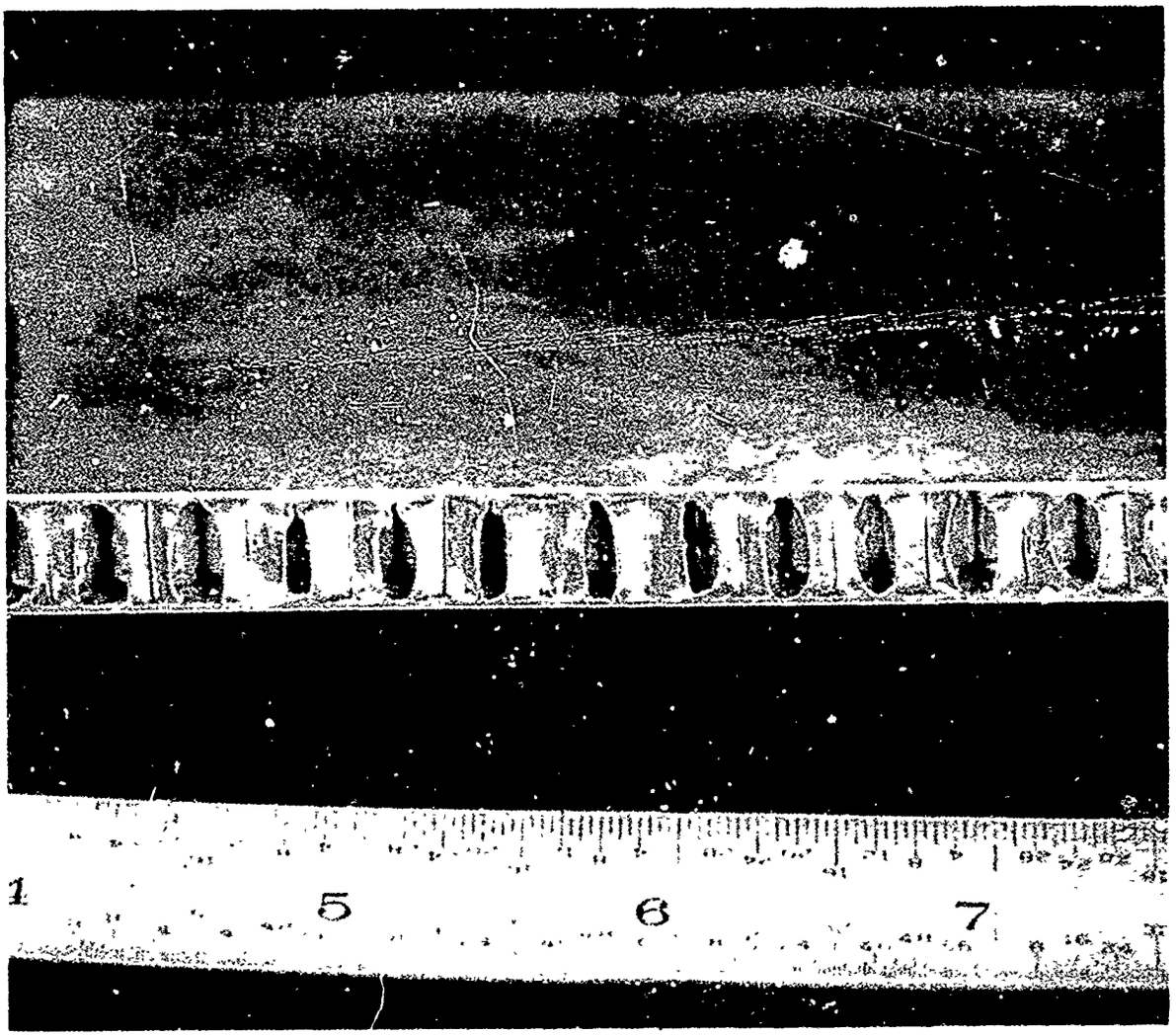

6" x 6" Honeycomb Sandwich Test Panel
Joined with AlSi + Ni Filler

Figure 9-1

Honeycomb Sandwich Brazed Joint

6061 Al - Ribbon
7005 Al - Face Sheet
AlSi + Ni - Braze Filler Metal

Mount #512
Etchant - None
Magnification - 50X

Illustrates - Massive Filleting

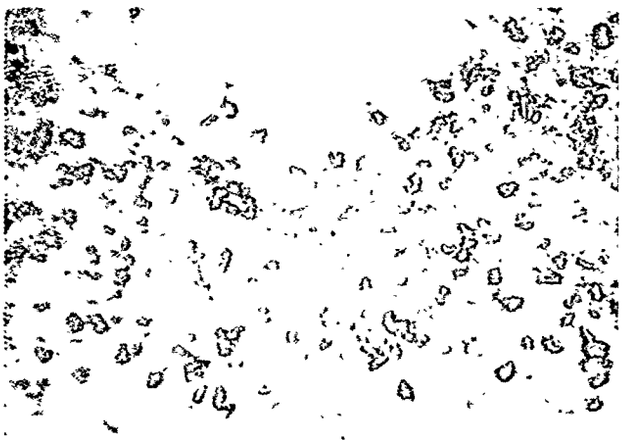

Mount #512
Etchant - None
Magnification - 200X

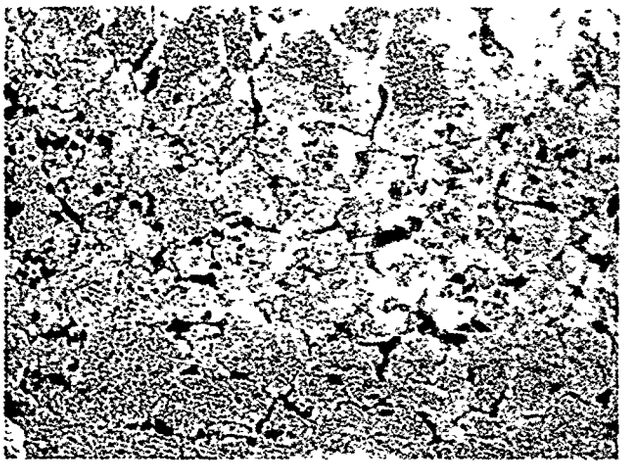

Mount #512
Etchant - Boric HF
Magnification - 200X

Figure 9-2

Honeycomb Sandwich Brazed Joint

6061 Al - Ribbon
7005 Al - Face Sheet
AlSi + Ni - Braze Filler Metal

Mount #513
Etchant - None
Magnification - 50X

Illustrates Negative Filleting

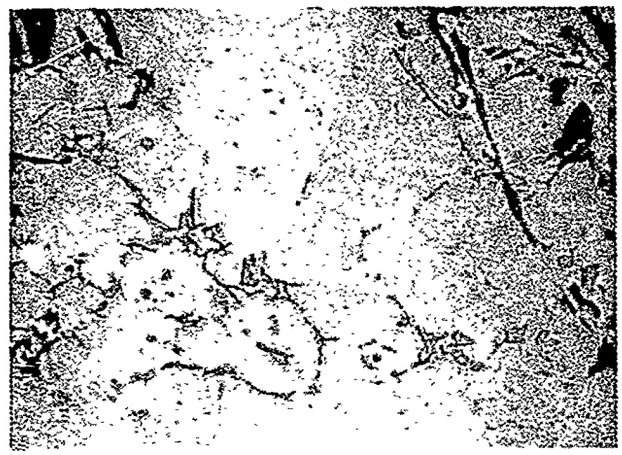

Mount #513
Etchant - None
Magnification - 200X

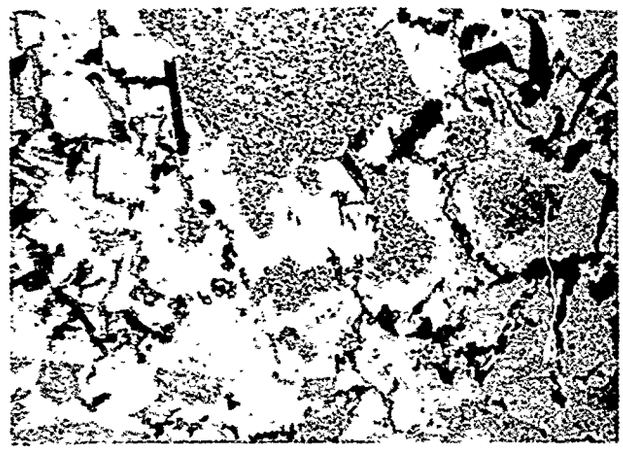

Mount #513
Etchant - Boric HF
Magnification - 200X

Figure 9-3